Transport Models for Non-Isobaric Electrolytes

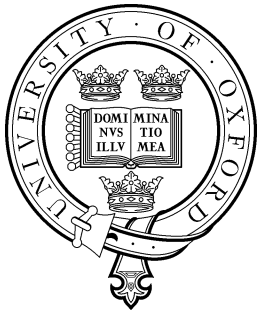

Priyamvada
St Peter's College
University of Oxford

A thesis submitted for the degree of
Doctor of Philosophy

Michaelmas 2018

Abstract

Conventionally, transport models employed for describing processes in electrochemical devices have been developed for liquid electrolytes under isobaric conditions [1]. The assumption of constant pressure starts to break down for solid or other viscoelastic electrolytes, which respond to internal or external stress and strain changes in a fundamentally different way. Mechanical effects and their coupling with charge and mass transfer have, therefore, become a key area of research [2]. The present work focuses on the Nafion ionomers used in polymer electrolyte membrane (PEM) fuel cells. The tendency of these membranes to swell upon solvent sorption in spatially constrained environments, when viewed in conjunction with the delicate water balance necessary for optimum operation and the durability requirements from the cell stacks, makes for a perfect case study of non-isobaric transport in electrolytes [3].

The thermodynamics underlying the transport model for a viscoelastic electrolyte such as a hydrated Nafion membrane was recently revisited by the authors [4]. A membrane (or more generally, a solid) can store energy in the form of elastic work obtained from deformation of the material, in addition to the pV compressive work, heat work, and electrochemical work; this introduces deformation stress as an additional intensive variable. Conservation laws for material, momentum, and energy, local equilibrium conditions, as well as material and momentum flux constitutive laws, have been developed using basic principles of classical and

irreversible thermodynamics to maintain congruency with this modified basis of thermodynamic intensive variables.

Electrochemical impedance spectroscopy (EIS) response of the model has been studied within the new framework to gain insight into electrochemical/mechanical coupling. EIS concentrates on the first-order effects and identifies the various time-scales, length-scales, and the dominant ranges of the modelled physical phenomena. For instance, current-induced pressure variations at high frequencies (~1 MHz) were found to manifest as resonance peaks on Bode plots, which can partially explain the high-frequency inductance observed in Nafion systems [5]. Further, a parameter study was performed to assess which material and mechanical properties are necessary to enhance or downplay stress effects in the model.

To my parents, *Pratima* & *Ambrish*

Contents

List of Figures

List of Tables

List of Symbols

Roman

a	Constant $[=]\,(1-\nu B_0)$. [unitless]
A	Cross-sectional area of the electrolyte. [m^2]
$\vec{b}_i$	Body force on species i exerted by external fields, see equation 3.109. [N/m^3]
B_i	Ratio of the partial molar volume of species i to that of the electrolyte e. [unitless]
c_T	Total molar concentration; relates to $\overline{V}$ through $c_T = 1/\overline{V}$; see equation 3.30. [mol/m^3]
c_i	Molar concentration of species i, $c_i = c_T y_i$. [mol/m^3]
C_p	Constant-pressure heat capacity, defined by equation 3.55. [J/K]
$\hat{C}_p$	Specific heat capacity, $\hat{C}_p = C_p/m_T$. [$J/kg \cdot K$]
$C_{\text{wave},k}$	Speed of sound in the electrolyte when modelled as k =elas; visc; visc,elas material. [m/s]
d	Dimensionality of the system/problem being solved. [unitless]
$\vec{d}_i$	Thermodynamic force driving diffusion of chemical species i, defined in equation 3.58. [N/m^3]
$\vec{\vec{d}}_A$	Diagonal tensor representing the components of $\vec{\vec{A}}$ along its principal axes, see equation 3.5 for $\vec{\vec{d}}_\tau$.[units of $\vec{\vec{\tau}}$]
$\mathscr{D}$	Thermodynamic diffusion coefficient, see Table 4.1. [m^2/s]
D	Fickian diffusion coefficient, $D = \mathscr{D}\chi$, see Table 4.1. [m^2/s]
$\{D_1, D_2\}$	Basis of thermodynamic deformation volumes derived from principal values of $\vec{\vec{V}}'$, see equation 3.9. [m^3]
$\{\overline{D}_1, \overline{D}_2\}$	Basis of molar deformation volumes, $\overline{D_i} = D_i/n_T$. [m^3/mol]
$\overline{D}_{ki}$	Partial molar deformation volume of species i, see equation 3.36. [m^3/mol]
$\mathscr{D}_{ij}$	Microscopic binary interaction parameter between species i and j, see equation 3.136. [m^2/s]
$\{\vec{e}_1, \vec{e}_2, \vec{e}_3\}$	Unit vectors representing an orthonormal, right-handed Cartesian coordinate basis. [unitless]
$\{\vec{e}^{\,\tau}_1, \vec{e}^{\,\tau}_2, \vec{e}^{\,\tau}_3\}$	Unit vectors representing the Cartesian principal axes of tensor $\vec{\vec{\tau}}$. [unitless]
$\vec{e}_n$	Unit outward surface normal vector. [unitless]
$\hat{E}$	Total specific energy, $\hat{E} = \hat{U} + \hat{K}$. [J/kg]
f	Frequency of the sinusoidal impedance current. [Hz]
$\vec{f}_i$	Sum of internal forces exerted by other species on species i. See equation 3.109. [N/m^3]
F	Faraday's constant, 96485.3 C/equivalent.
g_S	Homogeneous rate of entropy generation, defined in equation 3.128. [$J/K \cdot m^3 \cdot s$]
G	Gibbs free energy, defined by Euler's extensivity theorem 3.20. [J]
$\overline{G}$	Molar Gibbs free energy, $\overline{G} = G/n_T$. [J/mol]
G_{ij}	Thermodynamic modulus of elasticity, defined by equation 3.39. [Pa]
$\overline{G}_i$	Partial molar Gibbs energy of species i. Identifies with electrochemical potential μ_i. [J/mol]
$\hat{G}$	Specific Gibbs energy, $\hat{G} = G/m_T$. [J/kg]
G_{mech}	Mechanical contribution to the Gibbs free energy, see equation 3.1, 3.10, or 3.12. [J]
G_{shear}	Isotropic elastic shear modulus, see equation 3.43. [Pa]

H	Enthalpy, defined by equation 3.76. [J]
$\overline{H}_i$	Partial molar enthalpy of species i; through equation 3.76, $\mu_i = \overline{H}_i - T\overline{S}_i$. [J/mol]
$\hat{H}$	Specific enthalpy, $\hat{H} = H/m_\mathrm{T}$. [J/kg]
i_0	Impedance current density amplitude. [C/m$^2 \cdot$s]
$\vec{i}$	Current density, see equation 3.91. [C/m$^2 \cdot$s]
$\vec{\vec{I}}$	Identity tensor. [unitless]
$\vec{J}_i$	Excess molar flux of species i relative to the mass-average velocity, defined in equation 3.106. [mol/m$^2 \cdot$s]
$\vec{J}_i^{\psi}$	Excess molar flux of species i relative to $\vec{v}^{\psi}$, defined in equation 3.100. [mol/m$^2 \cdot$s]
K	Bulk modulus (or inverse isothermal compressibility), defined by equation 3.32. [Pa]
K_{ij}	Drag coefficients between species i and j, defined in equation 3.136. [N$\cdot$s/m^4]
$\hat{K}$	Specific kinetic energy associated with bulk flow, defined by equation 3.116. [J/kg]
L	Electrolyte thickness, distance between electrodes. [m]
m_i	Ratio of the molar mass of species i to that of the electrolyte e. [unitless]
m_T	Total mass, defined in equation 3.79. [kg]
$\overline{m}$	Total molar mass, see equation 3.81. [kg/mol]
$\overline{m}_i$	Molar mass of species i, see equation 3.79 *et seq.* [kg/mol]
Ma_D	Diffusion Mach number, see equation 4.51. [unitless]
Ma_M	Maxwell Mach number, see equation 4.60. [unitless]
n	Number of chemically distinct constituents comprising a material. [unitless]
n_i	Molar content of species i. [mol]
n_T	Total molar content; see equation 3.13. [mol]
$\vec{N}_i$	Total molar flux of species i relative to an inertial frame. [mol/m$^2 \cdot$s]
p	External pressure, related to Cauchy stress through $p = \frac{1}{3}\mathrm{tr}(\vec{\vec{\sigma}})$ and equation 3.2. [Pa]
p_dy	Spherical part of dynamic pressure, attributed to bulk viscosity effects. [Pa]
P	Scaled pressure. [unitless]
Pe^{ψ}	Scaled ψ-average velocity, formulated as Peclet numbers. [unitless]
$\vec{q}$	Heat flux (or excess heat flux relative to $\vec{v}$), introduced in equation 3.115. [J/m$^2 \cdot$s]
$\vec{q}'$	Irreversible heat flux (or excess heat flux relative to $\vec{v}^h$), defined by equation 3.124. [J/m$^2 \cdot$s]
$\vec{\vec{Q}}_A$	Rigid rotation that throws a tensor $\vec{\vec{A}}$ into its principal coordinates, see equation 3.5 for $\vec{\vec{Q}}_\tau$. [unitless]
R	Universal gas constant, 8.314 J/mol$\cdot$K
R_i	Generation rate of species i. [mol/m^3/s]
s_i	Stoichiometric coefficient of species i. [unitless]
S	System entropy, related to G through the Maxwell relation 3.17. [J/K]
$\overline{S}$	Molar entropy, $\overline{S} = S/n_\mathrm{T}$. [J/mol$\cdot$K]
$\hat{S}$	Specific entropy, $\hat{S} = S/m_\mathrm{T}$. [J/kg$\cdot$K]
$\overline{S}_i$	Partial molar entropy of species i, see equation 3.52. [J/mol$\cdot$K]
$\mathrm{Sc}_\mathrm{shear}$	Schmidt number based on shear viscosity, see equation 4.57. [unitless]
$\mathrm{Sc}_\mathrm{bulk}$	Schmidt number based on bulk viscosity. [unitless]
$\vec{t}$	Surface traction vector, $\vec{t} = -\vec{e}_\mathrm{n} \cdot \vec{\vec{\sigma}}$. [Pa]
t_A	Characteristic acoustic time, for corresponding frequency f_A see equation 4.73. [s]
t_D	Characteristic diffusion time, for corresponding frequency f_D see equation 4.72. [s]
t_M	Characteristic Maxwell time, for corresponding frequency f_M see equation 4.74. [s]

t_+^0	Transference number of cations with reference to the solvent. [unitless]
t_{bulk}	Bulk stress relaxation time [$= \mu_{\text{bulk}}/K$]. [s]
t_{shear}	Shear stress relaxation time [$= \mu_{\text{shear}}/G_{\text{shear}}$]. [s]
T	Absolute temperature. [K]
U	Internal energy, see equation 3.77. [J]
$\hat{U}$	Specific internal energy, see equation 3.82. [J/kg]
$\overline{U}$	Partial molar internal energy, see equation 3.82. [J/mol]
$\vec{v}$	Mass-average velocity, see equation 3.95. [m/s]
$\vec{v}^{\square}$	Volume-average velocity, see equation 3.88. [m/s]
$\vec{v}^{h}$	Enthalpy-average velocity. [m/s]
$\vec{v}^{\psi}$	ψ-average velocity, where ψ could be mass, mole, or volume fraction, see equation 3.101. [m/s]
$\vec{v}_i$	Velocity of species i, related to flux through equation 3.87. [m/s]
V	System volume, obtained from G *via* equation 3.17; $V = \frac{1}{3}\text{tr}(\vec{\vec{V}})$. [m^3]
$\hat{V}$	Specific volume, $\hat{V} = V/m_{\text{T}}$; relates to mass density through $\hat{V} = 1/\rho$. [m^3/kg]
$\overline{V}$	Molar volume, $\overline{V} = V/n_{\text{T}}$; relates to c_{T} through $\overline{V} = 1/c_{\text{T}}$. [m^3/mol]
$\overline{V}_i$	Partial molar volume of species i, see equation 3.26. [m^3/mol]
$\vec{\vec{V}}$	Volume tensor, introduced in equation 3.1. [m^3]
$\vec{\vec{V}}'$	Deformation volume tensor, defined by equation 3.3; $\text{tr}(\vec{\vec{V}}') = 0$. [m^3]
$\overline{\vec{\vec{V}}}_i'$	Partial molar deformation volume tensor for chemical species i, defined by 3.51. [m^3/mol]
$\{V_1', V_2', V_3'\}$	Principal values of $\vec{\vec{V}}'$; $V_3' = -(V_1' + V_2')$. [m^3]
W	Frequency scale, $W\left(= \Omega \text{Ma}_{\text{D}}^{\infty}/\sqrt{3}\right) \sim \mathcal{O}(1)$. [unitless]
X	Dimensionless position variable, fractional membrane thickness, see equation 4.44. [unitless]
$\tilde{X}$	Space variable for the left composition boundary layer, $\tilde{X} = \sqrt{\Omega}X$. [unitless]
$\hat{X}$	Space variable for the right composition boundary layer, $\hat{X} = \sqrt{\Omega}(X-1)$. [unitless]
y_i	Particle fraction of species i, defined by equation 3.14, constrained by equation 3.15. [unitless]
z_i	Equivalent charge carried by species i.[equivalent/mol]
Z	Area-specific impedance, see equation 4.75. [$\Omega \cdot \text{m}^2$]
Z_b	Ohmic overpotential contribution to area-specific impedance, see equation 4.76. [$\Omega \cdot \text{m}^2$]
Z_y	Composition overpotential contribution to area-specific impedance, see equation 4.77. [$\Omega \cdot \text{m}^2$]
Z_p	Pressure overpotential contribution to area-specific impedance, see equation 4.78. [$\Omega \cdot \text{m}^2$]

Greek

α	Transport coefficient for Nafion, see table 4.1. [$\mathrm{mol}^2/\mathrm{J}\cdot\mathrm{m}\cdot\mathrm{s}$]
α_{D_i}	Volumetric coefficient of thermal deformation, see equation 3.38; index i refers to τ_1 or τ_2. [1/K]
α_V	Volumetric coefficient of thermal expansion, defined in equation 3.32. [1/K]
$\vec{\mathrm{A}}'_D$	Thermal deformation tensor, defined in equation 3.50. [1/K]
β	Dimensionless group in the scaled transport model, see equation 4.61. [unitless]
ϵ_g	Global volumetric strain, see equation 5.11. [unitless]
$\vec{\bar{\epsilon}}'$	Deviatoric Eulerian strain tensor, defined by equation 3.11. [unitless]
$\vec{\bar{\dot{\epsilon}}}$	Rate-of-deformation tensor, defined by equation 3.120. [1/s]
η_k	Scaled molar flux of species k. [unitless]
θ_T	Scaled total concentration. [unitless]
I	Scaled current density. [unitless]
κ	Ionic conductivity of the electrolyte, see table 4.1. [S/m]
K	Scaled ionic conductivity. [unitless]
λ	Water content of Nafion $\lambda = n_{\mathrm{H_2O}}/n_{\mathrm{SO}_3^-}$. [unitless]
λ_{y_0}	Activity coefficient of the solvent on a mole-fraction basis, see equation 4.16. [unitless]
μ_bulk	Effective bulk viscosity of the system, see equation 3.140. [$\mathrm{Pa}\cdot\mathrm{s}$]
μ_shear	Effective shear viscosity of the system, see equation 3.141. [$\mathrm{Pa}\cdot\mathrm{s}$]
μ_i	Electrochemical potential of species i, defined by equation 3.19. [J/mol]
ν_i	Number of entities of species i in a formula unit of a compound, total entities $\nu = \sum_k \nu_k$. [unitless]
ν_PR	Poisson's ratio, see equation 4.43. [unitless]
ξ	Electroosmotic coefficient for Nafion, see table 4.1. [unitless]
ξ_coup	Coupling damping coefficient, see equation 4.88. [unitless]
ξ_visc	Viscous damping coefficient, see equation 4.89. [unitless]
$\xi^*_\mathrm{visc,elas}$	Viscoelastic damping coefficient, see equation 4.90. [unitless]
$\vec{\bar{\Xi}}$	Diffusion stress tensor, defined in equation 3.113. [Pa]
ρ	Mass density, defined in equation 3.80; relates to specific volume through $\rho = 1/\hat{V}$. [$\mathrm{kg/m^3}$]
ρ_i	Mass density of species i, defined by equation 3.93. [$\mathrm{kg/m^3}$]
ρ_e	Excess charge density, defined by equation 3.90. [$\mathrm{C/m^3}$]
$\vec{\bar{\sigma}}$	Cauchy stress tensor, see equation 3.1. [Pa]
$\vec{\bar{\sigma}}_\mathrm{t}$	Total stress tensor, see equation 3.109. [Pa]
$\vec{\bar{\sigma}}_\mathrm{dy}$	Dynamic stress tensor, see equation 3.110. [Pa]
$\vec{\bar{\tau}}$	Deformation stress, defined by equation 3.2. [Pa]
$\{\tau_1, \tau_2, \tau_3\}$	Principal deformation stresses, identified by diagonalizing $\vec{\bar{\tau}}$ with a rigid rotation; only two are independent, since $\tau_3 = -(\tau_1 + \tau_2)$. [Pa]
ϕ_i	Volume fraction occupied by species i, $\phi_i = \overline{V}_i c_\mathrm{T} y_i$, , constrained by $\sum_i \phi_i = 1$. [unitless]
ϕ	Scaled voltage. [unitless]
Φ	Electric Potential. [$\mathrm{J}\cdot\mathrm{C}^{-1}$]
φ	Scaled density. [unitless]
χ	Darken's thermodynamic factor, see equation 4.18. [unitless]
ψ	Symbol representing the fractional basis for $\vec{v}^\psi$.
ψ_i	Fractional variable associated with species i; constrained such that $\sum_i \psi_i = 1$. [unitless]
ω_i	Mass fraction of species i, defined in equation 3.94, constrained by $\sum_i \omega_i = 1$. [unitless]
ω	Angular frequency of the sinusoidal impedance current. [rad/s]
Ω	Scaled angular frequency, see equation 4.45. [rad]

Abbreviations

AC	Alternating current
EIS	Electrochemical impedance spectroscopy
EOS	Equation of state
LE	Liquid equilibrated
MEA	Membrane/electrode assembly
OSM	Onsager–Stefan–Maxwell
PEM	Polymer electrolyte membrane
RH	Relative humidity
VE	Vapour equilibrated

Subscript

$_0$	Solvent/neutral species, water in the case of hydrated Nafion.
$_+$	Cationic species in the electrolyte, protons in the case of hydrated Nafion.
$_-$	Anionic species in the electrolyte, stationary sulphonic acid sites in the case of hydrated Nafion.
$_e$	Neutral electrolyte salt/membrane.
$_{elas}$	Pertaining to the elastic medium.
$_{visc}$	Pertaining to the viscous medium.
$_{visc,elas}$	Pertaining to the viscoelastic medium.

Superscript

^{ref}	Quantity in the reference state; for Nafion, dry membrane is chosen as the reference state.
$^{\infty}$	Zero-order or steady-state value of a parameter; for EIS analysis, a steady-state of no-bias was chosen.
$^{(1)}$	First-order value of a parameter, obtained by a regular perturbation of the transport model.
$^{\square}$	Referring to a volume-average quantity.
^{h}	Referring to an enthalpy-average quantity.

Acknowledgements

Prof. Charles Monroe has been the involved, generous, and insightful supervisor, as well as the inspiring teacher I had hoped for in my D.Phil. journey. What came as a surprise was the research ethic he was able to instil in me, inconspicuously—one punctuation character at a time. His appreciation of the giants of science, unrelenting determination for doing things rigorously, and unwavering optimism to see a solution through are invaluable lessons that have shaped me as a researcher. I would like to thank Prof. Monroe for giving me freedom and guidance as necessary and helping me find some of the philosophy in the D.Phil.

I am grateful to the Monroe group for contributing to my everyday growth as a researcher, and for making it worthwhile to stay on course this occasionally uphill ride, specific shout-outs to: Jing for being ever willing to help; James for always being encouraging; Saber for his generosity and positivity; Howie for helping me find the humour on the worst days; Guanchen for being an effective sounding board; Kirk for putting up with the incessant ageist jokes; Andrew for reminding me to be a little less jaded; and Trishna (an honourary member) for being a much needed girlfriend. It is mostly because of the group members with experimental backgrounds that I have been able to step out of my theory bubble. I should also thank Valentin Sulzer from Math for helping me navigate the math-heavy parts of the impedance modelling project.

I would like to extend my gratitude towards the US Department of Energy, the Department of Engineering Science at Oxford, and the Faraday Institution for the financial support.

The move to Oxford from Michigan was bitter-sweet because of the family of friends I was leaving behind. The bonds I formed with Avan, Prao, Priyanka, Anadi, Sameer, Mohit, Mi, Dits, Koko, Sidd, and KP will continue to be life-long friendships. I was fortunate, however, to find a new family in Oxford: Amogh's amazing listening and Sambar skills, Usha's thoughtfulness and general omniscience, Abhilasha's idealism and unconditional love for food, Neeraj's level-headedness and appreciation of BoJack, Vitor's bear hugs and great Jazz recommendations, and Huma's unconditional support as well as great taste in poetry, books, and bad Bollywood movies have made many a dreary Oxford day brighter. Special thanks to Bhanu and Koushik for making me feel like I was home whenever it was most needed.

I can not thank my parents enough for their silent strength and unflinching belief, for having the courage to let me make my own mistakes and become my own person, and most of all for leading by example to "*Let your dreams be bigger than your fears...*" —M Scott Peck.

My husband, Bhavya, has been the solid ground beneath my feet through the vagaries of this journey. Among other countless things, I should thank him for inspiring me to be the best version of myself, and most of all for being my 2am friend, even if it's because of our different time-zones.

Chapter 1

Non-Isobaric Transport: Case Study for Nafion

1.1 Transport Modelling in Electrolytes

Modelling of transport in electrolytes has been a valuable tool to understand and address issues related to the functioning of electrochemical devices. Transport models not only aid in refining device design for improved performance, but may also be used to explore unfamiliar phenomena—achieving both these goals at far lower costs than experiments. A basic example demonstrating the efficacy of this approach is provided within the context of Li-ion-battery systems; electrolyte physics controls the limiting current, which informs design parameters and operational limits.

Transport modelling has also been beneficially applied to electrolytes within fuel cells, electrolysers *etc.* In 1965, Newman, Bennion, and Tobias [1] published a transport model for concentrated binary electrolytes, replacing the traditionally used Nernst–Planck dilute-solution theory. The rigour of concentrated-solution theory owes to its grounding in classical equilibrium thermodynamics as well as in irreversible thermodynamics through the Onsager–Stefan–Maxwell (OSM) transport formalism. OSM diffusion driving forces emerge from a Gibbs–Duhem relation among intensive-

property gradients; the fluxes conjugate to the OSM forces are identified by analysing the irreversible energy dissipation associated with dynamic processes [6, 7].

Newman's theory is parameterised by familiar equilibrium material properties, which depend on the same basis of intensive variables needed to specify an equilibrium state in classical thermodynamics. More specifically, properties such as volumetric heat capacity, isothermal compressibility, and molar volume appearing in Newman's theory can all in principle be extracted from isolated measurements of macroscopic systems at fixed composition and ambient conditions (temperature, pressure, *etc.*).

When applied to materials wherein properties vary locally, Newman's theory incorporates two assumptions of 'microscopic equilibrium'. First, the material properties in non-uniform dynamical systems are taken to depend pointwise on the instantaneous local values of the thermodynamic basis variables. Second, the local property dependences are assumed to identify with those observed for uniform, macroscopically equilibrated systems. These continuum-level hypotheses agree with those Onsager expressed when deriving his reciprocal relation [7].

Transport properties in Newman's theory have explicit roots in nonequilbrium statistical mechanics. Irreversible thermodynamics as deployed by Newman connects to microscopic statistics through fluctuation theory, which is supported by a regression hypothesis developed in broad strokes by Onsager, and more practically by Casimir [6, 8]. When applied to the OSM multicomponent diffusion model, fluctuation theory not only proves a symmetric reciprocal relation among the transport coefficients, but also justifies a statement that the transport coefficients depend on the same basis of thermodynamic state variables as the equilibrium material properties [9]. Wheeler and Newman have also drawn these conclusions without an overt regression hypothesis, from a nonequilibrium statistical-mechanical approach based on the fluctuation-dissipation theorem and Nyquist–Johnson linear-response theory [10, 11].

Fifty years later, the community still relies heavily on Newman's 'concentrated-solution theory', or variations thereof [12–21], since it provides one of the most general and thermodynamically rigorous continuum-scale frameworks for understanding transport phenomena and their relationship with performance for electrochemical systems. Some time ago Newman extended concentrated-solution theory to include thermoelectric effects when temperature, as well as composition, varies locally [22]. Monroe and Delacourt recently reported an extension for systems where local electroneutrality is violated [23], which also formalised the algorithm Newman used to develop flux-explicit transport laws for binary electrolytes in his seminal textbook [24] and extended it to multicomponent situations.

In response to a simplification made in the landmark battery model of Doyle, Fuller, and Newman [25, 26], Liu and Monroe studied phenomena arising from considering the variation of an electrolyte's density with respect to its local composition [27, 28]. They found that application of density's dependence on composition as a local constraint can substantially affect transport, particularly when electrolytes are non-aqueous.

Although concentrated-solution theory is highly developed, it has been applied primarily to liquid electrolytes. Many electrochemical devices, such as polymer-electrolyte fuel cells, solid-oxide fuel cells, and all-solid Li batteries, instead employ (or seek to employ) solid electrolytes of different kinds. Such solids include polymer membranes and ion-conductive ceramics [29–37]. Solid electrolytes, in addition to being leak-proof, offer higher thermal and mechanical stability, and consequent increased flexibility in cell design. On-going research on solid lithium-conducting electrolytes strives to make them have similar—if not higher—ionic conductivities to those of state-of-the-art liquid electrolytes [38].

Rather than starting from scratch, it is reasonable to adapt the well-established liquid-phase ion transport theory for modelling solids. A vital point of difference between liquid and solid electrolytes is that the latter can sustain deformation at equilibrium, which can arise either from externally imposed constraints or from changes that occur within the cell as it operates. This additional form of available energy can alter the macroscopic dynamical behaviour of solid electrolytes, necessitating modifications of the transport model to reflect the change. It would be useful to handle deformation or strain energy (more broadly, stress), in a local way, while also addressing the coupling that potentially exists between mass and momentum transport.

Various models of diffusive, electrochemical, and mechanical phenomena have been developed independently, often without acknowledging or intending that interplay between the phenomena might be significant in some systems. The main challenge when attempting to realise a general coupled transport model is, therefore, maintaining thermodynamic, kinematic, and dynamic consistency while amalgamating different aspects of electrolyte behaviour. An over-arching aim of this thesis is to identify a process for developing versatile frameworks for electrolytic transport modelling that only require minimal system-specific modifications for diverse applications.

A transport model applicable to solid electrolytes is formulated by laying down the fundamental balances and equations of state that augment concentrated-solution theory to include local pressure and deformation stress. The proposed model is then employed to identify transport constitutive laws applicable to elastic, ionically conductive electrolytic media such as ceramic electrolytes or swollen polymer gels. The remainder of this chapter justifies the choice of Nafion membranes as a case study, motivating the development of transport models for non-isobaric conditions where mechanical effects take centre-stage.

1.2 Electrochemical/Mechanical Coupling: Nafion

Polymer-electrolyte-membrane (PEM) fuel cells have been the focus of concerted research efforts over most of the last half-century, which have resulted in tremendous technological development. Although they are on the brink of commercial viability today, some issues related to water management in and durability of PEM fuel cells remain to be resolved [39]. The US Department of Energy report of 2013 published a target durability of 5000 hours for fuel cell stacks used in automotive applications; at the time the highest achieved durability was ~2500 hours, which was only half way to the target. The issues of water management and durability both relate to properties of the PEM most commonly used in these fuel cells—Nafion. It belongs to a class of polymers called ionomers, in which the polymeric repeat units end in ionic moieties. The ionised units lend ionomers unique functional characteristics, such as permselectivity, that make them suitable for a vast range of uses: as transport media, sensors, actuators, and components of biomedical devices [40–43]. Thus, the applications of ionomer research extend far beyond fuel-cell technology.

A cation-exchange membrane, Nafion has a regular comb structure comprising a hydrophobic Teflon (poly-tetrafluoroethylene) backbone, punctuated by pendant chains of perfluorovinylether that terminate in hydrophilic sulphonic-acid endgroups, as depicted in Figure 1.1.

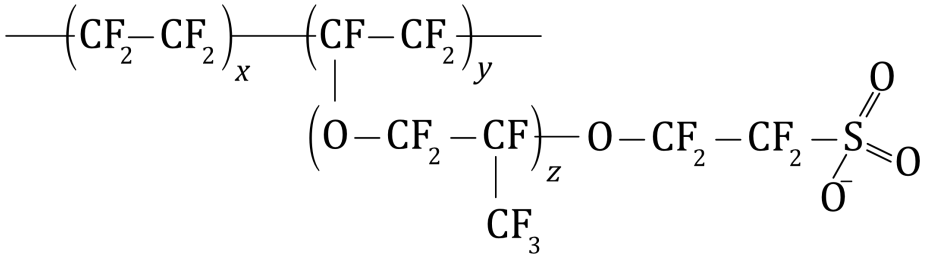

Figure 1.1: Chemical structure of Nafion

Definitive details of hydrated Nafion microstructure have proved elusive owing to its tendency to arrange into tertiary structures when permeated by a solvent. Hydrated Nafion segregates in to at least three interior microstructural phases [44, 45], which can reorganise upon increased water sorption: polymer domains, with a low degree of crystallinity; ionic clusters formed of hydrated sulphonic acid groups; and a second ionic domain with lower water content. The sensitivity of Nafion's structure to external conditions raises challenges specific to the experimental techniques employed to study its morphology. These techniques include small-angle X-ray scattering, electron microscopy, scanning transmission electron microscopy, and atomic force microscopy *etc.* as covered comprehensively in the review by Mauritz and Moore [46]. They proceed to discuss various attempts made to describe the features of dry and hydrated Nafion membranes observed in the experiments by means of structural models, namely the cluster-network model proposed by Gierke and Hsu [47, 48], the intraparticle core-shell model proposed by Fujimura *et al.* [49, 50], Kumar and Pineri's modified hard-sphere model which accounted for interference (Coulombic interactions) between non-interacting spheres [51], and several others.

Despite the debate about microstructure, it is well accepted that Nafion conducts protons only when sufficiently hydrated [52]. The cluster-network model [47, 48], even with its shortcomings, has stood the test of time as a useful starting point for morphology conversations as it explains this hydration-dependent aspect of Nafion's ionic conductivity well. Results of some molecular-dynamics simulations and experiments such as electron microscopy and atomic force microscopy endorse the cluster-network model [46, 53]. The model suggests that water solvates the ionic moieties, which phase-separate from the hydrophobic polymeric backbone into inverted micellar clusters (~4 nm across), further connected by continuously forming and disintegrating short narrow channels (~1 nm), as depicted in Figure 1.2.

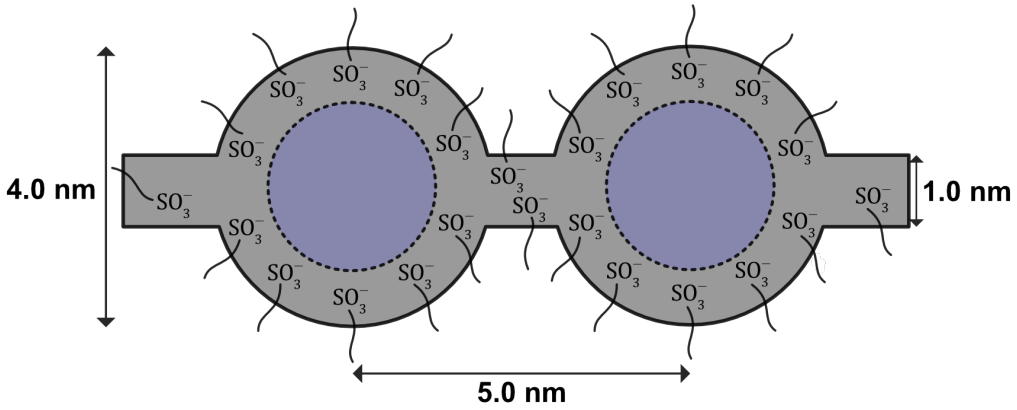

Figure 1.2: Inverted-micellar microstructural depiction of hydrated Nafion ionomers; adapted from Gierke and Hsu's cluster-network model [47, 48]. Grey area represents the double-layer ionic region of the polymeric backbone; purple area represents water clusters that solvate the ionic sites; hydrophilic, cation-conductive channels of partially hydrated sulphonic acid connect the micelles.

Since the sulphonic acid sites on the channel walls are both immobile and negatively charged, the membrane is selective towards cation transport. Ionic conductivity in Nafion is determined by the availability of the hydrophilic ionic clusters embedded in the hydrophobic matrix. As the water content of the membrane increases, the clusters become more connected; this makes it easier for cations to travel from one sulphonic site to another, thereby permitting conduction [54]. Thus, it is necessary to keep the membrane optimally hydrated during fuel-cell operation, and both the hydrogen and the oxygen gas feeds are humidified to ensure sufficient hydration.

Hydrogen ions, while being conducted from the anode to the cathode, also tend to drag their waters of hydration along—a phenomenon referred to as electroosmotic drag [55, 56]. At high current densities, a copious amount of water is dragged away from the anode side of a fuel cell in concordance with the high efflux of hydrogen ions, which can cause it to run dry, dangerously reducing the conductivity. On the other hand, a fuel cell generates water at the cathode as hydrogen ions combine with the incoming oxygen gas. Ironically, if this excess water is allowed to accumulate at the

cathode, it can lead to flooding, where water blocks incoming oxygen from reaching reaction sites. Managing the delicate water balance that keeps membranes hydrated enough to conduct while preventing flooding is essential to smooth functioning of a fuel cell. To devise strategies for performance optimisation, we should first understand the various modes of ionic and water transport, and the driving forces inducing these fluxes, pictorially represented in Figure 1.3. This requirement inspires the study of coupled water and charge transport in PEM fuel cells.

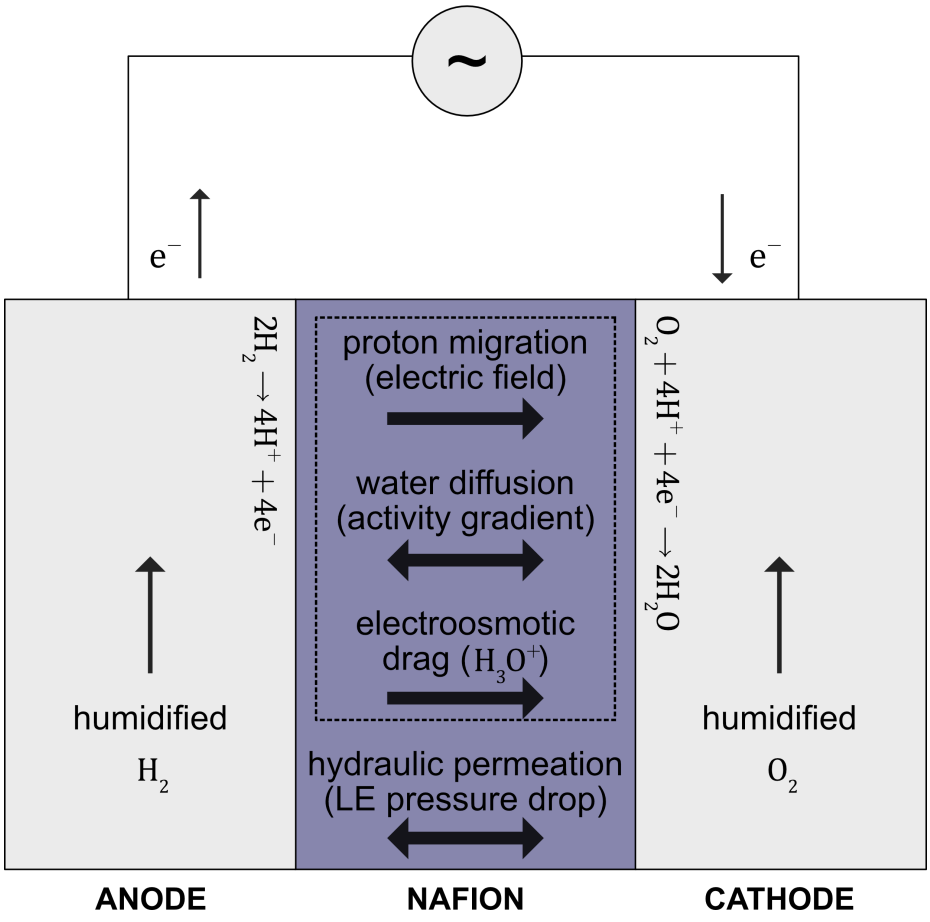

Figure 1.3: Illustration of the various fluxes across a Nafion membrane in a fuel cell environment, relevant to the water management problem; water produced at the cathode may lead to flooding and electroosmotic drag can dehydrate the anode. Adapted from Kumbur and Mench [57].

In addition to the strong and complex dependence of conductivity on hydration, Nafion tends to swell significantly upon water sorption. The swelling strain increases non-linearly with increasing water content. As much as a 74% volume increase has been observed for Nafion membranes equilibrated with liquid water [3]. Modelling this swelling tendency of membranes is an interesting exercise in itself, but it becomes more challenging when one recognizes that a membrane in a fuel-cell environment cannot swell freely.

The membrane/electrode assembly (MEA) is built under pressure to ensure good contact between layers; MEAs may also experience additional forces from clamping of the bipolar plates, external gas pressure, and other sources [58, 59]. There is consequently little scope within a fuel cell to accommodate the volume change of a water-swollen membrane. The interaction between the externally applied forces/constraints and swelling strain can cause stresses to develop across the membrane. Further, changes in the operating conditions such as humidity of the surrounding gases, temperature, external forces *etc.* can lead to a spatially and temporally variable stress profile, contributing to fatigue, mechanical degradation, and the practically observed MEA failure over time. In this way water uptake can also impact the mechanical durability of fuel cell membranes.

Different approaches to solving the issues of managing membrane conductivity and ensuring mechanical stability for long durations have been introduced in the past. However, a new dimension is added to the problem because of the plausibility of a two-way coupling between the stress gradients accounting for momentum transport and the mass transport of ions and water across the membrane. Understanding this diffusive/mechanical interplay could therefore help to better elucidate the performance and durability of PEM fuel cells.

1.3 Scope of the Thesis

By virtue of Nafion being an interesting and complex material, morphologically and functionally, as well as due to the lofty ideal of formulating a generalised non-isobaric transport model based solely on thermodynamic principles, the scope of this thesis becomes both wide and deep.

Chapter 2 provides a brief overview of ionic and water transport modelling in Nafion. This exercise provides background and a common language by which to illustrate the thought processes involved in the theoretical development of thermodynamically consistent coupled electrochemical/mechanical models. Literature abounds with countless studies on various aspects of this complex material, ranging from controversial morphological claims to its piezoelectric properties that may render Nafion suitable for sensor-actuator applications. The review section touches upon the most relevant of these studies, to afford us an informed starting point along with a reasonable and meaningful scope of study. Each section in the review chapter concludes with insights that systematically form the building blocks for our transport model.

Chapter 3 is the crux of the thesis, where the non-isobaric transport model for a viscoelastic electrolyte is developed. Starting from the fundamentals of classical thermodynamics, strain energy is built in to the first law along with compressive mechanical work. This contribution induces stress-driven components into the diffusion of water and cations. Further, overall mass, momentum, and energy balances are developed from species balances to ensure there is no double counting across phenomena. One of the highlights is the entropy generation law, which accounts for all the dissipative processes: mass diffusion, thermal conduction, and deformative momentum transport (usually viscous dissipation, although this could also include plastic or creep friction). The chapter ends with a statement of consistent mass and momen-

tum flux laws based on the entropy-generation expression, following the irreversible thermodynamics of Onsager.

Chapter 4 applies the non-isobaric transport model to analyse electrochemical impedance spectroscopy of hydrated Nafion. Since an alternating current acts as a linear perturbation to the electrolyte at equilibrium, all the second- or higher-order effects drop out, simplifying analysis of the coupled transport model to a great extent. This application is novel in its scope because the impedance signatures of mechanical effects have not been studied before in the context of electrolytic transport models. Additionally, impedance analysis in the frequency domain aids understanding, because it segregates physical processes based on their characteristic times. The dynamics of momentum change is expected to relax over a very short duration, which usually makes it irrelevant in the steady-state scenario; impedance becomes a tool to identify the time scale and nature of this relaxation. Impedance signatures of three special cases—Hookean-elastic, Newtonian-liquid, and isotropic-viscoelastic materials—are explored and analysed. Additionally, a parameter study allows this analysis to go beyond Nafion, to understand how electrochemical/mechanical coupling could be made more prominent and valuable for novel materials and applications.

Chapter 5 explores the steady-state case which approximates the low-frequency behaviour of the model. The simple case with uniform pressure (could be different from ambient) is explored as it offers the advantage of an analytically accessible solution. Chapter 6 casts a critical look back at the theory, model, and results presented in the thesis. In doing so, it returns to the salient features we wanted to build into the model, as delineated in Chapter 2. Although the thesis tries to enforce thermodynamic consistency for transport models with electrochemical/mechanical coupling, and this work is complete in itself, there are many more aspects of modelling transport in Nafion that remain to be explored.

Chapter 2

State of Nafion Modelling: A Review

A broad, deep review of perfluorosulphonic acid membranes, such as Nafion, was recently carried out by Weber and Kusoglu [42]; it was not only comprehensive but also insightful given the expertise both authors bring with them. This chapter does not intend to give a similarly complete historical account of models that describe Nafion-like membranes. Instead, we discuss a few models representative of the dominant ideologies regarding ionomer transport. A literature review makes it clear that transport modelling in Nafion has been a topic of contention for several decades. Numerous approaches have been proposed, tested, and revised over time. It is therefore surprising that the prime challenge in developing a transport model for Nafion still lies in rooting the system in thermodynamic first principles to maintain overall consistency, while ensuring that the model spans the entire space of physical and operational constraints. Reiterating for clarity: the focus of this work is to incorporate the coupling between electrochemical transport and mechanical facets of transport in Nafion-like (or other solid) electrolytes in the most rigorous way possible.

The first distinction typically made at the outset of transport-model formulation for Nafion is whether the membrane is exposed to humidified gas or to liquid water.

Gierke and Hsu's structural (cluster-network) model [47, 48] informs the qualitative transport mechanisms in Nafion proposed by Weber and Newman [54, 55] and by Kumbur and Mench [57]. As discussed in the context of ionic conductivity, cluster-network models argue that when the membrane is exposed to water vapour (a vapour equilibrated, or VE, state), absorbed water molecules bind to the ionic moieties within it, forming clusters that are connected by narrow collapsed hydrophilic channels that permit molecular diffusion of water and hydrogen ions. When ambient water vapour is replaced with liquid water (a liquid equilibrated, or LE, state), surface tension may push the collapsed channels open to form pore structures. The LE membrane consequently behaves as a medium that is porous, through which water can flow as a liquid.

The broadest classification of transport models divides them into *macroscopic*—based on macroscopic colligative properties observable at the continuum scale, and *microscopic*—reliant on molecular-scale microstructural information. Although our model falls under the macroscopic classification, ionomer morphology still must form its bedrock; the features that make Nafion interesting (permselectivity, propensity for water uptake), the characteristics which make it challenging to use and model (swelling/deformation tendencies), and the physical properties which govern its macroscopic behaviour (stress/strain behaviour, solvent uptake) all hinge on the energetic description of phase-separated hydrated ionic nanodomains dispersed across a semi-crystalline polymer matrix.

There are many examples of how microstructural explorations have stumbled upon phenomena relevant to meso/macroscale phenomena [46]. Many studies reported a disparity between microscopic swelling (dimension change of the ionic clusters) and macroscopic swelling (change in the observable dimensions of the membrane), a phenomenon commonly referred to as *non-affine swelling*. An inherent anisotropy within

the membrane induced by the extrusion process was identified. Equilibrium solvent-uptake isotherms were improved by recognising residual water (hysteresis), bound water (first-solvation-shell), and free water (electroosmotic drag) as distinct. *Schröder's paradox*—the observation that Nafion's equilibrium water uptake is different when exposed to saturated vapour or liquid, despite water's identical activity in these two states—can be resolved by considering that a very slow structural reorganisation within the membrane is required to achieve true equilibrium in a vapour-equilibrated state.

2.1 Equilibrium Water Uptake and Swelling

The primary aim of a transport model is to relate the mass, momentum, and energy fluxes through a system to the spatial and temporal distributions of a basis of intensive variables that define its local state such as pressure, temperature, and composition (most commonly). In addition to balance equations and flux laws, this requires defining equations of state, which describe microscopic equilibrium conditions. This section brings into focus a specific equation of state (EOS), which governs the equilibrium solvent uptake by a membrane upon exposure to various ambient humidities, temperatures *etc.* Thermodynamic models developed for this purpose apply solely to equilibrium, providing no information regarding the impact of the rate of solvent sorption. The general principle of the model is based on balancing the chemical energy of ionic solvation with the mechanical energy of polymer expansion to accommodate the solvation.

Choi *et al.* [60–64] developed one of the flagship models of equilibrium water uptake. Their model is rooted in the Flory–Huggins theory [65–67], which accounts for the enthalpic and entropic changes when a solvent is mixed with an entangled polymer

network. An extension of this is the Flory–Rehner theory [68, 69], which additionally includes entropic changes due to polymer deformation; this theory suggests that in cross-linked polymers, a maximum swelling state is reached when the osmotic pressure of the solvent in the polymer equals the elastic stretching force exerted by the polymer backbone, such that solvent in the polymer is in chemical equilibrium with the outside solvent. Choi *et al.* further discuss that Nafion remains stable in the presence of a solvent despite not being cross-linked because of the phase separation between the hydrophobic and hydrophilic domains. For the VE case, the swelling pressure in this model comprises capillary pressure at the vapour-liquid interface and the pressure which stretches the polymer matrix.

Different approaches, ranging from nanoscopic to macrosocopic, have been taken to understand the elastic pressure swollen polymers exert. One of the most widely-used of these is Freger's non-affine model [70], because it produces the correct behaviour of swelling pressure in the limit that the membrane is dry and incorporates the shear modulus of the membrane, which is a directly measurable macroscopic parameter. A more general mescoscale framework from Kusoglu *et al.* [71, 72] directly uses the domain spacing as an indication of the deformation, thereby organically taking into account effects of pre-treatments, external constraints, specific chemical nature of the membrane *etc.*

Eikerling *et al.* [73, 74] employed poroelectromechanics to fill in some gaps left by earlier work in predicting accurate sorption isotherms and explaining Schröder's paradox, among other things. Multiple conditions (as opposed to the single one in the thermodynamic approach) arose from the analysis of chemical and mechanical equilibria occurring at a single-pore level. The explicit assumption that pore-like channels are present robbed the model of generality, however, and the set of dependent variables, for instance, the various types of pressure used in different regions of the

pores, did not have thermodynamic clarity. Although the analysis was first carried out at a microscopic level, it was later extended to a macroscopic scale through consideration of pore-ensemble effects. The authors maintained that it was important to know the microstructural properties of the membrane very accurately to expect a quantitative agreement with experimental data. A central idea proposed by this paper is that the "internal driving forces for water fluxes and external conditions should be clearly distinguished."

The scope of our transport model is tangential to the models above, because by nature it describes non-equilibrium processes; our development will, however, require thermodynamic laws that accurately describe local equilibrium conditions. Sorption isotherms, which provide information on how the water content in the membrane varies in response to ambient water activity, could feed into the transport model through a thermodynamic factor that accounts for solution non-ideality, and in some cases through partition coefficients that determine absorbed water content at the boundaries.

In summary, a survey of work on water uptake supports the following observations:

- A thermodynamic basis should be preferred over a phenomenological one, to ensure first, that no physical constraints are violated, and second, that all model variables and properties have physical definitions that clearly explicate how they can be measured
- A macroscopic model will not account for structural features explicitly, but material- and transport-property variations within the membrane could ideally embody relevant nano/micro/mesoscale dependences, if any

- Given the uncertainty about morphology, an effort should be made to make as few assumptions about the structure of Nafion as possible; the only such differentiation in our model is based on the VE *vs.* LE classification
- The model should have consistency checks in place so that it converges to correct physical limits; for example, it should include parameters that match known values when the membrane is dry

2.2 Transport Models

This section narrows the scope to a particular range of membrane-transport models based on concentrated-solution theory. We borrow some of our knowledge from Weber and Newman's systematic review [75] of macroscopic transport models for PEM fuel cells and add to it a study of the models published since, in the fuel-cell field and beyond. Revisiting this journey opens a window into the evolution of understanding regarding these systems, allowing for a more refined and modular approach to the transport problem.

2.2.1 Single-Phase *vs.* Two-Phase Models

Traditionally, macroscopic transport models developed for Nafion have either been single-phase models, which assume diffusion (driven by a concentration difference) to be the only mode of water transport, or two-phase models, which consider only hydraulic permeation (driven by a pressure difference); both frameworks include migration of charge in response to an electric field. Zawodzinski *et al.* [76, 77], Nguyen *et al.* [78], Fuller and Newman [79], and Meyers and Newman [80–82] treated the membrane as a single phase, wherein water and protons dissolve. Alternatively, Bernardi and Verbrugge [83, 84] and Weber and Newman (LE model) [55] treated the mem-

brane as a two-phase porous medium (fully hydrated membrane), in which hydraulic flow of water is driven by a pressure gradient (according to Schlögl's equation [85] by Bernardi and Verbrugge [83], and a Darcy-type law [86] by Weber and Newman [55]). The two classes of models discussed above are exclusively applicable to strictly VE or strictly LE boundary conditions, and neither describes the full range of operating conditions experienced by a fuel-cell MEA. Weber and Newman [3, 55], therefore, proposed a combined model, which incorporated VE and LE models in parallel, with the fraction of collapsed and expanded channels respectively weighting the VE and LE contributions. Monroe *et al.* [87] and Benziger *et al.* [88] studied steady as well as dynamic water transport in this mode.

2.2.2 Dilute-Solution *vs.* Concentrated-Solution Theory

At the start, many scientists used (and continue to use [89]) Nernst–Planck laws to describe ion diffusion across ionomers, assuming dilute-solution theory to be valid for a fuel-cell environment [90]. It did not take long for others [79, 91] to observe that Nernst–Planck laws needed to be replaced with the more rigorous Stefan–Maxwell flux laws, not only because ions are typically concentrated in Nafion, but also to account for phenomena such as electroosmotic drag, and to mitigate the challenge of assigning the typical solute/solvent roles to water and the polymeric backbone of Nafion.

Pintauro and Bennion paved the way by formulating one of the initial models based on concentrated-solution theory for Nafion [91, 92]. Water flux was found to be driven by gradients in water chemical potential (which drives diffusion) and the ionic current density (which leads to electroosmotic drag). They, along with Fuller and Newman [79], soon followed with a modification of this model in which the electrochemical-potential gradient mass-diffusion driving force was replaced with

a more general force derived from irreversible thermodynamics, following the framework developed by Hirschfelder *et al.* [93] and Bird *et al.* [94]. The general diffusion driving force derives from the Gibbs–Duhem equation, and includes additional forces such as pressure gradients, which are expected to play a role in modelling viscoelastic electrolytes such as Nafion. Despite this added sophistication, a simplification was made by considering that the membrane backbone is the only species that bears all of the mechanical force, even when the membrane is modelled as a single-phase case. Since the validity of the Gibbs–Duhem equation requires linear dependence of the n^{th} species driving force on the $n-1$ remaining, the law describing membrane flux could be excluded from the development, thereby making mechanical forces appear inconsequential for water and proton transport. Fuller and Newman made another interesting observation: this multicomponent diffusion formalism also allows hydrodynamic flow to be accounted for in an LE membrane; no extraneous equations are required to specify how water flows under a pressure gradient, eliminating the need for a momentum balance.

Further, in congruence with Onsager's reciprocal relations [6], it was enforced that for an n-species system, only $n(n-1)/2$ independent transport properties are required to describe diffusion. Traditionally, the three physical properties used to specify transport in the 3-species hydrated-Nafion system [water (0), hydrogen ions (+), and anions embedded in the membrane backbone (–)] are ionic conductivity, electroosmotic coefficient (which replaces cation transference number), and the transport coefficient (which replaces the diffusion coefficient). The force-explicit Stefan–Maxwell laws were inverted into flux-explicit forms using the definitions of these three transport properties.

2.2.3 Treatment of Swelling in Transport Models

Macroscopic models of Nafion can further be classified based on how they treat the swelling phenomenon. Many models, such as those by Nguyen and White [78], and Bernardi and Verbrugge [83], neglect any strain that could arise in a membrane as a consequence of water sorption. Some other groups recognised and incorporated the strain, but in most such models [55, 76, 80] the membrane is taken to swell freely. For instance, Meyers and Newman [80] appended a framework that calculates water-induced swelling onto the Fuller model [79]. They found that it was important to consider swelling in order that the mass of membrane be conserved when going from a dry to a hydrated state.

The extent of swelling may vary spatially as a function of the local water composition, and can, therefore, affect a membrane's local density. This *excluded-volume effect*, defined by Liu and Monroe [27], is depicted in Figure 2.1. When the solute (grey) is replaced by the solvent species (purple), there is a clear change in the sample volume of the solution. The magnitude of this volume change ΔV is a function of the partial molar volumes and composition of all the species, as well as ambient conditions such as pressure.

A majority of transport models, even those based on concentrated-solution theory, ignore the composition dependence of membrane density. This effect has, however, been shown to be significant for liquid electrolytes in which the salt volume fraction is high, and may be similarly important for Nafion, wherein the volume fraction of water can be large. Further, the effect may be especially significant under non-isobaric conditions, where pressure can additionally affect the local volume and density, leading to a momentum flux. In simulations with multiple spatial dimensions, it appears that when a volume-explicit EOS is adopted to describe density, model closure requires

a momentum balance to be carried alongside the material balances [27]; Table 2.1 illustrates this closure conundrum. This begs for an investigation of effects arising from stress, which have not been studied in detail within Newman's theory.

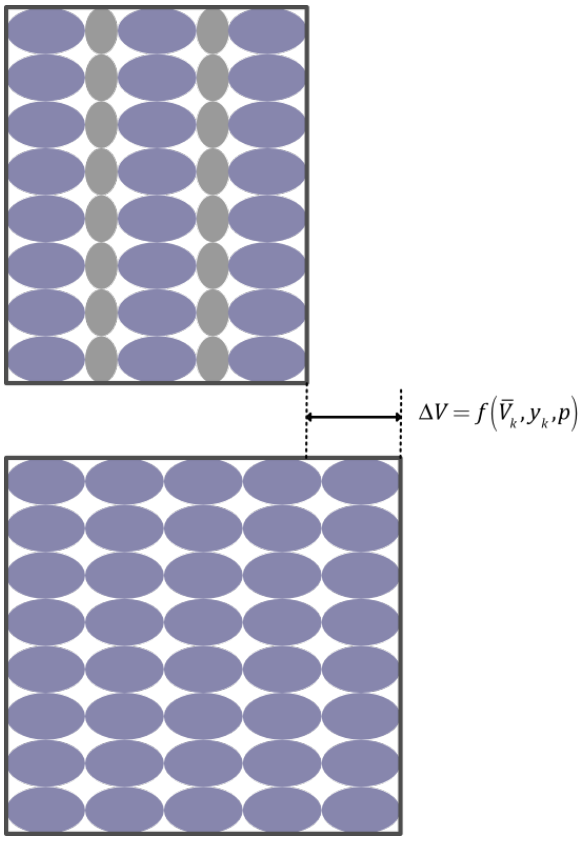

Figure 2.1: Pictorial representation of the excluded-volume effect: density can vary locally as composition changes because solute (grey) and solvent (purple) moieties have different molar volumes.

#	**variables**	#	**governing equations**
1	total concentration	1	equation of state
n	species mole fraction	1	particle-fraction sum
$n-1$	species electrochemical potential	$n-2$	material balance
1	electrical potential	1	volume continuity
d	volume-average velocity	1	charge continuity
d	current density	d	definition of volume-average velocity
nd	species molar flux	d	Faraday's law
		1	electroneutrality
		$n-1$	electrochemical-potential constitutive law
		$(n-1)\,d$	Stefan–Maxwell law
	$nd+2d+2n+1$	$\neq$	$nd+d+2n+2$
1	pressure	d	Cauchy momentum balance
d^2	deviatoric stress	d^2	stress-constitutive law
1	density	1	definition of density
d	mass-average velocity	d	definition of mass-average velcocity
	$d^2+nd+3d+2n+3$	$=$	$d^2+nd+3d+2n+3$

Table 2.1: General model structure for concentrated-solution theory. Recreated from Table 1 in Liu and Monroe [27] for a d-dimensional system comprising n species. The table explicitly lists the dependent variables and equations in the isothermal, isobaric model, and shows that the number of equations and unknowns differs by $d-1$, so the model closure is ensured in $1d$ systems only. Pressure/stress, specified by a momentum balance, and other associated equations need to be included for analyses in higher dimensions to ensure closure.

2.2.4 Consideration of Stresses and Constraints

Weber and Newman [3] were among the first to analyse membrane swelling under imposed physical constraints, doing so by building upon Newman's previous models (Fuller [79] and Meyers [80]). In the Weber–Newman model, a 'degree of constraint' was defined, as the ratio of volume changes under constrained and freely-swelling circumstances. A given degree of constraint can be experimentally realised by either compressing a swollen membrane to remain within a fixed volume (described as 'fully constrained' when this volume is same as the initial) or by applying a given force and then determining the consequent membrane volume ('freely swelling' indicates that there is no externally applied force). The volume strain, available from the degree of constraint and the water content of the membrane, was used to calculate the overall compressive stress in the membrane. The stress in the membrane can, however, be viewed as a consequence of the *local* swelling, rather than the global swelling; a non-uniform swelling profile could cause an uneven stress distribution in the membrane, which Weber and Newman do not consider. Nevertheless, the Weber–Newman model is a good starting point to understand the effects of physical constraints and the subsequent stresses in a swollen membrane.

Figure 2.2 illustrates the concept of local swelling in a membrane. Equally spaced markings on the dry membrane, which is the reference state, help track the local strain, as shown in Figure 2.2(a). If the membrane is exposed to humidified gas on both sides, with higher humidity on the right, the result will be a non-uniform water composition profile, which increases monotonically across the thickness of the membrane. Since this causes the local density to vary, the non-uniform water composition results in an uneven relative displacement of the markings on the membrane, schematised in Figure 2.2(b). Finally, Figure 2.2(c) shows how an external constraint (in this example exerting a compressive force) could further affect the local swelling.

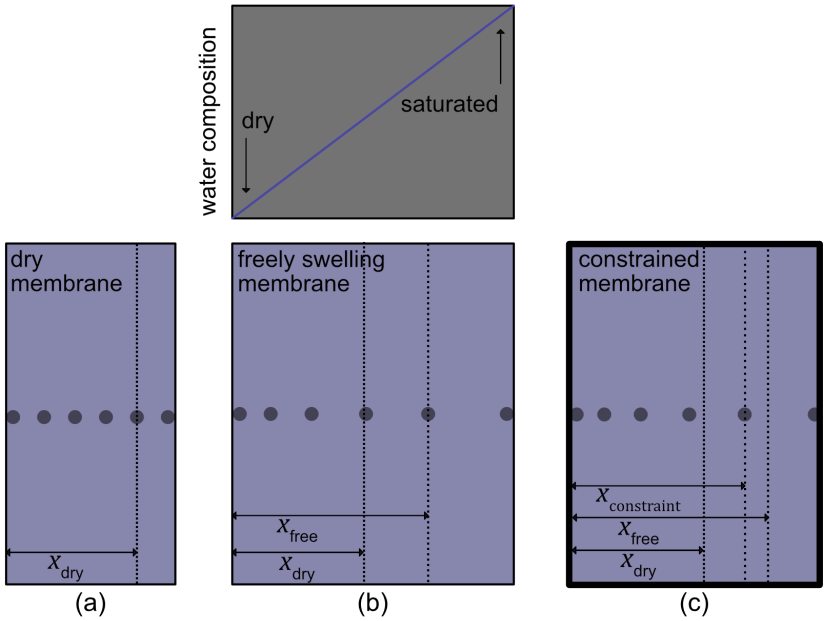

Figure 2.2: Illustration of how local swelling might distribute due to composition gradients and external constraints.

Kusoglu, Kientiz, and Weber [58] devised a way to resolve the multi-scale nature of swelling by marrying the macroscopic-constraint model developed by Weber and Newman [3] with Kusoglu's mechanics-based microscopic swelling model [71]; microscopic swelling was considered to be associated with the solvation of the ionic groups—the *bound water*—and macroscopic swelling with the growth of hydrophilic domains—the *free water*. The authors stressed the importance of considering nanoscale deformations and argued that ignoring them leads to a significantly underestimated water loss on compression.

In his doctoral thesis, Meyers [95] built on the Fuller–Newman model [79], in the context of direct-methanol fuel cells, to further explore the transport of species in a membrane under a pressure gradient by considering carrying a momentum balance alongside the other transport equations. Meyers acknowledged that a membrane such as Nafion may be able to sustain shear stresses in addition to compressive stresses,

but did not distinguish between pressure and normal deformation stress. Further, neglecting the composition dependence of density, as discussed in the previous section, enforces a condition of constant mass-average velocity, making any inertial effects in the momentum balance disappear. Finally, transients in mechanical equilibrium were assumed to be much shorter lived than the transients in concentration profiles, leading to negligible momentum accumulation. These assumptions simplified Meyers' momentum balance greatly, but may not be universally valid.

The most critical consequence of Meyers' simplified momentum balance was the conclusion that any imbalance in external pressure would be compensated by normal stresses exerted by the solid supports on either side of the membrane, leaving the internal membrane pressure a constant. In short, the model arrived at a condition of a quantifiable uniform pressure in the membrane, but at the expense of being unable to include a local pressure gradient to act as a driving force for pressure diffusion or hydraulic permeation (by means of the momentum balance).

In the spatially one-dimensional model developed by Nazarov and Promislow [96], the anode was assumed to be exposed to humidified gas whereas the cathode was exposed to liquid water—conditions which mimic the real operating conditions of a flooded fuel cell, but are not usually accommodated by fuel-cell water management models. They argued that an externally applied pressure would be partitioned between the polymer backbone and the water contained in the hydrophilic domains, making a clear distinction between the two phases. Their description of stresses did not derive from a strong theoretical foundation of thermodynamics or even the theory of elasticity or poroelasticity. The model should be credited, however, for identifying important gaps, such as the vague distinction between elastic and chemical components of total swelling, and the ambiguity in how these swelling modes are affected by external pressure.

2.2.5 Beyond Fuel Cells

Outside of the PEM fuel-cell field, Nafion has been observed to be a good choice for piezoelectric actuators, because it deforms under relatively small electric fields (of the order of 10 V/mm) and is mechanically robust over a sufficiently large number of cycles [40]. To describe Nafion's piezoelectric behaviour, Doi *et al.* [41, 97–100] developed a 3-dimensional macroscopic 'electrostress diffusion coupling' model, which can handle transient cases with mechanical constraints and externally applied forces on membranes. This model accounts for both hydraulic and electroosmotic fluxes but the coupling between the two is empirical/arbitrary.

In Doi's model [41, 97–100], the diffusion laws were based on dilute-solution theory, ionic concentration was assumed to be constant throughout the membrane, and the coupling between different transport modes was not based on a careful analysis of irreversible energy dissipation. Stress, however, was handled very convincingly, *via* a rigorous momentum balance and constitutive laws rooted in linear-elasticity theory. The authors believed that the model was able to predict correct dynamic behaviour because it included the mechanical coupling between solvent diffusion and polymer network stress, something not accounted for by most other models. Overall, the Doi model is useful for its approach to the mechanical part of the analysis, which can be used to complement an augmented concentrated-solution theory.

Olivier Coussy's work [101, 102] focused on porous solids, specifically in the context of soils, but the general principles developed in his analysis were explicitly derived in a thermodynamically consistent manner, by including the strain energy component for available energy. Coussy's development of poroelasticity theory can also be used as a building block for an LE transport model. The stress in Coussy's model is partitioned between the pore domains and the backbone, according to their respective

volume fractions, under an assumption that pore pressure is constant throughout the membrane. Coussy next employed the effective stress principle, a well-known tenet in the field of soil mechanics, which states that only the excess of stress over pore pressure causes deformation of the solid. Although this further simplifies stress partitioning, it requires an assumption that the solid in question is almost incompressible; this holds in the case of soils but is not valid for many other porous solids—an issue addressed in Coussy's own book [103]. The linear poroelasticity theory has been extended to describe large deformations, for applications in biomechanics and geomechanics, by replacing the theory of linear elasticity for the solid with Hencky's nonlinear elasticity by MacMinn *et al.* [104].

After reviewing the salient features of extant transport models and systematically laying out the assumptions made, both implicit and explicit, we identified a few functions and characteristics that an improved model should have:

- The scope of our model will be limited to vapour-equilibrated modes, a restriction that allows Nafion to be treated as a single phase, with possibly non-uniform internal distributions of mass, momentum, and energy
- The model should be based in concentrated-solution theory, incorporating a generalised diffusion driving force similar to the one developed by Hirschfelder, Curtiss, and Bird [93], but revisited for the case of a viscoelastic polymer capable of storing strain energy at equilibrium
- The model should be macroscopic, but swelling and stresses should be recognised as locally variable quantities; it is critical to include local relationships that establish how water content and stresses define swelling and deformation

- A local momentum balance with carefully considered boundary conditions should be included
- A distinction should be made between *spherical stress* or pressure (which causes volume change, preserving shape) and *deviatoric stress*, such as a viscous or elastic stress (which causes shape change, preserving volume)

2.3 Mechanical Behaviour of Nafion

Apart from its transport and thermodynamic properties, the mechanical properties of Nafion also play a significant role in determining its performance; mechanical properties should appear in a non-isobaric transport model when the physical mechanical processes and their coupling with electrochemical processes are represented in a proper way. Elastic properties of the hydrated membrane not only decide the balance between chemical and mechanical forces, which determines the equilibrium water uptake, but they also may play a role in deciding the rate of water sorption [105]. Once convinced that there is a good reason for non-uniform stresses to build up within a membrane, it becomes critical to understand how a membrane would respond to such a stress distribution.

Durability is a legitimate concern because Nafion has been identified as a viscoelastic material through scores of tests, and thereby tends to creep under a constant stress load, leading to thinning, pinhole formation, and delamination of MEAs [106, 107]. Fuel cells, during operation, are subjected to relative humidity (RH) cycling. Accelerated life tests performed for such RH cycling conditions on Nafion corroborate fears about membrane fatigue, creep, mechanical embrittlement, microcrack formation, *etc.* [108–111]. Efforts have been made to develop membrane materials with improved durability by enhancing their mechanical properties [112].

Benziger, Bocarsly and colleagues have performed a wide variety of mechanical tests to characterise the performance of Nafion under various conditions [88, 113–115]. The elastic moduli are found to be strong functions of ambient humidity (membrane water content in general) and the temperature of operation. Mechanical analysis experiments with RH cycling are challenging to realise, because the traditional measurement apparatus does not have sophisticated humidity control. Satterfield *et al.* carried out stress/strain tests to discover that elastic modulus tends to decrease as either temperature or humidity increases [115, 116]. Such a strong dependence on membrane hydration levels suggests a link between Young's modulus, or membrane stiffness, and the states of hydrophilic ionic clusters in the membrane. It was also found that Young's modulus remains practically same for the machine and transverse directions, validating the assumption of isotropy with regard to this property. Adding water was seen to slow down stress-relaxation rates, which is equivalent to increasing the relaxation times. Mechanical tensile creep tests were performed by Majsztrik *et al.* to find that around room temperature, water plasticizes Nafion, which decreases resistance to tensile creep strain [117].

The relevant question for us is: how can this behaviour be captured in a transport model? The first step towards that goal was to identify the state-of-the-art practice for building in the stress/strain behaviour of hydrated Nafion into macroscopic transport models. Hooke's law of linear elasticity would be the logical first choice of stress constitutive law to be integrated into a transport model, as was done by Doi *et al.* and many others [41, 97, 118]. All the experiments, however, point to there being a viscous component to Nafion stress response (in both dry and hydrated states).

Conventionally, viscoelastic materials are either modelled by a Maxwell model or a Kelvin–Voigt model [119, 120]. The Maxwell model considers the viscous (modelled by Newton's law of viscosity and represented by a damper) and the elastic (modelled

by Hooke's law of elasticity and represented by a spring) elements to be in series, as illustrated in Figure 2.3(a). The Maxwell fluid behaves like a liquid at long times, describing stress-relaxation behaviour well but failing to explain creep. The Kelvin–Voigt model is complementary to the Maxwell model, in the sense that it considers the viscous and elastic elements to be in parallel, as illustrated in Figure 2.3(b). A Kelvin–Voigt fluid behaves like a solid at long times, explaining creep well but not stress relaxation. A combination of the two models is able to capture most of the required phenomenological effects, but still does not entirely match the experimental data obtained for Nafion, especially given the coupling with hydration and temperature.

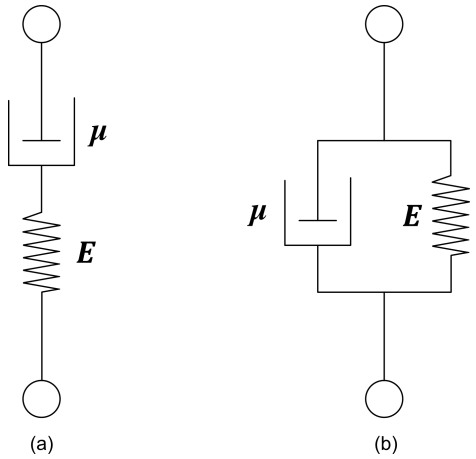

Figure 2.3: Common viscoelastic model depictions where the spring denotes elastic and the dashpot denotes viscous characteristics of the material (a) Maxwell model (b) Kelvin–Voigt model.

Two parameters, viscosity (μ) and Young's modulus (E), and their ratio (called the relaxation time) parameterise these models, which make them rooted in physical reality and convenient to implement. Satterfield *et al.* used the generalised Maxwell model to fit their stress-relaxation data by considering three spring-dashpot units in parallel with each other, leading to three widely disparate relaxation times ranging

from ~ 0.1 s–100 s [116]. It becomes tricky to attach physical meaning to the various time constants so obtained, though they fit the experimental data well.

Although existing literature provides a blueprint for modelling Nafion-like membranes, which can be tweaked to fit the main features of the experimental data by adding the appropriate dependences of properties on hydration *etc.* [116, 121–123], an effort should be made to root the description of stress in classical and irreversible thermodynamics [120]. This would ensure that stress derives from the same foundation as the other intensive variables; consistency of such a model would manifest an organic interaction between water content and stress both in dynamic and static regimes. To achieve this goal, we must consider the following:

- A rigorous description of deformation stress is needed, along with a stress constitutive law that describes the viscoelastic phenomena of creep and stress relaxation
- One must ensure that stress is rooted in classical thermodynamics, rather than being obtained from an *ad hoc* phenomenological description; this requires revisiting the entropy generation law that governs all dissipative processes, and examining how it depends on deformation stress
- Would deformation stress, identified as separate from pressure, affect local volume/density?
- Would gradients in deformation stress be linked to transport in the material, and would such transport be diffusive or convective?
- A consistency check is required to ensure that any stress/strain relationship proposed describes the extremes of a Newtonian liquid and a Hookean solid

- The combination of a deformation stress law with the momentum balance and equilibrium state equations should provide a framework to define the effective swelling in the material, or the stresses generated given an external physical constraint

Existing models and experimental data add many pieces to the jigsaw puzzle of transport in Nafion, from providing frameworks within which diffusive, hydraulic, and mechanical forces can be handled to carrying out detailed force balances within a membrane's pores. The challenge is to analyse how these pieces fit together, and construct a comprehensive model, founded in thermodynamic rigour and first principles. An approach based in non-equilibrium thermodynamics has been taken by researchers to develop transport and kinetic models for various applications: Latz and Zausch modelled ion and heat transport in porous cathodes for Li batteries [124]; Bazant described phase change behaviour in lithium iron phosphate [125]; and Pavelka modelled fuel cells [126], the example most relevant to our case.

Through the course of this literature review, we have recognised the different characteristics that should be built in to our model of Nafion, specifically emphasising stress-related effects, as summarised in Figure 2.4. First, the model must explore how stress (and its gradients) can affect the different transport mechanisms: diffusion, electroosmotic drag, hydraulic permeation and/or viscous flow of water, migration of protons *etc.* This is achieved by figuring out what role stress plays in the equilibrium state equations, conservation balance equations, and flux constitutive laws. Second, since Nafion is a solid material, elastic effects also become relevant: it is important to distinguish between purely compressive and purely deformational parts of stress, to understand their origins in classical thermodynamics, and to identify their functional ramifications. This is achieved by the means of clear definitions, as well as incorporating proper momentum flux laws and boundary conditions into the model.

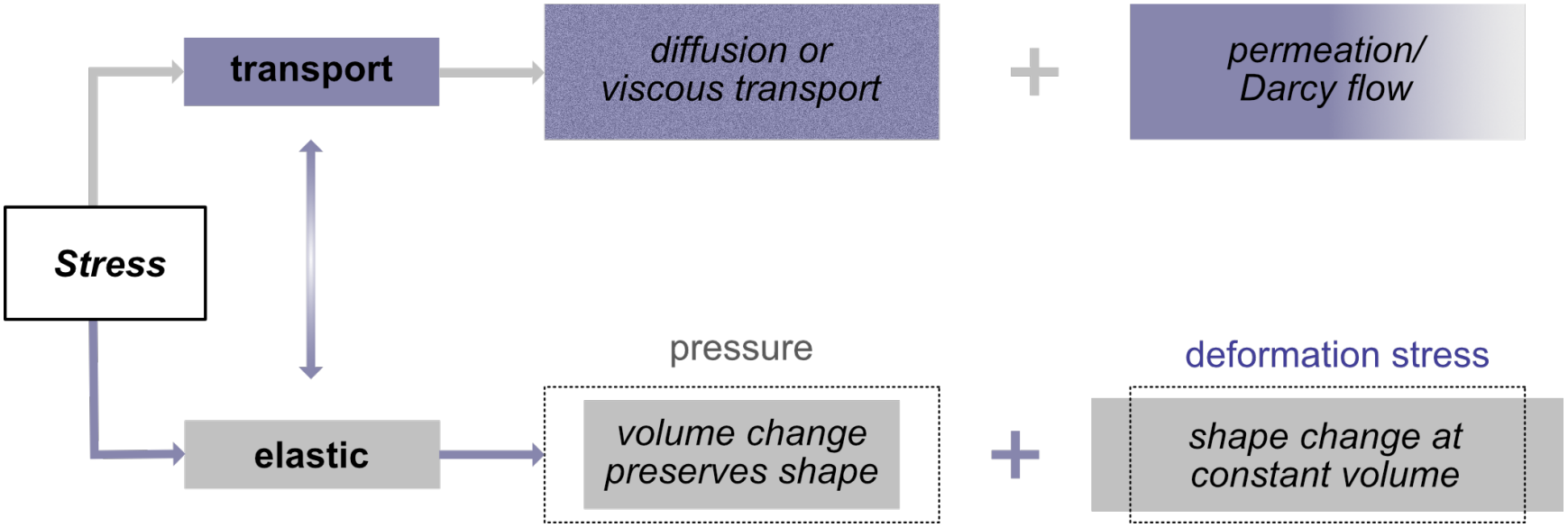

Figure 2.4: General model considerations for the case of non-isobaric transport in ionomers.

Chapter 3

Modelling Irreversible Transport in Viscoelastic Electrolytes

The description of viscoelastic electrolytes poses a substantial challenge because of the elastic component of their character; elasticity refers to a material's ability to sustain spatial deformations at equilibrium. Thus the classical-thermodynamic foundations of Newman's theory of transport in concentrated electrolytic solutions must be rebuilt, because the statement of the first law from which all the thermodynamic properties derive must account for this capacity for deformation, apart from the standard volume compression.

We set out here to develop elementary balance equations and flux laws that can be used to produce a concentrated-solution theory applicable to viscous liquids, elastic solids, and viscoelastic materials. The system of balances allows for multiphysical couplings between electrochemical and mechanical phenomena, and reveals the bases of fluxes and driving forces that should be involved in constitutive laws that account for diffusional coupling.

Deformation stresses, when included in the first law, are shown to propagate into the Gibbs–Duhem relation among intensive properties, and consequently to alter the familiar definition of the thermodynamic force that drives mass diffusion. Moreover, since the continuity of total energy is used to derive both the heat equation and the energy dissipation (local entropy generation), these macroscopic balances are both shown to require additional terms when describing solids. The long chapter that follows aims to achieve the above goals; it is divided in to clear sections to offer modularity as well as clarity about the changes made to the conventional thermodynamic construct.

The first section discusses how the first law of thermodynamics changes when strain energy is accounted for at equilibrium. This is followed by developing equations of state on volume, deformation, and entropy, which give local conditions of microscopic equilibrium. A very important juncture in this journey is the development of Gibbs–Duhem equations which relate the changes in intensive properties at equilibrium: they provide the driving forces to bring a system back to its equilibrium state. The second, third, and fourth sections deal with the development of material, momentum, and energy balances used in the model. These continuity equations are essentially dynamic, and therefore stand apart from (and on equal footing as) the thermodynamic relations.

The fifth section focuses on the dissipation function, equivalently the second law of thermodynamics, by developing an entropy generation expression. Following in Onsager's footsteps, this expression can be used to identify the conjugate driving forces and fluxes associated with irreversible processes, which are affected by adding the strain energy in the first law. Without making reference to any particular type of material, it is possible to formulate the general multicomponent transport problem and address the question of model closure. The sixth section summarises the

equations developed for a general electrolyte by means of an equation count, clearly specifying the need for material-specific constitutive flux laws to close the non-isobaric transport model. Finally, the seventh section uses the entropy generation function to develop flux laws for irreversible transport processes. Specifically, Onsager–Stefan–Maxwell (OSM) theory is employed to formulate linear mass transport laws for electrolytic solutions at constant temperature but with possibly varying stress. Further, instead of relying solely on phenomenology, the stress constitutive laws developed for viscoelastic materials are firmly rooted in the dissipation function. Despite the rather esoteric fundamental nature of the present enquiry, this effort is worthwhile, because it will permit the formulation of thermodynamically complete descriptions of ion transport in ionomer gels and ceramic electrolytes, both of which are important classes of electrochemical materials.

3.1 Thermodynamics

3.1.1 First Law of Thermodynamics: Viscoelastic Electrolytes

3.1.1.1 Mechanical Principles

A basic axiom of classical thermodynamics holds that every equilibrium colligative property of a homogeneous phase containing n chemically distinct species at ambient temperature T and external pressure p ultimately derives from a single scalar function, called the Gibbs function G, which measures the total energy available to be extracted from the phase *via* reversible processes. To account for deformation equilibria in elastic solids, this elementary framework must be extended by replacing the scalar external pressure p with the more general Cauchy stress tensor $\vec{\vec{\sigma}}$, which quantifies how any plane's orientation at a given location maps into a force vector acting on that plane. More precisely, the traction force $\vec{t}$ exerted on a plane whose outward

orientation is designated by the unit normal vector $\vec{e}_{\mathrm{n}}$ relates to the Cauchy stress through the projection $\vec{t} = -\vec{e}_{\mathrm{n}} \cdot \vec{\vec{\sigma}}$.

Classical thermodynamics is generally applied to simple fluids or, more generally, to systems in which only pure compression or dilation needs to be considered when computing mechanical contributions to the Gibbs function. In this mode the change in G arising from mechanical phenomena is familiarly written as $dG_{\mathrm{mech}} = V\,dp$, where V is the system volume. When a system is capable of sustaining deformation in addition to compression, one has instead that

$$dG_{\mathrm{mech}} = \frac{1}{3}\vec{\vec{V}} : d\vec{\vec{\sigma}}, \tag{3.1}$$

where $\vec{\vec{V}}$ is a tensor with units of volume that describes both the system volume and the extent to which that volume is deformed. Being conjugate to intensive property $\vec{\vec{\sigma}}$, $\vec{\vec{V}}$ must be extensive. Some properties of $\vec{\vec{\sigma}}$ are required by laws of mechanics; it is worth using those constraints to put equation 3.1 into a simpler form.

Stresses fall into two broad classes: *spherical* and *deviatoric*. Spherical stresses are uniformly compressive or dilatational, manifesting as purely normal tractions whose magnitudes are unaffected by the orientations of the surfaces on which they act. Deviatoric stresses, by contrast, embody tractions with all parts that transform with respect to the orientations of their planes of action. Equation A.10 can be used to prove that any spherical tensor is necessarily a scalar multiple of the identity tensor $\vec{\vec{I}}$. Thus pressure p is identified by decomposing the Cauchy stress into its unique spherical and deviatoric parts,

$$\vec{\vec{\sigma}} = p\vec{\vec{I}} + \vec{\vec{\tau}}. \tag{3.2}$$

Thermodynamic pressure identifies with the spherical stress, related to the first invariant, or trace, of the Cauchy stress through $p = \frac{1}{3}\mathrm{tr}(\vec{\vec{\sigma}})$. The deviatoric nature of the deformation stress, $\vec{\vec{\tau}}$, is expressed by the property $\mathrm{tr}(\vec{\vec{\tau}}) = 0$. Cauchy stress, at

this point, only includes forces which can be sustained at equilibrium. There may be other spherical or deviatoric components of stress, which only act in non-equilibrium situations, and will be dealt with later in the dynamic momentum balance section.

The volume tensor $\vec{\vec{V}}$ likewise decomposes uniquely into spherical and deviatoric parts,

$$\vec{\vec{V}} = V\vec{\vec{I}} + \vec{\vec{V}}', \tag{3.3}$$

where $V = \frac{1}{3}\mathrm{tr}(\vec{\vec{V}})$ is the familiar system volume; the deformation-volume tensor has the property $\mathrm{tr}(\vec{\vec{V}}') = 0$. Insertion of decompositions 3.2 and 3.3 into equation 3.1 gives

$$dG_{\mathrm{mech}} = V\,dp + \tfrac{1}{3}\vec{\vec{V}}' : d\vec{\vec{\tau}}, \tag{3.4}$$

because the vertical scalar product between spherical and deviatoric tensors generally vanishes (*cf.* equation A.9). Thus one recovers an expression for the change in the mechanical Gibbs function that reduces to the familiar form in the absence of deformation stress.

Additional simplifications can be made to the right side of equation 3.4 by considering some consequences of tensor symmetry. On physical grounds one expects that the content of a Cauchy stress should not change if the coordinate system under it is subjected to an arbitrary rigid motion. This invariance principle is equivalent to a statement that stress is symmetric, $\vec{\vec{\sigma}} = \vec{\vec{\sigma}}^{\,\mathrm{T}}$ [127]. Through equation 3.2 it also implies symmetry of the deformation stress, so that $\vec{\vec{\tau}} = \vec{\vec{\tau}}^{\,\mathrm{T}}$.

Since the vertical scalar product between an antisymmetric tensor and a symmetric tensor vanishes, it immediately follows from the symmetry of $\vec{\vec{\sigma}}$ that any antisymmetric part of the volume tensor will not contribute to the Gibbs energy. The requirement that all colligative equilibrium properties must derive from the Gibbs

function therefore amounts to a stipulation that $\vec{\vec{V}} = \vec{\vec{V}}^{\mathrm{T}}$, which implies symmetry of the deformation-volume tensor $\vec{\vec{V}}'$.

Properties of the deviators $\vec{\vec{\tau}}$ and $\vec{\vec{V}}'$ allow further simplification of equation 3.4. Given a deformation stress expressed relative to a particular right-handed Cartesian coordinate system, the spectral theorem (*cf.* Appendix A) says that one can always rigidly rotate the coordinate frame to make the tractions represented by the stress transform into three mutually perpendicular, purely normal forces. That is, for any $\vec{\vec{\tau}}$ there exists a principal representation

$$\vec{\vec{\tau}} = \vec{\vec{Q}}_{\tau}^{\mathrm{T}} \cdot \vec{\vec{d}}_{\tau} \cdot \vec{\vec{Q}}_{\tau}, \quad \text{where} \quad \vec{\vec{d}}_{\tau} = \sum_{k} \tau_k \vec{e}_k^{\tau} \otimes \vec{e}_k^{\tau}, \tag{3.5}$$

in which the diagonal entries $\{\tau_1, \tau_2, \tau_3\}$ of $\vec{\vec{d}}_{\tau}$ establish the magnitudes of the principal deformation stresses, and the rotation $\vec{\vec{Q}}_{\tau}^{\mathrm{T}}$ transforms the original coordinate basis under $\vec{\vec{\tau}}$ into the principal directions $\{\vec{e}_1^{\tau}, \vec{e}_2^{\tau}, \vec{e}_3^{\tau}\}$ of $\vec{\vec{\tau}}$.

Owing to its symmetry, the basis of the deformation-volume tensor $\vec{\vec{V}}'$ can similarly be rotated by some $\vec{\vec{Q}}_{V'}^{\mathrm{T}}$ to produce a principal representation that involves only the principal deformation volumes $\{V_1', V_2', V_3'\}$. Substitution of the principal representations of $d\vec{\vec{\tau}}$ and $\vec{\vec{V}}'$ allows one to demonstrate that

$$\vec{\vec{V}}' : d\vec{\vec{\tau}} = \left[\left(\vec{\vec{Q}}_{V'} \cdot \vec{\vec{Q}}_{d\tau}^{\mathrm{T}} \right)^{\mathrm{T}} \cdot \vec{\vec{d}}_{V'} \cdot \left(\vec{\vec{Q}}_{V'} \cdot \vec{\vec{Q}}_{d\tau}^{\mathrm{T}} \right) \right] : \vec{\vec{d}}_{d\tau}. \tag{3.6}$$

For certain classes of materials, for instance isotropic solids, the principal axes of deformation volume and deformation stress coincide, implying $\vec{\vec{Q}}_{V'} = \vec{\vec{Q}}_{d\tau}$. This physical notion of coincident principal axes is equivalent to the mathematical commutativity relation $\vec{\vec{V}}' \cdot \vec{\vec{\tau}} = \vec{\vec{\tau}} \cdot \vec{\vec{V}}'$. Supposing that the constitutive relation between stress and strain is such that this commutativity relation holds, it follows that

$$\vec{\vec{V}}' : d\vec{\vec{\tau}} = \vec{\vec{d}}_{V'} : \vec{\vec{d}}_{d\tau} = V_1' d\tau_1 + V_2' d\tau_2 + V_3' d\tau_3. \tag{3.7}$$

The principal values on the right are not independent, however, because both tensors involved are traceless. Equation A.12 therefore implies that $\tau_3 = -(\tau_1 + \tau_2)$ and

$V_3' = -(V_1' + V_2')$; consequently

$$dG_{\text{mech}} = V\,dp + \tfrac{1}{3}\left(2V_1' + V_2'\right)d\tau_1 + \tfrac{1}{3}\left(V_1' + 2V_2'\right)d\tau_2. \tag{3.8}$$

From this, one can identify extensive properties that associate strains with each independent principal deformation stress:

$$D_1 = \tfrac{1}{3}\left(2V_1' + V_2'\right) \quad \text{and} \quad D_2 = \tfrac{1}{3}\left(V_1' + 2V_2'\right), \tag{3.9}$$

so that a simple expression involving only scalar quantities,

$$dG_{\text{mech}} = V\,dp + D_1 d\tau_1 + D_2 d\tau_2, \tag{3.10}$$

encapsulates all the possible contributions that mechanical forces can make to changes in the Gibbs function.

Finally, it is useful to specify how the deformation-volume tensor $\vec{\vec{V}}'$ relates to the traceless Eulerian strain deviator $\vec{\vec{\epsilon}}'$ familiar from the continuum mechanics of solids. A suitable connection is provided by the definition

$$\tfrac{1}{3}\vec{\vec{V}}' = V\vec{\vec{\epsilon}}', \tag{3.11}$$

making the strain deviator dimensionless. This relationship is consistent with the use of strain in Coussy's comprehensive development of thermodynamics for poroelastic systems [128], but operates in an Eulerian, rather than a Lagrangian, frame. The challenge of functioning in a Lagrangian frame is having to define a reference frame for all the calculations; an Eulerian frame, however, is only concerned with the instantaneous properties of the system [104].

Working backward to reinsert the tensors on which the principal stresses and deformation volumes are based, equation 3.10 can be written equivalently in terms of the strain deviator as

$$dG_{\text{mech}} = V\,dp + V\vec{\vec{\epsilon}}' : d\vec{\vec{\tau}}, \tag{3.12}$$

a relationship that can also be obtained by direct substitution of equation 3.11 into equation 3.4. The scalar form (equation 3.10) is preferred here, however, as it offers convenience for scalar thermodynamic operations. Further, since $\vec{\vec{\epsilon}}'$ is a simple scalar multiple of $\vec{\vec{V}}'$, the strain deviator can be proven to share many of the fundamental properties possessed by $\vec{\vec{V}}'$. In particular, $\vec{\vec{\epsilon}}' = \vec{\vec{\epsilon}}'^{\mathrm{T}}$ and $\vec{\vec{\epsilon}}' \cdot \vec{\vec{\sigma}} = \vec{\vec{\sigma}} \cdot \vec{\vec{\epsilon}}'$.

3.1.1.2 Basis of the Gibbs Function

After adopting the mechanical principles developed above, one can establish a general Gibbs function to describe a homogeneous multicomponent phase. Assume that each chemically distinct constituent i has a given total molar content within the phase, which is given the symbol n_i; in an n-constituent phase, all the molar contents can be denumerated as an n-tuple $\{n_i\}_n$, which we take to be an ordered list for convenience. Further we assume that through the application of appropriate experimental controls, T, p, τ_1, τ_2, and each of the $\{n_i\}_n$ can be varied in isolation while holding all the other quantities constant. Mathematically speaking, the domain T, p, τ_1, τ_2, $\{n_i\}_n$ comprises a basis of independent scalar variables on which the available energy depends. Each of the members of this basis set of elementary state variables is real; all but τ_1 and τ_2 are strictly non-negative.

The free energy of a homogeneous, equilibrated phase is expressed as a continuous, differentiable scalar function $G\left(T, p, \tau_1, \tau_2, \{n_i\}_n\right)$. The Gibbs function is single-valued, but is not an injective mapping because multiple sets of the basis variables can in principle correspond to the same available energy.

Rather than treating individual species in isolation, it is convenient to define a set of alternative variables to describe composition, reserving the single quantity

$$n_{\mathrm{T}} = \sum_i n_i \tag{3.13}$$

to express the total molar content of a phase. With n_{T} in hand, one can define particle fractions

$$y_i = \frac{n_i}{n_{\mathrm{T}}}, \tag{3.14}$$

which are also non-negative, to describe local composition. Each y_i is individually bounded between zero and unity, and the whole n-tuple $\{y_i\}_n$ satisfies

$$\sum_i y_i = 1. \tag{3.15}$$

This constraint can be thought of as a 'phase rule': in an isolated phase, one of the composition descriptors necessarily depends on the others. In other words, specifying the $(n-1)$-tuple $\{y_i\}_{n-1}$ is sufficient to establish the composition of an n-ary phase unambiguously.

Hereafter, the term 'composition' should be taken to mean a specific set of values for the basis variables $\{y_i\}_{n-1}$. A material with $n = 1$ is called 'pure'. In pure materials $G(T, p, \tau_1, \tau_2, n_{\mathrm{T}})$ and particle fractions are unnecessary. Standard theories of thermomechanics tend to be restricted to pure materials.

Mole fractions (composition) are the basis variables of choice instead of molar concentration or volume fractions *etc.* for various reasons: they are bounded between 0 and 1 by definition, the phase rule acts as an intrinsic constraint on them, they do not refer to (or rely upon) any material properties which is especially useful when material properties of species (such as molecular weights or partial molar volumes) are starkly different, and most importantly for this non-isobaric study they are independent of pressure and temperature. This isolates all the mechanical effects from composition effects by design; composition variables involving volume have pressure convoluted within them.

3.1.1.3 Extensivity

With definitions 3.13 and 3.14 and property 3.15, one can show that the transformation from the composition basis $\{n_i\}_n$ to the basis n_T, $\{y_i\}_{n-1}$ is bijective (one-to-one and onto). Thus one can equivalently write the functionality of G as $G\left(T, p, \tau_1, \tau_2, \{y_i\}_{n-1}, n_\mathrm{T}\right)$ without loss of information.

The most elementary property of G is that it is an extensive state function. That is to say, given any positive scalar γ,

$$G\left(T, p, \tau_1, \tau_2, \{y_i\}_{n-1}, \gamma n_\mathrm{T}\right) = \gamma G\left(T, p, \tau_1, \tau_2, \{y_i\}_{n-1}, n_\mathrm{T}\right). \tag{3.16}$$

Adopting n_T as the only quantity that rescales the magnitude of G in this way amounts to a physical postulate: the magnitude of the available energy within a continuous material equilibrated at fixed temperature, pressure, deformation stress, and composition varies in direct proportion to the total number of particles the material contains.

The term 'extensive' can be applied to any other state variable or state function that has the property stated in equation 3.16. For example, equation 3.14 can be used to show that each of the state variables $\{n_i\}_n$ is extensive, because $n_i\left(T, p, \{y_i\}_{n-1}, n_\mathrm{T}\right) = y_i n_\mathrm{T}$ and $\gamma \cdot (y_i n_\mathrm{T}) = y_i \cdot (\gamma n_\mathrm{T})$. In general, the sum of extensive properties proves to be extensive, so it follows through equation 3.13 that n_T itself is extensive.

Conversely, a property is 'intensive' if its magnitude is insensitive to changes in n_T at fixed T, p, and composition. For example, the molar Gibbs energy, $\overline{G}$, is defined as $\overline{G} = G/n_\mathrm{T}$. By letting $\gamma = 1/n_\mathrm{T}$ in equation 3.16, one sees that $\overline{G}$ is an intensive state function, because its domain does not need to include n_T; specifically, $\overline{G}\left(T, p, \tau_1, \tau_2, \{y_i\}_{n-1}\right)$.

3.1.1.4 Euler's Theorem

Volume V and entropy S are important characteristics of a phase, which are identified as the conjugate variables of p and T, respectively. In this context 'conjugate' means they derive from G through the partial derivatives

$$V = \left(\frac{\partial G}{\partial p}\right)_{T,\tau_1,\tau_2,n_i} \qquad \text{and} \qquad S = -\left(\frac{\partial G}{\partial T}\right)_{p,\tau_1,\tau_2,n_i}. \tag{3.17}$$

The new extensive properties D_1 and D_2 associated with volume deformation can be seen to come from G through partial derivatives of the form

$$D_i = \left(\frac{\partial G}{\partial \tau_i}\right)_{T,p,\tau_{j\neq i},n_k}. \tag{3.18}$$

By a similar process one can define electrochemical potentials μ_i as conjugate variables associated with the n_i,

$$\mu_i = \left(\frac{\partial G}{\partial n_i}\right)_{T,p,\tau_1,\tau_2,n_{j\neq i}}. \tag{3.19}$$

Although electrochemical potentials are given a special symbol, any property obtained by applying the thermodynamic derivative on the right of equation 3.19 to an extensive property is called a 'partial molar property' of species i. Partial molar properties are notated by putting an overbar on the property from which they derive and appending a subscript to indicate the species involved in the derivative. For example, one can equivalently write $\mu_i = \overline{G}_i$.

In a phase at fixed temperature, pressure, deformation stress, and composition, the extensivity relation expressed by equation 3.16 implies that

$$G = \sum_i \mu_i n_i, \tag{3.20}$$

which is known as Euler's extensivity theorem for the grand canonical ensemble. The extensivity property from equation 3.16 can be used here to prove that the μ_i are intensive.

3.1.1.5 Gibbs Energy Form of First Law

Given the stated domain of the Gibbs function, the first law of thermodynamics can be written through definitions 3.17 through 3.19 as

$$dG = -SdT + Vdp + D_1 d\tau_1 + D_2 d\tau_2 + \sum_i \mu_i dn_i \tag{3.21}$$

or use equations 3.10 and 3.12 to write it in more general terms as,

$$dG = -SdT + Vdp + V\vec{\vec{\epsilon}}' : d\vec{\vec{\tau}} + \sum_i \mu_i dn_i. \tag{3.22}$$

This is the first principal result of this chapter which clearly lays out the first law of thermodynamics for a viscoelastic material. This form of the first law also provides a clear thermodynamic definition for the Eulerian strain tensor. Each component of the strain tensor can be defined as the per unit volume change in Gibbs free energy with respect to the corresponding component of the deviatoric stress tensor while holding temperature, pressure, molar content, and all other components of deviatoric stress constant,

$$\epsilon'_{ij} = \frac{1}{V}\left(\frac{\partial G}{\partial \tau_{ij}}\right)_{T,p,\tau_{mn\neq ij},n_k}. \tag{3.23}$$

Not all components of $\vec{\vec{\epsilon}}'$ are independent since the deviatoric stress tensor is symmetric and traceless.

This definition of strain does not make any assumptions about the material, and conceptually concurs with the idea of hyperelasticity which describes non-Hookean elastic materials capable of withstanding large deformations [129, 130], through a strain energy function similar to G_{mech}. It should be noted, however, that the strain definition 3.23 only accounts for quasi-equilibrated deformations. Irreversible deformations, such as those incurred due to the viscous or plastic behaviour of a material, would need to be quantified in excess of $\vec{\vec{\epsilon}}'$. Dynamic, irreversible, or permanent deformations are rooted not in the Gibbs but the dissipation function for the system [131].

By inserting the definitions $G = n_{\mathrm{T}}\overline{G}$, $S = n_{\mathrm{T}}\overline{S}$, $V = n_{\mathrm{T}}\overline{V}$, $D_i = n_{\mathrm{T}}\overline{D}_i$, and $n_i = n_{\mathrm{T}}y_i$ into equation 3.21 and applying equation 3.15, one can show with the product rule of differentiation that

$$d\overline{G} = -\overline{S}dT + \overline{V}dp + \overline{D}_1 d\tau_1 + \overline{D}_2 d\tau_2 + \sum_{i\neq n} (\mu_i - \mu_n)\, dy_i, \tag{3.24}$$

providing an intensive form of the first law. Since it was found that $\overline{G}\,(T, p, \tau_1, \tau_2, \{y\}_{n-1})$, equation 3.24 implies

$$\left(\frac{\partial \overline{G}}{\partial y_i}\right)_{T,p,\tau_1,\tau_2,y_{k\neq i,n}} = \mu_i - \mu_n. \tag{3.25}$$

Equations 3.24 and 3.25 can be useful for analyzing local energy balances. Equation 3.25 in particular was employed by Monroe, Wheeler, and Newman in their derivation of the symmetric reciprocal relation for isothermal, isobaric OSM diffusion [9].

3.1.2 Equations of State: Local Equilibrium

3.1.2.1 Volumetric Equation of State

Volume is the most fundamental descriptor of a material's kinematic state. In multicomponent materials, one must consider that the equilibrium volume can depend on composition. To quantify the contributions that individual species make to overall material volume, one can introduce partial molar volumes

$$\overline{V}_i = \left(\frac{\partial V}{\partial n_i}\right)_{T,p,\tau_1,\tau_2,n_{j\neq i}} = \left(\frac{\partial \mu_i}{\partial p}\right)_{T,\tau_1,\tau_2,n_j}. \tag{3.26}$$

The second equality here derives from a Maxwell relation, which may be easier to see if one recalls that $\mu_i = \overline{G}_i$. Because the molar contents are naturally independent of T, p, and τ_i, differentiation of equation 3.20 with respect to p at fixed T and deformation stress shows through equations 3.17 and 3.26 that

$$V = \sum_i \overline{V}_i n_i. \tag{3.27}$$

Equation 3.16 can be used to show that V is extensive; it follows that the properties $\left\{\overline{V}_i\right\}_n$ are intensive. Also, the extensivity of V proves that the molar volume $\overline{V} = V/n_{\mathrm{T}}$ is intensive.

There may be other physical constraints on the functionality of V, which can be seen as fundamental constitutive relationships. An important constraint applies to the mechanical part of G as a consequence of the physical definitions of spherical and deformation stresses. Discussions of these stresses often conflate a dynamical perspective with a kinematic perspective: deformation stress is typically defined heuristically as 'stress that leads to shape change without volume change', whereas spherical stress is 'stress that leads to volume change without shape change'. These concepts are intuitive, but practically imply thermodynamic constraints. To say that τ_i leads to shape change without volume change means that

$$\left(\frac{\partial V}{\partial \tau_i}\right)_{T,p,\tau_{j\neq i},n_k} = 0, \quad \text{whence} \quad \overline{V} = \overline{V}\left(T, p, \{y_i\}_{n-1}\right); \tag{3.28}$$

that is, the molar volume of a material cannot depend on deformation stress. In light of equation 3.27, this says that the volume occupied by different species in a solution will change when the system is compressed (or expanded), keeping the molar content the same, but will not change when the system is deformed. Further, through the Maxwell relation

$$\left(\frac{\partial V}{\partial \tau_i}\right)_{T,p,\tau_{j\neq i},n_k} = \left(\frac{\partial D_i}{\partial p}\right)_{T,\tau_1,\tau_2,n_j}, \tag{3.29}$$

it appears to follow that the deformation volumes D_1 and D_2 cannot depend on pressure p. This is a more complex statement because the deformation volumes are related to volume, which is a function of pressure. There should, therefore, be another quantity in the description of deformation volume which cancels out this pressure dependence; equations 3.9 and 3.11 suggest this quantity is the Eulerian strain $\vec{\epsilon}'$, dealt with in the next section on deformation.

The total molar concentration c_T is defined as the inverse of molar volume, $c_\mathrm{T} = 1/\overline{V}$, and has the same functionality, *i.e.*, $c_\mathrm{T}\left(T, p, \{y_i\}_{n-1}\right)$. Thus, in elastically deformable materials, the volume-explicit equation of state needs no modification from the form used for simple fluids. Through manipulation of equation 3.27 with the definitions above, any phase with properties embedded in G can be seen to obey a volumetric equation of state

$$\frac{1}{c_\mathrm{T}} = \sum_i \overline{V}_i y_i, \tag{3.30}$$

which provides a fundamental kinematic relation, used as a local equilibrium condition, to stand alongside the phase rule provided by equation 3.15. Every quantity that appears in equation 3.30 depends at most on T, p, and $\{y_i\}_{n-1}$. This is an important result which quantifies the local equilibrium relationship between volume and all intensive variables—composition, pressure, and temperature—therefore accounting for the excluded-volume effect [27]. This quantification of local volume represents the swelling in the case of hydrated Nafion membranes, which answers one of the more important modelling questions for these ionomers.

If desired, one can define the molar concentration of species i at this stage, through $c_i = c_\mathrm{T} y_i$. One can also identify the volume fraction of i, which relates to its concentration and partial molar volume through $\phi_i = \overline{V}_i c_i$. Equation 3.30 implies another phase rule stating: $\sum_i \phi_i = 1$. Both molar concentrations and species volume fractions are necessarily independent of the deformation stress.

Since volume is independent of deformation stress, all differential changes in V relate to changes in T, p, and $\{n_i\}_n$ through

$$dV = V\alpha_V dT - \frac{V}{K} dp + \sum_i \overline{V}_i dn_i. \tag{3.31}$$

This equation introduces the volumetric coefficient of thermal expansion, α_V, and the bulk modulus (isothermal compressibility) K, two familiar material properties that

are generally defined as

$$\alpha_V = \frac{1}{V}\left(\frac{\partial V}{\partial T}\right)_{p,\tau_1,\tau_2,n_i} \quad \text{and} \quad \frac{1}{K} = -\frac{1}{V}\left(\frac{\partial V}{\partial p}\right)_{T,\tau_1,\tau_2,n_i}; \tag{3.32}$$

being intensive, α_V and K are at most functions of temperature, pressure, and composition. Equation 3.31 forms the basis of local volume balance and the starting point for exploring the pressure dependence of partial molar volumes in the later sections.

3.1.2.2 Deformational Equations of State

Materials that can be deformed elastically need strain states, in addition to volume, to fully specify their kinematic state. This can be achieved *via* developing deformational equations of state to describe how deformation volumes or strains may depend on the intensive thermodynamic basis variables. The partial molar deformation volumes $\overline{V}'_{i,jk}$ are defined in a similar way as the partial molar volumes $\overline{V}_i$ except that they additionally depend on material orientation:

$$\overline{V}'_{i,jk} = \left(\frac{\partial V'_{jk}}{\partial n_i}\right)_{T,p,\tau_{lm},n_{q\neq i}} = \left(\frac{\partial \mu_i}{\partial \tau_{jk}}\right)_{T,p,\tau_{lm\neq jk},n_q}. \tag{3.33}$$

Thus the deformation borne by the material as a whole can be partitioned among the individual molecular species that comprise it, and the total deformation volume can be expressed as a sum of the individual contributions,

$$\vec{\vec{V}}' = \sum_i \vec{\vec{\overline{V}}}'_i n_i. \tag{3.34}$$

Further, using the definition of the deformation volume (equation 3.11), we can obtain a tensorial deformational equation of state (similar to equation 3.30 which is the volumetric equation of state)

$$3\vec{\vec{\epsilon}}' = c_{\mathrm{T}} \sum_i \vec{\vec{\overline{V}}}'_i y_i. \tag{3.35}$$

This equation of state provides another thermodynamic definition of the Eulerian strain as a function of other system variables and properties (the first being equation

3.23), without assuming anything about the mechanical behaviour of the material. The present approach differs from classical theories of linear elasticity, hyperelasticity, or even viscoelasticity, which typically define strain in terms of displacements, then derive relationships between stresses and strains based on phenomenological material-specific constitutive descriptions.

The discussion of the volumetric equation of state suggests that physical definitions of compressive stresses require that the deformation volumes D_1 and D_2 be independent of pressure, *i.e.*, $D_k\left(T, \tau_1, \tau_2, \{n_i\}_n\right)$. In light of this dependence the total differential of deformation strain D_k becomes

$$dD_k = V\alpha_{D_k}dT - \frac{V}{G_{k1}}d\tau_1 - \frac{V}{G_{k2}}d\tau_2 + \sum_i \overline{D}_{ki}dn_i. \tag{3.36}$$

The partial properties $\overline{D}_{ki}$ are defined in a similar way to the partial molar deformation volumes $\overline{V}'_{i,jk}$ except that they define independent principal strains,

$$\overline{D}_{ki} = \left(\frac{\partial D_k}{\partial n_i}\right)_{T,p,\tau_1,\tau_2,n_{j\neq i}}. \tag{3.37}$$

The 'volumetric coefficients of thermal deformation' are defined by analogy to the volumetric coefficient of thermal expansion:

$$\alpha_{D_k} = \frac{1}{V}\left(\frac{\partial D_k}{\partial T}\right)_{p,\tau_1,\tau_2,n_i}. \tag{3.38}$$

These equations further introduce four mechanical material properties,

$$\frac{1}{G_{ij}} = -\frac{1}{V}\left(\frac{\partial D_i}{\partial \tau_j}\right)_{T,p,\tau_{k\neq j},n_k}, \tag{3.39}$$

given the symbols G_{ij} because they are similar to shear moduli. Observe that the necessary pressure independence of D_i requires that the quotient V/G_{ij} is independent of pressure. Further note that there are only three independent moduli G_{ij} because a Maxwell relation based on equation 3.18,

$$\left(\frac{\partial D_i}{\partial \tau_j}\right)_{T,p,\tau_{k\neq j},n_k} = \left(\frac{\partial D_j}{\partial \tau_i}\right)_{T,p,\tau_{k\neq i},n_k}, \tag{3.40}$$

requires that $G_{12} = G_{21}$.

Instead of using the simpler but obscure formulation of D_k, we can revert to the deformation volume in principal coordinates V_k' using equation 3.9, and convert equation 3.36 to the following:

$$dV_1' = V\left(2\alpha_{D_1} - \alpha_{D_2}\right)dT - V\left(\frac{2}{G_{11}} - \frac{1}{G_{12}}\right)d\tau_1 - V\left(\frac{2}{G_{12}} - \frac{1}{G_{22}}\right)d\tau_2 + \sum_i \left(2\overline{D}_{1i} - \overline{D}_{2i}\right)dn_i \tag{3.41}$$

$$dV_2' = V\left(2\alpha_{D_2} - \alpha_{D_1}\right)dT - V\left(\frac{2}{G_{12}} - \frac{1}{G_{11}}\right)d\tau_1 - V\left(\frac{2}{G_{22}} - \frac{1}{G_{12}}\right)d\tau_2 + \sum_i \left(2\overline{D}_{2i} - \overline{D}_{1i}\right)dn_i \tag{3.42}$$

Until now, the only constraint on the material was that the principal axes of stress and strain coincide. Now, we additionally assume that the material is isotropic. This assumption imposes the condition that deformation in a principal direction should be a function of the principal stress in that direction alone, placing the following constraints on G_{ij}'s:

- since dV_1' should be independent of $d\tau_2$, the respective coefficient in equation 3.41 is set to zero,

$$\frac{2}{G_{12}} - \frac{1}{G_{22}} = 0 \text{ implying } \mathrm{G_{12}} = 2\mathrm{G_{22}},$$

- similarly, dV_2' should be independent of $d\tau_1$, making the following coefficient in equation 3.42 zero,

$$\frac{2}{G_{12}} - \frac{1}{G_{11}} = 0 \text{ implying } \mathrm{G_{12}} = 2\mathrm{G_{11}}.$$

Using these two conditions together, we have the simple result that deformation in an isotropic elastic system is characterised by a scalar property $G_{\text{shear}} = G_{11} = G_{22} = G_{12}/2$. Remembering that the same rotation sends stress and strain into their principal coordinates, equations 3.41–3.42 can be rotated back and condensed to:

$$d\vec{\vec{V}}' = V\vec{\vec{\mathrm{A}}}_D' dT - \frac{3}{2}\frac{V}{G_{\text{shear}}}d\vec{\vec{\tau}} + \sum_i \vec{\vec{V}}_i' dn_i. \tag{3.43}$$

At constant temperature and composition, the integrated form of equation 3.43 when combined with the definition of strain 3.11, can lead us to a relationship between stress and strain for an elastic material,

$$\vec{\vec{\tau}} = -2 \int_{\vec{\vec{\epsilon}}'_{\text{ref}}}^{\vec{\vec{\epsilon}}'} G_{\text{shear}} d\vec{\vec{\epsilon}}'. \tag{3.44}$$

In this analysis, therefore, G_{shear} identifies with the shear modulus used in the theory of elasticity. At this point, we have not related strain to displacement, or demanded that G_{shear} be a constant. This allows a broad range of isotropic elastic materials, and does not restrict the description to linear behaviour.

However, when we apply additional constraints such as not allowing for residual stress or demanding that G_{shear} not be a function of strain or stress, we can retrieve the linear expression,

$$\vec{\vec{\tau}} = -2G_{\text{shear}} \vec{\vec{\epsilon}}'. \tag{3.45}$$

The local deformation equilibrium condition, under the specific restrictions of isotropy and linearity, reduces to the classical Hooke's law expression, providing another definition for the Eulerian strain. This can be viewed as an alternate approach to hyperelasticity where a constitutive form for strain energy is not postulated at the outset.

The symmetric thermal deformation $\vec{\vec{\mathrm{A}}}'_D$ and partial-molar deformation $\overline{\vec{\vec{V}}}'_i$ tensors, appearing in equation 3.43, are defined such that they have zero trace and commute with the deformation-strain tensor, *i.e.*, let

$$\vec{\vec{\mathrm{A}}}'_D = (\vec{\vec{\mathrm{A}}}'_D)^{\mathrm{T}}, \quad \mathrm{tr}(\vec{\vec{\mathrm{A}}}'_D) = 0, \quad \text{and} \quad \vec{\vec{\mathrm{A}}}'_D \cdot \vec{\vec{\epsilon}}' = \vec{\vec{\epsilon}}' \cdot \vec{\vec{\mathrm{A}}}'_D, \tag{3.46}$$

$$\overline{\vec{\vec{V}}}'_i = (\overline{\vec{\vec{V}}}'_i)^{\mathrm{T}}, \quad \mathrm{tr}(\overline{\vec{\vec{V}}}'_i) = 0, \quad \text{and} \quad \overline{\vec{\vec{V}}}'_i \cdot \vec{\vec{\epsilon}}' = \vec{\vec{\epsilon}}' \cdot \overline{\vec{\vec{V}}}'_i. \tag{3.47}$$

These characteristics respectively ensure that $\vec{\vec{\mathrm{A}}}'_D$ and $\overline{\vec{\vec{V}}}'_i$ are diagonalizable, have at most two independent principal values respectively, and are diagonalised by the same

rotation tensor that diagonalises $\vec{\vec{\epsilon}}'$. Since this rotation also diagonalises $\vec{\vec{\tau}}$ (*cf.* the 'Mechanical principles' item in the Thermodynamics section), it follows that

$$\vec{\vec{\mathrm{A}}}'_D : \vec{\vec{\tau}} = (2\mathrm{A}_1 + \mathrm{A}_2)\,\tau_1 + (\mathrm{A}_1 + 2\mathrm{A}_2)\,\tau_2, \tag{3.48}$$

where A_1 and A_2 are the independent principal values of $\vec{\vec{\mathrm{A}}}'_D$ in the corresponding principal directions of $\vec{\vec{\tau}}$. The entries of $\vec{\vec{\mathrm{A}}}'_D$ are fully specified by defining

$$\mathrm{A}_1 = \tfrac{1}{3}\,(2\alpha_{D_1} - \alpha_{D_2}) \quad \text{and} \quad \mathrm{A}_2 = \tfrac{1}{3}\,(-\alpha_{D_1} + 2\alpha_{D_2})\,. \tag{3.49}$$

In short, given the principal axes of deformation strain and the coefficients of thermal deformation coincide, the thermal deformation tensor is formed by the similarity transformation

$$\vec{\vec{\mathrm{A}}}'_D = \vec{\vec{Q}}^{\mathrm{T}}_{\epsilon'} \cdot \vec{\vec{d}}_A \cdot \vec{\vec{Q}}_{\epsilon'}, \text{ where } \vec{\vec{d}}_A = \alpha_{D1}\vec{e}_1 \otimes \vec{e}_1 + \alpha_{D2}\vec{e}_2 \otimes \vec{e}_2 - \tfrac{1}{3}\,(\alpha_{D1} + \alpha_{D2})\,\vec{\vec{I}}. \tag{3.50}$$

The rotations here can also be extracted from deformation stress, Cauchy stress, *etc.*, because the principal axes of these quantities coincide. For example, $\vec{\vec{Q}}_{\epsilon'} = \vec{\vec{Q}}_{\tau}$. An analogous process can be followed for the molar deformation tensor $\vec{\vec{\overline{V}}}'_i$ to obtain

$$\vec{\vec{\overline{V}}}'_i = \vec{\vec{Q}}^{\mathrm{T}}_{\epsilon'} \cdot \vec{\vec{d}}_{\overline{V}_i{}'} \cdot \vec{\vec{Q}}_{\epsilon'}, \text{ where } \vec{\vec{d}}_{\overline{V}'_i} = \overline{V}'_{1i}\vec{e}_1 \otimes \vec{e}_1 + \overline{V}'_{2i}\vec{e}_2 \otimes \vec{e}_2 - \tfrac{1}{3}\left(\overline{V}'_{1i} + \overline{V}'_{2i}\right)\vec{\vec{I}}. \tag{3.51}$$

3.1.2.3 Entropic Equation of State

From the thermodynamic standpoint, a phase's entropy S can be treated similarly to its volume. Individual species' contributions to S are quantified by defining partial molar entropies $\overline{S}_i$; these relate to electrochemical potentials through the Maxwell relation

$$\overline{S}_i = \left(\frac{\partial S}{\partial n_i}\right)_{T,p,\tau_1,\tau_2,n_{j\neq i}} = -\left(\frac{\partial \mu_i}{\partial T}\right)_{p,\tau_1,\tau_2,n_j}. \tag{3.52}$$

Unlike $\overline{V}_i$, $\overline{S}_i$ may vary with the deformation stress.

With the domain of the Gibbs function specified as described in the paragraphs preceding equation 3.13, the definition of entropy through a temperature derivative in equation 3.17 shows in combination with equations 3.20 and 3.52 that

$$S = \sum_i \overline{S}_i n_i. \tag{3.53}$$

Thus entropy can be allocated to various species in the same way as the Gibbs energy and the volume.

For a system based in the Gibbs function, entropy can be obtained through temperature derivatives of G, and must consequently depend on the same basis of state variables: $S\left(T, p, \tau_1, \tau_2, \{n_i\}_n\right)$. The total differential of entropy can therefore be written as

$$dS = \frac{C_p}{T} dT - V\alpha_V dp - V\alpha_{D_1} d\tau_1 - V\alpha_{D_2} d\tau_2 + \sum_i \overline{S}_i dn_i. \tag{3.54}$$

This includes the familiar constant-pressure heat capacity, defined as

$$C_p = T\left(\frac{\partial S}{\partial T}\right)_{p,\tau_1,\tau_2,n_i}. \tag{3.55}$$

The material properties α_V, α_{D_1}, and α_{D_2} defined by equations 3.32 and 3.38 arise in equation 3.54 through

$$\left(\frac{\partial V}{\partial T}\right)_{p,\tau_1,\tau_2,n_i} = -\left(\frac{\partial S}{\partial p}\right)_{T,\tau_1,\tau_2,n_i} \quad \text{and} \quad \left(\frac{\partial D_i}{\partial T}\right)_{p,\tau_1,\tau_2,n_j} = -\left(\frac{\partial S}{\partial \tau_i}\right)_{T,p,\tau_{j\neq i},n_k}, \tag{3.56}$$

which are Maxwell relations that connect the strain state to entropy.

Equation 3.54 differs from the other thermodynamic relationships in that the terms associated with mechanical forces do not involve products of the principal deformation stress and principal deformation volume. To allow the concise formulation of dynamical balances later on, it will be convenient to embody the information contained in properties α_{D_1} and α_{D_2} into a tensor quantity, which we will call the thermal deformation tensor $\vec{\vec{\mathrm{A}}}'_D$.

3.1.3 Gibbs–Duhem Relations

A canonical Gibbs–Duhem equation arises directly from the Gibbs function, by combining the first law from equation 3.22 with the total differential of equation 3.20 to get

$$\sum_i n_i d\mu_i = -SdT + Vdp + V\vec{\vec{\epsilon}}' : d\vec{\vec{\tau}}. \tag{3.57}$$

This equation shows how thermodynamic-property gradients associated with diffusion may result in mechanical forces. (One phenomenon illustrating this connection is osmotic pressure, which arises from chemical-potential differences induced by variations in composition.) Thermodynamic mechanical forces are identified *via* the procedure of Hirschfelder, Curtiss, and Bird [93]. The spatial variations of intensive properties in each direction are taken to satisfy the differential relationship established by Gibbs–Duhem equation 3.57. After introducing the Euler equation for entropy from equation 3.53, then dividing both sides by V, one can identify a thermodynamic force $\vec{d}_i$ acting on a species i, with units of force per volume,

$$\vec{d}_i = -c_{\mathrm{T}} y_i \left[\vec{\nabla}\mu_i + \overline{S}_i \vec{\nabla} T - \frac{\overline{m}_i}{\rho} \left(\vec{\nabla} p + \vec{\vec{\epsilon}}' : \vec{\nabla}\vec{\vec{\tau}} \right) \right]. \tag{3.58}$$

This equation is recalled in key derivations during the course of this chapter to relate the changes in various intensive properties for a given species. Further, this definition recasts the Gibbs–Duhem equation as

$$\sum_i \vec{d}_i = \vec{0}. \tag{3.59}$$

The local balance of thermodynamic forces on individual species can be viewed as a statement of Newton's third law of motion for systems in microscopic equilibrium [132].

Insertion of equation 3.27 into equation 3.31 reveals that partial molar volumes satisfy a Gibbs–Duhem equation

$$c_{\mathrm{T}} \sum_i y_i d\overline{V}_i = \alpha_V dT - \frac{1}{K} dp, \tag{3.60}$$

showing that partial molar volumes have no natural dependence on deformation stress. This result can be applied in various ways: the relations

$$\sum_i y_i \frac{\partial \overline{V}_i}{\partial t} = \frac{\alpha_V}{c_{\mathrm{T}}} \frac{\partial T}{\partial t} - \frac{1}{K c_{\mathrm{T}}} \frac{\partial p}{\partial t} \quad \text{and}$$

$$\vec{\nabla} \overline{V}_n = -\sum_{i \neq n} \frac{y_i}{y_n} \vec{\nabla} \overline{V}_i + \frac{\alpha_V}{c_{\mathrm{T}} y_n} \vec{\nabla} T - \frac{1}{K c_{\mathrm{T}} y_n} \vec{\nabla} p \tag{3.61}$$

are both useful. Equations 3.27 and 3.60 can also be used in combination with equation 3.30 to show that

$$0 = -\alpha_V dT + \frac{1}{K} dp - \sum_i \overline{V}_i d\left(c_{\mathrm{T}} y_i\right), \tag{3.62}$$

which expresses how changes in temperature, pressure, and intensive composition variables are linked.

Analogous to a Gibbs–Duhem equation on partial molar volumes, we get the following equation of partial molar deformations by inserting equation 3.34 into equation 3.43,

$$c_{\mathrm{T}} \sum_i y_i d\vec{\vec{\overline{V}}}'_i = \vec{\vec{\mathrm{A}}}'_D dT - \frac{3}{2} \frac{1}{G_{\mathrm{shear}}} d\vec{\vec{\tau}} \tag{3.63}$$

This can be further simplified by inserting equation 3.35 into equation 3.63:

$$-3 d\vec{\vec{\epsilon}}' = -\vec{\vec{\mathrm{A}}}'_D dT + \frac{3}{2} \frac{1}{G_{\mathrm{shear}}} d\vec{\vec{\tau}} - \sum_i \vec{\vec{\overline{V}}}'_i d\left(c_{\mathrm{T}} y_i\right). \tag{3.64}$$

This is a wholly new and interesting result which relates the change in equilibrium deformation of the solid system given the changes in the associated intensive variables—temperature, deformation stress, and composition. Equations 3.62 and 3.64 are interesting to look at together because they provide the total elastic effects, compressive as well as deformational, brought about by changes in any intensive variable.

Last, equations 3.53, 3.54, 3.48, and 3.50 can be combined to get a Gibbs–Duhem equation

$$\sum_i n_i d\overline{S}_i = \frac{C_p}{T} dT - V\alpha_V dp - V\vec{\vec{\mathrm{A}}}'_D : d\vec{\vec{\tau}}, \tag{3.65}$$

which derives from the system entropy.

3.1.3.1 Consequences of Gibbs–Duhem Relations

Pressure Dependence of Partial Molar Volumes.—If external pressure p is increased on a system, thereby compressing the volume, the total concentration c_T will increase provided the total number of moles remain unchanged in this process. The volumetric equation of state, equation 3.30, illustrates that partial molar volumes $\overline{V}_i$ are required to depend on pressure to be consistent with this change in c_T (y_i's are independent of pressure). We postulate that this pressure dependence is the same for all species,

$$\overline{V}_i = \overline{V}_i^{\mathrm{ref}} f_p, \tag{3.66}$$

leading to the following form of the equation of state,

$$f_p \sum_i c_\mathrm{T} y_i \overline{V}_i^{\mathrm{ref}} = 1. \tag{3.67}$$

Differentiating this equation, and combining it with the isothermal Gibbs–Duhem equation, equation 3.60, we obtain

$$\frac{df_p}{f_p} = -\frac{1}{K} dp. \tag{3.68}$$

Integrating this from a reference state ($p^{\mathrm{ref}}, f_p^{\mathrm{ref}} = 1$) to an arbitrary state (p, f_p), and assuming that K is constant with pressure, we obtain the pressure dependence of partial molar volumes as,

$$\overline{V}_i = \overline{V}_i^{\mathrm{ref}} \exp\left(-\frac{p - p^{\mathrm{ref}}}{K}\right). \tag{3.69}$$

This makes the following assertion: under increased pressure the change in total volume made by the addition of a mole of any species is less than what it would be

under the reference pressure. Finally, the volumetric equation of state can be written with an explicit pressure dependence as follows,

$$c_{\mathrm{T}}\left(\sum_i \overline{V}_i^{\mathrm{ref}} y_i\right)\exp\left(-\frac{p-p^{\mathrm{ref}}}{K}\right)=1. \tag{3.70}$$

Deformation Stress Dependence of Partial Molar Deformation Volumes.—Analogous to the previous section, based on the deformational equation of state, equation 3.35, we postulate that the partial molar deformation volumes will have to provide any stress functionality. Assuming that this dependence is the same for all the species and directions,

$$\overline{V}'_{i,jk}=\overline{V}'^{\mathrm{ref}}_{i,jk}\ f_\tau, \tag{3.71}$$

leading to the following form of the deformational equation of state, written out in the component form,

$$3\epsilon'_{jk}=f_\tau\sum_i \overline{V}'^{\mathrm{ref}}_{i,jk}c_{\mathrm{T}}y_i. \tag{3.72}$$

Consider the component form of the isothermal Gibbs–Duhem equation for deformation, equation 3.63, combined with equations 3.71 and 3.72,

$$d\tau_{jk}=-\left(2G_{\mathrm{shear}}\epsilon'_{jk}\right)d\ln f_\tau. \tag{3.73}$$

Further, equation 3.45 implies that at constant temperature and composition, Hooke's law $\tau_{jk}=-2G_{\mathrm{shear}}\epsilon'_{jk}$ returns

$$d\ln f_\tau=d\ln\tau_{jk}\Rightarrow f_\tau\propto\tau_{jk}. \tag{3.74}$$

The deformational EOS can therefore be interpreted as a version of Hooke's law where $\epsilon'_{jk}\propto f_\tau\propto\tau_{jk}$ with a composition dependent constant of proportionality, implying

$$c_{\mathrm{T}}\sum_i \overline{V}'^{\mathrm{ref}}_{i,jk}y_i\propto\frac{1}{G_{\mathrm{shear}}}. \tag{3.75}$$

3.1.4 Beyond Gibbs Energy: Internal Energy and Enthalpy

From the standpoint of irreversible thermodynamics, the constitutive laws for transport derive from inspection of the local entropy generation within a nonequilibrated material. In developing this balance one must consider the distribution of total energy, which includes additional information beyond that described by the available energy function G. Two quantities that are useful in the Energy Balances section below are the enthalpy, H, which relates to G through the Legendre transformation

$$H = G + TS, \tag{3.76}$$

and the internal energy U, defined as

$$\begin{aligned} U &= G + TS - pV - \tau_1 D_1 - \tau_2 D_2 \\ &= G + TS - pV - V\vec{\vec{\epsilon}}' : \vec{\vec{\tau}}. \end{aligned} \tag{3.77}$$

Terms associated with deformation have been included in the Legendre transformation from G to U. Taking total derivatives of both sides of equation 3.77 and inserting equation 3.21 shows that

$$dU = TdS - pdV - \tau_1 dD_1 - \tau_2 dD_2 + \sum_i \mu_i dn_i, \tag{3.78}$$

which provides a statement of the first law that associates an extensive quantifier (entropy, volume, deformation volume, and species molar content) with every distinct mode of energy exchange (thermal, compressive, deformational, and chemical, respectively).

3.1.4.1 Specific Internal Energy, Volume, and Entropy

Unlike the intensive variables on which G depends, the basis variables in equation 3.78 can be accounted in terms of accumulation, flux, and generation; the dynamics of

how extensive properties are distributed is readily described by balance equations. In locally inhomogeneous systems, extensive-property balances are stated as differential equations that govern the densities of the properties, *i.e.*, their amounts per unit of system volume.

Energy is carried by massive particles that occupy volume, rather than being a property of the volume itself, so it is convenient to refer extensive-property densities to mass. The total mass of a system is designated by the symbol m_{T}; mass is commonly understood to be independent of temperature, pressure, and deformation stress. Total mass does depend on system composition, however, relating to species molar contents through

$$dm_{\mathrm{T}} = \sum_i \overline{m}_i dn_i, \qquad \text{or} \qquad m_{\mathrm{T}} = \sum_i \overline{m}_i n_i, \tag{3.79}$$

where $\overline{m}_i$ is the molar mass of species i. (Formally $\overline{m}_i$ is a partial molar property, explaining its notation here.) The molecular hypothesis essentially states that species masses relate uniquely to their molar contents, through $m_i = \overline{m}_i n_i$, and that, for any given species i, $\overline{m}_i$ is a constant independent of temperature, stress, and composition. Both total mass and the individual species masses are extensive.

With the total mass in hand, one can define the mass density ρ as

$$\rho = \frac{m_{\mathrm{T}}}{V} = c_{\mathrm{T}} \left[\overline{m}_n + \sum_{i \neq n} (\overline{m}_i - \overline{m}_n) y_i \right], \tag{3.80}$$

an intensive property. Owing to the property dependence of c_{T} established by the volumetric equation of state and the constancy of molar masses, the density proves to be determined by only temperature, pressure, and composition: $\rho = \rho(T, p, \{y_i\}_{n-1})$. Moreover, the quotient ρ/c_{T}, which identifies with the total molar mass $\overline{m}$,

$$\frac{\rho}{c_{\mathrm{T}}} = \overline{m} = \frac{m_{\mathrm{T}}}{n_{\mathrm{T}}} = \overline{m}_n + \sum_{i \neq n} (\overline{m}_i - \overline{m}_n) y_i, \tag{3.81}$$

depends on composition alone.

Any extensive property can be expressed per unit of system mass to produce an intensive property. Quantities normalized in this way are referred to as 'specific' properties, and notated with a carat. For instance, specific internal energy can be written in various ways:

$$\hat{U} = \frac{U}{m_{\mathrm{T}}} = \frac{U}{\rho V} = \frac{\overline{U}}{\overline{m}} = \frac{c_{\mathrm{T}}\overline{U}}{\rho}, \tag{3.82}$$

and specific volume equals inverse mass density, $\hat{V} = 1/\rho$. Note that the internal energy per unit volume can be written either as $\rho\hat{U}$ or $c_{\mathrm{T}}\overline{U}$.

A form of the first law involving specific internal energy can be derived as follows. Use equations 3.77 and 3.20 to express the total internal energy in terms of the state variables. Then divide this relation by m_{T} and apply equation 3.82 to get an expression for $\hat{U}$ in terms of fundamental intensive variables and the specific versions of their extensive conjugates. Take a total differential, then eliminate the differential intensive properties using Gibbs–Duhem equation 3.57 divided by m_{T}. Finally, insert $\hat{V} = 1/\rho$ and $\hat{n}_i = c_{\mathrm{T}} y_i/\rho$, then use equations 3.10 and 3.12 to show that

$$\rho d\hat{U} = T\rho d\hat{S} + \left(p + \vec{\vec{\tau}} : \vec{\vec{\epsilon}}'\right) d\ln\rho - \vec{\vec{\tau}} : d\vec{\vec{\epsilon}}' + c_{\mathrm{T}} \sum_i \mu_i y_i \left[d\ln\left(c_{\mathrm{T}} y_i\right) - d\ln\rho\right]. \tag{3.83}$$

This result is needed when deriving the dynamical form of the second law in the Energy Balances section. Because the equation contains $\hat{S}$, a state variable that is hard to control, some further analysis is still helpful.

In particular, it is useful to have a form of equation 3.83 wherein the entropy dependence is eliminated in favor of dependences on composition, temperature, and stress, which can be produced as follows. Put equation 3.53 in terms of specific quantities by dividing both sides by m_{T}; take a total differential of this result and use equation 3.65 to eliminate partial-molar-entropy changes. Thus

$$\rho d\hat{S} = \frac{\rho\hat{C}_p}{T} dT - \alpha_V dp - \vec{\vec{\mathrm{A}}}'_D : d\vec{\vec{\tau}} + c_{\mathrm{T}} \sum_i \overline{S}_i y_i \left[d\ln\left(c_{\mathrm{T}} y_i\right) - d\ln\rho\right], \tag{3.84}$$

which incorporates the thermal deformation tensor defined by equation 3.50. Equations 3.84 and 3.83 combine to produce an expression for internal-energy change that does not explicitly include the entropy:

$$\rho d\hat{U} = \rho\hat{C}_p dT + \left(p + \vec{\vec{\tau}} : \vec{\vec{\epsilon}}'\right) d\ln\rho - \vec{\vec{\tau}} : d\vec{\vec{\epsilon}}' - T\alpha_V dp \\ - T\vec{\vec{\mathrm{A}}}'_D : d\vec{\vec{\tau}} + c_{\mathrm{T}} \sum_i \overline{H}_i y_i \left[d\ln\left(c_{\mathrm{T}} y_i\right) - d\ln\rho\right]. \quad (3.85)$$

This final result of thermodynamic analysis is key to the derivation of the heat equation in the Energy Balances section below.

3.2 Material Balances

The macroscopic description of local dynamics within an n-ary phase begins with statements of local balance equations that express how the local time variations of properties connect to their flow. These conservation laws introduce the notions that systems change transiently and that properties differ from place to place. The most elementary expressions of continuity are universal, in the sense that the governing equations hold regardless of the particular material in question. Dynamical continuity equations complement the thermodynamic information in G and are of equivalent fundamental importance.

Material is the most basic conserved quantity. In multicomponent transport systems one must consider that each individual species within a phase obeys a continuity equation, as well as the phase as a whole. This section shows how the equations that locally express the continuity of volume, charge, and mass can be derived by combining species material balances with thermodynamic and electrical state equations. In many cases it is convenient to replace one or more of the n species balances in an n-ary system with one of these broader laws of continuity.

3.2.1 Molar Species Continuity

The most basic governing equations Newman uses to express the local balances of material can be written as

$$\frac{\partial c_{\mathrm{T}} y_i}{\partial t} = -\vec{\nabla} \cdot \vec{N}_i, \tag{3.86}$$

where $\vec{N}_i$ is a spatial vector representing the total molar flux of species i relative to an inertial reference frame.[1] (Recall that $c_i = c_{\mathrm{T}} y_i$.) Each constituent i within an n-ary phase obeys a local material balance in the form of equation 3.86. The set of these continuity laws and the set of molar fluxes are both n-tuples, *e.g.*, $\left\{\vec{N}_i\right\}_n$.

It is also sometimes convenient to speak in terms of velocities, rather than fluxes. These can be extracted from molar fluxes through

$$\vec{N}_i = c_{\mathrm{T}} y_i \vec{v}_i, \tag{3.87}$$

which introduces a species velocity $\vec{v}_i$ (*i.e.*, a weighted average of individual particle velocities over all particles of type i in a volume element). The set of species velocities is also an n-tuple, $\{\vec{v}_i\}_n$.

3.2.2 Volume Continuity

Alongside c_{T} — a thermodynamic variable associated with the static volume a material occupies — it is useful to have a dynamic variable that describes how material carries volume with it as it moves. The volume-average velocity, defined as

$$\vec{v}^{\square} = \sum_i \overline{V}_i \vec{N}_i = \sum_i \phi_i \vec{v}_i, \tag{3.88}$$

[1] Homogeneous generation of material has been neglected in equation 3.86 for simplicity. To include generation of material by homogeneous processes, equation 3.86 can be extended to read

$$\frac{\partial c_{\mathrm{T}} y_i}{\partial t} = -\vec{\nabla} \cdot \vec{N}_i + R_i,$$

where R_i quantifies the generation rate of species i in moles per volume per time.

provides an elementary kinematic quantity useful to establish a local description of how a material moves in total relative to an inertial frame of reference.

A macroscopic volume balance can be derived by taking the partial time derivative of equation 3.62, then using the material balances from equation 3.86 to eliminate terms with $\partial(c_{\mathrm{T}} y_i)/\partial t$. Application of the vector identity $\vec{\nabla}\cdot(s\vec{v}) = s\vec{\nabla}\cdot\vec{v} + \vec{v}\cdot\vec{\nabla}s$ then yields

$$\frac{1}{K}\frac{\partial p}{\partial t} - \alpha_V \frac{\partial T}{\partial t} = -\vec{\nabla}\cdot\vec{v}^{\square} + \sum_i \vec{N}_i \cdot \vec{\nabla}\overline{V}_i. \tag{3.89}$$

The strategy used to derive this result was first presented by Newman and Chapman, whose analysis of restricted diffusion produced a volume balance for isothermal, isobaric binary electrolytes [133]. Note that one can reduce the range of the summation on the right of equation 3.89 by applying the spatial identity given in equation 3.61. It is often convenient to replace one of the n local material balances with volume continuity, particularly when modelling systems where T and p are both constant.

3.2.3 Charge Continuity

Particle numbers can be connected to total charge, as well as total volume. Charge is an extensive quantity; the excess charge density

$$\rho_{\mathrm{e}} = F c_{\mathrm{T}} \sum_i z_i y_i, \tag{3.90}$$

where z_i stands for the equivalent charge carried by species i and F is Faraday's constant, provides an intensive description of the static electrical state. The current density $\vec{i}$ provides a dynamic variable describing charge flow, connected to molar fluxes through Faraday's law:

$$\vec{i} = F \sum_i z_i \vec{N}_i. \tag{3.91}$$

Multiplying equation 3.86 by $F z_i$, then summing over all species and incorporating equations 3.90 and 3.91, yields an equation that describes the local balance of charge.

Thus, if definitions 3.90 and 3.91 are adopted, and if at least one species in a system carries a nonzero equivalent charge, one of the material balances can be replaced with

$$\frac{\partial \rho_{\mathrm{e}}}{\partial t} = -\vec{\nabla} \cdot \vec{i}, \tag{3.92}$$

which expresses charge continuity. It is common when analyzing electrochemical systems to simplify the set of material balances by replacing one of them with the charge balance.

3.2.4 Mass Continuity

One quantity that has not yet been discussed is the species mass density, defined as

$$\rho_i = \overline{m}_i c_i = c_{\mathrm{T}} \overline{m}_i y_i. \tag{3.93}$$

This can also be used to identify the mass fraction of species i,

$$\omega_i = \frac{\rho_i}{\rho} = \frac{c_{\mathrm{T}} y_i \overline{m}_i}{\rho}, \tag{3.94}$$

a composition variable that, like y_i, is constrained such that $\sum_i \omega_i = 1$. Equation 3.81 can be inserted into equation 3.94 to show that species mass fractions are similar to particle fractions in that they do not vary with temperature or stress.

The total mass flux provides a dynamic variable that can be associated with convective flow of material, but it is more common to employ the mass-average velocity $\vec{v}$. This velocity is embedded in the mass flux $\rho\vec{v}$ and relates to species fluxes as

$$\rho\vec{v} = \sum_i \overline{m}_i \vec{N}_i = \sum_i \rho_i \vec{v}_i, \quad \text{or} \quad \vec{v} = \sum_i \frac{\overline{m}_i \vec{N}_i}{\rho} = \sum_i \omega_i \vec{v}_i. \tag{3.95}$$

Here the last equalities follow from the species velocity defined in equation 3.87; $\rho_i \vec{v}_i$ represents the mass flux associated with the motion of species i.

Multiplication of both sides of equation 3.86 by $\overline{m}_i$ illustrates the continuity of individual species masses,

$$\frac{\partial \rho_i}{\partial t} = -\vec{\nabla} \cdot (\rho_i \vec{v}_i), \tag{3.96}$$

and summing this result across all n species demonstrates overall mass continuity,

$$\frac{\partial \rho}{\partial t} = -\vec{\nabla} \cdot (\rho \vec{v}). \tag{3.97}$$

Thus the elementary 'continuity equation' from fluid mechanics derives from the n material balances, and necessarily involves the mass-average velocity $\vec{v}$.

3.2.5 Change of Composition and Flux Bases

It should be emphasized that the n species balances expressed in the form of equation 3.86 involve only $n-1$ primary scalar composition variables — and that specifying the composition $\{y_i\}_{n-1}$ suffices to determine uniquely any choice of intensive composition variables (mass fractions, volume fractions, species molalities, species molarities, species mass densities, *etc.*) at fixed T and p.

In combination with the particle-fraction sum from equation 3.15, the discussions of the volumetric equation of state, specific volume, and charge continuity above have put forward definitions that establish c_{T}, ρ, and ρ_{e} as functions of T, p, and $\{y_i\}_{n-1}$. In the analysis of some transport problems, it may be convenient to invert the state equations for c_{T}, ρ, or ρ_{e} to exchange one of the concentrations that makes up the composition basis for the molar, mass, or charge density. For example, Newman used this strategy to solve the Poisson–Nernst–Planck equations in his analysis of current flow in polarized diffuse double layers, replacing one of the species concentrations with ρ_{e} [1].

Similarly, there are only n primary flux variables in the n species balances, equations 3.86. In some cases it is convenient to use the current density $\vec{i}$ or a bulk velocity, say, $\vec{v}^{\,\square}$, in place of one of the molar fluxes $\vec{N}_i$.

3.2.6 Convective Velocities and Excess Fluxes

Continuity equation 3.97 is often written in a Lagrangian frame, by incorporating a convective derivative

$$\frac{D}{Dt} = \frac{\partial}{\partial t} + \vec{v} \cdot \vec{\nabla}, \tag{3.98}$$

whence vector identities can be used to show that

$$\frac{D\rho}{Dt} = -\rho \vec{\nabla} \cdot \vec{v}. \tag{3.99}$$

The definition in equation 3.98 implicitly assumes that the mass-average velocity $\vec{v}$ is the correct choice of reference velocity for convection. In fact a variety of reference velocities is available, and it is worth generally developing the many ways one can parse convective contributions to the molar flux $\vec{N}_i$.

Only the part of species motion that is in excess of some 'bulk flow velocity' $\vec{v}^{\psi}$ should be associated with dissipative modes of mass transport (diffusion, migration, *etc.*). One can define the excess molar flux of i relative to $\vec{v}^{\psi}$ as

$$\vec{J}_i^{\psi} = \vec{N}_i - c_{\mathrm{T}} y_i \vec{v}^{\psi} \tag{3.100}$$

to produce a set of fluxes that isolate non-convective phenomena and are therefore more natural for the formulation of transport constitutive laws.

There is some ambiguity in the definition of the 'bulk flow velocity'. The convention used when defining substantial derivatives suggests $\vec{v}$, but we have already seen another viable candidate — the volume-average velocity $\vec{v}^{\square}$ — and there are many more, including familiar examples like the mole-average velocity [94], and less familiar ones like the enthalpy-average velocity, which Hirschfelder *et al.* suggest might be a natural reference for heat convection [93]. Every reference velocity is defined through a sum of the form

$$\vec{v}^{\psi} = \sum_i \psi_i \vec{v}_i = \sum_i \frac{\psi_i}{c_{\mathrm{T}} y_i} \vec{N}_i; \tag{3.101}$$

if one calls $\vec{v}^{\psi}$ the 'ψ-average velocity', then one understands ψ_i to be an n-tuple of variables defined in terms of masses or equilibrium properties that follow from the Gibbs function; these variables should also be 'fractional', in the sense that they are constrained by a relation

$$\sum_i \psi_i = 1. \tag{3.102}$$

For instance, if one identifies the fractional variable as the mass fraction, $\omega_i \to \psi_i$, then equation 3.101 defines the mass-average velocity $\vec{v}$; if it is identified as the species volume fraction, $\phi_i \to \psi_i$, the equation defines the volume-average velocity $\vec{v}^{\square}$; one can also identify the mole-average velocity $\vec{v}^{*}$ by making the substitution $y_i \to \psi_i$, or the enthalpy-average velocity $\vec{v}^{h}$ by $c_{\mathrm{T}}\overline{H}_i y_i/\rho\hat{H} \to \psi_i$.

The choice of reference velocity generally constrains the n-tuple of excess fluxes relative to that velocity. Equations 3.100 and 3.101 can be combined to yield

$$\sum_i \frac{\psi_i \vec{J}_i^{\psi}}{c_{\mathrm{T}} y_i} = \vec{0}, \tag{3.103}$$

a kinematic relation showing that only $n-1$ of the n excess fluxes relative to $\vec{v}^{\psi}$ are independently variable.

In some sense, the particular choice of convective velocity is immaterial, since the difference between any two reference velocities can be determined from either independent set of excess fluxes. For reference velocities $\vec{v}^{\psi}$ and $\vec{v}^{\psi'}$ based on fractions ψ_i and ψ'_i, the relations

$$\vec{v}^{\psi'} - \vec{v}^{\psi} = \sum_{i \neq n} \left(\frac{\psi'_i}{\psi_i} - \frac{\psi'_n}{\psi_n} \right) \frac{\psi_i \vec{J}_i^{\psi}}{c_{\mathrm{T}} y_i} = \sum_{i \neq n} \left(\frac{\psi_n}{\psi'_n} - \frac{\psi_i}{\psi'_i} \right) \frac{\psi'_i \vec{J}_i^{\psi'}}{c_{\mathrm{T}} y_i} \tag{3.104}$$

follow directly from fraction-sum 3.102 and kinematic relation 3.103. One can use this difference to show that

$$\vec{J}_i^{\psi} = \sum_{j \neq n} \left[\delta_{ij} + \left(\frac{\psi_n}{\psi'_n} - \frac{\psi_j}{\psi'_j} \right) \frac{\psi'_j y_i}{y_j} \right] \vec{J}_j^{\psi'}, \tag{3.105}$$

which is an invertible, homogeneous transformation that can be used to convert any set of independent excess fluxes into any other. Monroe and Newman have shown that linear transformations of this type preserve the symmetry of the Onsager reciprocal relation in transport constitutive laws of the Stefan–Maxwell form [7], emphasizing that no particular choice of excess fluxes needs be made when developing constitutive laws for transport.

In the discussion of momentum it will be convenient to introduce a particular set of excess fluxes. We will use the set of molar fluxes relative to the mass-average velocity,

$$\vec{J}_i = c_{\mathrm{T}} y_i \left(\vec{v}_i - \vec{v} \right), \tag{3.106}$$

which are constrained by a kinematic relation

$$\sum_i \overline{m}_i \vec{J}_i = \vec{0}, \tag{3.107}$$

but wish to emphasize that this choice is purely one of convenience. In particular, these excess fluxes preserve the standard definition of the substantial derivative, allowing one to write the familiar expression

$$\frac{D c_{\mathrm{T}} y_i}{Dt} = -\vec{\nabla} \cdot \vec{J}_i - c_{\mathrm{T}} y_i \vec{\nabla} \cdot \vec{v} \tag{3.108}$$

for the balance of species i in a frame following the bulk motion of the material.

3.3 Momentum Balance

An overall local momentum balance accounts for how external forces drive material motion. When deriving this balance, which is typically expressed for pure phases by the Cauchy equation, it is not so clear what convective velocity should be involved. (This issue received substantial attention from Brenner in the early 2000s [134].) By

starting with species material balances above, the mass-average velocity $\vec{v}$ was successfully identified as the relevant velocity in the traditional mass-continuity equation. A similar tack will be taken here, and the total momentum balance will be derived by combining individual species momentum balances, which avoids giving precedence to a particular bulk velocity.

3.3.1 Momentum Continuity

As well as being the mass flux of i, $\rho_i \vec{v}_i = \overline{m}_i \vec{N}_i$ represents the contribution that species i makes to the local momentum density.[2] Momentum continuity for an individual species in a phase can then be expressed as

$$\frac{\partial \rho_i \vec{v}_i}{\partial t} = -\vec{\nabla} \cdot \left(\omega_i \vec{\vec{\sigma}}_{\mathrm{t}} + \rho_i \vec{v}_i \otimes \vec{v}_i \right) + \vec{f}_i + \vec{b}_i. \tag{3.109}$$

Total stress $\vec{\vec{\sigma}}_{\mathrm{t}}$, apportioned among species according to their mass fractions, ω_i in this equation, extends the definition of Cauchy stress $\vec{\vec{\sigma}}$ introduced in the classical thermodynamics sections to include a purely dynamic component, $\vec{\vec{\sigma}}_{\mathrm{dy}}$, in addition to the equilibrium contributions: thermodynamic pressure, p, and the traceless deviatoric stress, $\vec{\vec{\tau}}$,

$$\vec{\vec{\sigma}}_{\mathrm{t}} = \left(p\vec{\vec{I}} + \vec{\vec{\tau}} \right) + \vec{\vec{\sigma}}_{\mathrm{dy}}. \tag{3.110}$$

The dynamic stress component allows the model to account for momentum generation through phenomena which are only relevant in non-equilibrium conditions, such as sound attenuation due to bulk viscosity. This provides additional avenues of momentum dissipation, as explored in the later sections.

[2] Brenner's work suggests that this statement amounts to a physical postulate, which may require additional justification [134]. Here we have left the microscopic definition of $\vec{v}_i$ ambiguous intentionally, with the understanding that an appropriate choice might address Brenner's concerns. For example, choosing a microscopic averaging process such that $\vec{v}_i$ is, in Brenner's terms, a 'volume velocity' of species i may resolve the problem. Of course, this contradicts the usual interpretation of $\vec{v}_i$ as a number-average velocity over all particles of type i.

The only significant deviation from the overall Cauchy momentum balance in the species momentum continuity is the inclusion of the internal force $\vec{f}_i$ which all the other species exert on species i, constrained by

$$\sum_i \vec{f}_i = 0. \tag{3.111}$$

At this point, we do not make any assumptions regarding the specific form of this internal force. The vector $\vec{b}_i$ represents all the body forces imposed on i by external fields not already considered in the Thermodynamics section. Examples of such body forces include gravity and the Lorentz force, both of which are governed by complementary sets of field equations that can be appended to the present model without contradiction.

Summation of equation 3.109 over all species yields an overall momentum balance. Unlike the summation of species material balances, which results in the familiar continuity equation, the overall balance derived from species momenta contains an additional convective term, because

$$\sum_i \rho_i \vec{v}_i \otimes \vec{v}_i = \rho \vec{v} \otimes \vec{v} + \vec{\vec{\Xi}}, \tag{3.112}$$

an identity that can be derived by applying equations 3.106 and 3.107. The diffusion stress $\vec{\vec{\Xi}}$, defined as

$$\vec{\vec{\Xi}} = \sum_i \frac{\overline{m}_i}{c_{\mathrm{T}} y_i} \vec{J}_i \otimes \vec{J}_i, \tag{3.113}$$

accounts for inertia due to excess momentum convection, which exists because species carry momentum with them at $\vec{v}_i$, rather than at the bulk velocity $\vec{v}$. This idea that volume, momentum, energy, and entropy can be carried by mechanisms other than mass convection has been explored extensively by Howard Brenner in his bi-velocity reformulation of transport models [134–136].

In the overall momentum balance, equation 3.111 shows that the contributions of the internal forces vanish; application of mass continuity from equation 3.97, in-

troduction of the convective derivative from equation 3.98, and insertion of equation 3.110 further simplify the sum to

$$\rho \frac{D\vec{v}}{Dt} = -\vec{\nabla} \cdot \left(\vec{\vec{\sigma}}_{\mathrm{t}} + \vec{\vec{\Xi}} \right) + \sum_i \vec{b}_i. \tag{3.114}$$

This looks much like the familiar Cauchy equation, save for the added diffusion stress. It is interesting to note that the form of the diffusion stress term is similar to Reynolds' stress, which is obtained from averaging the momentum balance (Navier–Stokes Equation) over turbulent fluctuations. Several other sources in the literature have arrived at a similar term from summing the species momentum balance over all species [137–141]. However, the preference to comply with the standard form of Cauchy equation led them to postulate that diffusion stress can be combined with the deviatoric part of the Cauchy stress, since both tensors deal with the non-convective part of momentum exchange. For instance, Bearman and Kirkwood [139] assumed that the deviatoric stress is made up of two parts, an intermolecular contribution such as viscous stress, and a kinetic contribution (which identifies with our diffusion stress).

Although the perspective wherein deviatoric Cauchy stress and diffusion stress are grouped together yields a convenient form of the Cauchy equation, it may lead to inconsistencies unless great care is taken when formulating stress constitutive laws. This may not be the case for materials where the deviatoric Cauchy stress does not play a role in classical thermodynamics (for viscous liquids, for instance), and hence does not have a very clear definition at the stage of momentum-continuity formulation.

3.4 Energy Balance

The heat equation ultimately arises as a consequence of the balance of total energy, which is the sum of specific kinetic energy and specific internal energy. Total specific energy $\hat{E}$ can accumulate locally within a material element as a consequence of heat exchange with its surroundings, exchange of mechanical energy with its surroundings, or energy absorption due to the action of external fields:

$$\rho \frac{D\hat{E}}{Dt} = -\vec{\nabla} \cdot \vec{q} - \vec{\nabla} \cdot \left[\left(\vec{\vec{\sigma}}_{\mathrm{t}} + \vec{\vec{\Xi}} \right) \cdot \vec{v} \right] + \vec{v} \cdot \sum_i \vec{b}_i. \tag{3.115}$$

This equation introduces the heat flux $\vec{q}$, whose definition will be refined somewhat in the sequel. Equation 3.115 basically matches the forms used by Hirscshfelder *et al.*, Bird *et al.*, and Gyarmati [93, 94, 137], except that it includes energy gained as a consequence of diffusion stress.

Continuity of kinetic energy is a consequence of the modified Cauchy equation. Dot $\vec{v}$ into both sides of equation 3.114, then identify the specific kinetic energy

$$\hat{K} = \tfrac{1}{2} \vec{v} \cdot \vec{v} \tag{3.116}$$

to show that

$$\rho \frac{D\hat{K}}{Dt} = -\vec{v} \cdot \left[\vec{\nabla} \cdot \left(\vec{\vec{\sigma}}_{\mathrm{t}} + \vec{\vec{\Xi}} \right) \right] + \vec{v} \cdot \sum_i \vec{b}_i. \tag{3.117}$$

Again this expression matches canonical results [94], save for the addition of $\vec{\vec{\Xi}}$.

Subtraction of equation 3.117 from equation 3.115, followed by the recognition that

$$\hat{E} = \hat{U} + \hat{K}, \tag{3.118}$$

yields a balance of internal energy,

$$\rho \frac{D\hat{U}}{Dt} = -\vec{\nabla} \cdot \vec{q} - \left(\vec{\vec{\sigma}}_{\mathrm{t}} + \vec{\vec{\Xi}} \right) : \vec{\nabla} \vec{v}, \tag{3.119}$$

which has been simplified with the tensor identity $\vec{\nabla}\cdot\left(\vec{\vec{u}}\cdot\vec{v}\right)=\vec{v}\cdot\left(\vec{\nabla}\cdot\vec{\vec{u}}\right)+\vec{\vec{u}}:\vec{\nabla}\vec{v}$.

The form of the last term on the right of equation 3.119 can be clarified in several ways. To emphasize that the antisymmetric part of $\vec{\nabla}\vec{v}$ does not contribute to the double dot product, replace $\vec{\nabla}\vec{v}$ with the rate-of-deformation tensor

$$\vec{\vec{\epsilon}}=-\tfrac{1}{2}\left[\vec{\nabla}\vec{v}+(\vec{\nabla}\vec{v})^{\mathrm{T}}\right], \tag{3.120}$$

a quantity familiar from fluid mechanics. In place of the total stress, introduce pressure and deformation stress with equation 3.110, then apply the identity $\vec{\vec{I}}:\vec{\nabla}\vec{v}=\vec{\nabla}\cdot\vec{v}$ to simplify the pressure term. Finally, put the diffusion stress back in terms of fluxes using equation 3.113 and apply tensor identities to obtain

$$\rho\frac{D\hat{U}}{Dt}=-\vec{\nabla}\cdot\vec{q}-p\vec{\nabla}\cdot\vec{v}+\vec{\vec{\tau}}:\vec{\vec{\epsilon}}+\vec{\vec{\sigma}}_{\mathrm{dy}}:\vec{\vec{\epsilon}}+\sum_i\frac{\vec{J}_i}{c_{\mathrm{T}}y_i}\cdot\vec{\vec{\epsilon}}\cdot\overline{m}_i\vec{J}_i. \tag{3.121}$$

It only remains to express the left side of equation 3.121 in terms of thermodynamic basis variables and quantities that describe the elastic state.

Following Hirschfelder *et al.*, use equation 3.85 to express a relationship among the substantial derivatives of the quantities involved, *i.e.*,

$$\begin{aligned}\rho\frac{D\hat{U}}{Dt}=\rho\hat{C}_p\frac{DT}{Dt}+\left(p+\vec{\vec{\tau}}:\vec{\vec{\epsilon}}'\right)\frac{D\ln\rho}{Dt}-\vec{\vec{\tau}}:\frac{D\vec{\vec{\epsilon}}'}{Dt}\\ -T\alpha_V\frac{Dp}{Dt}-T\vec{\vec{\mathrm{A}}}'_D:\frac{D\vec{\vec{\tau}}}{Dt}+c_{\mathrm{T}}\sum_i\overline{H}_iy_i\frac{D(c_{\mathrm{T}}y_i/\rho)}{Dt}.\end{aligned} \tag{3.122}$$

The derivatives of ρ and $c_{\mathrm{T}}y_i$ can be eliminated in favor of flux divergences using equations 3.99 and 3.108, respectively. With this in hand, one can eliminate $D\hat{U}/Dt$ with equation 3.121, after which some straightforward rearrangement gives

$$\begin{aligned}\rho\hat{C}_p\frac{DT}{Dt}=-\vec{\nabla}\cdot\left(\vec{q}-\sum_i\overline{H}_i\vec{J}_i\right)+T\left(\alpha_V\frac{Dp}{Dt}+\vec{\vec{\mathrm{A}}}'_D:\frac{D\vec{\vec{\tau}}}{Dt}\right)\\ +\sum_i\vec{J}_i\cdot\left(\vec{\vec{\epsilon}}\cdot\frac{\overline{m}_i\vec{J}_i}{c_{\mathrm{T}}y_i}-\vec{\nabla}\overline{H}_i\right)+\vec{\vec{\tau}}:\left(\vec{\vec{\epsilon}}+\vec{\vec{\epsilon}}'\vec{\nabla}\cdot\vec{v}+\frac{D\vec{\vec{\epsilon}}'}{Dt}\right)+\vec{\vec{\sigma}}_{\mathrm{dy}}:\vec{\vec{\epsilon}}.\end{aligned} \tag{3.123}$$

A final simplification is provided by recognizing that the heat flux $\vec{q}$ has contributions both from irreversible heat flux — by mechanisms like conduction — and the latent heat carried by excess species fluxes. To separate these, introduce the irreversible heat flux

$$\vec{q}' = \vec{q} - \sum_i \overline{H}_i \vec{J}_i, \tag{3.124}$$

which isolates the flow of heat associated with purely dynamical processes. (Hirschfelder *et al.* introduced $\vec{q}'$ [93]; whereas $\vec{q}$ is the excess enthalpy flux relative to $\vec{v}$, $\vec{q}'$ is the excess enthalpy flux relative to $\vec{v}^h$.)

Putting equations 3.123 and 3.124 together, one achieves a thermal energy balance applicable to elastic, multicomponent materials:

$$\begin{aligned}\rho \hat{C}_p \frac{DT}{Dt} = -\vec{\nabla}\cdot\vec{q}' + T\left(\alpha_V \frac{Dp}{Dt} + \vec{\vec{\mathrm{A}}}'_D : \frac{D\vec{\vec{\tau}}}{Dt}\right) \\ + \sum_i \vec{J}_i \cdot \left(\vec{\vec{\epsilon}}\cdot\frac{\overline{m}_i \vec{J}_i}{c_{\mathrm{T}} y_i} - \vec{\nabla}\overline{H}_i\right) + \vec{\vec{\tau}} : \left(\vec{\vec{\epsilon}} + \vec{\vec{\epsilon}}'\vec{\nabla}\cdot\vec{v} + \frac{D\vec{\vec{\epsilon}}'}{Dt}\right) + \vec{\vec{\sigma}}_{\mathrm{dy}} : \vec{\vec{\epsilon}}.\end{aligned} \tag{3.125}$$

This form of the general heat equation matches the expression given by Bird, Stewart, and Lightfoot [94], save for four differences, three of which arise solely from considering elasticity. Elastic heating can arise from transient changes in deformation stress through $\vec{\vec{\mathrm{A}}}'_D : D\vec{\vec{\tau}}/Dt$; as a consequence of transient changes in deformation strain through $\vec{\vec{\tau}} : D\vec{\vec{\epsilon}}'/Dt$; and, in deformed materials that are transiently compressed or dilated, through $\vec{\vec{\tau}} : \vec{\vec{\epsilon}}'\vec{\nabla}\cdot\vec{v}$.

To get a heat equation that applies to typical fluids (*e.g.* Newtonian fluids, or non-Newtonian fluids with no elasticity in response to shear), one needs only set $\vec{\vec{\mathrm{A}}}'_D = \vec{\vec{0}}$ and $\vec{\vec{\epsilon}}' = \vec{\vec{0}}$ in equation 3.125. In that case the heat equation almost exactly agrees with Bird, Stewart, and Lightfoot's multicomponent heat balance [94]. The only discrepancy in this limit is the term arising from diffusion stress (adjacent to $\vec{\nabla}\overline{H}_i$ in the diffusion term of equation 3.125). Although we are aware of no sources in the literature that consider this source of heat generation, it must be present to ensure

consistency of the individual species momentum balances with the overall momentum balance.

Thermodynamic differentiation of equation 3.76 with n_i shows that partial molar properties are connected by $\mu_i = \overline{H}_i - T\overline{S}_i$. Thus, insertion of equation 3.58 shows that

$$\vec{\nabla}\overline{H}_i = T\vec{\nabla}\overline{S}_i - \frac{\vec{d}_i}{c_{\mathrm{T}} y_i} + \frac{\overline{m}_i}{\rho}\left(\vec{\nabla}p + \vec{\vec{\epsilon}}' : \vec{\nabla}\vec{\vec{\tau}}\right). \tag{3.126}$$

When dotted with $\vec{J}_i$ and summed over all species, the term at the far right vanishes because of kinematic relation 3.107. Thus an equivalent form of the heat equation is

$$\rho\hat{C}_p\frac{DT}{Dt} = -\vec{\nabla}\cdot\vec{q}' + T\left(\alpha_V\frac{Dp}{Dt} + \vec{\vec{\mathrm{A}}}'_D : \frac{D\vec{\vec{\tau}}}{Dt}\right) + \sum_i \frac{\vec{J}_i\cdot\vec{d}_i}{c_{\mathrm{T}} y_i} + \vec{\vec{\Xi}} : \vec{\vec{\epsilon}} + \vec{\vec{\tau}} : \left(\vec{\vec{\epsilon}} + \vec{\vec{\epsilon}}'\vec{\nabla}\cdot\vec{v} + \frac{D\vec{\vec{\epsilon}}'}{Dt}\right) + \vec{\vec{\sigma}}_{\mathrm{dy}} : \vec{\vec{\epsilon}} + T\sum_i \vec{J}_i\cdot\vec{\nabla}\overline{S}_i. \tag{3.127}$$

Reading in order from left to right, the terms signify: heat accumulation, heat efflux due to dynamical processes, reversible energy accumulation associated with compression and deformation (that is, entropic heat from mechanical processes), energy dissipation from diffusional stress, diffusion, and friction, and heating from excess entropy convection.

3.5 The Dissipation Function

The development now culminates with a transient statement of the second law of thermodynamics. Within Onsager's transport theory [142], and within the field of nonequilibrium thermodynamics in general [143], this law is derived by performing a dynamical entropy balance, then using thermodynamic relationships and the continuity equations for mass, momentum, and energy to express the entropy generation in terms of a sum over pairs of conjugate fluxes and driving forces.

A general continuity equation for entropy can be written as

$$\frac{\partial}{\partial t}\left(\rho\hat{S}\right) = -\vec{\nabla}\cdot\left(\frac{\vec{q}'}{T} + \sum_i \overline{S}_i\vec{N}_i\right) + g_S, \tag{3.128}$$

in which g_S represents the rate of entropy generation. Introduction of the substantial derivative from equation 3.98, the excess molar fluxes from equation 3.106, and application of Euler equation 3.53 and continuity equations 3.97 and 3.108 show that

$$\rho\frac{D\hat{S}}{Dt} = -\vec{\nabla}\cdot\left(\frac{\vec{q}'}{T}\right) - \sum_i \vec{J}_i\cdot\vec{\nabla}\overline{S}_i + c_\mathrm{T}\sum_i \overline{S}_i y_i\frac{D\ln\left(c_\mathrm{T}y_i/\rho\right)}{Dt} + g_S. \tag{3.129}$$

Another formula for the substantial derivative of entropy can be obtained by combining the substantial derivative of equation 3.83 with equations 3.97 and 3.108 to express $D\hat{U}/Dt$, which can be eliminated with a combination of equations 3.121 and 3.124 to get

$$\begin{aligned} T\rho\frac{D\hat{S}}{Dt} = -\vec{\nabla}\cdot\vec{q}' + c_\mathrm{T}\sum_i T\overline{S}_i y_i\frac{D\ln\left(c_\mathrm{T}y_i/\rho\right)}{Dt} - \sum_i \vec{J}_i\cdot\vec{\nabla}\overline{H}_i \\ + \vec{\vec{\tau}} : \left(\vec{\vec{\epsilon}} + \vec{\vec{\epsilon}}'\vec{\nabla}\cdot\vec{v} + \frac{D\vec{\vec{\epsilon}}'}{Dt}\right) + \vec{\vec{\sigma}}_\mathrm{dy} : \vec{\vec{\epsilon}} + \sum_i \frac{\vec{J}_i}{c_\mathrm{T}y_i}\cdot\vec{\vec{\epsilon}}\cdot\overline{m}_i\vec{J}_i. \end{aligned} \tag{3.130}$$

Elimination of $D\hat{S}/Dt$ between equations 3.129 and 3.130 and insertion of equation 3.126 yields

$$Tg_S = -\vec{q}'\cdot\vec{\nabla}\ln T + \sum_i \frac{\vec{J}_i}{c_\mathrm{T}y_i}\cdot\left(\vec{d}_i + \vec{\vec{\epsilon}}\cdot\overline{m}_i\vec{J}_i\right) + \vec{\vec{\tau}} : \left(\vec{\vec{\epsilon}} + \vec{\vec{\epsilon}}'\vec{\nabla}\cdot\vec{v} + \frac{D\vec{\vec{\epsilon}}'}{Dt}\right) + \vec{\vec{\sigma}}_\mathrm{dy} : \vec{\vec{\epsilon}}. \tag{3.131}$$

One final simplification allows the energy dissipation to be expressed in terms of independent fluxes and driving forces: application of kinematic relation 3.107 and Gibbs–Duhem equation 3.59 can be used to eliminate the n^th term from the sum in equation 3.131.

Ultimately the energy dissipation is given as a sum over pairs of independent fluxes and their conjugate driving forces:

$$\begin{aligned} Tg_S = \sum_{i\neq n}\left(\frac{\vec{J}_i}{c_\mathrm{T}y_i} - \frac{\vec{J}_n}{c_\mathrm{T}y_n}\right)\cdot\left(\vec{d}_i + \vec{\vec{\epsilon}}\cdot\overline{m}_i\vec{J}_i\right) \\ + \vec{q}'\cdot\left(-\vec{\nabla}\ln T\right) + \vec{\vec{\tau}} : \left(\vec{\vec{\epsilon}} + \vec{\vec{\epsilon}}'\vec{\nabla}\cdot\vec{v} + \frac{D\vec{\vec{\epsilon}}'}{Dt}\right) + \vec{\vec{\sigma}}_\mathrm{dy} : \vec{\vec{\epsilon}}. \end{aligned} \tag{3.132}$$

In this expression the first term on the right illustrates the fundamental fluxes and forces that appear in the constitutive laws for OSM diffusion [9]; the term with $\vec{q}'$ underpins Fourier's law of heat conduction, and can be used in combination with the diffusion term to rationalize the Soret/Dufour effects [22, 93, 94, 144]; the last two terms justify the Navier–Stokes constitutive law for Newtonian fluids. Several new quantities involving the deformation strain $\vec{\vec{\epsilon}}'$ appear in the equation, providing a logical basis for the formulation of dynamical constitutive laws that apply to viscoelastic or plastic materials.

The term with $\dot{\vec{\vec{\epsilon}}} \cdot \overline{m}_i \vec{J}_i$ is a cause for concern because it suggests that diffusion stress, as well as the thermodynamic force $\vec{d}_i$, can drive mass diffusion. This factor is typically not included in the OSM formalism. Its addition may lead to difficulties, since it will result in transport constitutive laws that mix fluxes and driving forces, which Monroe and Newman have shown can affect the symmetric Onsager reciprocal relation one expects among the transport coefficients [7]. Probably this is not an issue, however, because the derivation of a reciprocal relation *via* Onsager–Casimir fluctuation theory involves linearizing the transport constitutive laws around an equilibrium state [9]. For equilibrium fluctuations $\dot{\vec{\vec{\epsilon}}} \cdot \overline{m}_i \vec{J}_i$ is a term of higher than linear order.

Another way of handling the problem with the $\dot{\vec{\vec{\epsilon}}} \cdot \overline{m}_i \vec{J}_i$ term is to introduce the diffusion stress, and rewrite equation 3.132 as

$$T g_S = \sum_{i \neq n} \left(\frac{\vec{J}_i}{c_{\mathrm{T}} y_i} - \frac{\vec{J}_n}{c_{\mathrm{T}} y_n} \right) \cdot \vec{d}_i + \vec{q}' \cdot \left(-\vec{\nabla} \ln T \right) + \vec{\vec{\Xi}} : \dot{\vec{\vec{\epsilon}}} + \vec{\vec{\tau}} : \left(\dot{\vec{\vec{\epsilon}}} + \vec{\vec{\epsilon}}' \vec{\nabla} \cdot \vec{v} + \frac{D \vec{\vec{\epsilon}}'}{Dt} \right) + \vec{\vec{\sigma}}_{\mathrm{dy}} : \dot{\vec{\vec{\epsilon}}}. \quad (3.133)$$

Here diffusion stress is identified as a type of momentum flux, with the rate-of-deformation tensor providing the conjugate driving force. This formulation seems to require a separate constitutive relationship to connect $\vec{\vec{\Xi}}$ with $\dot{\vec{\vec{\epsilon}}}$, however.

In closing, the second law of thermodynamics can be stated simply as

$$g_S \geq 0, \quad (3.134)$$

with equality holding only at equilibrium. This completes the development of the general equilibrium governing equations and dynamical balance laws applicable to elastically deformable multicomponent electrolytes.

3.6 Equation Count

Most of the quantities introduced here are familiar from prior implementations of multicomponent diffusion theory [93, 94, 132, 137, 138, 143]. The new model essentially reduces to those prior developments with only a few minor modifications, most of which involve the strain.

The development here has provided the groundwork needed to state a sufficient set of balances and variable definitions for a description of simultaneous transport of material, momentum, and heat within an electrochemically active material. For an n-ary material in a d-dimensional geometry, equations 3.15, 3.30, 3.81, 3.99, 3.107, 3.113, 3.114, 3.120, and 3.127, along with $n-1$ of equations 3.108 and n of equation 3.58, constitute a set of $4+n+nd+2d+2d^2$ scalar equations (each vector equation being counted d times, and each tensor equation, d^2 times); these involve $4+n+2nd+2d+5d^2$ scalar dependent variables (with vector quantities counted d times, and tensors, d^2 times): $\{y_i\}_n$, T, p, c_T, ρ, $\vec{\vec{\tau}}$, $\vec{\vec{\sigma}}_\mathrm{dy}$, $\vec{v}$, $\left\{\vec{J}_i\right\}_n$, $\vec{q}'$, $\left\{\vec{d}_i\right\}_n$, $\vec{\vec{\epsilon}}'$, $\dot{\vec{\vec{\epsilon}}}$, and $\vec{\vec{\Xi}}$. The electrical state of the material is described by adopting equations 3.90 and 3.91, which introduce the excess charge density ρ_e and current density $\vec{i}$ without changing the balance of equations and unknowns. In some cases it may be helpful to describe kinematics with the volume-average velocity, which can be computed by appending equation 3.88; this allows one species material balance to be replaced with equation 3.89.

The governing equations also involve various equilibrium material properties, which, being based in the Gibbs function, depend at most on temperature, stress,

and composition: $\{\overline{m}_i\}_n$, $\{\mu_i\}_n$, $\{\overline{V}_i\}_n$, $\left\{\overline{\vec{\vec{V}}}'_i\right\}_n$, $\{\overline{S}_i\}_n$, α_V, $\vec{\vec{\mathrm{A}}}'_D$, and $\hat{C}_p$. Description of the electrical state also involves the species charges $\{z_i\}_n$. If a volume balance is adopted, one may also require the material's modulus K. One should be careful to ensure that the electrochemical potentials relate to partial molar volumes and entropies through appropriate Maxwell relations (equations 3.26 and 3.52). The Euler equation for V, equation 3.27, shows that α_V and K, as defined by equation 3.32, are determined by the constitutive laws for electrochemical potential; the Euler equation for S, equation 3.53, leads to a similar connection between the set of μ_i and $\hat{C}_p$. All the partial molar properties must be properly constrained by Gibbs–Duhem relations (equations 3.57, 3.60, and 3.65); these will in turn ensure that the diffusion driving forces satisfy equation 3.59, which is a fundamental law in OSM transport theory [142].

Finally it is possible to provide a count of how many flux constitutive laws are needed to close the governing system of transport equations. The number of scalar dependent-variable components is greater than the number of scalar governing equations by $nd + 3d^2$. Of these remaining degrees of freedom, d^2 can be specified by adopting an equilibrium constitutive law for deformation strain like equation 3.45. Inspection of the entropy generation in the form of equation 3.132 suggests that transport constitutive laws should close nd degrees of freedom by relating fluxes $\vec{q}'$ and $\left\{\vec{J}_i/c_{\mathrm{T}}y_i - \vec{J}_n/c_{\mathrm{T}}y_n\right\}_{n-1}$ to the independent forces $-\vec{\nabla}\ln T$ and $\left\{\vec{d}_i + \dot{\vec{\vec{\epsilon}}}\cdot\overline{m}_i\vec{J}_i\right\}_{n-1}$; the last $2d^2$ degrees of freedom are closed by expressing the flux $\vec{\vec{\tau}}$ as a function of the rate-of-deformation tensor $\dot{\vec{\vec{\epsilon}}}$, the substantial derivative of the deformation strain tensor $\vec{\vec{\epsilon}}'$, and $\vec{\vec{\epsilon}}'\vec{\nabla}\cdot\vec{v}$, and the flux σ_{dy} in terms of its conjugate driving force, $\dot{\vec{\vec{\epsilon}}}$. The following sections deal with the explicit formulation of these transport constitutive laws.

3.7 Formulation of Irreversible Flux Laws

Onsager states that the rate of entropy generation for a system affords conjugate pairs of driving forces and fluxes for irreversible processes, such as mass diffusion, thermal conduction, and viscoelastic stress, which lead to energy dissipation [142]. Diffusion involves the relative motion of different species present in the system, conduction involves the relative transfer of heat among molecules through vibration, and viscoelastic flow involves the relative motion or displacement between neighbouring parts of a material.

A unique feature of the OSM formalism is its ability to account for 'coupled diffusion' processes, in which a driving force induces fluxes to which it is not conjugate in the function describing local energy dissipation. Diffusion in binary electrolytes typifies a coupled process, because the gradient of a given species' electrochemical potential can generally drive the flux of a different species. (A lucid example is provided by electroosmotic drag in low-temperature fuel-cell membranes: an electric field drives migration of mobile ions relative to the membrane backbone; these ions exert a drag force on dissolved water that causes it to move relative to the membrane as well; thus electric fields apparently drive water flux, despite the fact that water molecules carry no net charge [145].) This physical content distinguishes OSM theory from the more common Nernst–Planck transport formalism, which ignores solute/solute interactions entirely. Newman's theory is more 'complete' than Nernst–Planck theory in the sense that it incorporates one transport coefficient for every pair of chemically distinct diffusing species, in line with the principles of irreversible thermodynamics laid out by Onsager [142, 146].

Coupled diffusion is illustrated more starkly in systems where multiple types of transport occur simultaneously, whose analysis is entirely outside the scope of Nernst–

Planck theory. An example is provided by materials in which temperature gradients induce charge flux or potential gradients induce heat flux, which have been of interest to electrochemists for decades [147]. Newman has extended concentrated-solution theory to rationalize this 'Thompson–Peltier effect' by incorporating terms associated with Soret and Dufour fluxes, in accord with the principles of irreversible thermodynamics [22]. This work is developing a theory which incorporates the phenomenon of pressure diffusion with similar depth and rigour.

Multiphysics, where the assumption of isothermal, isobaric conditions are relaxed, leads to another, subtler type of coupling: fluxes across a material can be affected by the local variation of material properties with respect to the distributions of thermodynamic basis variables. This coupling is consequently driven primarily by the general balance equations, rather than being explicitly seen in the transport constitutive laws. For example, when a current passes through a liquid electrolyte, Joule heating (or 'I^2R' heating) can cause substantial local enthalpy generation [148], which, when distributed according to the local thermal-energy balance, induces temperature gradients. If, say, the electrolyte diffusivity depends strongly on temperature, then the local change in diffusivity with temperature will augment composition-gradient-driven material fluxes in proportion to the temperature gradient — a thermophoretic force that is inherently macroscopic, and therefore distinct from the Soret effect. Since transport properties often depend strongly on temperature and composition [149], this 'multiphysical coupling', although more obscure in its origins, can sometimes outweigh the diffusional coupling built into the OSM laws.

The present work employs these various concepts and approaches to coupling for the specific case of transport in Nafion where other than the coupled electroosmotic flow already discussed, mechanical forces could be driving diffusive mass transport and local solvent/water composition could not only be affecting mechanical properties

directly but also the microscopic thermodynamic equilibria. It is important to mention that this transport model continues to assume isothermal conditions; therefore, only material and momentum flux laws, without any thermal coupling, are discussed.

3.7.1 Mass Flux Laws

Mass diffusion is an inherently coupled phenomenon, where force on one species affects the diffusion for all other species involved. Dilute-solution theory for electrolyte transport, based on the phenomenological Nernst–Planck laws (extended Fick's law with ionic migration), neglects species/species interactions among solutes [24]. Maxwell, however, placed the inter-species interaction at the centre of his hydrodynamical approach for describing diffusion in a binary gas mixture [150]. Stefan further formalised Maxwell's approach, quantified the resistance experienced by every species due to every other species present in the system *via* binary diffusion coefficients, and extended the theory to liquids [151]. Hirschfelder, Curtiss, and Bird proved that the Stefan–Maxwell laws agreed with the Chapman–Enskog kinetic theory approach to a considerable extent [93], making them more rigorous than Fick's laws. In the same work, Hirschfelder *et al.* extended the Stefan–Maxwell theory to multicomponent systems by considering a force balance where the drag every species experiences due to every other species present in the system (from hydrodynamics) is balanced by the mass diffusion driving force acting on the species (from thermodynamics). The foundation of Newman's concentrated-solution theory for describing transport in electrolytes was based on replacing the Nernst–Planck laws with the multicomponent Stefan–Maxwell mass flux laws [133]. Onsager's approach to formulating flux laws based on entropy generation, equation 3.132, leads us to a similar result, expressed as follows:

$$\vec{d}_i + \vec{\vec{\epsilon}} \cdot \overline{m}_i \vec{J}_i = \sum_{j \neq i} K_{ij} \left(\frac{\vec{J}_i}{c_{\mathrm{T}} y_i} - \frac{\vec{J}_j}{c_{\mathrm{T}} y_j} \right) = \sum_{j \neq i} K_{ij} \left(\vec{v}_i - \vec{v}_j \right), \tag{3.135}$$

where K_{ij} are the associated drag coefficients between species i and j; these equations are formulated in a way which renders them independent of a reference velocity.

Hydrodynamics dictates the following form for K_{ij}:

$$K_{ij} = RTc_{\mathrm{T}}\frac{y_i y_j}{\mathscr{D}_{ij}}. \tag{3.136}$$

Onsager reciprocal relationships for the microscopic transport coefficients $\mathscr{D}_{ij} = \mathscr{D}_{ji}$, proved by means of fluctuation theory and principle of microscopic reversibility, assert, through equation 3.136, that drag coefficients must be symmetric as well: $K_{ij} = K_{ji}$. If the thermodynamic mass driving force on species i is given by equation 3.58, the mass flux law can be written using the gradients in intensive variables as:

$$-c_{\mathrm{T}}y_i\left[\vec{\nabla}\mu_i + \overline{S}_i\vec{\nabla}T - \frac{\overline{m}_i}{\rho}\left(\vec{\nabla}p + \vec{\vec{\epsilon}}' : \vec{\nabla}\vec{\vec{\tau}}\right)\right] + \vec{\vec{\epsilon}}\cdot\overline{m}_i\vec{J}_i = \sum_{j\neq i}\frac{RT}{\mathscr{D}_{ij}}\left(y_j\vec{J}_i - y_i\vec{J}_j\right). \tag{3.137}$$

This equation clearly indicates that pressure and deviatoric stress gradients play a role in the diffusion of every species present in the system. Gibbs–Duhem equation (equation 3.59) requires that the sum of mass diffusion driving forces of all the species in a system is equal to zero. This constraint implies that in a system with n species, $n-1$ driving forces are enough to specify the entire range of diffusive transport in the system, because the n^{th} driving force is linearly dependent on the rest.

Since the flux-explicit form is more commonly used in the modelling literature, Monroe and Delacourt developed a general process for the conversion of force-explicit transport laws for multicomponent non-neutral electrolytes but it can't be used directly in this context because it assumes isothermal and isobaric conditions [23]. In this conversion process, it is possible to identify how the macroscopic transport properties appearing in the flux-explicit form are related to the microscopic binary interaction coefficients $\mathscr{D}_{ij}$ of the force-explicit form. Instead of carrying out a generalised conversion, we prefer to invert flux laws as and when required in the later chapters where this transport model is applied to specific applications.

3.7.1.1 Revisiting the Species Momentum Balance

Earlier, when formulating species momentum continuity, no specific form was postulated for the internal force acting on species i, $\vec{f}_i$ (*cf.* equation 3.109). These terms were, however, defined with the expectation that they encompass all possible internal species/species momentum exchange. The entropy generation function, equation 3.132, accounts for all the dissipative processes in the system, and should therefore also account for the inter-species momentum exchange. Since, the mass-diffusion driving force $\left(\vec{d}_i + \vec{\vec{\epsilon}} \cdot \overline{m}_i \vec{J}_i\right)$ is the only term which quantifies species-species interactions in the entropy generation expression, it identifies with $\vec{f}_i$. Further, the Gibbs–Duhem relation, equation 3.59 and the kinematic relation, equation 3.107, imply that

$$\sum_i \left(\vec{d}_i + \vec{\vec{\epsilon}} \cdot \overline{m}_i \vec{J}_i\right) = 0, \tag{3.138}$$

thereby fulfilling the constraint $\sum_i \vec{f}_i = 0$. Going one step further, one can use the mass flux law, equation 3.135, to identify that $\left(\vec{d}_i + \vec{\vec{\epsilon}} \cdot \overline{m}_i \vec{J}_i\right)$ can be replaced by the equivalent drag term $\sum_{j \neq i} K_{ij} \left(\vec{v}_i - \vec{v}_j\right)$, which also adds up to zero when summed over all species. In accordance with this observation, one can write the species momentum continuity equation with more detail, as

$$\frac{\partial \rho_i \vec{v}_i}{\partial t} = -\vec{\nabla} \cdot \left(\omega_i \vec{\vec{\sigma}}_{\mathrm{t}} + \rho_i \vec{v}_i \otimes \vec{v}_i\right) + \sum_{j \neq i} K_{ij} \left(\vec{v}_i - \vec{v}_j\right) + \vec{b}_i. \tag{3.139}$$

Although the two formulations with $\left(\vec{d}_i + \vec{\vec{\epsilon}} \cdot \overline{m}_i \vec{J}_i\right)$ and $\sum_{j \neq i} K_{ij} \left(\vec{v}_i - \vec{v}_j\right)$ are equivalent, the latter expression of internal force in terms of a dynamic inter-species drag force may be more intuitive for researchers familiar with the kinetic theory.

3.7.2 Formulation of Momentum Flux Laws

The dissipation function, equation 3.132, can now be leveraged to formulate transport constitutive laws. The entropy generation equation reveals that there are two sources of momentum dissipation: in the first, flux is characterised by the molecular stress tensor $\vec{\vec{\tau}}$, which is conjugate to the driving force $\left(\vec{\vec{\epsilon}} + \vec{\vec{\epsilon}}'\vec{\nabla} \cdot \vec{v} + \frac{D\vec{\vec{\epsilon}}'}{Dt}\right)$; in the second, flux is characterised by the dynamic stress $\vec{\vec{\sigma}}_{\mathrm{dy}}$, taking the rate of deformation $\vec{\vec{\epsilon}}$ as a conjugate driving force.

The simplest constitutive laws from nonequilibrium thermodynamics relate fluxes to driving forces in linear, homogeneous relationships [142]. Based on the conjugate variables appearing in the dissipation function, one can write a constitutive law for the traceless deviatoric stress in an isotropic material,

$$\vec{\vec{\tau}} = 2\mu_{\mathrm{shear}}\left[\left(\vec{\vec{\epsilon}} + \tfrac{1}{3}\vec{\vec{I}}\vec{\nabla} \cdot \vec{v}\right) + \vec{\vec{\epsilon}}'\vec{\nabla} \cdot \vec{v} + \frac{D\vec{\vec{\epsilon}}'}{Dt}\right]. \tag{3.140}$$

This choice of the proportionality constant, involving an effective shear viscosity of the system μ_{shear}, ensures consistency with Newton's law of viscosity (obtained by following the same procedure for viscous liquids, in which $\vec{\vec{\epsilon}}' = \vec{\vec{0}}$). Also, the spherical part $\frac{1}{3}\vec{\vec{I}}\vec{\nabla} \cdot \vec{v}$ of the rate of deformation tensor $\vec{\vec{\epsilon}}$ has been excluded, since only the deviatoric components of the tensor quantity in square brackets contribute to $\vec{\vec{\tau}}$. The other driving force of the same tensorial order in the entropy generation function is the rate of deformation tensor. This is already a part of the conjugate driving force for $\vec{\vec{\tau}}$, and therefore a separate term containing it would be redundant. The second stress law is formulated to relate the dynamic stress $\vec{\vec{\sigma}}_{\mathrm{dy}}$ to the rate of deformation tensor. Since momentum dissipation from the deviatoric part of the rate of deformation tensor was already accounted for in the previous law, this law is formulated for the dissipation occurring due to the spherical part as follows,

$$\vec{\vec{\sigma}}_{\mathrm{dy}} = p_{\mathrm{dy}}\vec{\vec{I}} = -\mu_{\mathrm{bulk}}\vec{\vec{I}}\vec{\nabla} \cdot \vec{v}. \tag{3.141}$$

This law can be seen to quantify effects of bulk viscosity μ_{bulk}, which arise when transient volume changes cause dissipation. The dynamic pressure p_{dy} is therefore seen to account for the excess local non-equilibrated part of uniform stress, which is often discussed in the fluid dynamics literature. To close the transport model, these two stress constitutive laws should be plugged into Cauchy's equation (equation 3.114). In theory, it is possible for equation 3.141 to include a coupling term because of the traceless driving force of equation 3.140, which may be able to explain purely dynamical deformation behaviour such as plastic deformation. However, this possibility is not explored further in the present study.

3.7.2.1 Development of a Viscoelastic Stress Model

The form of the stress constitutive law in equation 3.140 looks different from the conventional expressions usually used such as Hooke's law of elasticity, Newton's law of viscosity, or Maxwell/Kelvin–Voigt models used for viscoelastics. Inspecting the individual terms of the driving force carefully, one sees that the rate of deformation tensor is fully specified in terms of the mass average velocity, equation 3.120; the Eulerian deformation strain $\vec{\vec{\epsilon}}'$ can be related to the material state through the deformational equation of state or Hooke's law, equation 3.45, which is justified by the principle of microscopic equilibrium. Eliminating the deformation strain and its substantial derivative with Hooke's law, one finds an alternative form of equation 3.140:

$$\vec{\vec{\tau}} = 2\mu_{\text{shear}}\left(\vec{\vec{\dot{\epsilon}}} + \tfrac{1}{3}\vec{\vec{I}}\vec{\nabla}\cdot\vec{v}\right) - \tfrac{\mu_{\text{shear}}}{G_{\text{shear}}}\vec{\vec{\tau}}\ \vec{\nabla}\cdot\vec{v} - \mu_{\text{shear}}\frac{D\left(\vec{\vec{\tau}}/G_{\text{shear}}\right)}{Dt}. \tag{3.142}$$

The last term can be simplified by using the chain rule of differentiation. Collecting terms with common factors together, using mass continuity equation 3.97, and defining $t_{\text{shear}} = \mu_{\text{shear}}/G_{\text{shear}}$ as a relaxation time of the material yields a compact form of

the stress law,

$$\vec{\vec{\tau}} = \frac{2\mu_{\text{shear}}\left(\vec{\vec{\epsilon}} + \frac{1}{3}\vec{\vec{I}}\vec{\nabla}\cdot\vec{v}\right) - t_{\text{shear}}\dfrac{D\vec{\vec{\tau}}}{Dt}}{1 - t_{\text{shear}}\frac{D\ln\rho G_{\text{shear}}}{Dt}}. \tag{3.143}$$

This form of the stress law more clearly begins to resemble the Maxwell model for viscoelastic materials. One can rearrange equation 3.143 to illustrate how viscous and elastic strain rates add together to produce the total strain rate,

$$\underbrace{\frac{1}{\delta}\left(\vec{\vec{\epsilon}} + \frac{1}{3}\vec{\vec{I}}\vec{\nabla}\cdot\vec{v}\right)}_{\text{total strain rate}} = \underbrace{\frac{\vec{\vec{\tau}}}{2\mu_{\text{shear}}}}_{\text{viscous strain rate}} + \underbrace{\frac{1}{2G_{\text{shear}}\delta}\frac{D\vec{\vec{\tau}}}{Dt}}_{\text{elastic strain rate}}, \tag{3.144}$$

where effects of variability in the density and shear modulus are lumped into the term

$$\delta = \left(1 - t_{\text{shear}}\frac{D\ln\rho G_{\text{shear}}}{Dt}\right). \tag{3.145}$$

Maxwell models are good at explaining the viscoelastic stress relaxation phenomenon. This is illustrated by applying a condition of zero total strain rate to equation 3.144, i.e., when $\vec{\vec{\epsilon}} + \frac{1}{3}\vec{\vec{I}}\vec{\nabla}\cdot\vec{v} = 0$, the stress will relax according to the equation

$$\frac{D\vec{\vec{\tau}}}{Dt} + \frac{\delta}{t_{\text{shear}}}\vec{\vec{\tau}} = 0. \tag{3.146}$$

Standard Maxwell models, however, usually predict a linear increase in strain at constant stress, which does not match the viscoelastic non-linear creep behavior. For this modified model, however, the presence of δ may be a way to introduce the correct non-linearity in creep response.

Further, for theoretical analysis, new proposed laws converging to familiar laws for ideally behaving materials functions may function as a form of validation. Towards this end, the following analysis explores the form of the stress constitutive law, equation 3.143, in two extremes of material relaxation times t_{shear}:

- *Small relaxation time* ($t_{\text{shear}} \sim 0$), material responds to stress (or strain) almost instantly thereby behaving more like a liquid, and the stress law corresponds to

Newton's law of viscosity:

$$\vec{\vec{\tau}} = 2\mu_{\text{shear}}\left(\vec{\vec{\epsilon}} + \frac{1}{3}\vec{\vec{I}}\vec{\nabla}\cdot\vec{v}\right). \tag{3.147}$$

- *Large relaxation time* ($t_{\text{shear}} \sim \infty$) reduces the stress law to

$$\tau_{jk} \propto \rho G_{\text{shear}}. \tag{3.148}$$

With a proportionality constant $k = -\frac{2\epsilon'_{jk}}{\rho}$, this equation returns Hooke's law of elasticity. System closure becomes problematic in this situation, however, because constitutive laws for strain (Deformation EOS, equation 3.45) and stress (from the dissipation function, equation 3.148) collapse into the same equation. The next chapter explores this case in detail under the assumption that Nafion behaves like an ideal elastic material, and it is seen that boundary conditions then help close the problem.

3.7.2.2 Relevance of Dynamic Pressure

A further analysis can be performed for the second stress constitutive law, equation 3.141, to illustrate when the dynamic pressure becomes significant. This analysis is straightforward for a single-component case where the mass- and volume-average velocities are indistinguishable. Volume continuity, equation 3.89, for an isothermal case, can be used to replace $\vec{\nabla}\cdot\vec{v}$, yielding an expression for the dynamic pressure of the form,

$$p_{\text{dy}} = t_{\text{bulk}}\frac{Dp}{Dt}, \tag{3.149}$$

where a second relaxation time for the material has been introduced, $t_{\text{bulk}} = \mu_{\text{bulk}}/K$.

The multi-component case, however, is more complex. The mass- and volume-average velocities are not equivalent anymore, the difference being quantified by ap-

plication of kinematic relation 4.25:

$$\vec{v}^{\square} - \vec{v} = \sum_{i \neq n} \left(\frac{\phi_i}{\omega_i} - \frac{\phi_n}{\omega_n} \right) \frac{\omega_i \vec{J}_i}{c_{\mathrm{T}} y_i} = -\overline{V}_n \sum_{i \neq n} \left(\frac{\overline{m}_i}{\overline{m}_n} - \frac{\overline{V}_i}{\overline{V}_n} \right) \vec{J}_i. \tag{3.150}$$

Given that molar masses are independent of pressure and that the pressure dependence of all species is assumed to be the same, the coefficient $\left(\frac{\overline{m}_i}{\overline{m}_n} - \frac{\overline{V}_i}{\overline{V}_n} \right)$ can be considered to be constant if composition dependence is neglected. To relate this kinematic relation to the dynamic pressure, equation 3.143, take the divergence of equation 3.150, eliminate $\vec{\nabla} \cdot \vec{v}^{\square}$ using the isothermal version of volume continuity 3.89, consider the pressure dependence of partial molar volumes 3.69, and use the material balance 3.108, to get the following expression for dynamic pressure,

$$p_{\mathrm{dy}} = t_{\mathrm{bulk}} \frac{Dp}{Dt} - \mu_{\mathrm{bulk}} c_{\mathrm{T}} \sum_i \left(\overline{V}_i - \frac{\overline{m}_i}{\rho} \right) \frac{Dy_i}{Dt}, \tag{3.151}$$

which relates it to transients in pressure as well as composition. For a single-component case, $\rho = \overline{m}_n / \overline{V}_n$, thereby reducing equation 3.151 to 3.149. Similar to considering the extremes of t_{shear} in the viscoelastic case, it is also informative to consider the extremes of this second relaxation time:

- *Small relaxation time* ($t_{\mathrm{bulk}} \sim 0$)
  - for the single-component case, equation (3.149) returns that $p_{\mathrm{dy}} \sim 0$, implying that for a fast-relaxing material local mechanical equilibrium is readily established, and therefore thermodynamic pressure can be used directly in Cauchy momentum balance.
  - for the multicomponent case, however, we have,

    $$p_{\mathrm{dy}} = -\mu_{\mathrm{bulk}} c_{\mathrm{T}} \sum_i \left(\overline{V}_i - \frac{\overline{m}_i}{\rho} \right) \frac{Dy_i}{Dt}. \tag{3.152}$$

    This expression implies that even for a rapidly relaxing material, there may be an excess pressure over the thermodynamic pressure, which comes

from composition transients alone scaled by the difference between mass and volume fractions of the respective species.

- *Large relaxation time* ($t_{\text{bulk}} \sim \infty$)
  - for the single-component case,

$$\frac{Dp}{Dt} = \frac{p_{\text{dy}}}{t_{\text{bulk}}} \sim 0. \tag{3.153}$$

  - for the multicomponent case,

$$\frac{Dp}{Dt} \sim K c_{\text{T}} \sum_i \left(\overline{V}_i - \frac{\overline{m}_i}{\rho} \right) \frac{Dy_i}{Dt}. \tag{3.154}$$

In general, these expressions show that change in pressure happens very slowly in the limit of a large relaxation time, possibly rendering dynamic pressure vastly different than the thermodynamic pressure.

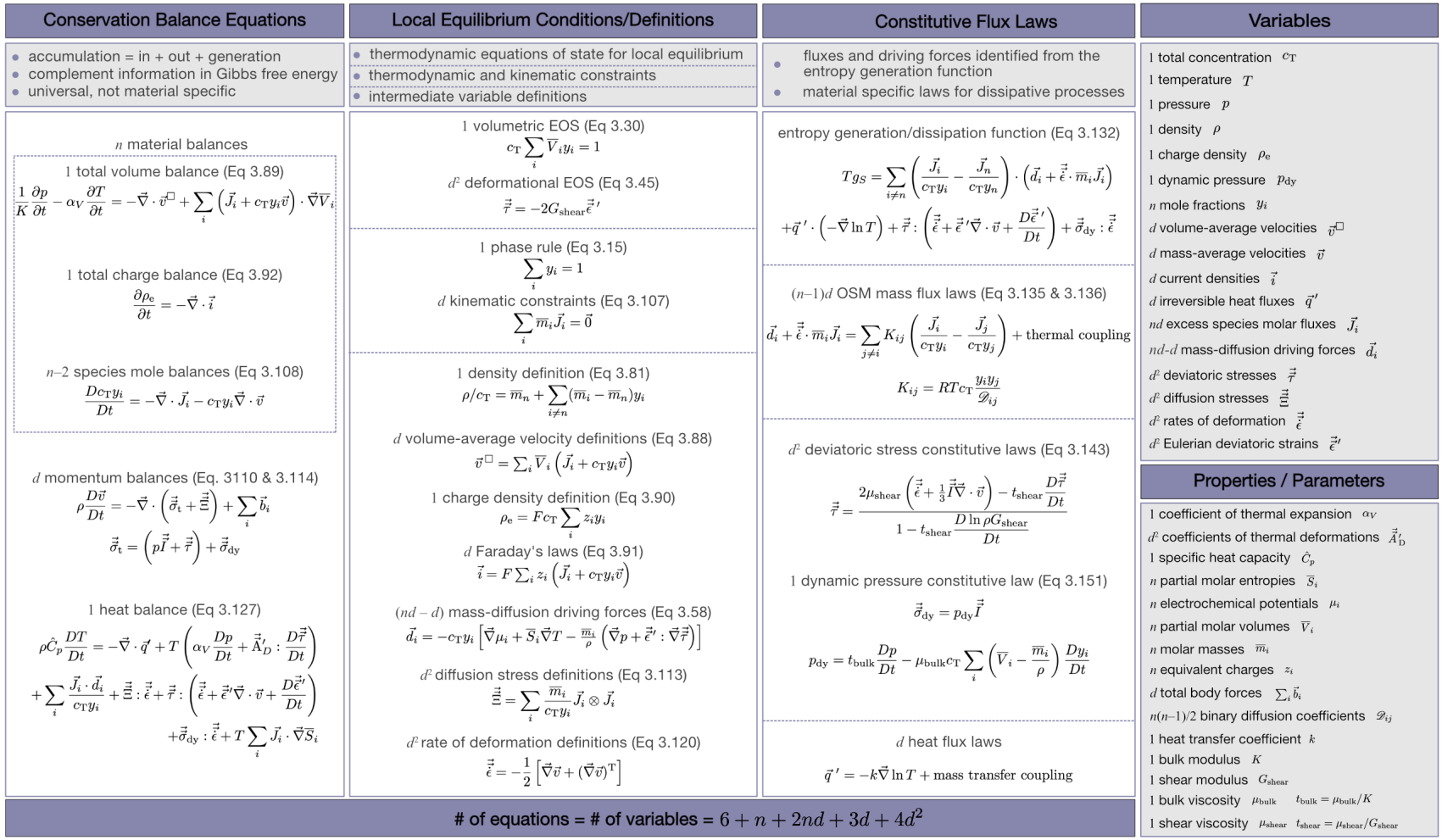

Figure 3.1: Building blocks of a continuum-level electrolyte transport model with electrochemical/mechanical coupling, with equation and variable count. In some cases, the total molar flux of species i, $\vec{N}_i$, has been recast in terms of the excess molar flux of i relative to the mass-average velocity, $\vec{J}_i$, by using the definition $\vec{J}_i = \vec{N}_i - c_T y_i \vec{v}$.

Chapter 4

Non-Isobaric Transport: Impedance Modelling

Electrochemical impedance spectroscopy is an analytical technique commonly applied to batteries, fuel cells, and supercapacitors, which experimentally probes the electrical nature of physical processes without considering the physio-chemical mechanistic details [152]. Some microscopic processes are represented by known electrical circuit elements: interfacial kinetics has been identified to act like a nonlinear resistor, and double-layer charging like a nonlinear capacitor [153]. Attempts to describe other processes have led to the identification of less familiar current/voltage relationships, such as the *Warburg element* that characterises mass diffusion [154] and the *constant-phase element*, which is used to justify non-ideal behaviour such as time-constant dispersion caused by electrode roughness [155]. This chapter explores the impedance signatures of a transport model applied to hydrated ionomeric membranes used as electrolytes in PEM fuel cells, augmenting standard approaches by including local mechanical effects.

Specifically for PEMFCs, impedance analysis has been employed to characterise a variety of processes [156–158] such as catalyst-layer kinetics and gas-phase transport limitations [159], the variation of oxygen-transport impedance with polarization [160],

non-uniformities along flow channels [161], [162] *etc.*. Most of this work has relied on 'equivalent-circuit models', which fit data by employing *ad hoc* networks of traditional circuit elements. More information can be extracted from EIS, however, if the data is instead interpreted by employing detailed physical models that explicitly describe the various processes occurring in the device. For instance, by employing a detailed continuum model, it was discovered that formation of oxygen-reduction-reaction intermediates, oxide-layer growth, and, to some extent, water build-up in Nafion during fuel-cell operation can manifest low-frequency inductive loops on Nyquist plots [5]—a counter-intuitive observation because almost all known electrochemical processes are resistive, capacitive, Warburg, or constant-phase. When taken in tandem with a mechanistic model, impedance data can also be relied upon for quantitative purposes such as estimating transport or kinetic properties of the electrolyte-electrode system. Warburg signatures on Nyquist plots have been used to obtain diffusion coefficients [163] and transference numbers [164].

In the context of this thesis, impedance analysis of Nafion is a potentially insightful analytical tool for several reasons: first, the Nyquist and Bode plot signatures of mechanical effects and diffusion/momentum-transport coupling remain largely unidentified; second, EIS is useful for studying systems involving phenomena with starkly different relaxation times, a condition likely for mechanical and diffusive effects in Nafion; third, the inherently dynamical nature of EIS helps to resolve information that can be lost in steady-state (direct-current) analysis; fourth, carrying out the time-to-frequency regime transformation in a linear window of current-voltage response to model the EIS procedure dramatically simplifies the coupled non-linear model, making the contributions of disparate phenomena to the system response easier to parse, while retaining interesting characteristics. More concretely, literature studies have shown inductive signatures at high frequencies for Nafion and other electrolytes (both solid and liquid) [5], which cannot be attributed to any physical process

included in present-day transport models; we may be able to explain high-frequency inductance by including mechanical effects.

This chapter first applies the theory developed in Chapter 3 to model a hypothetical EIS experiment, stating the relevant governing equations, constitutive laws, and boundary conditions, as well as executing the linearisation process that allows conversion from the time regime to the AC frequency regime. A dimensional analysis of the linearised model is carried out, both to improve computational stability and also to equip ourselves with the appropriate means to clarify the system's fundamental physical behaviour. Rescaled versions of the linear model are analysed to obtain the impedance response in various frequency regimes. Bode and Nyquist plots are produced over a wide range of practical frequencies and the resulting signatures are associated with probable physical processes that emerge from the coupled electrochemical-mechanical transport model. The features of mass and momentum transport are understood through spatial profiles of concentration and pressure across the membrane, respectively. Three distinct cases of membrane mechanical behaviour are considered—elastic (Hookean solid), viscous (Newtonian liquid), and generally viscoelastic—and their impedance signatures, as well as concentration and pressure profiles, are compared.

During the scaling of the model, the effects of dimensionless-parameter values on the resultant impedance plots are obtained and explored. A sensitivity study is carried out to understand what the roles of various parameters are in determining the impedance response, as well as their relative importance. The aim is to uncover ways that signatures of electrochemical/mechanical coupling can be enhanced, not only to gain insight but also to develop property targets for novel materials useful for applications such as piezoelectric sensors and actuators.

4.1 Transport Model for Impedance Analysis

The transport model considers a hydrated Nafion membrane exposed to symmetric humidified hydrogen feeds on both sides [165]. Dissolution of molecular hydrogen in the membrane is ignored: the membrane is treated like a simple binary electrolyte, containing one solvent (0, water) and one salt of the form MX comprising ν_+ cations (+, hydrogen ions) and ν_- anions (−, stationary sulphonic acid sites attached to the polymeric backbone) with z_+ and z_- representing equivalent charges in a formula unit whose stoichiometry satisfies the Guggenheim condition:

$$\nu_+ z_+ + \nu_- z_- = 0. \tag{4.1}$$

When current is passed through this cell, hydrogen dissociates into hydrogen ions at the anode. These ions subsequently travel to the cathode, under the action of gradients of activity or stress, which drives diffusion, as well as the electric field, which drives migration. Upon reaching the other side of the cell, the hydrogen ions recombine to form gaseous molecular hydrogen. The half-reactions at the electrodes are identical, $H_2 - 2H^+ \rightleftharpoons 2e^-$, although electrons are produced on one side and consumed on the other. Since only cations react at the electrodes, the stoichiometric coefficients for the half reactions are: $s_+ = -2; s_- = 0; s_0 = 0$.

In the remainder of this section, mass-conservation laws are developed in a way that highlights the effect of compressibility on the local volume balance. The momentum balance is discussed, along with stress constitutive laws for the deviatoric stress component for a range of materials. Coupling of diffusive flux and potential drop with stress gradients, in accord with thermodynamic laws and OSM theory, is presented next. Finally, a kinematic relationship between mass- and volume-average velocities condenses the information contained in the auxiliary algebraic relations and definitions to close the system.

4.1.1 Material Conservation Laws

For this 3-species scenario, the water mole balance is the first of three balances needed to establish local mass conservation,

$$\frac{\partial \left(c_{\mathrm{T}} y_0 \right)}{\partial t} = -\vec{\nabla} \cdot \vec{N}_0. \tag{4.2}$$

The other two species material balances, which express the mole balances of cations and anions, can be linearly recombined through Faraday's law (equation 3.91) and the definition of volume-average velocity (equation 3.88) to produce a charge balance and a volume balance that can be used in their place. For a locally electroneutral solution in which charge density ρ_{e} is approximately zero,

$$\rho_{\mathrm{e}} = c_{\mathrm{T}} \sum_i z_i y_i \simeq 0, \tag{4.3}$$

the local charge balance is reduced to

$$\vec{\nabla} \cdot \vec{i} = \vec{0}. \tag{4.4}$$

The volume balance elucidates the role of the material's compressive response, and encompasses the effects of changing pressure, both temporal (through the accumulation term) and spatial (through the pressure dependences of species partial molar volumes):

$$\vec{\nabla} \cdot \vec{v}^{\square} = -\frac{1}{K} \frac{\partial p}{\partial t} + \sum_i \vec{N}_i \cdot \vec{\nabla} \overline{V}_i. \tag{4.5}$$

In this expression, the bulk modulus K tends to be several orders of magnitude higher than the gauge pressure within the material, making the time-constant associated with compressive forces characteristically small; mechanical relaxation is, therefore, assumed to be very fast and can be neglected in most cases. The term is retained here because impedance analysis enables specific probing of timescales where compressive pressure effects can be relevant.

Further, the pressure dependence of partial molar volumes simplifies the volume balance (4.5) to

$$\vec{\nabla} \cdot \vec{v}^{\square} = -\frac{1}{K}\left(\frac{\partial p}{\partial t} + \vec{v}^{\square} \cdot \vec{\nabla} p\right) = -\frac{1}{K}\frac{D^{\square} p}{Dt}, \tag{4.6}$$

where $D^{\square}p/Dt$ is the substantial derivative of pressure, taken with the volume-average velocity $\vec{v}^{\square}$, rather than the barycentric velocity $\vec{v}$, as the reference for convection. Approximately, this implies that the local flux of volume leads to pressure accumulation in the material coordinate.

4.1.2 Kinematic Mechanical Effects: Considering Excluded-Volume

Liu and Monroe [27] implemented a description of the excluded-volume effect *via* incorporating a volumetric equation of state with an explicit pressure dependence (equation 3.70), which replaced the implicit assumption of constant solvent concentration (or mass density). The volumetric state equation expresses the constraint that a unit volume of electrolyte must be composed of individual species volume fractions $\phi_i = c_{\mathrm{T}} y_i \overline{V}_i$,

$$\sum_i \phi_i = 1. \tag{4.7}$$

4.1.3 Momentum Balance and Associated Quantities

In addition to the material balances, a locally non-isobaric system also needs a momentum balance, which can be taken to obey Cauchy's equation in the following form,

$$\rho \frac{\partial \vec{v}}{\partial t} + \rho \vec{v} \cdot \vec{\nabla} \vec{v} = -\vec{\nabla} p - \vec{\nabla} \cdot \vec{\vec{\tau}}. \tag{4.8}$$

For this study, phenomena associated with bulk viscosity, diffusion stress, and body forces are assumed to be insignificant or absent.

In Cauchy's equation, the mass density depends locally on composition: its definition can be rephrased to say that a unit mass must be made up of species mass fractions $\omega_i = c_\mathrm{T} y_i \overline{m}_i / \rho$,

$$\rho = c_\mathrm{T} \sum_i y_i \overline{m}_i \qquad \text{or} \qquad \sum_\mathrm{i} \omega_\mathrm{i} = 1. \tag{4.9}$$

Also, the mass-average velocity can be rephrased as an average of the species momentum density through equation 3.95.

As discussed in the previous chapter at length, stress constitutive laws developed from the entropy generation function characterise deviatoric stresses. Treating hydrated Nafion as a viscoelastic solution, we can either use the general form of equation 3.140, which embodies complex mechanical behaviour directly, or we can build our understanding by starting with the archetypal solid and liquid materials before proceeding to the viscoelastic case. The latter approach is taken; impedance is, therefore, studied for the following three kinds of materials:

Elastic Case: usually described by Hooke's law of linear elasticity, parameterised by the shear modulus G_shear for an isotropic material, which was derived from the deformational equation of state in the previous chapter as equation 3.45 [$\vec{\vec{\tau}} = -2G_\mathrm{shear}\vec{\vec{\epsilon}}'$].

Most models, based on the theory of linear elasticity, operate in the Lagrangian frame which allows for a straightforward definition of elastic deviatoric deformation strain $\vec{\vec{\epsilon}}'$ in terms of the displacement usually from an equilibrated, undeformed initial position (a hypothetical 'material coordinate'), to close the system. For the present model, however, we choose to operate in an Eulerian frame, similar to MacMinn et al. [104], which need make no reference to a material coordinate. Generally, in a d-dimensional system, d^2 stress laws derived from the dissipation function can be seen as describing d^2 deviatoric stresses $\vec{\vec{\tau}}$, while the d^2 deformational equations of state derived from classical thermodynamics describe d^2 the elastic deviatoric strains

$\vec{\epsilon}'$. However, in Chapter 3, Section 3.7.2.1, the viscoelastic stress law was seen to converge to the deformation equation of state/Hooke's law in the limit of a large shear relaxation time, which is the elastic solid limit. This leaves us with a model closure issue as $2d^2$ variables now only have d^2 equations [$\vec{\tau} = -2G_{\text{shear}}\vec{\epsilon}'$] to determine them. Therefore, additional input is needed to close the transport model for an elastic medium.

It is observed that even though changes are assumed to occur only in the through-plane (x) direction in our system, information about stress variation in the in-plane directions (y-z) has an impact on the deviatoric stress in the primary direction. In this case, boundary conditions, such as exposure to ambient pressure or maintaining constant volume, used in conjunction with the momentum balance can provide model closure by directly determining the deviatoric stress distribution in the system. It is inferred that stress must be invariant in the y- and z-directions based on the constraint that the mass, charge, and hence momentum transport only occur in the x-direction:

$$\sigma_{yy} = \sigma_{zz} = \text{constant} = p^{\infty}, \tag{4.10}$$

where p^{∞} is the ambient pressure (or stress) surrounding the system. In reality, since impedance measurements are inherently transient in nature, there may be a lag associated with the boundaries achieving this ambient pressure p^{∞}, and consequently for this boundary information to propagate into the bulk. Here, we press ahead with an assumption of quasi-steady state with respect to the stress boundary conditions and ignore the possibility of such a lag. Further, if there is no shear acting on the system,

$$\tau_{ij} = 0, \tag{4.11}$$

the y- and z-components of stress can be written as:

$$\left.\begin{aligned} \sigma_{yy} = p^{\infty} = p + \tau_{yy} \\ \sigma_{zz} = p^{\infty} = p + \tau_{zz} \end{aligned}\right\} \Rightarrow \tau_{yy} = \tau_{zz} = p^{\infty} - p. \tag{4.12}$$

Stress decomposes uniquely in to spherical and deviatoric parts, so its deviatoric part must be traceless. One can thus identify the deviatoric stress normal to the x direction

$$\tau_{xx} = -\left(\tau_{yy} + \tau_{zz}\right) = 2p - 2p^{\infty}. \tag{4.13}$$

Thus the excess or gauge pressure over the ambient pressure necessarily works to deform the material. This is similar to the effective-stress principle used in soil mechanics [104, 128]. With d^2 equations 4.11–4.13 providing descriptions of deviatoric stresses in terms of the boundary information and pressure distributions within the membrane, Hooke's law (equation 3.45) can again be perceived as a definition for deviatoric strains, thereby closing the model.

It is worth emphasising that in this one-dimensional elastic case, the stress boundary conditions in the in-plane directions imply that no mechanical properties are explicitly needed to describe the distribution of deviatoric stresses. Strain calculation, however, must incorporate properties: calculation of Eulerian spherical strain through the equation of state (equation 3.70) involves the bulk modulus, K; calculation of deviatoric strain through Hooke's law (equation 3.45) involves the shear modulus G_{shear}.

Viscous Case: assuming linearity and isotropy, Newton's law generally applies, characterised by the shear μ_{shear} and bulk μ_{bulk} viscosities of the material,

$$\vec{\vec{\tau}} = -\mu_{\text{shear}}\left[\vec{\nabla}\vec{v} + \left(\vec{\nabla}\vec{v}\right)^{\text{T}} - \tfrac{2}{3}\vec{\vec{I}}\vec{\nabla}\cdot\vec{v}\right]. \tag{4.14}$$

This law defines deformation stress in terms of the traceless part of the rate of deformation tensor $\dot{\vec{\vec{\epsilon}}}$, which is expressed in terms of mass-average velocity gradients. This closes the problem without the need for providing additional information, since the mass-average velocity has already been defined. The challenge, here, is to quantify the effective viscosity of hydrated Nafion.

Viscoelastic Case: this is the stress constitutive derived from the entropy generation law in chapter 3 (equation 3.143), which deals with a more complex material similar to a Maxwell fluid,

$$\vec{\vec{\tau}} = \frac{2\mu_{\text{shear}}\left(\vec{\vec{\epsilon}} + \frac{1}{3}\vec{\vec{I}}\vec{\nabla}\cdot\vec{v}\right) - t_{\text{shear}}\dfrac{D\vec{\vec{\tau}}}{Dt}}{1 - t_{\text{shear}}\frac{D\ln\rho G_{\text{shear}}}{Dt}},$$

parameterised by the shear viscosity, the shear modulus, and a ratio of the two—the stress relaxation time $t_{\text{shear}} = \mu_{\text{shear}}/G_{\text{shear}}$. For finite values ($0 < t_{\text{shear}} < \infty$) of the relaxation time, the material can be classified as viscoelastic.

4.1.4 Mass Transport Flux Laws with Stress Diffusion

The momentum balance and associated equations, the compressibility effects in the volume balance, and the kinematic effects built in through the equation of state describe only a part of the mechanical response: they are insufficient to describe the various ways in which spatial or temporal stress gradients can impact the transport of species in an electrolytic solution; the impact of stress variation on the driving force for diffusive transport should also be considered. Recall that the Gibbs–Duhem equation allows only $n-1$ independent driving forces in an n species system; to these there correspond $n-1$ flux laws in each of the d spatial dimensions. For the 1-dimensional, 3-species system, we therefore write only 2 flux laws.

4.1.4.1 Solvent Flux Law

In the force-explicit form of the Onsager–Stefan–Maxwell formalism, the general flux law 3.137 can be adapted for the solvent as

$$-c_{\text{T}}y_0\left[\vec{\nabla}\mu_0 + \overline{S}_0\vec{\nabla}T - \frac{\overline{m}_0}{\rho}\left(\vec{\nabla}p + \vec{\vec{\epsilon}}' : \vec{\nabla}\vec{\vec{\tau}}\right)\right] = \sum_{j\neq 0}\frac{RT}{\mathscr{D}_{0j}}\left(y_j\vec{N}_0 - y_0\vec{N}_j\right). \tag{4.15}$$

The local gradient of the electrochemical potential for the solvent, $\mu_0 = \mu_0\left(T, p, \vec{\bar{\tau}}, y_0\right)$ can be expressed in terms of gradients of the basis variables as

$$\vec{\nabla}\mu_0 = -\overline{S}_0\vec{\nabla}T + \overline{V}_0\vec{\nabla}p + \overline{V}_0\vec{\bar{\epsilon}}' : \vec{\nabla}\vec{\bar{\tau}} + RT\vec{\nabla}\ln\left(y_0\lambda_{y_0}\right), \tag{4.16}$$

where λ_{y_0} is the activity coefficient of the solvent on a mole-fraction basis. Note that electric potential or charge plays no part in determining the energy state of the solvent, since it is a neutral species with $z_0 = 0$. It should also be noted that the chemical potential of a viscoelastic or solid material depends on the deviatoric stress and strain. Equations 4.15 and 4.16 combine to yield

$$-c_{\mathrm{T}}y_0\left[RT\chi\vec{\nabla}\ln y_0 + \left(\overline{V}_0 - \frac{\overline{m}_0}{\rho}\right)\left(\vec{\nabla}p + \vec{\bar{\epsilon}}' : \vec{\nabla}\vec{\bar{\tau}}\right)\right] = \sum_{j\neq 0}\frac{RT}{\mathscr{D}_{0j}}\left(y_j\vec{N}_0 - y_0\vec{N}_j\right). \tag{4.17}$$

Here the temperature dependence of the electrochemical potential μ_0 is cancelled by the partial-molar-entropy term in the definition of the diffusion driving force. Darken's thermodynamic factor χ, quantifying the non-ideality of the electrolyte, is defined through

$$\vec{\nabla}\ln\left(y_0\lambda_{y_0}\right) = \left(1 + \frac{d\ln\lambda_{y_0}}{d\ln y_0}\right)\vec{\nabla}\ln y_0 = \chi\vec{\nabla}\ln y_0. \tag{4.18}$$

As seen earlier in this chapter, the diffusive flux $\vec{J}_i$ is replaced by the total molar flux $\vec{N}_i$ in this version of the model. For a simple binary electrolyte, the algorithm presented by Monroe and Delacourt [23] can be employed to invert equation 4.17 (into a ~Nernst–Planck form): use Faraday's law (equation 3.91) and the principle of electroneutrality (equation 4.3) to eliminate anion molar flux and mole fraction, proceed by using the definition of volume-average velocity (equation 3.88) to eliminate cation molar flux, use the Guggenheim condition (equation 4.1) and the equation of state (equation 3.30) to further simplify the law. The explicit steps for the inversion are provided in Appendix B. The ultimate result of this procedure in a flux-explicit law for water diffusion:

$$\vec{N}_0 = -c_{\mathrm{T}}^2\overline{V}_{\mathrm{e}}y_0\frac{D}{\nu}\left\{\vec{\nabla}\ln y_0 + \frac{1}{RT\chi}\left[\left(\overline{V}_0 - \frac{\overline{m}_0}{\rho}\right)\left(\vec{\nabla}p + \vec{\bar{\epsilon}}' : \vec{\nabla}\vec{\bar{\tau}}\right)\right]\right\} + c_{\mathrm{T}}y_0\vec{v}^{\square}, \tag{4.19}$$

where $D = \mathscr{D}\chi$ is the macroscopic Fickian diffusion coefficient and $\nu = \sum_i \nu_i$ stands for the total number of ions in a formula unit. The salt chemical potential μ_e, partial molar volume $\overline{V}_e$, and molecular weight $\overline{m}_e$ are stoichiometric combinations of the corresponding properties of its constituent ions; for instance, $\overline{V}_e$ for a binary electrolyte would be $\overline{V}_e = \nu_+\overline{V}_+ + \nu_-\overline{V}_-$. By definition, the partial molar volume of a species measures how a solution changes volume when the molar content of a given species is changed in isolation; since global electroneutrality must be maintained, this physical process is not possible for a charged species. Hence, only the partial molar volume of the salt $\overline{V}_e$ is practically measurable; following the convention developed by Newman and Chapman, $\overline{V}_e$ can be decomposed into partial molar volumes of the cations and anions: $\overline{V}_+ = \frac{1-t_+^0}{\nu_+}\overline{V}_e$ and $\overline{V}_- = \frac{t_+^0}{\nu_-}\overline{V}_e$. Further details of this decomposition are detailed in Appendix B.

According to the solvent flux law (equation 4.19), in addition to composition-gradient-driven ($\vec{\nabla} y_0$) and bulk convective transport ($\vec{v}^{\square}$), the Cauchy stress gradients, $\vec{\nabla} p$ and $\vec{\nabla}\vec{\tilde{\tau}}$, can lead to solvent diffusion but only when the volume and mass fraction of the solvent are different. Additionally, the contribution of deformation stress gradient is scaled by the deformation strain; for instance, this term will be small for a purely viscous liquid exhibiting negligible deformation.

4.1.4.2 MacInnes Equation

The second OSM flux law describes the transport of hydrogen ions. It differs in form from the solvent flux law because the electrochemical potential of protons μ_+ can be directly related to the voltage measured by a reference electrode, and therefore needs not be broken into activity-, stress-, and temperature-dependent components. In an

isothermal system, the force-explicit form of the hydrogen-ion flux is given by

$$-c_{\mathrm{T}} y_{+}\left[\vec{\nabla}\mu_{+}-\frac{\overline{m}_{+}}{\rho}\left(\vec{\nabla}p+\vec{\vec{\epsilon}}':\vec{\nabla}\vec{\vec{\tau}}\right)\right]=\sum_{j\neq+}\frac{RT}{\mathscr{D}_{+j}}\left(y_{j}\vec{N}_{+}-y_{+}\vec{N}_{j}\right). \tag{4.20}$$

In another inversion process (also explicitly carried out in Appendix B), this equation transforms into a MacInnes equation (modified form of Ohm's law) by combining Faraday's law (equation 3.91), the definition of volume-average velocity (equation 3.88), and the recently inverted solvent flux law (equation 4.19):

$$\vec{\nabla}\Phi=-\frac{\vec{i}}{\kappa}-\frac{\nu RT\left(1-t_{+}^{0}\right)\chi}{Fz_{+}\nu_{+}\left(1-y_{0}\right)}\vec{\nabla}y_{0}+\frac{1}{Fz_{+}}\left[\frac{\overline{m}_{+}}{\rho}-\frac{\nu\left(1-t_{+}^{0}\right)y_{0}}{\nu_{+}\left(1-y_{0}\right)}\left(\overline{V}_{0}-\frac{\overline{m}_{0}}{\rho}\right)\right]\left(\vec{\nabla}p+\vec{\vec{\epsilon}}':\vec{\nabla}\vec{\vec{\tau}}\right). \tag{4.21}$$

Here, t_{+}^{0} is the transference number of cations relative to the solvent and κ is the ionic conductivity, which is explicitly a function of local concentration. These, together with the Fickian diffusivity $D=\mathscr{D}\chi$, are the measurable macroscopic properties which are necessary to completely describe transport in a binary system; their relations to the microscopic transport and thermodynamic properties are shown in Table 4.1. The electrochemical-potential gradient has been related to a gradient of potential Φ by assuming that the reference electrode used to measure said potential is reversible only to cations

$$\vec{\nabla}\Phi=\frac{\vec{\nabla}\mu_{+}}{Fz_{+}}\ . \tag{4.22}$$

Although the properties laid out above are typically used for liquid electrolytes, conventional properties used in the Nafion literature are somewhat different. The *transport coefficient* α is used instead of the thermodynamic diffusion coefficient D, and the *electroosmotic drag coefficient* ξ is used instead of the cation transference number t_{+}^{0} [79]. Transport laws in terms of these alternative properties, unsurprisingly, look simpler,

$$\left(\vec{N}_{0}-c_{\mathrm{T}}y_{0}\vec{v}^{\square}\right)=-\left(1-c_{\mathrm{T}}y_{0}\overline{V}_{0}\right)\alpha\vec{d}_{0}, \tag{4.23}$$

$$\vec{i}=-\frac{\kappa}{Fz_{+}}\left(\vec{d}_{+}+\xi\vec{d}_{0}\right). \tag{4.24}$$

The relationships between the two sets of macroscopic transport properties are included in Table 4.1. For the sake of generality, we adhere to the conventional set of transport properties used for binary electrolytes—κ, D, t_+^0.

Equation 4.21 attributes changes in cation electrochemical potential to various sources such as ohmic losses quantified by the solution conductivity, concentration overpotential expressed in terms of the mole-fraction gradient, and a novel 'stress overpotential' originating in the mechanical dependences of the electrochemical potential and the diffusion driving force. These last terms relating to stress, mainly, will form the basis of the novel signatures in Nyquist and Bode plots that will be developed later in this chapter.

property description	expression
Thermodynamic Properties	
Thermodynamic Diffusion Coefficient	$\mathscr{D} = \dfrac{\nu \mathscr{D}_{0+}\mathscr{D}_{0-}}{\nu_+ \mathscr{D}_{0-} + \nu_- \mathscr{D}_{0+}}$
Thermodynamic Darken Factor	$\chi = 1 + \dfrac{d \ln \lambda_{y_0}}{d \ln y_0}$
Macroscopic Transport Properties	
Fickian Diffusion Coefficient	$D = \mathscr{D}\chi$
Cation Transference Number	$t_+^0 = \dfrac{\nu_- \mathscr{D}_{0+}}{\nu_+ \mathscr{D}_{0-} + \nu_- \mathscr{D}_{0+}}$
Electrolyte Conductivity	$\dfrac{1}{\kappa} = \dfrac{RT\nu_+\nu_-}{\left(Fz_+\nu_+\right)^2 c_{\mathrm{T}} y_+} \left(\dfrac{y_+}{\mathscr{D}_{+-}} + \dfrac{\nu_+ y_0}{\nu_+ \mathscr{D}_{0-} + \nu_- \mathscr{D}_{0+}} \right)$
Nafion-specific Transport Properties	
Transport Coefficient	$\alpha = \dfrac{c_{\mathrm{T}}}{RT} \dfrac{y_0}{1 - y_0} \mathscr{D}$
Electroosmotic Drag Coefficient	$\xi = \dfrac{\nu}{\nu_+} \dfrac{y_0}{1 - y_0} \left(1 - t_+^0\right)$

Table 4.1: Relationships of measurable macroscopic properties to microscopic binary transport coefficients and activity coefficients.

4.1.5 Model Closure: Kinematic Relationship for Reference Velocities

The two velocities used so far in the model are relevant to different physical phenomena occurring in the system: the mass-average velocity $\vec{v}$ is concerned with the flow of mass and momentum in the system whereas the volume-average velocity $\vec{v}^{\square}$ quantifies local volume flow. A linear relationship expresses the difference between the two reference velocities in terms of the independent excess fluxes. Such an expression is convenient from a modelling point of view because it can supplant several algebraic equations—the Guggenheim condition, the principle of electroneutrality, Faraday's law (equation 3.91), the definition of volume-average velocity (equation 3.88), and the definition of mass-average velocity (equation 3.95)—to yield a compact and closed system of governing equations. In terms of the flux variables of the model—solvent flux, current density, and volume-average velocity—the mass-average velocity can be written as

$$\vec{v} = \frac{\overline{m}_{\mathrm{e}}}{\rho\overline{V}_{\mathrm{e}}}\left(\frac{\overline{m}_0}{\overline{m}_{\mathrm{e}}} - \frac{\overline{V}_0}{\overline{V}_{\mathrm{e}}}\right)\overline{V}_{\mathrm{e}}\vec{N}_0 + \frac{\overline{m}_{\mathrm{e}}}{\rho\overline{V}_{\mathrm{e}}}\left(\frac{\overline{m}_-}{\overline{m}_{\mathrm{e}}} - \frac{\overline{V}_-}{\overline{V}_{\mathrm{e}}}\right)\frac{\overline{V}_{\mathrm{e}}\vec{i}}{Fz_-} + \frac{\overline{m}_{\mathrm{e}}}{\rho\overline{V}_{\mathrm{e}}}\vec{v}^{\square}. \tag{4.25}$$

Further, the solvent flux here can be replaced with flux law 4.19 for a different perspective; also using the definition of density (equation 4.9) and the equation of state (equation 3.30), one finds

$$\vec{v} - \vec{v}^{\square} = -c_{\mathrm{T}}^2\overline{V}_{\mathrm{e}}\frac{\overline{m}_{\mathrm{e}}}{\rho\overline{V}_{\mathrm{e}}}\left(\frac{\overline{m}_0}{\overline{m}_{\mathrm{e}}} - \frac{\overline{V}_0}{\overline{V}_{\mathrm{e}}}\right)\frac{D}{\nu}\left\{\vec{\nabla}\ln y_0 + \frac{1}{RT\chi}\left[\left(\overline{V}_0 - \frac{\overline{m}_0}{\rho}\right)\left(\vec{\nabla}p + \vec{\vec{\epsilon}}' : \vec{\nabla}\vec{\vec{\tau}}\right)\right]\right\} + \frac{\overline{m}_{\mathrm{e}}}{\rho\overline{V}_{\mathrm{e}}}\left(\frac{\overline{m}_-}{\overline{m}_{\mathrm{e}}} - \frac{\overline{V}_-}{\overline{V}_{\mathrm{e}}}\right)\frac{\overline{V}_{\mathrm{e}}\vec{i}}{Fz_-}. \tag{4.26}$$

This suggests that there will be net movement in a multicomponent electrolytic solution under the influence of composition gradients, stress (pressure or deformation) gradients, or a current density, leading to a difference between the mass-average and volume-average velocities. Only if the mass and volume fractions of the salt and sol-

vent equate, and those of the anion and salt, will the two velocities be identical for all combinations of fluxes and driving forces.

Table 4.2 summarises the system of transport equations that will be solved to simulate the signatures of electrochemical/mechanical coupling in Nafion membranes, along with the counts of dependent variables and equations. The model is closed in the sense that the numbers of variables and equations match in the membrane's interior points, but a more rigorous assessment of model closure can only be made after the initial and boundary conditions are considered.

#	**variables**	#	**governing equations**	**equation #**
1	total concentration, c_{T}	1	equation of state	3.70
d	solvent flux, $\vec{N}_0$	1	solvent mole balance	4.2
d	current density, $\vec{i}$	1	charge balance	4.4
d	volume-average velocity, $\vec{v}^{\square}$	1	volume balance	4.6
1	solvent mole fraction, y_0	d	solvent flux law	4.19
1	potential, Φ	d	cation flux law	4.21
1	pressure, p	d	momentum balance	4.8
1	density, ρ	1	definition of density	4.9
d	mass-average velocity, $\vec{v}$	d	kinematic velocity relations	4.25
d^2	deformation stresses, $\vec{\vec{\tau}}$	d^2	stress constitutive laws	4.13,4.14, & 3.143
d^2	Eulerian strain, $\vec{\vec{e}}'$	d^2	strain constitutive laws	3.45
	$2d^2 + 4d + 5$	$=$	$2d^2 + 4d + 5$	***closed***

Table 4.2: Summary of the impedance transport model equations with counts

4.2 Linearised Impedance Transport Model

At equilibrium, we imagine that the cell rests at open circuit under ambient pressure p^∞ and temperature T, which results in null molar species fluxes, volume-average velocity, and current density,

$$\vec{N}_i^\infty = \vec{i}^\infty = \vec{v}^{\square,\infty} = 0. \tag{4.27}$$

Assuming that no significant changes occur across the in-plane direction (in the y-z plane), the model is solved only in the through-plane dimension (x-direction) characterised by the equilibrium thickness, L^∞, which depends on the equilibrium water content λ^∞. The reduction to one spatial dimension is justified given the typical aspect ratios of Nafion membranes, whose thicknesses are much smaller than their other dimensions. This steady-state (or equilibrium) membrane system with uniform average composition, pressure, and temperature works as the initial condition for the model.

To carry out an impedance analysis on this system, a galvanostat is assumed to deliver a sinusoidal current density of the form

$$i = i_0 \operatorname{Re}\{\exp(j\omega t)\} \tag{4.28}$$

with an amplitude $|i_0|$ small enough to incite a linear voltage response from the cell (equivalently, a small alternating voltage could be applied from a potentiostat to induce a current); ω is the radial frequency of the applied waveform measured in radians/s, and is related to the practical frequency measured in Hz as

$$f = \frac{\omega}{2\pi}. \tag{4.29}$$

Owing to the small amplitude, the AC current density acts as a first-order regular perturbation to the system of equations modelling ion transport in such a cell. Thus,

once a periodic steady state is reached, variables and properties vary according to

$$g = g^{\infty} + \mathrm{Re}\left\{g^{(1)}\left(x, y, z\right)\exp\left(j\omega t\right)\right\}, \tag{4.30}$$

where g^{∞} is the uniform equilibrium response and $g^{(1)}$ is the first-order response; in a periodic steady state all the time-dependence arises from the sinusoidal term. Applying this perturbation transforms all the derivatives of the form $\partial g/\partial t$ into $\mathrm{Re}\{j\omega g^{(1)}\exp\left(j\omega t\right)\}$, as well as converts all partial differential equations to ordinary differential equations (over space). The zero-order problem produces the uniform steady-state discussed above, in which fluxes and property gradients vanish. A linear problem governing first-order, $\mathcal{O}(1)$, terms is obtained by neglecting terms of second and higher order, noting that the product of two first-order terms is $\mathcal{O}(2)$. Given the form of the perturbation ansatz, the time dependences of all dependent variables are exchanged for a parametric frequency dependence in the first-order perturbed system.

Following the procedure delineated above, equations listed in Table 4.2 are linearised and can be solved together to obtain spatial distributions of the dependent variables along electrolyte thickness x at each frequency ω, subject to the boundary conditions discussed in the following subsection.

4.2.1 Boundary Conditions

The differential-algebraic system derived from linearising the equations in Table 4.2, and in the process converting them from the time to the frequency regime, contains six first-order ordinary differential equations, which require one boundary condition each to close the system of equations. The faces of the electrolytic membrane that interface with the electrodes are considered as the physical boundaries of this system (at $x = 0$ & $x = L$).

The first boundary condition corresponds directly to the application of an alternating impedance current, which induces a constant amplitude current density in the first-order perturbation,

$$i^{(1)}\Big|_0 = i_0. \tag{4.31}$$

Assuming that the membrane does not take up any water from the surroundings during the course of the impedance experiment, the water molar flux at both the boundaries in this first-order system vanishes, giving us the second and third boundary conditions,

$$N_0^{(1)}\Big|_0 = N_0^{(1)}\Big|_L \sim 0. \tag{4.32}$$

Only hydrogen-ions/cations participate in the interfacial redox reactions driven by the impedance current. The resulting cation flux is quantified through,

$$N_+^{(1)}\Big|_0 = \left.\frac{s_+ i^{(1)}}{F z_{\mathrm{e}^-} n_{\mathrm{e}^-}}\right|_0 \qquad N_+^{(1)}\Big|_L = \left.\frac{s_+ i^{(1)}}{F z_{\mathrm{e}^-} n_{\mathrm{e}^-}}\right|_L. \tag{4.33}$$

However, cation flux is not one of the dependent variables in this system (as seen from Table 4.2). Condition 4.33 is, instead, expressed in terms of the volume-average velocity at the boundaries. This quantifies *Faradaic convection*, a solute-volume effect discussed by Liu and Monroe [27], which arises because the molar flux of hydrogen ions across the interface manifests as a net volume flow into the electrolyte. The interfacial volume-average velocities, proportional to the current density, are then expressed as,

$$v^{\square,(1)}\Big|_0 = \left.\frac{\Delta \overline{V}_{\mathrm{rxn}}^{\mathrm{sol},\,\infty} i^{(1)}}{F z_{\mathrm{e}^-} n_{\mathrm{e}^-}}\right|_0 \qquad v^{\square,(1)}\Big|_L = \left.\frac{\Delta \overline{V}_{\mathrm{rxn}}^{\mathrm{sol},\,\infty} i^{(1)}}{F z_{\mathrm{e}^-} n_{\mathrm{e}^-}}\right|_L, \tag{4.34}$$

providing the fourth and fifth boundary conditions. The molar volume change due to reaction in the solution phase is given by $\Delta \overline{V}_{\mathrm{rxn}}^{\mathrm{sol}} = \sum_i s_i \overline{V}_i$. For the symmetric hydrogen cell under consideration, anions and solvent do not contribute towards the change, so $\Delta \overline{V}_{\mathrm{rxn}}^{\mathrm{sol}} = s_+ \overline{V}_+$ at both boundaries. Finally, to close the $1d$ differential-algebraic system of equations, a reference potential needs to be set at either boundary

as the sixth boundary condition,

$$\Phi^{(1)}\big|_{L} = 0. \tag{4.35}$$

Only one condition is needed because potential only appears as a gradient in the model.

Nafion membranes are known to swell upon solvent sorption, so it is important to consider the effect of impedance current, through the induced composition and pressure changes, on the first-order change to membrane thickness $(L - L^{\infty})^{(1)}$. This can be analysed formally by comparing the mass of membrane before and during the passage of current. Assuming that the cross-sectional area remains unchanged, membrane moles are conserved during the swelling process:

$$\int_0^{L^{\infty}} c_{\mathrm{T}}^{\infty} y_{\mathrm{e}}^{\infty} dx = \int_0^{L} c_{\mathrm{T}} y_{\mathrm{e}} dx. \tag{4.36}$$

Linearising the right hand side, we obtain

$$\int_0^{L^{\infty}} c_{\mathrm{T}}^{\infty} y_{\mathrm{e}}^{\infty} dx = \int_0^{L^{\infty}} c_{\mathrm{T}}^{\infty} y_{\mathrm{e}}^{\infty} dx + \int_{L^{\infty}}^{L} c_{\mathrm{T}}^{\infty} y_{\mathrm{e}}^{\infty} dx + \int_0^{L^{\infty}} c_{\mathrm{T}}^{\infty} y_{\mathrm{e}}^{(1)} dx + \int_0^{L^{\infty}} c_{\mathrm{T}}^{(1)} y_{\mathrm{e}}^{\infty} dx. \tag{4.37}$$

Simplifying this leads to an expression for the first-order change in membrane thickness,

$$c_{\mathrm{T}}^{\infty} y_{\mathrm{e}}^{\infty} (L - L^{\infty})^{(1)} = - \int_0^{L^{\infty}} (c_{\mathrm{T}}^{\infty} y_{\mathrm{e}}^{(1)} + c_{\mathrm{T}}^{(1)} y_{\mathrm{e}}^{\infty}) dx. \tag{4.38}$$

This shows that the first-order change in thickness, or rather the extent to which the boundary moves, depends on the integral of the first-order change in the average membrane/electrolyte molar concentration. We do not have an explicit solution for concentration at this juncture to be able to quantify the integral directly, however. Instead we consider the cation material balance to get more insight,

$$-j\omega\nu_{+}(c_{\mathrm{T}}^{\infty} y_{\mathrm{e}}^{(1)} + c_{\mathrm{T}}^{(1)} y_{\mathrm{e}}^{\infty}) = \frac{dN_{+}^{(1)}}{dx}. \tag{4.39}$$

Integrating this from 0 to L^{∞} to get all the first-order integrands, we find that

$$- \int_0^{L^{\infty}} (c_{\mathrm{T}}^{\infty} y_{\mathrm{e}}^{(1)} + c_{\mathrm{T}}^{(1)} y_{\mathrm{e}}^{\infty}) dx = \frac{1}{j\omega\nu_{+}} dN_{+}^{(1)} = \frac{1}{j\omega\nu_{+}} \left(N_{+}^{(1)}\Big|_{L^{\infty}} - N_{+}^{(1)}\Big|_{0} \right). \tag{4.40}$$

This result suggests that the average membrane concentration can only be affected by the impedance current if the cation fluxes at the two boundaries differ. For the symmetric hydrogen cell, however, cations are produced at the anode and consumed at the cathode at the same rate, rendering $N_+^{(1)}\big|_{L^\infty} = N_+^{(1)}\big|_0$. Further combining the first-order change in membrane thickness expression, equation 4.38 and the integrated cation balance, equation 4.40 provides an alternate perspective into the first-order change in electrolyte thickness,

$$c_{\mathrm{T}}^{\infty} y_{\mathrm{e}}^{\infty} (L - L^{\infty})^{(1)} = \frac{1}{j\omega\nu_+} \left(N_+^{(1)}\Big|_{L^\infty} - N_+^{(1)}\Big|_0 \right). \tag{4.41}$$

This expression clearly establishes the fact that for the stripping/plating framework we consider for this study, there is no first-order change in electrolyte thickness; thus the boundaries do not move due to the passage of impedance current, even though local pressure is free to vary.

To crystallise our understanding of the relation between pressure and boundary movement, we proceed by integrating the linearised volume balance and isolating the first-order integrands,

$$v^{\square,(1)}\big|_{L^\infty} - v^{\square,(1)}\big|_0 = -j\omega \frac{1}{K^\infty} \int_0^{L^\infty} p^{(1)} dx. \tag{4.42}$$

Again, since the cell is symmetric and current density is constant across it, the volume-average velocity at the two boundaries is the same, suggesting that the first-order pressure perturbation integrates to 0. Impedance current does not, therefore, alter the average pressure in the membrane, as long as the volume flow out of the cell is the same as the volume flow into it. Although the local pressure is allowed to vary, it is constrained to an odd profile about the centre of the membrane to keep the average unchanged. This analysis may be key in building a piezoelectric application where a change in the thickness, materialised by ensuring different fluxes/velocities at the two boundaries (*e.g.* equal and opposite velocities manifesting as alternating squeezing and stretching actions on the membrane), could be linked to a change in voltage.

We place the left boundary at $x = 0$, implicitly assuming that the origin of coordinates is fixed there and that any change in thickness will manifest only in the right boundary position, $x = L(t)$. The above analysis proved $(L - L^{\infty})^{(1)} \sim 0$, allowing all conditions at L to be moved to L^{∞} in the first-order perturbation. Schematic diagrams of the symmetric hydrogen cell with boundary conditions at zero and first order are shown in Figure 4.1.

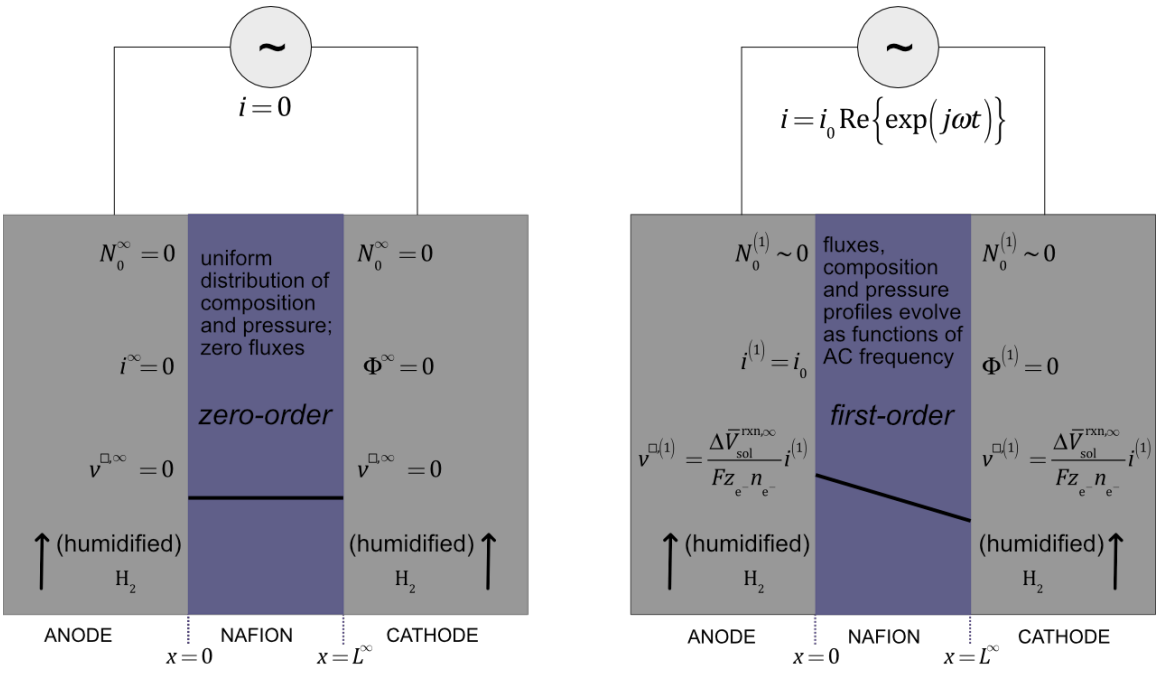

Figure 4.1: Schematic of the symmetric hydrogen cell showing (a) zero-order and (b) first-order behaviour.

A complete 'band-map' of the linearised transport equations and boundary conditions for the symmetric hydrogen cell is laid out in Figure 4.2, demonstrating closure of the problem. Linearisation of the equations makes certain higher-order effects disappear; for instance the pressure dependence of partial molar volumes appears in product with a flux term in the local volume balance, thereby becoming a higher-order term and hence dropping out from equation 4.5. The first-order density does not play a role in the model after the linearisation. The equilibrium total concentration c_{T}^{∞}, density ρ^{∞}, and solvent composition y_0^{∞} are model parameters that emerge from solving the zero-order problem, whose statement is relatively trivial because there are no fluxes or gradients.

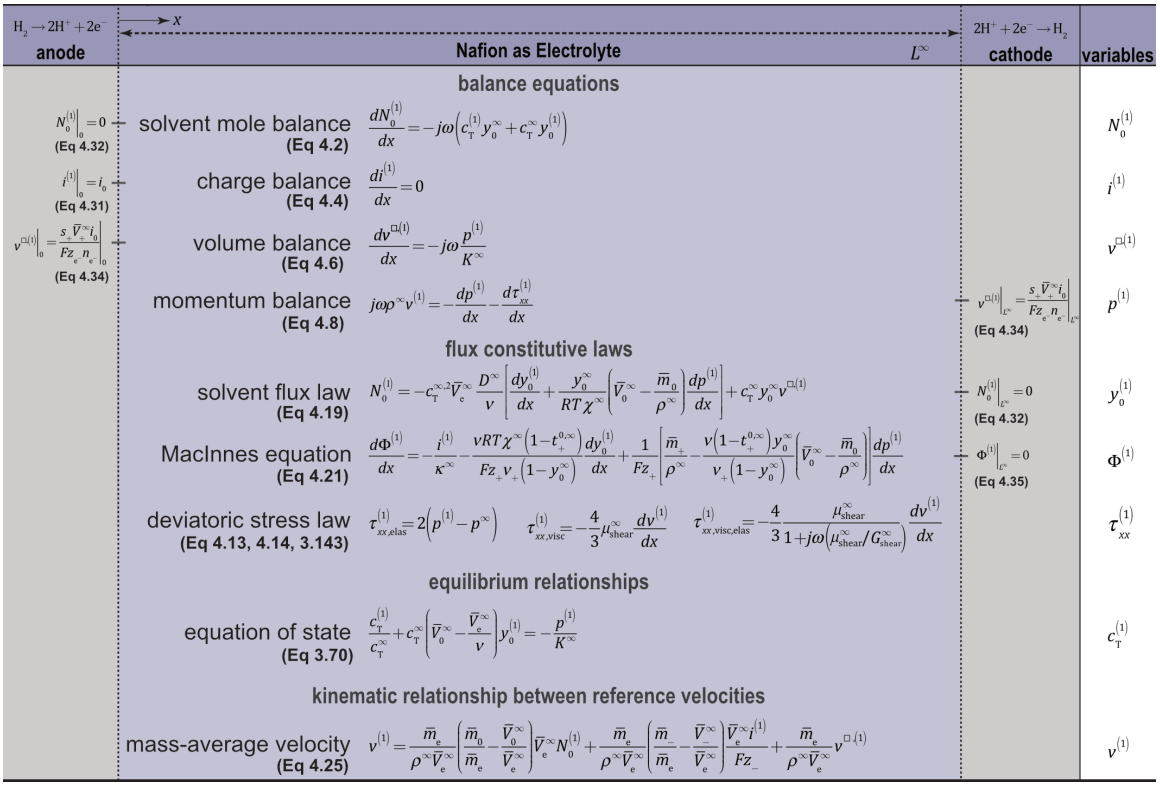

Figure 4.2: Linearised impedance transport models with applied boundary conditions.

Also in the linear problem, higher-order dependences of the material properties on dependent variables vanish. The zero-order properties listed in Table 4.3: transport properties $D^\infty, t_+^{0,\infty}, \kappa^\infty$; thermodynamic properties $\chi^\infty, \overline{V}_k^\infty, \overline{m}_i$; and mechanical properties K^∞, $\mu_{\text{shear}}^\infty$, ν_{PR}^∞, take the values measured at equilibrium y_0^∞, p^∞, T. Note that the shear modulus, G_{shear}^∞ has been replaced by Poisson's ratio ν_{PR}^∞ following the standard definition [118]

$$G_{\text{shear}}^\infty = \frac{3}{2}\frac{1-2\nu_{\text{PR}}}{1+\nu_{\text{PR}}}K^\infty. \tag{4.43}$$

Macroscopic transport parameters can be calculated from the microscopic transport and thermodynamic properties specified in the table.

property description	**value**	**reference**
Mechanical Properties		
Bulk Modulus, K^∞	76 MPa	[3]
Poisson's Ratio, ν_{PR}^∞	0.25	[166]
Viscosity, $\mu_{\text{shear}}^\infty$	3.5 mPa · s	[167]
Binary Interaction Parameters		
$\mathscr{D}_{0+}^\infty$	6.6×10^{-9} m$^2 \cdot$ s^{-1}	[168]
$\mathscr{D}_{0-}^\infty$	1.05×10^{-9} m$^2 \cdot$ s^{-1}	[168]
$\mathscr{D}_{+-}^\infty$	5.02×10^{-10} m$^2 \cdot$ s^{-1}	[168]
Macroscopic Transport Properties		
Fick's Diffusion Coefficient, D^∞	1.8×10^{-9} m$^2 \cdot$ s^{-1}	Table 4.1
Cation Transference Number, $t_+^{0,\infty}$	0.86	Table 4.1
Ionic Conductivity, κ^∞	18.74 S · m^{-1}	Table 4.1
Thermodynamic Properties		
Water Partial Molar Volume, $\overline{V}_0^\infty$	1.63×10^{-5} m$^3 \cdot$ mol^{-1}	[168]
Membrane Partial Molar Volume, $\overline{V}_{\text{e}}^\infty$	5.66×10^{-4} m$^3 \cdot$ mol^{-1}	[168]
Darken Thermodynamic Factor, χ^∞	1	assume ideality
Water Molar Mass, $\overline{m}_0$	18 g · mol^{-1}	
Membrane Molar Mass, $\overline{m}_{\text{e}}$	1100 g · mol^{-1}	[168]
Zero-Order Variables		
Density, ρ^∞	1.755 g · cm^{-3}	eq 4.9
Total Concentration, c_{T}^∞	16.46 M	eq 3.30
Hydrated Nafion Thickness, L^∞	229 μm	eq 4.36

Table 4.3: Property values for hydrated 117 Nafion membranes with λ^∞ = 10 and dry thickness = 177.8 μm assembled from various sources as mentioned.

4.3 Dimensional Analysis of the Linear Model

Rescaling the variables in the linear system with reasonable characteristic values reveals a number of dimensionless parameter groups, whose magnitudes determine the relative importances of various physical phenomena at different excitation frequencies. The two independent variables are position and frequency; the former scales with the equilibrium membrane thickness,

$$X = x/L^{\infty} \tag{4.44}$$

and the latter by the characteristic diffusion frequency,

$$\Omega = \omega/\left(D^{\infty}/L^{\infty 2}\right). \tag{4.45}$$

Given the characteristic length and frequency, a characteristic current density can be introduced by adopting parameter $Fz_+/\overline{V}_{\mathrm{e}}$ to establish the scale of the membrane's "ionic strength"

$$\mathrm{I} = \frac{i\overline{V}_{\mathrm{e}}^{\infty} L^{\infty}}{Fz_+ D^{\infty}}. \tag{4.46}$$

This parameter should be small in comparison to unity to guarantee that the applied current is in the regime of linear response.

Whereas the water mole fraction y_0^{∞} is already dimensionless and bounded, finding an appropriate scale for pressure is a subtler exercise, because pressure gradients are associated with both inertia and diffusion. Thus a geometric mean of the two characteristic system velocities— the characteristic diffusion speed D^{∞}/L^{∞} and the speed of sound in the medium, (approximately) $\sqrt{K^{\infty}/\rho^{\infty}}$—is used instead of favouring either end of the velocity spectrum:

$$P = \frac{p}{\rho^{\infty}\dfrac{D^{\infty}}{L^{\infty}}\sqrt{\dfrac{K^{\infty}}{\rho^{\infty}}}}. \tag{4.47}$$

Further, transforming the two characteristic velocities into Peclet numbers, $\mathrm{Pe}^{\square} = v^{\square}L^{\infty}/D^{\infty}$ and $\mathrm{Pe} = vL^{\infty}/D^{\infty}$, ensures that they are compatible with the scaled current density, which is the primary stimulator for transport in this cell. Similarly, the solvent flux is scaled by molar flux at the diffusional velocity, $\eta_0 = N_0/\left(\nu_+ c^{\infty} D^{\infty}/L^{\infty}\right)$. Total concentration is scaled by the molar volume $\theta_{\mathrm{T}} = c_{\mathrm{T}}\overline{V}_{\mathrm{e}}^{\infty}$, and would be unity for a dry membrane.

The described non-dimensionalisation scheme converts the first-order material conservation laws—material, charge, volume balances—as follows,

$$\frac{d\eta_0^{(1)}}{dX} = -j\Omega\left(\theta_{\mathrm{T}}^{(1)} y_0^{\infty} + \theta_{\mathrm{T}}^{\infty} y_0^{(1)}\right), \tag{4.48}$$

$$\frac{d\mathrm{I}^{(1)}}{dX} = 0, \tag{4.49}$$

$$\frac{d\mathrm{Pe}^{\square,(1)}}{dX} = -j\Omega\mathrm{Ma}_{\mathrm{D}}^{\infty} P^{(1)}, \tag{4.50}$$

in the process introducing the first dimensionless parameter

$$\mathrm{Ma}_{\mathrm{D}}^{\infty} = \frac{D^{\infty}/L^{\infty}}{\sqrt{K^{\infty}/\rho^{\infty}}}. \tag{4.51}$$

Using properties from Table 4.3, we can estimate $\mathrm{Ma}_{\mathrm{D}}^{\infty} \sim \mathcal{O}\left(10^{-8}\right)$. It is a 'diffusion Mach Number', which quantifies the characteristic diffusion speed in units of the speed of sound in the membrane. The magnitude of $\mathrm{Ma}_{\mathrm{D}}^{\infty}$ indicates the frequency range at which compressibility will become relevant in the system; this happens when scaled frequency $W = \mathrm{Ma}_{\mathrm{D}}^{\infty}\Omega \sim 1$ as can be gleaned from the scaled volume balance, equation 4.50.

The diffusion Mach number also appears in the scaled equation of state alongside another dimensionless parameter $B_i = \overline{V}_i^{\infty}/\overline{V}_{\mathrm{e}}^{\infty}$:

$$\frac{\theta_{\mathrm{T}}^{(1)}}{\theta_{\mathrm{T}}^{\infty}} + \theta_{\mathrm{T}}^{\infty}\left(B_0 - \frac{1}{\nu}\right) y_0^{(1)} - \mathrm{Ma}_{\mathrm{D}}^{\infty} P^{(1)} = 0. \tag{4.52}$$

B_0 characterises the partial molar volumes occupied by water and the membrane backbone: for Nafion, $B_0 = \mathcal{O}(10^{-2})$.

In the present analysis, we will explore all three stress constitutive laws discussed in the modelling section. The first assumes Nafion to be a Hookean elastic solid. Given the one-dimensional geometry, the deviatoric stress gradient becomes proportional to the gradient of local pressure through

$$\frac{d\tau^{(1)}_{xx,\mathrm{elas}}}{dx} = 2\frac{dp^{(1)}}{dx}. \tag{4.53}$$

The resulting compact momentum balance (analogous to the volume balance) suggests that above a certain frequency ($W \sim 1$), local momentum accumulation ($j\Omega \mathrm{Pe}^{(1)}$) begins to set up significant pressure gradients across the membrane,

$$3\frac{dP^{(1)}}{dX} = -j\Omega \mathrm{Ma}^{\infty}_{\mathrm{D}} \mathrm{Pe}^{(1)}. \tag{4.54}$$

On the other hand, for a viscous material, the deviatoric stress tensor derived from Newton's law of viscosity takes the familiar form

$$\tau^{(1)}_{xx,\mathrm{visc}} = -\tfrac{4}{3}\mu^{\infty}_{\mathrm{shear}}\frac{dv^{(1)}}{dx}, \tag{4.55}$$

which produces an alternate form of the scaled momentum balance,

$$j\Omega \mathrm{Ma}^{\infty}_{\mathrm{D}} \mathrm{Pe}^{(1)} = -\frac{dP^{(1)}}{dX} + \tfrac{4}{3}\mathrm{Sc}^{\infty}_{\mathrm{shear}}\mathrm{Ma}^{\infty}_{\mathrm{D}}\frac{d^2\mathrm{Pe}^{(1)}}{dX^2}. \tag{4.56}$$

This introduces a second dimensionless parameter, the familiar Schmidt number

$$\mathrm{Sc}^{\infty}_{\mathrm{shear}} = \frac{\mu^{\infty}_{\mathrm{shear}}/\rho^{\infty}}{D^{\infty}}, \tag{4.57}$$

which reflects whether viscosity or diffusion dominates in the system.

The viscoelastic stress constitutive law simplifies down substantially in the limit of linear response, to

$$\tau^{(1)}_{xx,\mathrm{visc,elas}} = -\frac{\frac{4}{3}\mu^{\infty}_{\mathrm{shear}}}{1 + j\omega\left(\mu^{\infty}_{\mathrm{shear}}/G^{\infty}_{\mathrm{shear}}\right)}\frac{dv^{(1)}}{dx}. \tag{4.58}$$

This is similar in form to the viscous law, but produces a complex effective viscosity, *i.e.*, there can be a phase shift in the stress response that depends on the material's

relaxation time $t^{\infty}_{\text{shear}} = \mu^{\infty}_{\text{shear}}/G^{\infty}_{\text{shear}}$. Recalling that bulk modulus and shear modulus relate through equation 4.43, this stress law is substituted into the momentum balance to produce a scaled law involving the already defined dimensionless numbers $\text{Sc}^{\infty}_{\text{shear}}$ and $\text{Ma}^{\infty}_{\text{D}}$, as well as the Poisson's ration ν_{PR}:

$$j\Omega \text{Ma}^{\infty}_{\text{D}} \text{Pe}^{(1)} = -\frac{dP^{(1)}}{dX} + \frac{\frac{4}{3}\text{Sc}^{\infty}_{\text{shear}}\text{Ma}^{\infty}_{\text{D}}}{1 + j\Omega\dfrac{2\left(1+\nu_{\text{PR}}\right)}{3\left(1-2\nu_{\text{PR}}\right)}\text{Sc}^{\infty}_{\text{shear}}\text{Ma}^{\infty}_{\text{D}}}\frac{d^2\text{Pe}^{(1)}}{dX^2}. \tag{4.59}$$

A third dimensionless group of parameters, $\text{Ma}^{\infty}_{\text{M}} \sim \mathcal{O}(1)$, emerges from scaling the transport flux laws,

$$\text{Ma}^{\infty}_{\text{M}} = \sqrt{\frac{RT\chi^{\infty}c^{\infty}_{\text{T}}/\rho^{\infty}}{K^{\infty}/\rho^{\infty}}}. \tag{4.60}$$

This 'Maxwell Mach number' puts the Maxwell speed (the average speed associated with thermal motion of molecules in the system) in units of the membrane's speed of sound. In the solvent flux law, this parameter determines the contribution of pressure diffusion,

$$\eta_0^{(1)} = -\frac{\theta^{\infty^2}_{\text{T}}}{\nu}\left[\frac{dy_0^{(1)}}{dX} + \frac{\text{Ma}^{\infty}_{\text{D}}}{\text{Ma}^{\infty^2}_{\text{M}}}\beta^{\infty}y_0^{\infty}\left(1-y_0^{\infty}\right)\frac{dP^{(1)}}{dX}\right] + \theta^{\infty}_{\text{T}}y_0^{\infty}\text{Pe}^{\square,(1)}. \tag{4.61}$$

The quantity $\beta^{\infty} = \frac{\theta^{\infty^2}_{\text{T}}}{\nu\varphi^{\infty}}(B_0 - m_0)$ has a few dimensionless parameters hidden within it, the new ones are: ratio of molar masses, $m_i = \overline{m}_i/\overline{m}_{\text{e}}$ and density scaled by the dry membrane density, $\varphi = \rho/\left(\overline{m}_{\text{e}}/\overline{V}^{\infty}_{\text{e}}\right)$. The difference $(B_0 - m_0)$, which is a measure of the difference in the volume and mass fractions of the solvent in the solution, scales pressure diffusion. A similar term in the MacInnes equation controls the contribution of the impedance signature of mechanical effects, which arise as a combination of compressibility and momentum accumulation,

$$\frac{d\phi^{(1)}}{dX} = -\frac{\text{I}^{(1)}}{\text{K}^{\infty}} - \frac{\nu\chi^{\infty}}{z_+\nu_+}\frac{1-t_+^{0,\infty}}{1-y_0^{\infty}}\left[\frac{dy_0^{(1)}}{dX} + \beta^{\infty}y_0^{\infty}\left(1-y_0^{\infty}\right)\frac{\text{Ma}^{\infty}_{\text{D}}}{\text{Ma}^{\infty^2}_{\text{M}}}\left(1 - \frac{1}{1-\varphi^{\infty}}\frac{\nu_+m_+}{1-t_+^{0,\infty}}\right)\frac{dP^{(1)}}{dX}\right].$$

Here the ionic conductivity is scaled as $\text{K}^{\infty} = RT\overline{V}^{\infty}_{\text{e}}\kappa^{\infty}/F^2z_+D^{\infty}$ and potential is scaled as $\phi = F\Phi/RT$. The strain-energy term, which shows how deviatoric stress

drives diffusion, does not contribute to the flux laws or impedance calculations,

$$\mathcal{O}(1)\left[\vec{\vec{\epsilon}}' : \vec{\nabla}\vec{\vec{\tau}}\right] = \underbrace{\epsilon'^{\infty}_{xx}}_{=0}\frac{d\tau^{(1)}}{dx} + \epsilon'^{(1)}_{xx}\underbrace{\frac{d\tau^{\infty}}{dx}}_{=0} = 0, \tag{4.62}$$

because it is at least a second-order term. The above result makes the explicit assumption that the system is neither deformed nor voltage-biased at zero-order. The contribution of pressure overpotential survives, however. It will be novel to explore how this pressure overpotential affects impedance spectra.

Finally, the kinematic relationship between the reference velocities rescales as

$$\mathrm{Pe}^{(1)} = \frac{1}{\varphi^{\infty}}\left(m_0 - B_0\right)\eta_0^{(1)} + \frac{z_+}{z_-}\frac{1}{\varphi^{\infty}}\left(m_- - B_-\right)\mathrm{I}^{(1)} + \frac{1}{\varphi^{\infty}}\mathrm{Pe}^{\square,(1)}, \tag{4.63}$$

an expression that involves previously defined dimensionless parameters.

4.3.1 Bulk Viscosity Effects

Although the momentum constitutive laws discussed so far in this chapter have excluded bulk viscosity, the mathematical framework needed to account for it was discussed in Chapter 3. Inclusion of bulk viscosity would change the respective momentum balances as follows:

Elastic Momentum Balance: Equations 4.10–4.13 should be modified to include the contribution of the bulk-viscosity-induced dynamic stress $p_{\mathrm{dy}} = -\mu_{\mathrm{bulk}}\vec{\nabla}\cdot\vec{v}$. The lateral-direction momentum balances and deformation stresses for $1d$ motion where $\vec{\nabla}\cdot\vec{v} = \frac{\partial v}{\partial x}$ are updated to

$$\left.\begin{aligned}\sigma_{yy} &= p + \tau_{yy} - \mu_{\mathrm{bulk}}\frac{\partial v}{\partial x} = p^{\infty}\\ \sigma_{zz} &= p + \tau_{zz} - \mu_{\mathrm{bulk}}\frac{\partial v}{\partial x} = p^{\infty}\end{aligned}\right\} \Rightarrow \tau_{yy} = \tau_{zz} = p^{\infty} - p + \mu_{\mathrm{bulk}}\frac{\partial v}{\partial x}. \tag{4.64}$$

The shear stresses are still zero, $\tau_{ij} = 0$. The traceless property of the deformation stress gives us τ_{xx} as follows,

$$\tau_{xx} = -\left(\tau_{yy} + \tau_{zz}\right) = 2\left(p - p^{\infty}\right) - 2\mu_{\text{bulk}}\frac{\partial v}{\partial x}. \tag{4.65}$$

Using equation 4.65, the linearised and scaled elastic momentum balance can be written as

$$j\Omega \text{Ma}_{\text{D}}^{\infty}\text{Pe}^{(1)} = -3\frac{dP^{(1)}}{dX} + 3\text{Sc}_{\text{bulk}}^{\infty}\text{Ma}_{\text{D}}^{\infty}\frac{d^2\text{Pe}^{(1)}}{dX^2}. \tag{4.66}$$

It can be observed that this elastic momentum balance with bulk viscosity, equation 4.68, has the same structure as the viscous momentum balance.

The modification of viscous and viscoelastic momentum balances is more straightforward. The dynamic pressure due to bulk viscosity simply gets added to the viscous stress, leading to effective viscosities (hence, Schmidt numbers) for both the cases,

Viscous Momentum Balance:

$$j\Omega \text{Ma}_{\text{D}}^{\infty}\text{Pe}^{(1)} = -\frac{dP^{(1)}}{dX} + \underbrace{\left(\tfrac{4}{3}\text{Sc}_{\text{shear}}^{\infty} + \text{Sc}_{\text{bulk}}^{\infty}\right)}_{\text{Sc}_{\text{eff}}^{\infty}}\text{Ma}_{\text{D}}^{\infty}\frac{d^2\text{Pe}^{(1)}}{dX^2} \tag{4.67}$$

Viscoelastic Momentum Balance:

$$j\Omega \text{Ma}_{\text{D}}^{\infty}\text{Pe}^{(1)} = -\frac{dP^{(1)}}{dX} + \left[\frac{\frac{4}{3}\text{Sc}_{\text{shear}}^{\infty}}{1 + j\Omega\frac{2(1+\nu_{\text{PR}})}{3(1-2\nu_{\text{PR}})}\text{Sc}_{\text{shear}}^{\infty}\text{Ma}_{\text{D}}^{\infty}} + \text{Sc}_{\text{bulk}}^{\infty}\right]\text{Ma}_{\text{D}}^{\infty}\frac{d^2\text{Pe}^{(1)}}{dX^2} \tag{4.68}$$

The paucity of reliable measurements for bulk viscosity, in general [169–171], but more specifically for polymers [172], motivated the choice of not including its effect in the current discussion. There are theoretical frameworks to estimate the bulk viscosity of dilute gases, which start to break down for denser gases, liquids, and solids. Most of the few experimental studies available in the literature employ acoustic absorption methods for the measurements, but it is not trivial to separate the

absorption coefficient thus measured into shear, thermal, and bulk contributions. Graves and Argrow [169] review the scarce experimental data from absorption experiments to conclude that bulk viscosity tends to be the same order of magnitude ($0.25 < \mu_{\text{bulk}}/\mu_{\text{shear}} < 4$) as the shear viscosity for dilute as well as dense gases. Dukhin and Goetz [170] drew a similar conclusion for several common Newtonian liquids, including water ($\mu_{\text{bulk}}/\mu_{\text{shear}} \sim 3$). Even though there is no conclusive source for bulk viscosity measurements, the upcoming parameter study section will shed light on the general behaviour expected from a system where bulk viscosity effects are significant.

4.4 Exploring the Mathematical Behaviour of the Linearised Transport Model

4.4.1 Diffusion Equation on Composition

The scaled linear solvent material balance (equation 4.48) can be combined with the space-differentiated solvent flux law (equation 4.61), while substituting for the volume-average velocity gradient from the volume balance (equation 4.50) and for the total concentration time-gradient from the time-differentiated equation of state (equation 4.52), as well as the zero-order scaled total concentration $\theta_{\text{T}}^{\infty} = \frac{\nu}{1+(\nu B_0 - 1)y_0^{\infty}}$, to give Fick's second law of diffusion, albeit with a correction coming from pressure diffusion (derived explicitly in Appendix C):

$$\underbrace{\boxed{j\Omega y_0^{(1)} = \frac{d^2 y_0^{(1)}}{dX^2}}}_{\text{Fick's law of diffusion}} + \underbrace{\beta^{\infty} y_0^{\infty}\left(1 - y_0^{\infty}\right)\frac{\text{Ma}_{\text{D}}^{\infty}}{\text{Ma}_{\text{M}}^{\infty^2}}\frac{d^2 P^{(1)}}{dX^2}}_{\text{pressure diffusion correction}}. \tag{4.69}$$

4.4.2 Wave Equation on Pressure

An equation governing the distribution and evolution of pressure in the electrolyte can be obtained as follows: time-differentiate the volume balance (equation 4.50), space-differentiate the elastic momentum balance (equation 4.54), use the linearised version of the kinematic relationship (equation 4.63) to replace mass-average velocity from the momentum balance, time-differentiate the solvent balance (equation 4.48) and the linearised equation of state (equation 4.52). This results in a wave equation with a composition correction,

$$\underbrace{\boxed{j^2\Omega^2\frac{\mathrm{Ma}_{\mathrm{D}}^{\infty^2}}{3}P^{(1)} = \frac{d^2P^{(1)}}{dX^2}}}_{\text{pressure wave equation}} + \underbrace{j^2\Omega^2\frac{\mathrm{Ma}_{\mathrm{D}}^{\infty}}{3}\beta^{\infty}y_0^{(1)}}_{\text{composition correction}}. \tag{4.70}$$

The pressure wave in the membrane is realised by changes in the local thickness of the electrolyte, even as the global thickness of the membrane remains unaffected.

A similar analysis can be performed for the viscous and viscoelastic cases as well, detailed in Appendix C. The form of the equations remain wave-equation-like with wave speed (dimensionless) identified as

$$C_{\text{wave, elas}} = \frac{\sqrt{3}}{\mathrm{Ma}_{\mathrm{D}}^{\infty}} \quad \text{and} \quad C_{\text{wave, visc/visc,elas}} = \frac{1}{\mathrm{Ma}_{\mathrm{D}}^{\infty}}. \tag{4.71}$$

4.4.3 Characteristic Time Constants

The linearised model describing transport in Nafion-like ionomers under the influence of a small alternating impedance current, while accounting for compressibility effects and the interplay between mass and momentum transport affords three time-constants or characteristic frequencies, as evident from the diffusion equation (4.69) and the wave equation (4.70):

- **Composition Diffusion Time Constant**, $t_{\mathrm{D}} = \dfrac{L^2}{D} \sim \mathcal{O}\,(10\ \mathrm{s})$

  For Nafion, this is usually the practically observable time scale at which mass diffusion due to composition differences dominates the system behaviour. This is controlled by the diffusivity D and the thickness L of the sample. The associated characteristic frequency is

$$\omega_{\mathrm{D}} = \frac{D}{L^2};\, f_{\mathrm{D}} = \frac{1}{2\pi L}\frac{D}{L} \sim \mathcal{O}\,(0.01\ \mathrm{Hz})\,. \tag{4.72}$$

  In this frequency range, the impedance response is expected to reduce to typical Warburg behaviour.

- **Acoustic Wave Time Constant**, $t_{\mathrm{A}} = \dfrac{L}{\sqrt{K/\rho}} \sim \mathcal{O}\,(1\ \mu\mathrm{s})$

  When the membrane is excited at this short time scale, acoustic pressure waves travel across it. The acoustic timescale is controlled by the membrane thickness L and the characteristic speed of sound, which depends on the nature of the specific medium: a generic speed $\sqrt{K/\rho}$ is used here but it can be modified accordingly for elastic, viscous, and viscoelastic situations following equations 4.71. In terms of the dimensional parameters identified in the previous section, the acoustic frequency is

$$f_{\mathrm{A}} = \frac{f_{\mathrm{D}}}{\mathrm{Ma}_{\mathrm{D}}} = \frac{1}{2\pi L}\sqrt{\frac{K}{\rho}} \sim \mathcal{O}\,(0.1\ \mathrm{MHz})\,, \tag{4.73}$$

  showing that in a material with a fixed diffusion frequency, a decrease in the diffusion Mach number will increase the acoustic frequency. When the frequency of the applied AC signal reaches this range $\mathcal{O}\,(0.1\ \mathrm{MHz})$, impedance signatures associated with mechanical effects are expected to appear.

- **Pressure Diffusion Time Constant**, $t_{\mathrm{M}} = \dfrac{L}{\sqrt{RT\chi c_{\mathrm{T}}/\rho}} \sim \mathcal{O}\,(1\ \mu\mathrm{s})$

  This is the timescale at which mass diffusion due to local pressure gradients becomes important in the system; the gradients themselves become significant when the acoustic response does. Maxwell speed denotes the average speed of

the molecules due to their thermal energy. This speed determines the osmotic pressure exerted by the system; pressure diffusion becomes relevant only when the mechanical/thermodynamic pressure becomes comparable to the osmotic pressure. Maxwell speed is controlled by the system temperature T, Darken's thermodynamic factor χ, and the ratio of density to the total concentration $\rho/c_{\mathrm{T}} = \sum_i \overline{m}_i y_i$. For Nafion, the acoustic and pressure-diffusion time constants are very close to each other, implying that the two effects are not well isolated. The Maxwell frequency can also be expressed in terms of the dimensionless parameters obtained earlier in the scaling process in the previous section,

$$f_{\mathrm{M}} = f_{\mathrm{A}}\mathrm{Ma}_{\mathrm{M}} = \frac{f_{\mathrm{D}}\mathrm{Ma}_{\mathrm{M}}}{\mathrm{Ma}_{\mathrm{D}}} = \frac{1}{2\pi L}\sqrt{\frac{RT\chi c_{\mathrm{T}}}{\rho}} \sim \mathcal{O}\left(0.1\ \mathrm{MHz}\right). \tag{4.74}$$

If diffusion frequency and acoustic frequency are held constant, Maxwell frequency will decrease as the Maxwell Mach number decreases.

Additional parameters, such as the solvent/membrane molecular weight ratio m_0 and partial-molar-volume ratio B_0, as well as the zero-order scaled total concentration $\theta_{\mathrm{T}}^{\infty}$ and density ρ^{∞}, which are in turn functions of the equilibrium extent of hydration y_0^{∞}, also play roles in determining the impedance signatures presented below. The magnitudes of the dimensionless groups help to identify practical frequencies at which different effects dominate, thereby allowing their segregation and identification in impedance data. Moreover, the parameter magnitudes suggest how voltage at any frequency can be parsed according to its constituent phenomena. Figure 4.3 summarises the scaling of the variables, as well as the definitions and physical interpretations, and typical magnitudes of the dimensionless parameters.

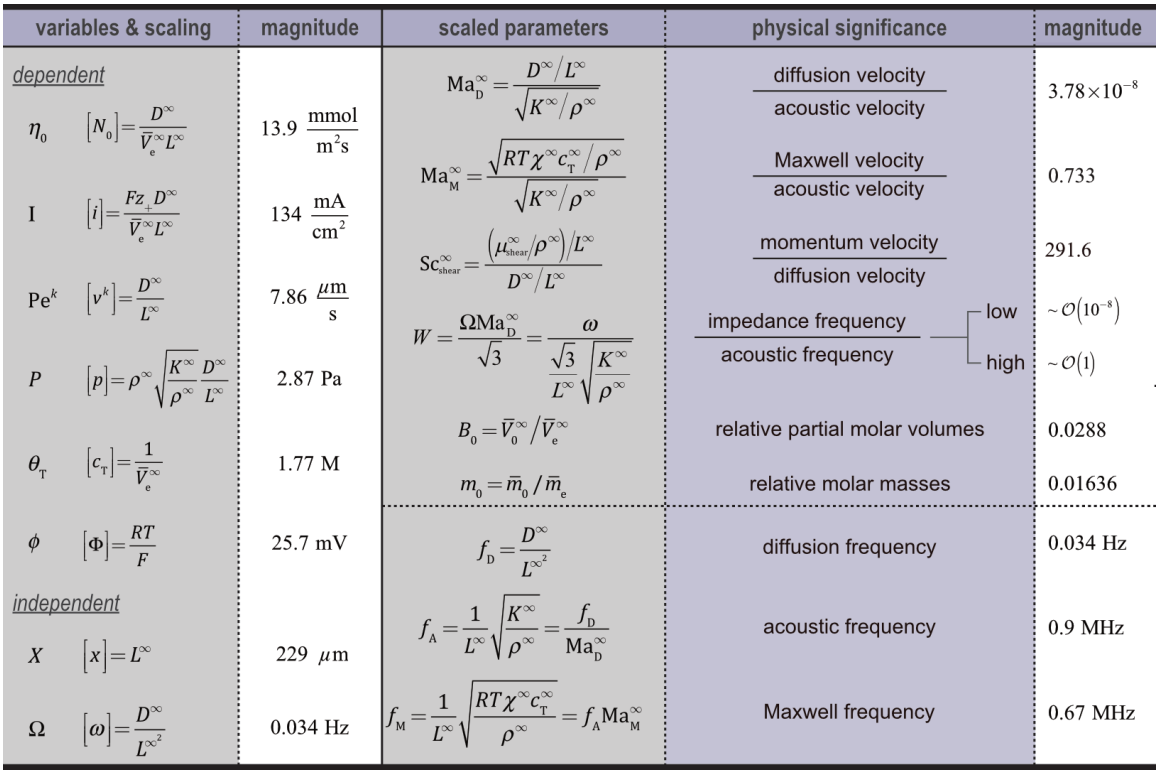

Figure 4.3: Summary of variable scalings and important dimensionless parameters. The first two columns present the scaling used to non-dimensionalise variables in the system, and their approximate magnitudes. The last three columns provide information about the dimensionless parameters and their combinations, which govern the behaviour of electrochemical/mechanical coupling

4.5 Impedance Signatures of Non-Isobaric Transport in Nafion

4.5.1 MacInnes Equation and Impedance

After the rescaling, the linearly perturbed model, expressed as a system of first-order ordinary differential equations, was solved using the bvp4c function in MATLAB. The system response was probed for a scaled impedance current density, I, with a small amplitude $\sim 10^{-3}$ to ensure linearity, over the range of frequencies discussed in the previous section—low, where diffusion dominates to high, where pressure effects become comparable in magnitude. Integration of the linearised MacInnes equation over the thickness of the membrane ($1d$ system) to obtain $\Delta\Phi = \Phi^{(1)}\big|_0 - \Phi^{(1)}\big|_{L^\infty}$ and subsequent division by the impedance current density amplitude $|i_0|$, yield the complex area-specific impedance $Z\,[\Omega\mathrm{m}^2]$ as shown in the expression below,

$$Z = \frac{\Phi^{(1)}\big|_0 - \Phi^{(1)}\big|_{L^\infty}}{|i_0|} = Z_\mathrm{b} + Z_y + Z_p. \tag{4.75}$$

The individual contributions of bulk electrolyte impedance, mass-diffusion impedance (arising from composition overpotential), and pressure-diffusion impedance (arising from stress overpotential) are respectively provided by

$$Z_\mathrm{b} = \frac{L^\infty}{\kappa^\infty}, \tag{4.76}$$

$$Z_y = \frac{\nu RT\left(1 - t_+^{0,\infty}\right)\chi^\infty}{F z_+ \nu_+ \left(1 - y_0^\infty\right) i_0}\, y^{(1)}\Big|_0^{L^\infty}, \tag{4.77}$$

$$Z_p = \frac{1}{F z_+ \nu_+ i_0}\left[\frac{\nu y_0^\infty\left(1 - t_+^{0,\infty}\right)}{1 - y_0^\infty}\left(\overline{V}_0^\infty - \frac{\overline{m}_0}{\rho^\infty}\right) - \frac{\nu_+ \overline{m}_+}{\rho^\infty}\right] p^{(1)}\Big|_0^{L^\infty}. \tag{4.78}$$

4.5.2 Low Frequency Regime: Warburg Behaviour

Nyquist and Bode plots are the two most common representations of impedance data. We use these tools to illustrate the impedance produced by equations 4.75– 4.78.

Nyquist representation: A Nyquist plot is a modified Argand diagram, on which impedance data is plotted as a parametric function of frequency. Since capacitive behaviour is more common than inductive behaviour, the ordinate axis describes the negative imaginary part of impedance; the real part of impedance lies along the abscissa. Although this approach obscures the frequency information, the loci of points on Nyquist plots have identifiable signatures that can be readily associated with physical processes. For example, a point on the real axis denotes a pure resistance, a vertical line in the first-quadrant at a non-zero real value denotes a resistance and capacitance in series, and a semi-circle in the first quadrant corresponds to a resistance and capacitance in parallel. Any signature in the second, third, or fourth quadrant indicates the presence of an inductive element in the system. Figure 4.4 depicts some of the common Nyquist signatures of electrical circuits.

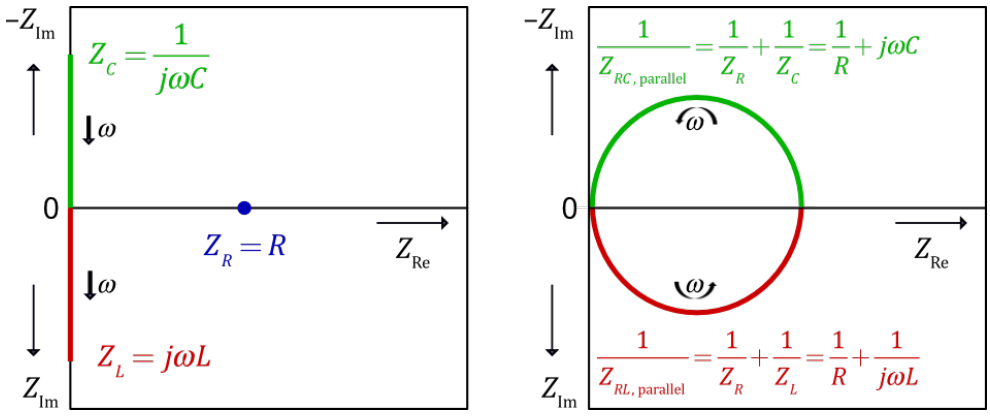

Figure 4.4: Nyquist representation of common linear circuit elements

Figure 4.5(a) presents a Nyquist plot yielded by a simulation using the typical properties of Nafion from Table 4.3, in which frequency spanned the low to moderate frequency range of 1 mHz to 100 kHz used in experiments. In such a plot, the high-frequency (leftmost) intercept on the real axis generally gives bulk ionic resistance, but this was subtracted from the total impedance here to clarify other phenomena. The data in Figure 4.5(a) shows a semi-circular arc (going from right to left with increasing frequency) that ends in a line inclined at 45 degrees relative to the real axis, indicating that the real and imaginary components of impedance match. This signature is known as the Warburg impedance, which suggests a diffusive transport process occurring in the electrolyte.

Pollard and Comte [163] analytically solved a system similar to the isobaric, inviscid limit of ours, involving concentrated-solution transport equations and a MacInnes equation to describe voltage. Solving the transport system for an isobaric concentrated, inviscid, binary liquid electrolyte subject to Faradaic convection, they derived a formula for an impedance element that produces this Warburg signature. The previous section showed that our model also reduces to the isobaric convective-diffusion equation at low frequencies where diffusion dominates. Following the procedure of Pollard and Comte, the system can be solved analytically to produce a composition distribution:

$$y_0^{(1)} = \frac{1}{2}\frac{s_+ z_+}{n_{e^-} z_{e^-}}\frac{\nu y_0^\infty}{\theta_T^\infty} B_+ \mathrm{I}_0 \frac{1}{\sqrt{\frac{j\Omega}{4}}} \frac{\sinh\left[\sqrt{\frac{j\Omega}{4}}\,(2X-1)\right]}{\cosh\left(\sqrt{\frac{j\Omega}{4}}\right)}. \tag{4.79}$$

The composition contribution to impedance can be obtained by integrating the appropriate term of MacInnes equation 4.77:

$$Z_y = \frac{s_+ z_+}{n_{e^-} z_{e^-}} \frac{\nu^2\left(1-t_+^{0,\infty}\right)^2 \chi^\infty}{z_+ \nu_+ \left(1-y_0^\infty\right)} \frac{y_0^\infty}{\theta_T^\infty} \frac{\overline{V}_e^\infty L^\infty}{F z_+ D^\infty} \frac{RT}{F} \frac{1}{\sqrt{\frac{j\Omega}{4}}} \tanh\left(\sqrt{\frac{j\Omega}{4}}\right). \tag{4.80}$$

Figure 4.5(a) compares the analytical (red solid lines) and simulation (black triangular markers $\triangleright$) results obtained by using the same material properties. Further analysis

was performed to identify that the maximum height of the Nyquist Warburg signature along the vertical axis occurs at frequency

$$\Omega_{\max} = \frac{\omega_{\max} {L^{\infty}}^2}{D^{\infty}} \simeq 10.16. \tag{4.81}$$

This can be used in conjunction with experimental data to directly estimate the diffusion coefficient of the electrolyte, following Pollard and Comte [163]. The detailed derivation of the expressions above is carried out in Appendix D.

Bode representation: the other popular graphical representations of impedance data are Bode gain and phase plots, which can be presented in various forms. For instance, in one popular version, the magnitude of impedance (in decibel units) is plotted against the logarithm of frequency, and the phase lag between voltage and current at different frequencies is plotted on a semi-log scale. There can be alternate styles in which uniform scales are used instead of logarithmic scales, or the magnitudes of the real and imaginary parts of impedance are plotted rather than the modulus and argument. The choice of style depends on the intended use of the plot. Phase plots are easier to read, because the common electrochemical elements correspond to single-valued bounded angles: a resistance has a 0 degree lag, a capacitor has a –90 degree lag (*i.e.*, a 90 degree lead), an inductor has a 90 degree lag, and a Warburg element has a –45 degree lag.

Figure 4.5(b) shows a Bode gain plot with a log-log scale, and Figure 4.5(c) is semi-log Bode phase plot. Unlike the Nyquist plot, these directly show frequency-dependent behaviour, and evenly distribute frequency data. The plots show archetypal Warburg behaviour as identified by the 0.5 slope on the gain plot and the –45 degree phase difference on the phase plot, respectively, at high and moderate frequencies and resistive behaviour as the frequency approaches zero. The Bode plots also show good agreement between the analytical and numerical solutions.

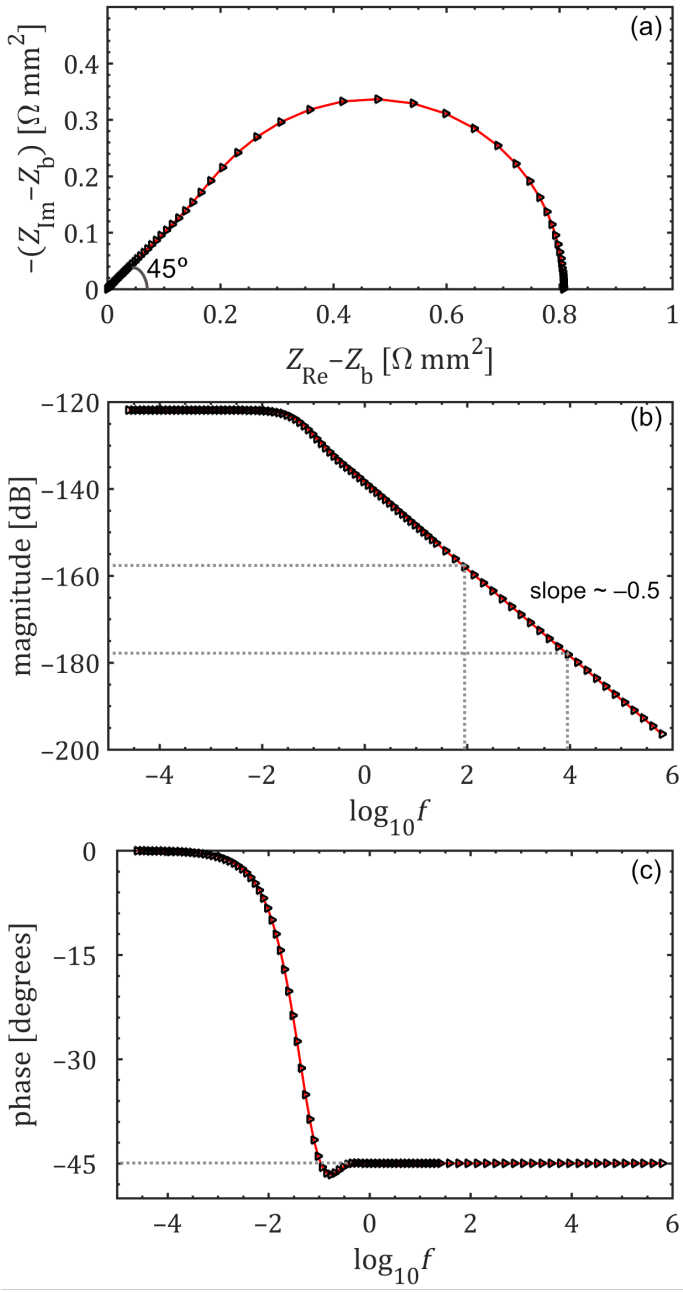

Figure 4.5: Electrolyte-resistance-corrected impedance plots in the low to moderate frequency regime showing typical Warburg behaviour (a) Nyquist plot (b) Bode gain plot (c) Bode phase plot. The analytical solution (red –) and the numerical solution (black ◁) show a very good match, indicating that the pressure overpotential plays an insignificant role at low to moderate frequencies for the Nafion system.

4.5.3 High Frequency Regime: Resonance & Anti-Resonance

The mathematical analysis leading to the diffusion and wave equations and subsequent discussion of characteristic frequencies suggested that pressure effects become increasingly important when the frequency of the impedance excitation rises above the range just discussed. A general feature of the observed responses is that the diffusion-dominated, mechanical-property-independent Warburg impedance persists at high frequency, but there are occasional deviations as frequency rises into the MHz range (the range of acoustic frequencies f_{A}). Before diving deeper in to the cause and nature of these deviations, some distinctions must be made according to the stress constitutive laws used.

4.5.3.1 Elastic Case

The Nyquist plot for an ideal elastic membrane is shown in Figure 4.6(a). In this case the response remains Warburg-like over a broad frequency range. At very high frequencies, however, the system impedance dips into positive imaginary parts, which suggests the presence of an inductive response. In the high frequency limit, points on the Nyquist plot are close together and the magnitudes of deviations induced by mechanics are small compared to the dominating Warburg signature, making them invisible in the Nyquist representation.

The Bode gain plot in Figure 4.6(b), however, reveals interesting features at high frequencies, precisely in the range where the dimensional analysis suggests that mechanical effects should become important. As seen in the plot, the analytical solution neglecting mechanical effects, and the numerical solution of the complete model begin to have a mismatch when the frequency is higher than a critical value, above which the Bode plot shows intermittent spikes. At frequencies above each spike in gain, the

numerical solution returns to the diffusion-dominated Warburg behaviour until the next spike is reached.

The Bode phase plot, Figure 4.6(c), is the most telling of the three impedance diagrams. Although the spikes on the Bode gain plot were significant enough to be noticed, the frequency range over which the gain spikes occur is narrow and the amplitudes of the spikes are relatively small; consequently the gain effect could be missed, or even be unnoticeable in the presence of experimental noise. Even in such a case, the Bode phase plot will be useful because the size of the spikes is not proportional to the magnitude but instead depends on the nature of the deviation. The Bode phase plot is more informative because it reveals the nature of the deviation of impedance, independent of the amplitude of the effect. The discrete locations of the spikes in frequency, match the locations of the spikes in the gain plot. The phase, however, spans from –90 degrees to 90 degrees, indicating both capacitive and inductive behaviour. None of these features are explained by simple diffusion physics.

As mentioned before, these new impedance signatures occur in the frequency range, $W\left(=\Omega \mathrm{Ma}_{\mathrm{D}}^{\infty}/\sqrt{3}\right) \sim \mathcal{O}\left(1\right)$, above which dimensional analysis suggests that coupling of mechanical response and diffusion should be triggered. The sudden passage of impedance current through the system engenders a dynamic mechanical response from the cell that relaxes very quickly; the high frequency simulations access this behaviour at time-scales smaller than a μs.

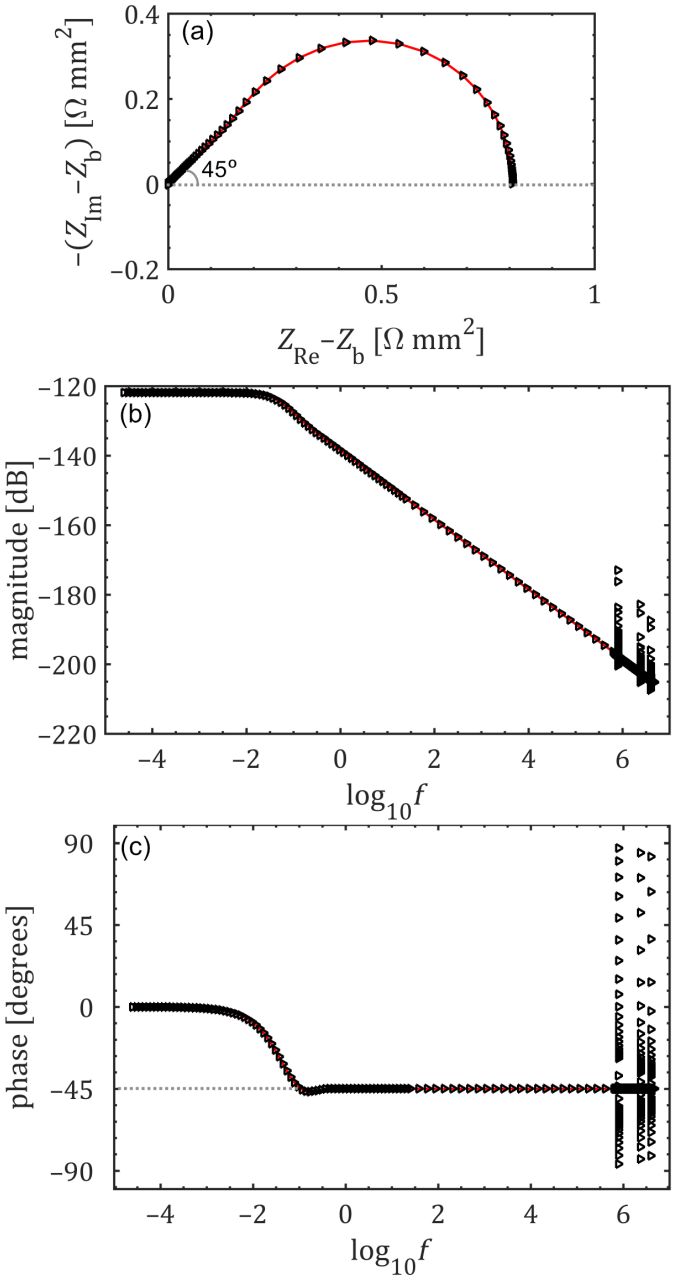

Figure 4.6: Elastic case: electrolyte-resistance-corrected impedance plots in a wide frequency regime exploring deviations from typical Warburg behaviour: (a) Nyquist plot (b) Bode gain plot (c) Bode phase plot. The analytical solution neglecting mechanical coupling (red –) and the numerical solution including mechanics (black ▷) match well except for the appearance of discrete spikes on the numerical Bode plots, which likely originate from the pressure overpotential.

It is worth plotting the high frequency data exclusively to aid qualitative analysis. Figure 4.7(a) shows the leftmost part of the Nyquist plot, which retains the trailing 45 degree Warburg behaviour, with disruptions at the higher frequency end.

Bode plots in Figures 4.7(b)–(c) use a linear frequency scale to examine the peaks in impedance magnitude, which appear periodically at fixed frequency intervals. This observation reveals a resonant behaviour: whenever the frequency of the AC impedance signal matches the fundamental acoustic frequency of the system (determined by the speed of sound in the electrolyte and its thickness), or odd integer overtones of this frequency, a vibration resonance occurs, producing the spikes in gain visualised in Figure 4.7(b). Figure 4.7(c) shows the corresponding Bode phase plot, in which spikes are readily spotted because they span the entire range of phase.

Assuming that the harmonic behaviour of this system is similar to that of an open air tube or a vibrating string, we propose a form for the harmonic frequencies,

$$\omega_N = \frac{N\pi\sqrt{3}}{L}\sqrt{\frac{K}{\rho}} \qquad \text{and} \qquad f_{\mathrm{N}} = \frac{N\sqrt{3}}{2L}\sqrt{\frac{K}{\rho}}, \tag{4.82}$$

where N =1,2,3... represents the various harmonics of vibration. The additional factor of $\sqrt{3}$ comes from the wave equation (equation 4.70). Since $\Omega = \omega L^2/D$, this yields

$$\Omega_N = \frac{N\pi\sqrt{3}}{\dfrac{D/L}{\sqrt{K/\rho}}} = \frac{W\sqrt{3}}{\mathrm{Ma}_{\mathrm{D}}^{\infty}}. \tag{4.83}$$

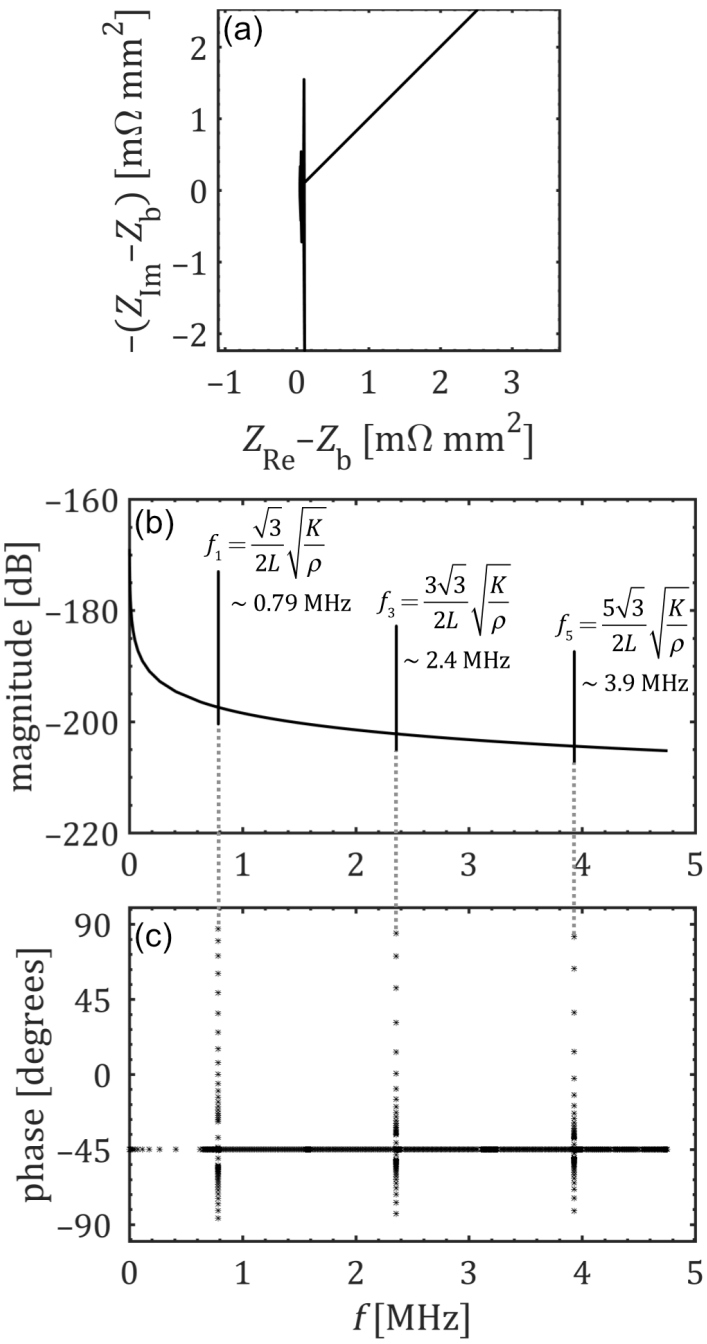

Figure 4.7: Elastic case: electrolyte-resistance-corrected impedance in the high frequency regime with mechanical resonance events (a) small spikes tacked on Warburg behaviour as seen in the Nyquist plot (b) regularly-spaced spikes on Bode gain plot (c) regularly-spaced spikes going from –90 to 90 degrees on Bode phase plot.

Further examination of the plots in Figure 4.7 suggests that resonance only occurs at odd harmonics, skipping even overtones. This is sensible because the boundary conditions on flux necessitate equal slopes of concentration at either end of the symmetric cell, which is only possible when harmonics of the acoustic frequency are odd.

$$W \sim (2N - 1)\,\pi. \tag{4.84}$$

When values of the parameters are used from Table 4.3, the frequencies associated with the peaks in Figure 4.7 are consistent with equations 4.83 and 4.84.

The nature and origin of the resonance phenomenon is clarified by examining the components of overpotential arising from composition and pressure individually. The composition impedance plots, Figures 4.8(a)–(c) show exact Warburg behaviour without any deviations, implying that all deviations originate in the pressure overpotential. The data presented in Figures 4.8(d)–(f) are consistent with this hypothesis; in fact, the pressure impedance plots are even richer in information than the overall impedance plots from Figures 4.7. The Nyquist plot, Figure 4.8(d) shows no Warburg-like behaviour. Note that the scale has been deliberately skewed to visualise the shapes of pressure impedance rather than showing indiscriminate spikes.

The Bode plots in Figures 4.8(e)–(f), are similar to those found in acoustic systems, showing peaks in amplitudes at the fundamental acoustic frequency and its odd overtones. The impedance also shows valleys at even overtones, pointing to anti-resonance which reduces the impedance magnitude to a minimum. Passive band-pass filters based on RLC circuits also show impedance peaks on Bode plots, suggesting that pressure effects act similarly, although such filters usually show a single resonance, rather than a periodic one [173]. The blue dashed lines on the pressure Bode gain plot show the envelope of the impedance as a function of frequency. The peaks appear to maintain approximately the same height, indicating that there is negligible dissipation in the system.

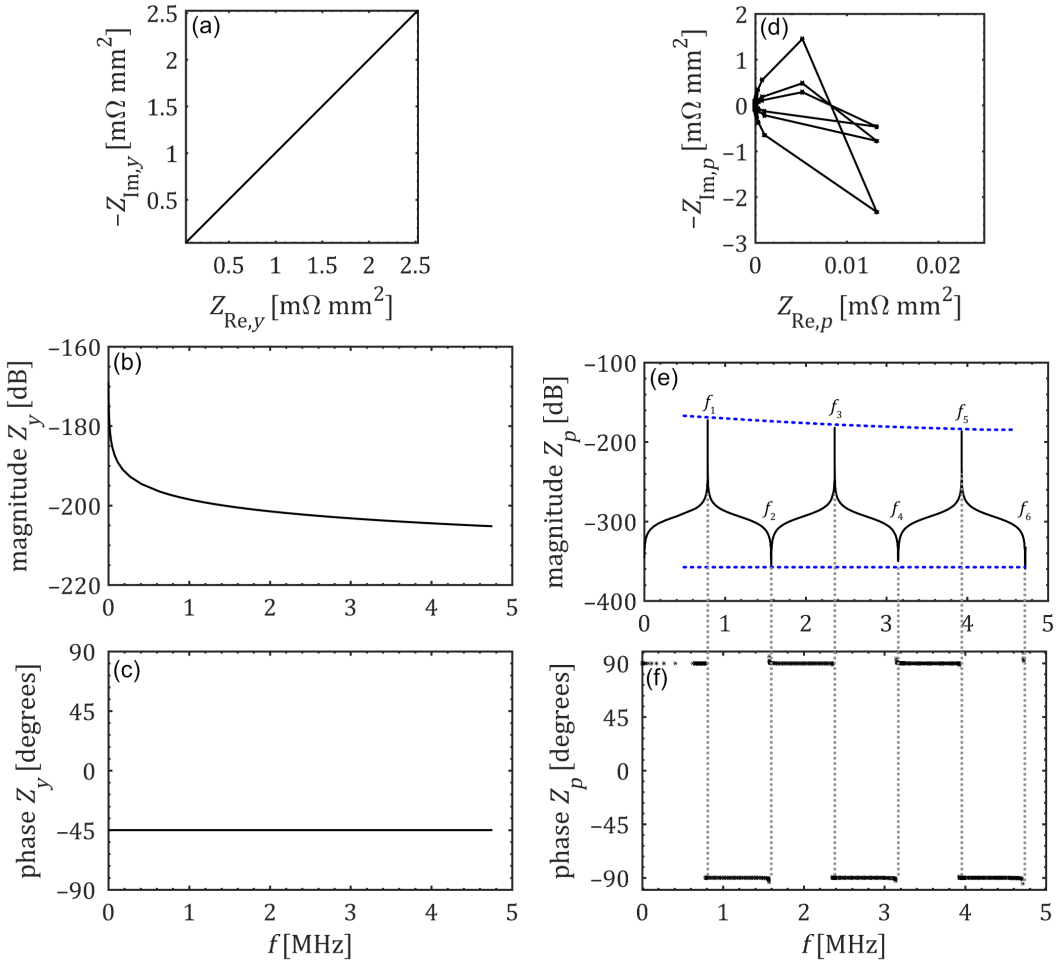

Figure 4.8: Elastic case: individual composition and pressure overpotential impedance plots at high frequencies (a) composition Nyquist (b) composition Bode gain plot (c) composition Bode phase plot (d) pressure Nyquist (e) pressure Bode gain plot: resonance and anti-resonance (f) pressure Bode phase plot.

4.5.3.2 Viscous Case

Through the next set of figures, we seek to elucidate the response when the system has viscous, rather than elastic behaviour. Again, the high-frequency Nyquist plot, Figure 4.9(a), shows a dominant Warburg response, but with loops superimposed on it, rather than the spikes seen in the elastic Nyquist plot (Figure 4.7(a)). The largest loop is the first, with successive loops becoming smaller, indicating dissipation. Whereas a vertical spike on the Nyquist plot usually indicates an inductive-capacitive resonance, a loop denotes the presence of an additional resistive component, which in this case can be attributed to viscosity. The magnitudes of the loops remain in a similar range as the magnitudes of the spikes in the elastic case, which are again relatively small in comparison to the dominant Warburg impedance.

Figure 4.9(b), the Bode gain plot, shows similar resonance events as the elastic case. At regular frequency intervals, which we now identify as the fundamental acoustic frequency and its odd overtones, impedance shows sudden changes in magnitude. Over a very narrow range of frequencies, a significant increase over the Warburg magnitude is followed by a small decrease below it. As one proceeds to higher frequencies, two things happen: the total size of the spike decreases and a higher fraction of the spike shifts below the Warburg impedance curve.

Figure 4.9(c) is the Bode phase plot, which is in agreement with the Nyquist and Bode gain plots. The increase in impedance magnitude on the gain plot is accompanied by the phase deviating from –45 degrees to approach –90 degrees, capacitive behaviour, and then continuing all the way to being completely out of phase (–180 degrees). Similarly, the decrease in magnitude on the gain plot leads to the phase decreasing from 180 to 90 degrees, inductive behaviour, down to 0 degrees before hitting –45 degrees as it returns to Warburg behaviour, completing the loop.

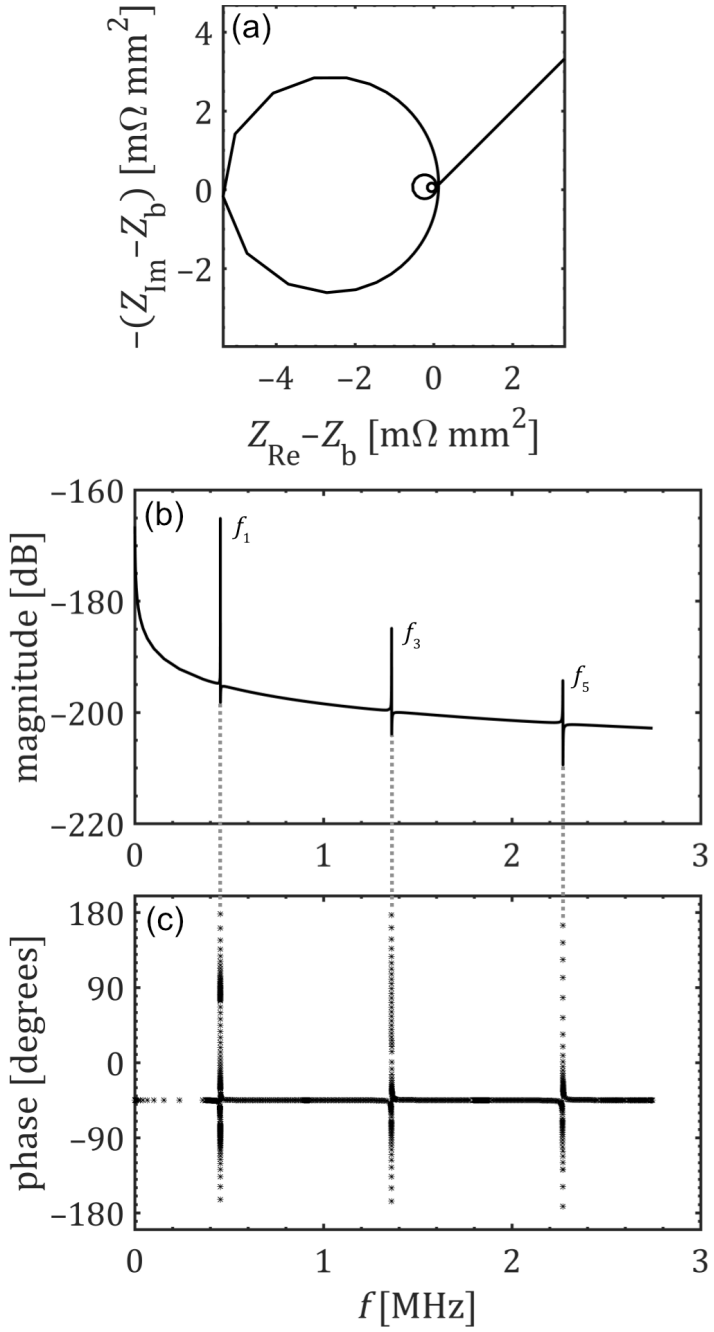

Figure 4.9: Viscous case: electrolyte-resistance-corrected impedance plots in the high frequency regime showing mechanical resonance events (a) loops tacked on Warburg behaviour as seen in the Nyquist plot (b) regularly-spaced, successively smaller, spikes on Bode gain plot (c) regularly-spaced spikes going from –180 to 180 degrees on Bode phase plot.

As we saw in the elastic case, the composition overpotential plots continue to follow the typical Warburg behaviour. The impedance solely arising from pressure overpotential is presented in Figure 4.10.

As expected, the Nyquist plot, Figure 4.10(a), shows perfect circular loops, which clearly map onto the Nyquist plot of overall impedance. A negative real part of impedance is not commonly observed in electrochemical systems, as it hints at the presence of an element that behaves like a negative resistor.

The Bode gain plot of pressure overpotential, Figure 4.10(b), helps explain the overall behaviour more clearly. The envelope identified by the dashed blue lines shows that the resonance peaks decrease in height with frequency. The anti-resonance valleys also increase in magnitude, and therefore should have a higher impact on the total impedance, as shown by the increasing fraction of the spike that lies below the Warburg line on the overall Bode gain plot, Figure 4.9(b).

The pressure Bode phase plot, Figure 4.10(c), does not show a Warburg signature. The anti-clockwise semi-circular half of the loop on the Nyquist plot conforms with the increasing part of the peak on the gain plot and the –90 degree plateau on the gain plot. At resonance, the Nyquist plot crosses over the real axis, the gain plot reverses sign towards decreasing magnitudes and the gain plot rapidly goes from –180 to 180 degrees. Following through, until the anti-resonance valley is reached on the gain plot, the 90 degree phase lead drops to being in-phase or 0 degrees (crossing the real axis again to form a new loop on the Nyquist plot) and then back to –90 degrees until the next resonance, and so on.

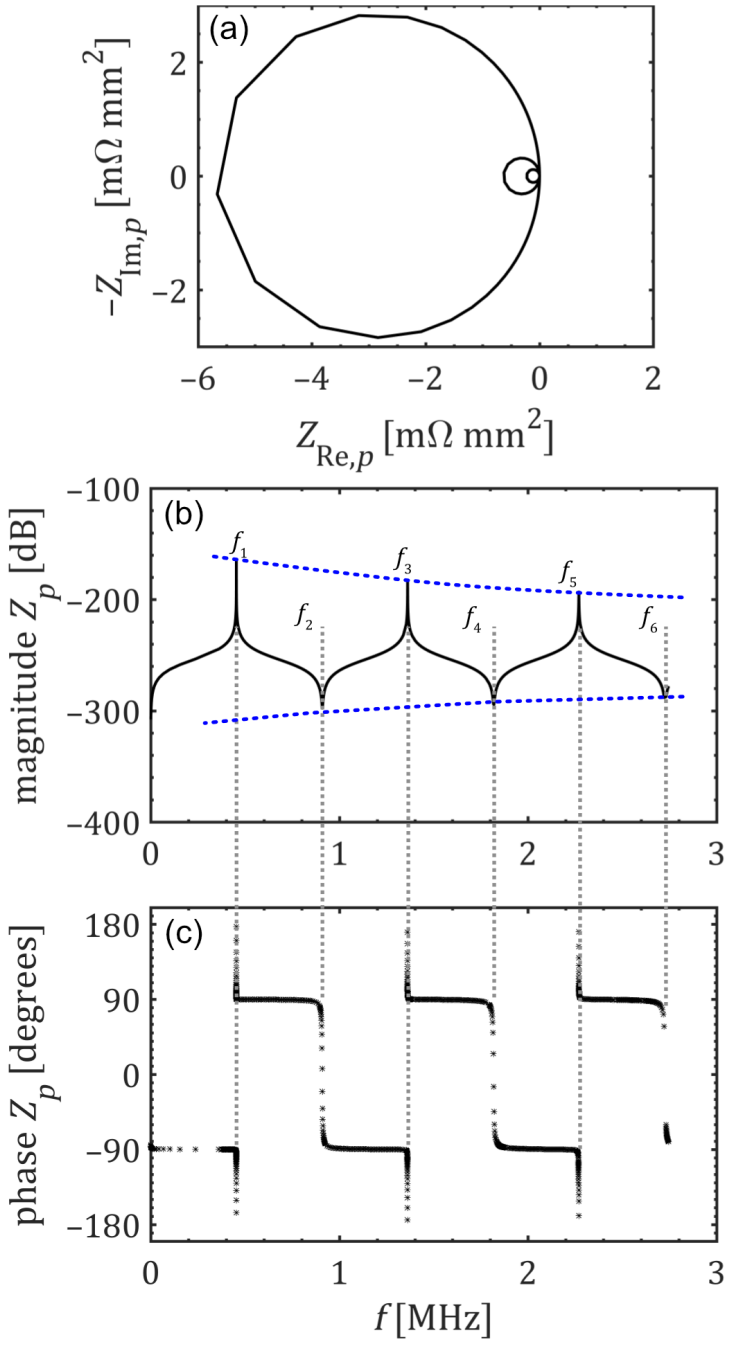

Figure 4.10: Viscous case: individual pressure overpotential impedance plots at high frequencies (a) pressure Nyquist (b) pressure Bode gain plot (c) pressure Bode phase plot.

4.5.3.3 Viscoelastic Case

As expected, the viscoelastic impedance plots yield a combination of elastic and viscous features, shown in the overall impedance plots in Figure 4.11(a)–(c). The Nyquist plot, Figure 4.11(a), returns to showing spikes instead of loops. The magnitudes of the gain spikes in Figure 4.11(b) decrease with frequency, as they did in the viscous case. Even the Bode phase plot, 4.11(c), shows the typical capacitive-inductive resonance.

Impedance plots derived from pressure overpotential, Figrue 4.12(a)–(c) follow suit. The Nyquist plot, Figure 4.12 (a), does not show circular loops like the viscous case. The Bode gain plot, Figure 4.12 (b), does have a decreasing amplitude envelope similar to the viscous case, signifying viscous dissipation, but the Bode phase plot, Figure 4.12 (c) does not seem to traverse the –180 to 180 degree shift, or perhaps it is happening over a narrower frequency range which wasn't accessible in the numerical simulation.

To facilitate comparison, the Bode gain plot of the pressure impedance is presented for all three cases—elastic, viscous, and viscoelastic—in Figure 4.13. On average, the magnitudes of viscous and viscoelastic impedance are higher than that of the elastic impedance. The peak heights in the elastic case seem to remain unchanged with frequency, since there is no significant source of mechanical dissipation, as signified by an envelope with almost parallel horizontal lines. Peak magnitudes in the viscoelastic case are higher than the viscous case, but reduce at similar rates with respect to frequency in both cases. As frequency increases, the magnitudes of the anti-resonance valleys increase at similar rates for both the viscous and viscoelastic cases as well, but the viscoelastic magnitude remains consistently lower, and hence plays a smaller part in the overall impedance.

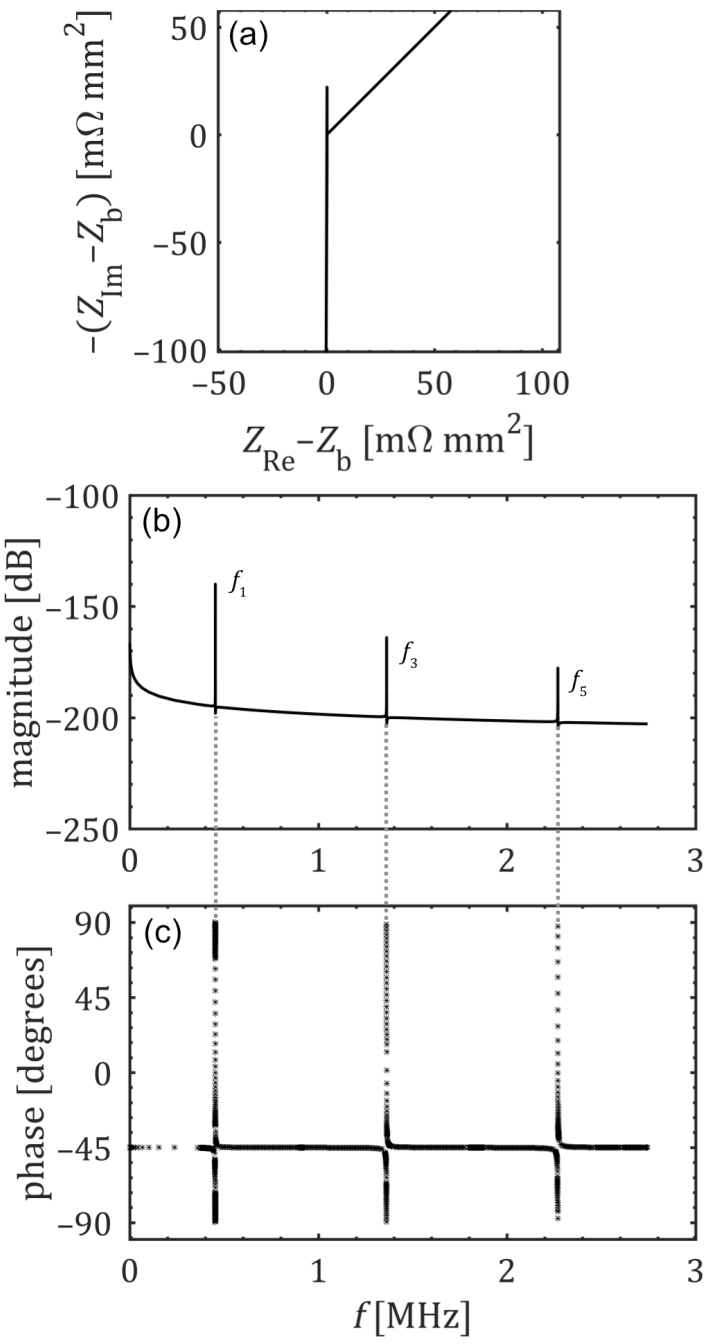

Figure 4.11: Viscoelastic case: electrolyte-resistance-corrected impedance in the high frequency regime showing mechanical resonance events (a) spikes tacked on Warburg behaviour as seen in the Nyquist plot (b) regularly-spaced, successively smaller, spikes on Bode gain plot (c) regularly-spaced spikes going from –90 to 90 degrees on Bode phase plot.

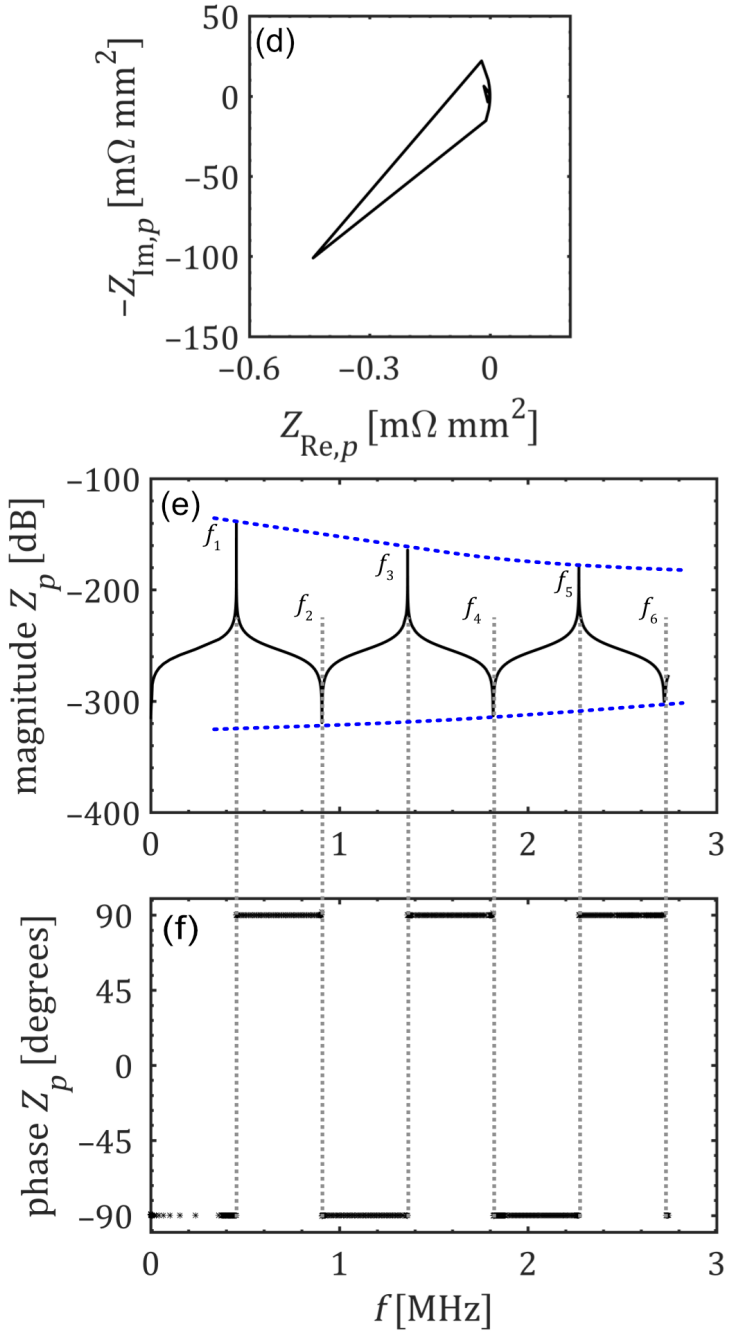

Figure 4.12: Viscoelastic case: individual pressure overpotential impedance plots at high frequencies (a) pressure Nyquist (b) pressure Bode gain plot (c) pressure Bode phase plot.

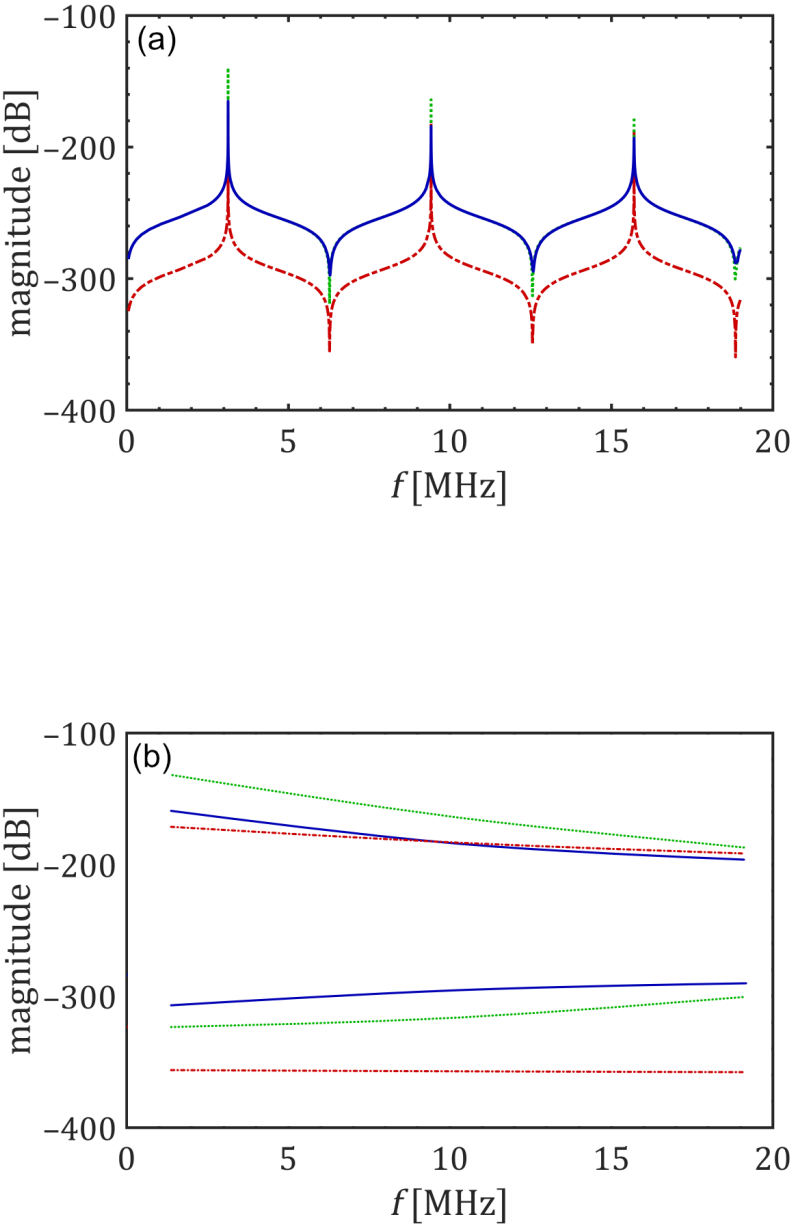

Figure 4.13: (a) Comparison of pressure overpotential contribution to Bode gain plots for the elastic (–. red), viscous (– blue), and viscoelastic case (: green) (b) The envelopes containing information about how the magnitudes of peaks and valleys change with frequency for the three cases of materials.

4.5.4 Boundary Layers

Having established the time ranges and frequencies of interest and significance, it is helpful to examine how the diffusion and wave equations behave in different frequency extremes of excitation frequency. At low frequencies which are characteristic of diffusion, $\Omega \sim \mathcal{O}(1)$, $W \sim \mathcal{O}(\mathrm{Ma}_{\mathrm{D}}^{\infty}) \ll 1$, the wave equation reduces to

$$\frac{d^2P^{(1)}}{dX^2} = j^2W^2P^{(1)} - j^2W^2\beta^{\infty}y_0^{(1)} \sim 0. \tag{4.85}$$

Since the pressure gradient across the membrane is negligible, it reduces the problem to the conventional isobaric diffusion problem:

$$j\Omega y_0^{(1)} = \frac{d^2y_0^{(1)}}{dX^2}. \tag{4.86}$$

Figure 4.14(a) shows solvent mole fraction profiles across Nafion's zero-order thickness for four different frequencies ranging from 10^{-5} Hz to 1 Hz. This large frequency range captures a vast spectrum of solvent composition distribution and evolution. The very low frequency cases [10^{-5} Hz and 10^{-2} Hz] approach steady-state distributions, in which the water concentration has ample time to reach a linear profile across the membrane. As the frequency increases, the time allowed for change, before polarity of the current signal changes, is not enough to achieve a steady-state, and the composition manifests increasingly bowed profiles. Although the absolute values of surface mole-fractions (at both electrodes) decrease through this process, the slope of the composition gradients, being controlled by the cation flux and consequently determined by the magnitude of impedance current, remains equal at both the boundaries.

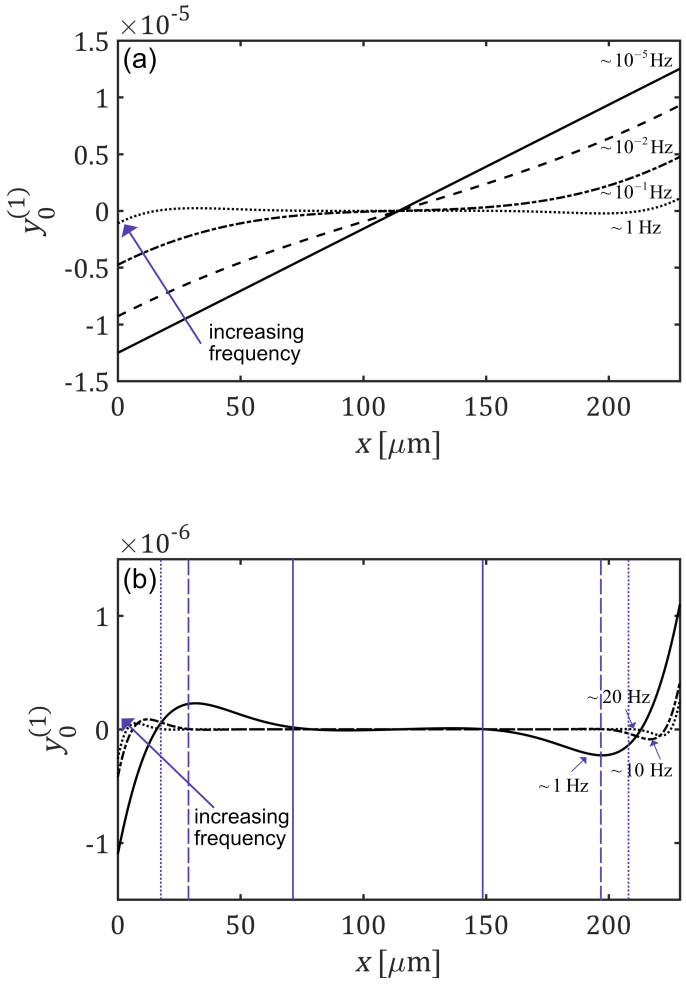

Figure 4.14: Profiles of first-order solvent mole-fraction across Nafion thickness in the (a) low-frequency range (b) mid-frequency range.

However, at frequencies $W = \Omega \mathrm{Ma}_{\mathrm{D}}^{\infty} \sim \mathcal{O}(1)$, which are much higher than typical diffusion frequencies, equation 4.69 suggests that $y_0^{(1)}(X) \sim 0$, which violates the boundary conditions that require composition gradients to be proportional to current density. This conflict suggests the existence of diffusion boundary layers, which contain the gradient; for the bulk of the solution, the condition $y_0^{(1)}(X) \sim 0$ would hold true. The length-scale of the diffusion boundary layer can be determined by defining a new space variable, which subsumes the high frequency to make the equation converge for the given boundary conditions; for the left boundary this new space variable

can be formed as $\tilde{X} = \sqrt{\Omega}X$, which resolves the issue:

$$jy_0^{(1)} = \frac{d^2 y_0^{(1)}}{d\tilde{X}^2} + \beta^\infty \frac{\mathrm{Ma}_\mathrm{D}^\infty}{\mathrm{Ma}_\mathrm{M}^{\infty^2}} y_0^\infty \left(1 - y_0^\infty\right) \frac{d^2 P^{(1)}}{d\tilde{X}^2}. \tag{4.87}$$

A similar asymptotic analysis could be performed for the right boundary by reformulating the space variable as $\hat{X} = \sqrt{\Omega}\,(X - 1)$.

Owing to the wide frequency range, the magnitudes of higher-frequency distributions are hard to see in Figure 4.14(a). Composition profiles for the mid-frequency range >1 Hz and <100 Hz are, therefore, plotted separately in Figure 4.14(b). The boundary-layer separation in the electrolyte insinuated by equation 4.87, which causes Warburg impedance response, can be observed in this range. As frequency increases, the bulk has shorter and shorter time to respond to the current input; only ions close to the electrodes are mobilised, forming symmetric boundary layers whose thicknesses are proportional to $1/\sqrt{\Omega}$. The boundary domains near the electrodes are delineated by vertical lines (line style matches composition profile at corresponding frequency).

The composition change becomes smaller as frequency nears the range where mechanical effects become significant (~ 1 MHz), as demonstrated in Figure 4.15(a)–(b). These plots specifically focuses on the solvent-concentration boundary layers at resonant frequencies (where the system response should be greatest). The layers at this stage are contained within regions of $\mathcal{O}(0.1\ \mu\mathrm{m})$. This could be a concern at much higher frequencies, when the thickness of the concentration boundary layer could become comparable to Debye length, bringing the assumption of electroneutrality into question. (This aspect does not receive further deliberation in the present study.)

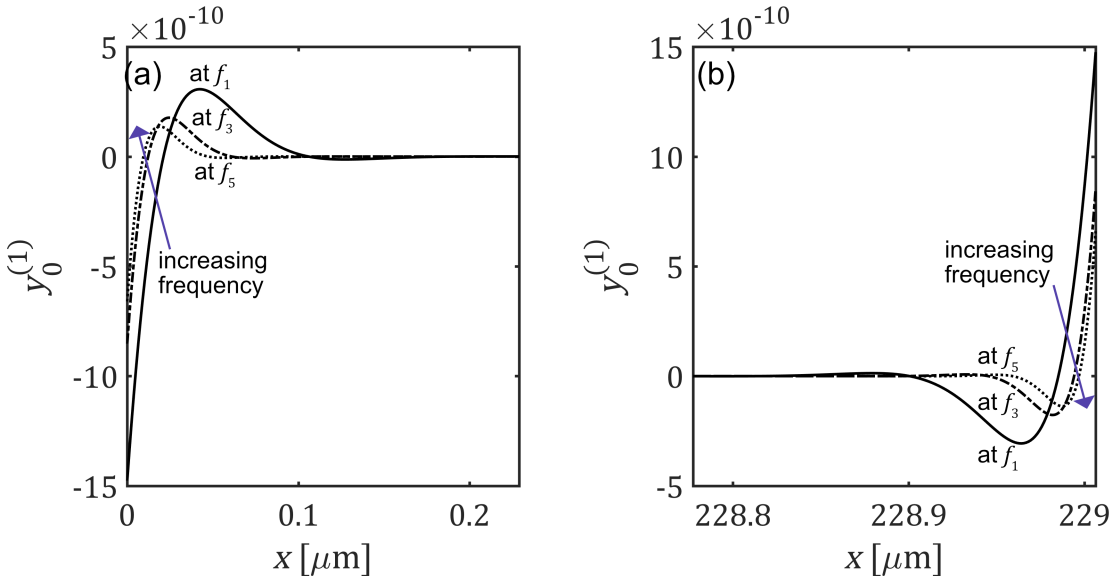

Figure 4.15: Illustration of thin composition boundary layers formed at the (a) left and (b) right electrode/electrolyte interfaces at high frequencies.

Pressure distributions across an elastic membrane are shown in Figures 4.16(a)–(b). At low frequencies, Figure 4.16(a), the magnitude of pressure change is too small to be significant, and can be ignored. As frequency rises sufficiently, pressure's wave behaviour dominates diffusion, yielding the characteristic behaviour depicted in Figure 4.16(b). The three lines represent the first three odd harmonics of the acoustic frequency, where the magnitude of the pressure effect is the highest: the first harmonic wave exhibits half a wavelength, the second, one-and-a-half wavelengths, and the third, two-and-a-half wavelengths. This figure corroborates the understanding that at very short times (suggested by the high resonance frequencies), as changes in composition are restricted to thin boundary layers near the electrodes, information from one boundary is communicated to the other boundary through these mechanical waves. If frequency is lowered the wave nature of pressure starts dying down while the composition boundary layers start growing and become the dominant way of communication in the electrolyte.

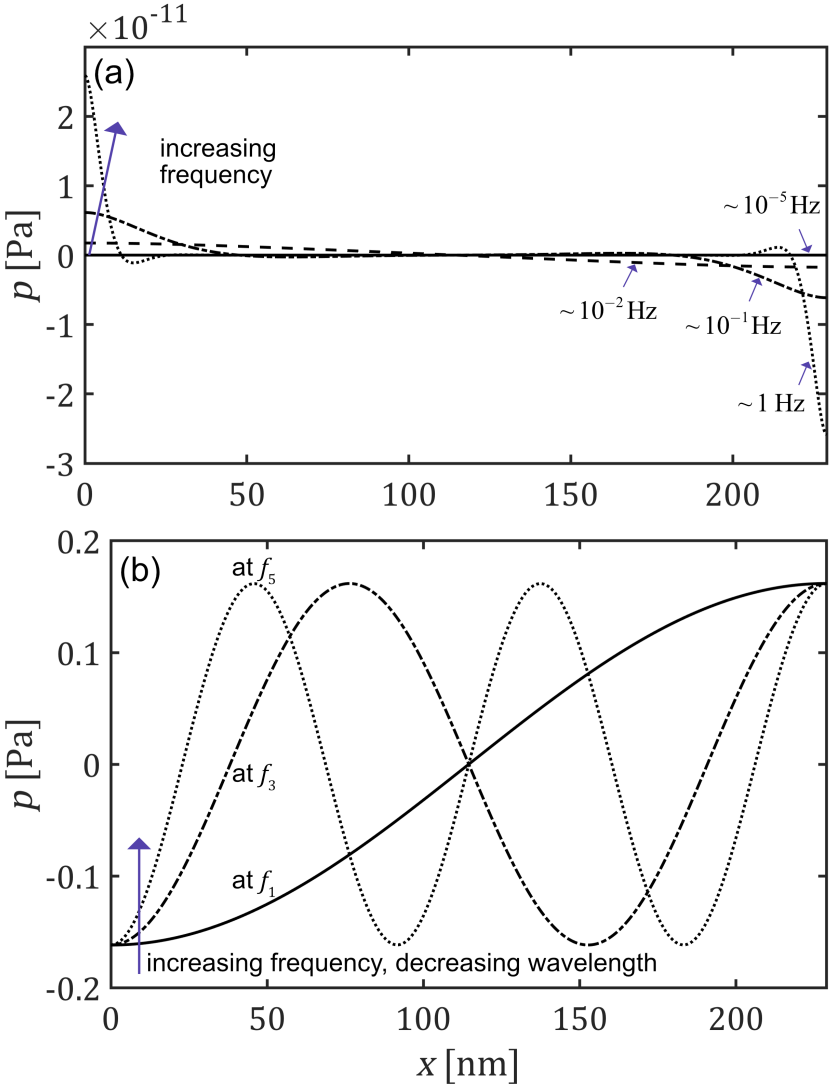

Figure 4.16: Pressure profiles across Nafion thickness, modelled as an elastic material (a) low frequencies, dominated by diffusion (b) first three resonance frequencies, dominated by mechanical response showing wave behaviour.

At low frequencies, pressure is negligible in both the viscous and viscoelastic cases. Figures 4.17(a)–(b), shows the pressure waves at resonance for these cases. Wave amplitude, which remained constant for the elastic case across the three frequencies, decreases significantly for the viscous as well as the viscoelastic case, in accordance with the discussion of decreasing peak heights earlier. The amplitude of the first resonant wave is highest for the viscoelastic case.

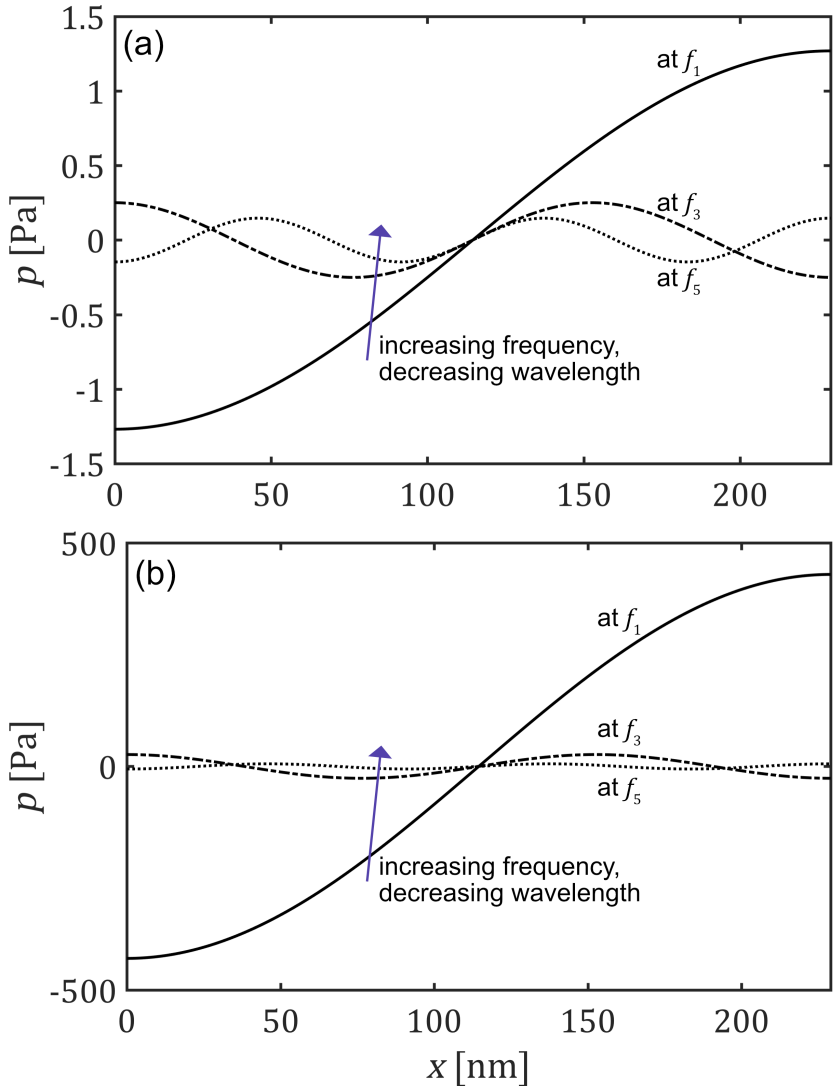

Figure 4.17: Wave behaviour of spatial pressure profiles at resonance frequencies when Nafion is modelled as a (a) viscous and (b) viscoelastic material.

To summarise, at high frequencies $W \sim \mathcal{O}(1)$, the period over which current changes is too short to permit diffusional relaxation. The excitation timescale is only long enough to produce composition boundary layers with thickness $\propto 1/\sqrt{\Omega}$, which are unable to propagate into the bulk, where concentration remains uniform. On this timescale, the much faster mechanical relaxation manifests as wave-like pressure vibrations in the membrane.

4.6 Beyond Nafion

This section aims to study how variations in dimensionless numbers, whose physical significances have been discussed in the context of characteristic frequencies, will affect impedance signatures. This may help to guide the development of ionomers in which mechanical effects are more dominant than they are in Nafion, or in which the electrochemical/mechanical coupling is even stronger.

4.6.1 Parameter Study: Transport & Mechanical Properties

Section 4.5 described interesting impedance features originating in the pressure overpotential part of MacInnes equation. The fundamental acoustic frequency at which resonance events begin to occur is fairly high, however. The first order of business is to understand how one could engineer a material with a lower fundamental frequency; not only could this help validate our theory, but in the long run, such a feature could be useful for piezoelectric applications. Second, even if resonance frequencies were lower, it might still not be possible to observe resonance experimentally due to the extremely narrow band of frequencies over which it occurs. Therefore, it is critical to widen the frequency band, to make electrochemical phenomena both practically accessible and useful.

Table 4.4 lists the values of each dimensionless parameter that were studied. The corresponding changes in the associated macroscopic property values are given in Table 4.5. When each parameter is varied in isolation, it causes a range of changes in dimensional properties to keep the other dimensionless parameters constant. For instance, $\mathrm{Ma}_{\mathrm{D}}^{\infty}$ can be decreased by an order of magnitude by decreasing the Fick's diffusion coefficient D^{∞} proportionally; in secondary effects, $\mu_{\mathrm{shear}}^{\infty}$ and κ^{∞} must de-

crease proportionally, since D^∞ also appears in $\mathrm{Sc}^\infty_{\mathrm{shear}}$ and K^∞, which are maintained as constants.

parameter	value 1	value 2	value 3	value 4
$\mathrm{Ma}^\infty_{\mathrm{D}} = \dfrac{D^\infty/L^\infty}{\sqrt{K^\infty/\rho^\infty}}$	3.778×10^{-9}	3.778×10^{-8}	3.778×10^{-7}	3.778×10^{-6}
$\mathrm{Ma}^\infty_{\mathrm{M}} = \sqrt{\dfrac{RT\chi^\infty c^\infty_{\mathrm{T}}/\rho^\infty}{K^\infty/\rho^\infty}}$	7.33×10^{-3}	3.665×10^{-2}	7.33×10^{-2}	7.33×10^{-1}
$\mathrm{Sc}^\infty_{\mathrm{shear}} = \dfrac{\mu^\infty_{\mathrm{shear}}/\rho^\infty}{D^\infty}$	2.91×10^{2}	1.455×10^{3}	2.91×10^{3}	2.91×10^{4}
$\mathrm{K}^\infty = \dfrac{RT\overline{V}^\infty_{\mathrm{e}}\kappa^\infty}{F^2 z_+ D^\infty}$	1.57×10^{-1}	1.57	1.57×10^{1}	1.57×10^{2}

Table 4.4: Values of the dimensionless parameters directly affecting transport and mechanical properties of the system used in the study. Parameter values for Nafion are shown in blue.

	transport properties		mechanical properties	
parameter	$D^\infty = \mathrm{Ma}^\infty_{\mathrm{D}} L^\infty \sqrt{\dfrac{K^\infty}{\rho^\infty}}$	$\kappa^\infty = \mathrm{K}^\infty \dfrac{F^2 z_+ D^\infty}{RT\overline{V}^\infty_{\mathrm{e}}}$	$K^\infty = \dfrac{RT\chi^\infty c^\infty_{\mathrm{T}}}{\mathrm{Ma}^{\infty^2}_{\mathrm{M}}}$	$\mu^\infty_{\mathrm{shear}} = \mathrm{Sc}^\infty_{\mathrm{shear}} D^\infty \rho^\infty$
$\Delta\mathrm{Ma}^\infty_{\mathrm{D}} = \uparrow \mathcal{O}(1)$	$\uparrow \mathcal{O}(1)$	$\uparrow \mathcal{O}(1)$	–	$\uparrow \mathcal{O}(1)$
$\Delta\mathrm{Ma}^\infty_{\mathrm{M}} = \downarrow \mathcal{O}(1)$	$\uparrow \mathcal{O}(1)$	$\uparrow \mathcal{O}(1)$	$\uparrow \mathcal{O}(2)$	$\uparrow \mathcal{O}(1)$
$\Delta\mathrm{Sc}^\infty_{\mathrm{shear}} = \uparrow \mathcal{O}(1)$	–	–	–	$\uparrow \mathcal{O}(1)$
$\Delta\mathrm{K}^\infty = \uparrow \mathcal{O}(1)$	–	$\uparrow \mathcal{O}(1)$	–	–

Table 4.5: A map of how variations in the dimensionless parameters selected for the study affect transport as well as mechanical properties of the system.

The present study only deals with dimensionless parameters that appear in the diffusion and wave equations (4.69 and 4.70), and involve dynamical transport or mechanical properties. The transference number $t_+^{0,\infty}$, is not studied. Its effect on impedance is evidenced by looking at the composition and the pressure overpotential contributions in equations 4.77–4.78. If $t_+^{0,\infty} = 1$, the composition overpotential vanishes, and the solvent effects from the pressure overpotential do also, leaving only

the pressure overpotential caused by cations, which is effectively zero due to the negligible mass of hydrogen ions. As $t_+^{0,\infty}$ decreases, both composition and pressure overpotentials increase.

4.6.1.1 Discussion of the Diffusion Mach Number

Increasing the diffusion Mach number is achieved by increasing the diffusion coefficient, which varies the diffusion frequency in direct proportion, while leaving the acoustic and Maxwell frequencies constant. Such an increase brings the diffusive and mechanical effects closer together in the frequency spectrum. For Nafion, the diffusion coefficient would have to be impractically high $D^\infty \sim \mathcal{O}\left(10^{-2}\ \mathrm{m^2/s}\right)$ for the frequencies to overlap completely.

An initial study showed that increasing $\mathrm{Ma}_\mathrm{D}^\infty$ beyond its standard value for Nafion achieves the goal of widening the resonance peaks. Figure 4.18 illustrates this effect through the gain and phase behaviour for the elastic (a)–(b), viscous (c)–(d), and viscoelastic (e)–(f) cases. Looking at the three gain plots we observe that the peaks become visibly wider with increasing $\mathrm{Ma}_\mathrm{D}^\infty$ for all the cases, although the effects are less pronounced for the elastic case.

The phase plots show a similar trend. Whereas for the standard value, the resonance events for all the three cases were isolated, they become convoluted as $\mathrm{Ma}_\mathrm{D}^\infty$ increases. The polarity with respect to the capacitive-like and inductive-like features is inverted for the elastic case compared to the viscous and the viscoelastic cases. Apart from the resonance convolution, phase tends to plateau around the capacitive and inductive behaviour for wider frequency ranges as $\mathrm{Ma}_\mathrm{D}^\infty$ increases. This must be owing to be components in pressure overpotential which resemble L-C behaviour becoming larger as the diffusion Mach number increases.

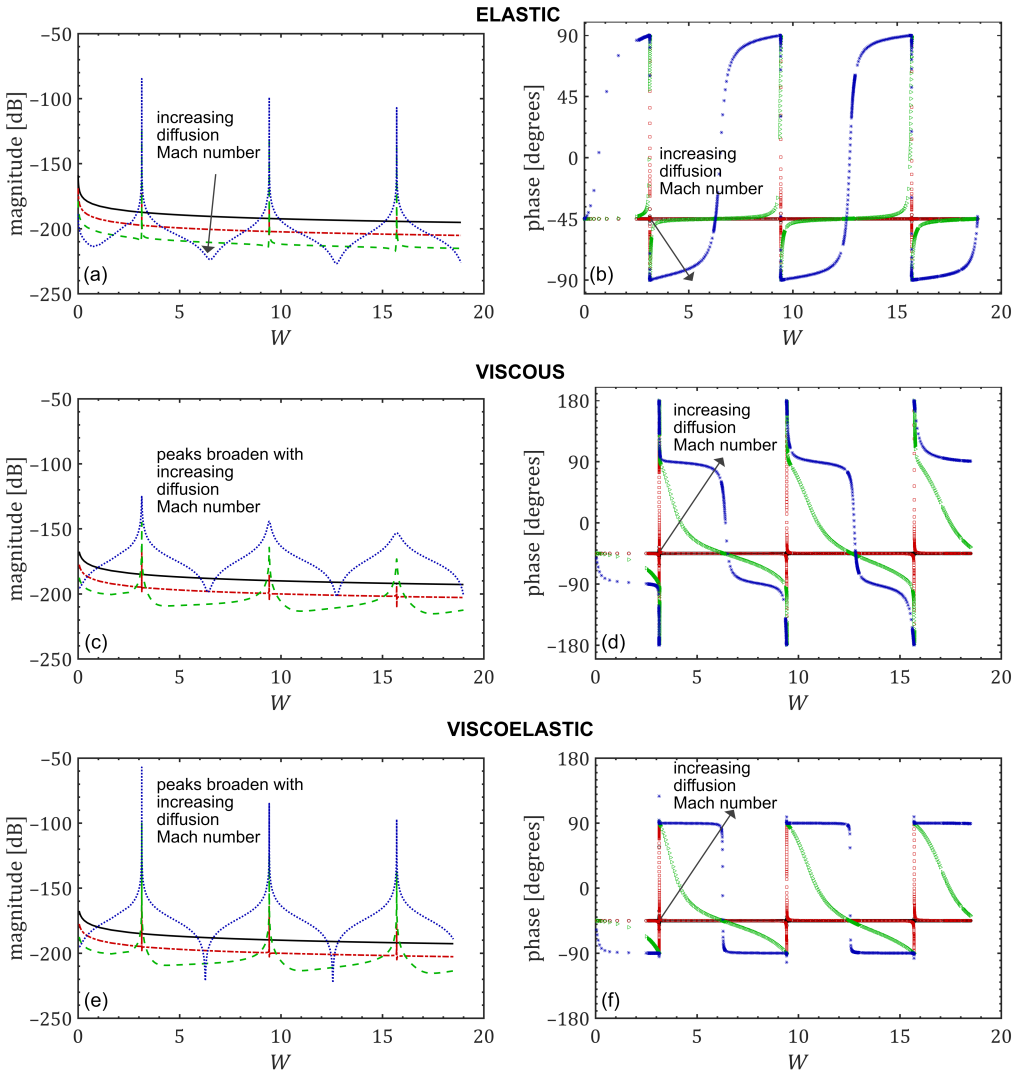

Figure 4.18: Effect of changing the diffusion Mach number $\mathrm{Ma}_{\mathrm{D}}^{\infty}$ on Bode plots for (a) elastic gain (b) elastic phase (c) viscous gain (d) viscous phase (e) viscoelastic gain (f) viscoelastic phase. In ascending order of parameter values: black (–) & (o), 3.778×10^{-9}; red (–.) & (□) , 3.778×10^{-8}; green (––) & (▷), 3.778×10^{-7}; and blue (:) & (∗), 3.778×10^{-6}.

4.6.1.2 Discussion of the Maxwell Mach Number

The Maxwell Mach number measures the Maxwell velocity in the units of the speed of sound in the material. From running a variety of trials, it was concluded that it is more valuable to decrease $\mathrm{Ma}_{\mathrm{M}}^{\infty}$. At the standard value for Nafion $\mathrm{Ma}_{\mathrm{M}}^{\infty} \sim 1$, which suggests that the Maxwell velocity is the same order of magnitude as the speed of sound; in other words, the Maxwell frequency is the same magnitude as the acoustic frequency. Decreasing $\mathrm{Ma}_{\mathrm{M}}^{\infty}$ therefore makes the Maxwell speed and frequency smaller than the acoustic speed and frequency. In the present case, this was achieved by increasing the bulk modulus K^{∞}. This is unfavourable from the experimental point of view because the resonant frequencies may become impractically high, but the features themselves become more interesting, so we accept the trade-off.

In the gain plots for the elastic, viscous, and viscoelastic cases, shown in Figures 4.19(a),(c),(e), the peaks become drastically wider as $\mathrm{Ma}_{\mathrm{M}}^{\infty}$ decreases, making them much more viable for experimental observation. It can also be seen that whereas the peak widens and changes curvature across all three cases, the peak heights and depths seem to change more drastically in the viscous case, and to an intermediate extent in the viscoelastic case. The one thing to keep in mind here is that an order of magnitude decrease in $\mathrm{Ma}_{\mathrm{M}}^{\infty}$ requires a hundredfold increase in bulk modulus K^{∞}. Since the resonance frequencies scale with K^{∞}, the gain is plotted against the scaled frequency W instead, to allow comparison of peak shapes. This also ensures uniformity across the discussion of various dimensionless parameters which may affect resonant frequencies in different ways, if at all. Finally, the phase plots, Figures 4.19(b),(d),(f), show similar trends as the gain plots. The convolution of resonance modes increases with decreasing $\mathrm{Ma}_{\mathrm{M}}^{\infty}$.

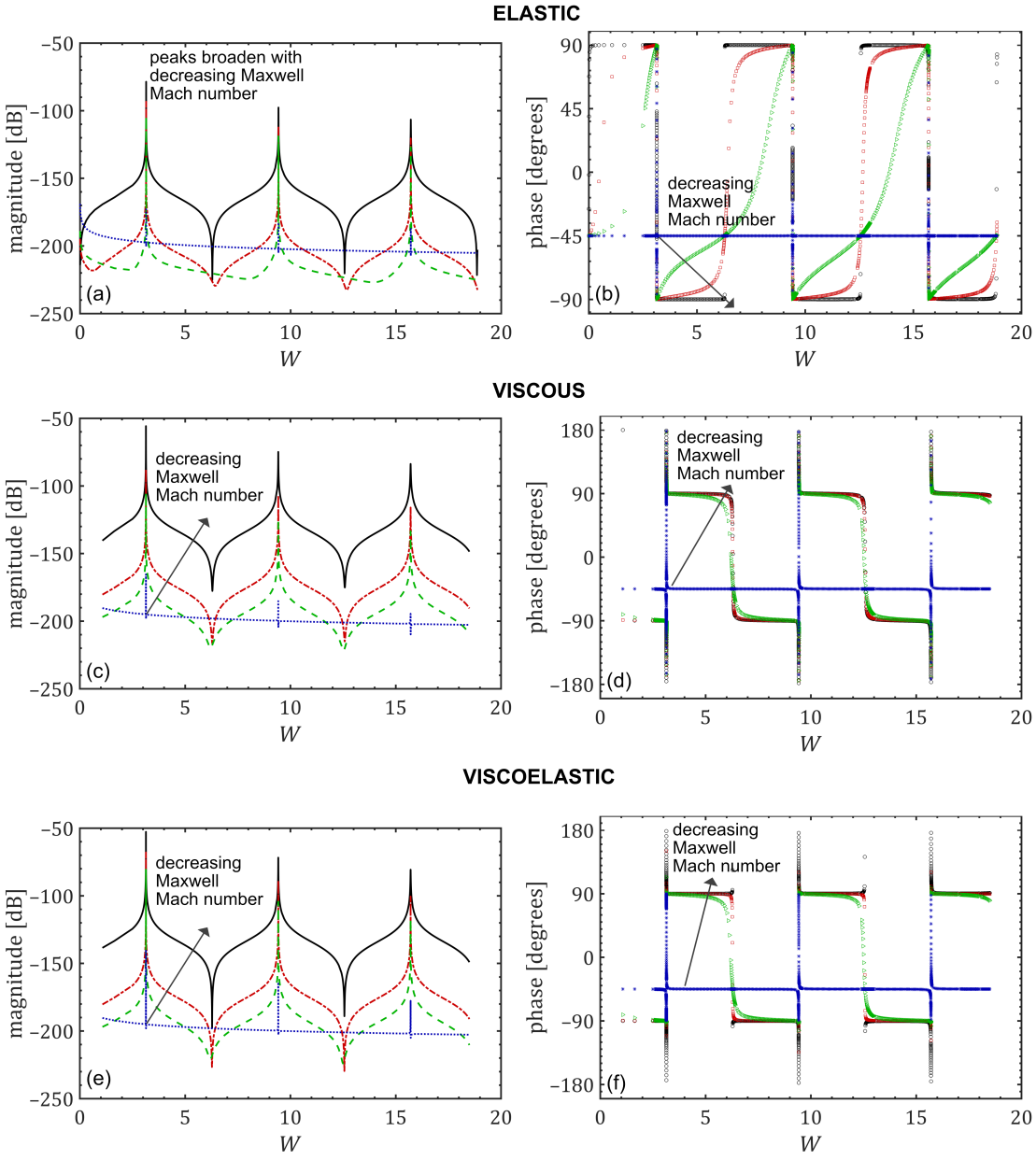

Figure 4.19: Effect of changing the Maxwell Mach number $\mathrm{Ma}_{\mathrm{M}}^{\infty}$ on Bode plots for (a) elastic gain (b) elastic phase (c) viscous gain (d) viscous phase (e) viscoelastic gain (f) viscoelastic phase. In ascending order of parameter values: black (–) & (o), 7.33×10^{-3}; red (–.) & (□), 3.665×10^{-2}; green (––) & (▷), 7.33×10^{-2}; and blue (:) & (∗), 7.33×10^{-1}.

4.6.1.3 Discussion of the Schmidt Number

As the viscosity increases, there is no discernible effect on resonant frequency or peak width, but the peak heights dwindle significantly. The plots in Figure 4.20(a) and (b) show how gain and phase plots change in the viscous case. To be able to understand the peak height decrease better, the gain due to pressure overpotential is plotted in 4.20(c) to show an overall decreasing envelope as $\mathrm{Sc}^{\infty}_{\mathrm{shear}}$ and therefore $\mu^{\infty}_{\mathrm{shear}}$ increases. The final plot, 4.20(d), shows a zoomed-in view of the first peak and valley, which clearly demonstrates that as the material becomes increasingly viscous, its ability to resonate reduces drastically. Results from the viscoelastic case lead to the same qualitative inferences and are therefore not explicitly shown.

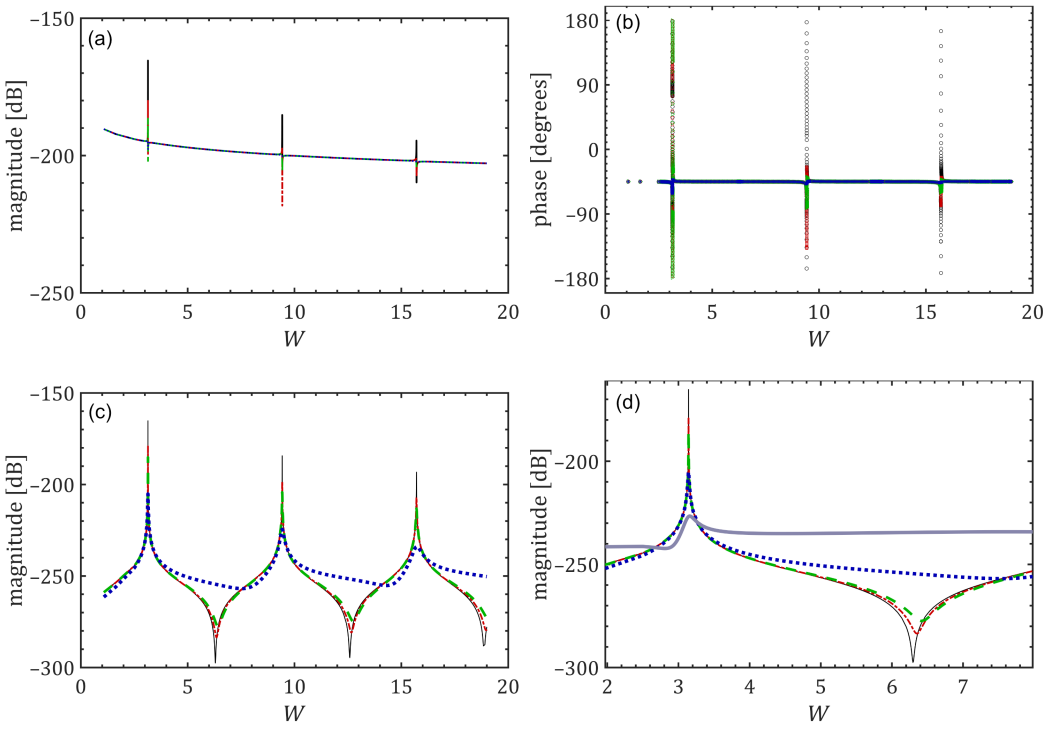

Figure 4.20: Effect of changing $\mathrm{Sc}^{\infty}_{\mathrm{shear}}$ for the viscous case on Bode plots (a) total gain (b) total phase (c) pressure gain (d) zoomed-in view of (c). In order of ascending parameter values: black (–) & (o), 2.91×10^2; red (–.) & (□), 1.455×10^3; green (−−) & (▷), 2.91×10^3; blue (:) & (∗), 2.91×10^4.

Lastly, since changing K^{∞} (scaled conductivity) and hence the bulk ionic conductivity κ^{∞} only changes the real intercept on the Nyquist plot, and the base magnitudes of the gain plots, its value does not affect the shape or the interaction of the resonance events, its impact is relatively trivial and that study is not formally carried out.

4.6.2 Parameter Study: Material & Chemical Properties

This section looks at the effect of changing material properties such as the ratio of molecular weights, partial molar properties, thickness of the membrane, activity coefficients, and the effect of zero-order hydration level of the membrane. This is an interesting way of studying how mechanical effects depend on the average water content of the membrane.

Information about material properties such as m_0 and B_0 can help choose the correct combination of electrolyte and solvent to magnify pressure effects. To carry out a systematic study, a broad range of the parameters was explored, as laid out in Table 4.6.

parameter	**value 1**	**value 2**	**value 3**	**value 4**
$B_0 = \overline{V}_0/\overline{V}_e$	–	0.0288	1	288
$m_0 = \overline{m}_0/\overline{m}_e$	–	0.01636	1	163.6
$\lambda^{\infty} = \dfrac{\nu y_0^{\infty}}{1 - y_0^{\infty}}$	2	6	10	14

Table 4.6: Values of the dimensionless parameters related to material and thermodynamics properties of the system.

4.6.2.1 Discussion of Solvent Mass and Volume Fractions

The black line on the Bode gain plot, Figure 4.21(a), represents typical Nafion behaviour, where $B_0 = \overline{V}_0/\overline{V}_e = \mathcal{O}(10^{-2}) = 0.0288$. When the partial molar volume of solvent becomes comparable to the partial mole volume of the polymer backbone, such that the two occupy similar volume fractions, the very narrow peak becomes broader, as seen by the red dashed line. A similar effect is seen on the phase plot, Figure 4.21(b). Whereas the oscillation between the capacitive and inductive behaviour is confined to a very narrow band of frequency (approaching a single frequency) for Nafion (black line), increasing B_0 to $\mathcal{O}(1)$ makes this change more gradual, thereby widening the peak and introducing a convolution of resonance modes. Going to the other extreme, in which the solvent occupies a much higher volume fraction of the solution than the membrane, $B_0 = \mathcal{O}(10^2)$, is represented by the green line (:) on both gain and phase plots in Figures 4.21(a) and (b), respectively. Resonance features are very prominent, since the pressure overpotential component of impedance is scaled by a factor of $B_0 - m_0$; the anti-resonance troughs show prominently because pressure overpotential dominates the composition overpotential.

A similar range of magnitudes is explored for $m_0 = \overline{m}_0/\overline{m}_e$. The typical Nafion case with $m_0 = \mathcal{O}(10^{-2})$ is represented by the black line in the Bode gain and phase plots, Figures 4.21 (c)–(d). Increasing m_0 to $\mathcal{O}(1)$, where the mass fractions of the solvent and the membrane are similar, and even to $\mathcal{O}(10^2)$, where solvent occupies a much larger mass fraction, cause little change in the impedance signatures. The increase in peak width on the gain plot or in the convolution between resonance modes on the phase plot is not significant enough to be practically advantageous. Both m_0 and B_0 also affect other zero-order parameters, such as total concentration θ_T^∞ and density φ^∞, so as to change the β^∞ factor appearing in diffusion and wave equations. This is interesting because making m_0 greater than B_0 may change the polarity of the term

in which it does not appear as a square, introducing contradictory effects.

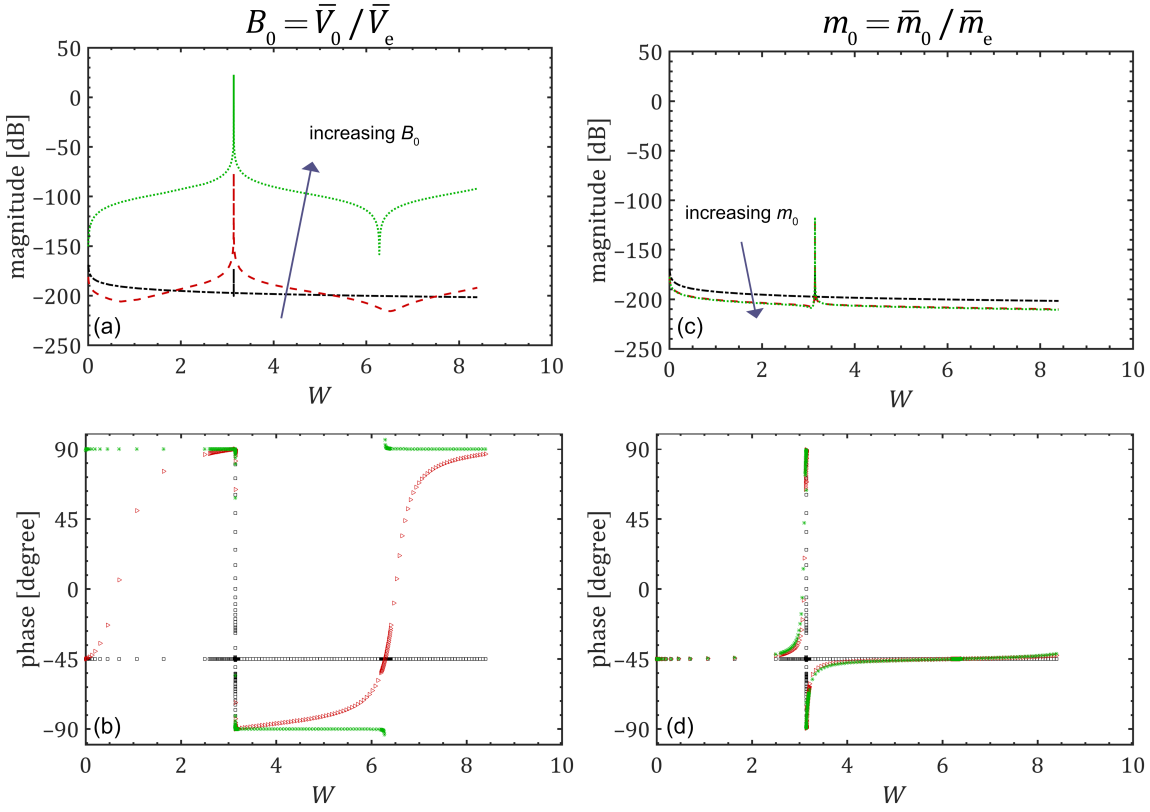

Figure 4.21: Plots showing the effects of varying relative material properties such as molar masses and partial molar volumes of the solvent and the electrolyte. (a) Bode gain plot and (b) Bode phase plot for the following B_0 values: black (–.) & (□), 0.0288; red (––) & (▷), 1; green (:) & (∗), 288.8. (c) Bode gain plot and (d) Bode phase plot for the following m_0 values: black (–.) & (□), 0.01636; red (––) & (▷), 1; green (:) & (∗), 163.36.

Attention should be given to a special case in which the mass fraction occupied by the solvent is the same as the volume fraction occupied by it, $m_0 = B_0$, causing the ubiquitous factor $(B_0 - m_0) = 0$ to vanish. This condition affects the mechanical effects in the system immensely, because it is primarily through the difference between the mass and volume fraction that pressure is coupled to diffusion, and therefore impedance. Firstly, the pressure diffusion term in the diffusion equation 4.69 com-

pletely drops out; secondly the composition term from the wave equation drops out, uniformly for the elastic 4.70, viscous C.16, and viscoelastic cases C.17; and finally, most importantly in the present context, the pressure overpotential term effectively gets reduced to zero ($m_+ = \overline{m}_+/\overline{m}_e \sim 0$ when protons are the cations).

4.6.2.2 Discussion of Average Solvent Content

The equilibrium hydration level of the membrane was varied last. It must be kept in mind that water composition is a bounded variable, $0 \leq y_0 \leq 1$ so its numerical value cannot be drastically changed. Given that many zero-order parameters depend on the membrane water content, it is worthwhile to list them and understand how they change with λ (water content), as shown in Table 4.7. Whereas θ_T^∞, φ^∞, and β^∞ increase with water content, the product $y_0^\infty\left(1-y_0^\infty\right)$ which occurs in many equations naturally decreases. A combination of these parameters can, therefore, produce complex effects with changing water content.

parameter	$\lambda = 2$	$\lambda = 6$	$\lambda = 10$	$\lambda = 14$
$y_0^\infty = \frac{\lambda^\infty}{\nu+\lambda^\infty}$	0.5	0.75	0.833	0.875
$\theta_T^\infty = \frac{\nu}{1+(\nu B_0-1)y_0^\infty}$	3.78	6.82	9.32	11.4
$\varphi^\infty = \frac{1+(\nu m_0-1)y_0^\infty}{1+(\nu B_0-1)y_0^\infty}$	3.87	7.28	10.31	13.01
$\beta^\infty = \frac{{\theta_T^\infty}^2(B_0-m_0)}{\nu\varphi^\infty}$	0.023	0.031	0.042	0.053
$y_0^\infty\left(1-y_0^\infty\right)$	0.025	0.187	0.139	0.109

Table 4.7: Values of the dimensionless parameters related to the water content of the membrane.

Unsurprisingly, changing the average water content of the membrane while leaving other material properties constant did not have a substantial effect on impedance signatures. This can be clearly seen in Figures 4.22 (a) and (c), which are Bode gain and phase plots. The inset Figure 4.22(b) shows the overall Bode plot, whereas

the main plot expands the axes near the resonance peak to show that although the peak width varies little, the peak height changes by several orders of magnitude, a desirable effect for making pressure effects more substantial. The change in peak magnitude appears to be non-linear; the change is big while going from $\lambda = 2$ to $\lambda = 6$, slows down towards $\lambda = 10$ and then shoots up again for $\lambda = 14$. This is partly because $y_0 = \frac{\lambda}{(\lambda+\nu)}$ is a non-linear function in itself but also because of the complex dependences of parameters on y_0 as laid out in Table 4.7.

The shortcoming of this analysis is that it does not take into account how material properties such as diffusion coefficient and bulk modulus depend on equilibrium water content. These dependences would likely exaggerate the observed effects, but are generally not well understood experimentally. Also, it serves us well to keep in mind that all of these plots are corrected for bulk-resistance, which also varies strongly with composition.

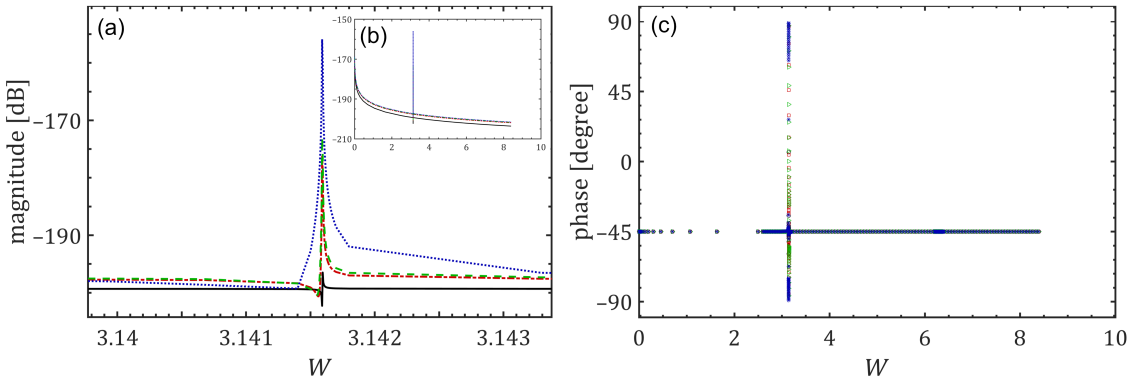

Figure 4.22: Plots showing the effects of varying the zero-order water content of the membrane on impedance (a) Bode gain plot and (b) Bode phase plot for the following λ values: black (–), 2; red (–.), 6; green (––), 10; blue (:), 14 [vapour-equilibrated case].

4.6.3 Damping Factors and Parameter Study

An eigenvalue analysis of the system of diffusion and wave equations for elastic, viscous, and viscoelastic systems in carried out in Appendix C.3. Apart from the quantities denoting the distinct eigenmodes of diffusion and wave equations, three kinds of coefficients appear in the eigenvalue expressions,

- a coupling coefficient showing the degree of association between the two eigenmodes (which appears for all three kinds of material behaviour)

$$\xi^{\infty}_{\text{coup}} = \frac{\text{Ma}^{\infty}_{\text{D}}}{\sqrt{3}} \frac{1}{\text{Ma}^{\infty^2}_{\text{M}}} \left[\frac{\theta^{\infty^2}_{\text{T}} \left(B_0 - m_0 \right)}{\nu \varphi^{\infty}} \right]^2 y^{\infty}_0 \left(1 - y^{\infty}_0 \right), \tag{4.88}$$

- a viscous coefficient denoting shear losses, and

$$\xi^{\infty}_{\text{visc}} = \frac{4}{3} \text{Sc}^{\infty}_{\text{shear}} \text{Ma}^{\infty}_{\text{D}}, \tag{4.89}$$

- a viscoelastic coefficient combining the viscous and the elastic characteristics,

$$\xi^{*,\infty}_{\text{visc,elas}} = \frac{\xi^{\infty}_{\text{visc}}}{1 + W^2 \left[\frac{1+\nu_{\text{PR}}}{2(1-2\nu_{\text{PR}})} \right]^2 C^{\infty^2}_{\text{visc}} \xi^{\infty^2}_{\text{visc}}} - j \frac{W \frac{1+\nu_{\text{PR}}}{2(1-2\nu_{\text{PR}})} C^{\infty}_{\text{visc}} \xi^{\infty^2}_{\text{visc}}}{1 + W^2 \left[\frac{1+\nu_{\text{PR}}}{2(1-2\nu_{\text{PR}})} \right]^2 C^{\infty^2}_{\text{visc}} \xi^{\infty^2}_{\text{visc}}}. \tag{4.90}$$

It is seen that all the three coefficients tend to cause damping of the impedance resonance peaks. A "damped" peak appears broader and shorter on the Bode gain plot, and the corresponding effect can be observed on the phase plot as well. The previous section related this broadening to the various dimensionless parameters such as $\text{Ma}^{\infty}_{\text{D}}$, $\text{Ma}^{\infty}_{\text{M}}$, $\text{Sc}^{\infty}_{\text{shear}}$ *etc.* through a numerical inquiry. However, the expressions above present a more exact relationship for the same.

For instance, as shown in the expression 4.88, the coupling damping coefficient, $\xi^{\infty}_{\text{coup}}$, and therefore the width of the resonance peak, is expected to vary linearly with the diffusion Mach number, $\text{Ma}^{\infty}_{\text{D}}$ but inversely with the square of the Maxwell Mach

number, $\mathrm{Ma}_{\mathrm{M}}^{\infty}$. The same conclusions were drawn through the analysis of Figures 4.18 and 4.19. Similarly, expression 4.89 shows that $\xi_{\mathrm{visc}}^{\infty}$ varies linearly with the Schmidt number, $\mathrm{Sc}_{\mathrm{shear}}^{\infty}$, as was also suggested by the numerical results in Figure 4.20. Information from these damping coefficients can, therefore, be utilised directly in the design of an electrolyte for exploring mechanical effects, thereby reducing if not eliminating the need for numerical simulations.

Further, if bulk viscosity effects are included in the momentum balance, an additional damping factor may be defined as follows:

$$\xi_{\mathrm{visc,bulk}}^{\infty} = \mathrm{Sc}_{\mathrm{bulk}}^{\infty}\mathrm{Ma}_{\mathrm{D}}^{\infty}. \tag{4.91}$$

The elastic system now has this bulk viscous damping in addition to $\xi_{\mathrm{coup}}^{\infty}$, which makes its impedance behaviour mimic the shear viscous case. Damping coefficients of the viscous and viscoelastic cases are accordingly updated as follows,

$$\xi_{\mathrm{visc,eff}}^{\infty} = \xi_{\mathrm{visc}}^{\infty} + \xi_{\mathrm{visc,bulk}}^{\infty}, \tag{4.92}$$

$$\xi_{\mathrm{visc,elas,eff}}^{*,\infty} = \xi_{\mathrm{visc,elas}}^{*,\infty} + \xi_{\mathrm{visc,bulk}}^{\infty}. \tag{4.93}$$

It is, however, seen that their fundamental mathematical behaviour remains the same. Given a reliable estimation of the bulk viscosity, the extent of damping in the system can be evaluated from the expressions above. As damping increases, the resonance peaks become broader, and hence more accessible in terms of frequency range, but also shorter in terms of magnitude; an optimum degree of damping is desired to balance the trade-off from the two features.

Table 4.8 lists the various damping factors, their expressions in terms of the dimensionless parameters as well as their orders of magnitude for the Nafion system (around impedance frequency $W \sim \mathcal{O}(1)$, where mechanical effects become important). It can be seen that most damping factors tend to be smaller than unity for this system, suggesting underdamping of the resonance peaks. Also, since the viscous

and viscoelastic damping factors are much larger, they dominate over any damping due to coupling of diffusion and mechanics.

damping factor	**expression**	**order of magnitude**
$\xi^{\infty}_{\text{coup}}$	$\frac{\text{Ma}^{\infty}_{\text{D}}}{\sqrt{3}} \frac{1}{\text{Ma}^{\infty^2}_{\text{M}}} \left[\frac{\theta^{\infty^2}_{\text{T}}(B_0 - m_0)}{\nu\varphi^{\infty}}\right]^2 y^{\infty}_0 \left(1 - y^{\infty}_0\right)$	$\mathcal{O}\left(10^{-9}\right)$
$\xi^{\infty}_{\text{visc}}$	$\frac{4}{3}\text{Sc}^{\infty}_{\text{shear}}\text{Ma}^{\infty}_{\text{D}}$	$\mathcal{O}\left(10^{-5}\right)$
$\xi^{*,\infty}_{\text{visc,elas}}$	$\frac{\xi^{\infty}_{\text{visc}}}{1+W^2\left[\frac{1+\nu_{\text{PR}}}{2(1-2\nu_{\text{PR}})}\right]^2 C^{\infty^2}_{\text{visc}}\xi^{\infty^2}_{\text{visc}}} - jW\frac{\frac{1+\nu_{\text{PR}}}{2(1-2\nu_{\text{PR}})}C^{\infty}_{\text{visc}}\xi^{\infty^2}_{\text{visc}}}{1+W^2\left[\frac{1+\nu_{\text{PR}}}{2(1-2\nu_{\text{PR}})}\right]^2 C^{\infty^2}_{\text{visc}}\xi^{\infty^2}_{\text{visc}}}$	Real:$\mathcal{O}\left(10^{-6}\right)$
$\xi^{\infty}_{\text{visc,bulk}}$	$\text{Sc}^{\infty}_{\text{bulk}}\text{Ma}^{\infty}_{\text{D}}$	$\mathcal{O}\left(\mu_{\text{bulk}} \times 10^{-2}\ \text{Pa}^{-1} \cdot \text{s}^{-1}\right)$

Table 4.8: Damping coefficients identified from the eigenvalue analysis in Appendix C in terms of the dimensionless groups identified earlier, along with the typical orders of magnitudes for Nafion. The small magnitudes ($<< 1$) suggest underdamping, resulting in resonance peaks.

It is difficult to estimate the order of magnitude of $\xi^{\infty}_{\text{visc,bulk}}$ because the magnitude of bulk viscosity for different systems varies greatly, ranging from being of the order of the shear viscosity to being three orders of magnitude higher [171]. As an example, if the electrolyte was aqueous ($\mu_{\text{bulk}}/\mu_{\text{shear}} \sim 3$) [170], the effective damping factor would only be 4 times as big as viscous damping factor, which would not change the mathematical behaviour drastically. If the bulk viscosity, however, is indeed very large ($> 100\text{Pa} \cdot \text{s}$), it may lead to overdamping in the system, thereby suppressing the resonance peaks.

4.7 Conclusions

A closed system of governing equations accounting for kinematic and dynamic mechanical effects in an electrochemical cell was formulated, yielding a system of nonlinear coupled partial differential equations to be solved. To simplify the problem without losing physical relevance, the framework was perturbed to model electrochemical impedance spectroscopy. Linearising the model in this way led to a system of ordinary differential equations, and the assumption of an unbiased steady state ensured that the model only contained constant properties, whose values were set by the equilibrium water content of the membrane.

Mechanical coupling becomes important at the resonance frequencies of the cell, which occur in the frequency range of MHz for the symmetric hydrogen-cell with Nafion considered in the study. The compressibility of the medium, produces peaks on Bode plots and irregular loops on Nyquist plots, both of which suggest the presence of RLC-like components in the pressure contribution to impedance [173]. A part of the inductance often observed experimentally at high frequencies may be attributed to these mechanical resonance events.

This simplified model can form a foundation upon which various other modifications, depending upon the application, can be appended. Double-layer charging and interfacial kinetic resistance could be incorporated to explore their interaction with the mechanical resonance. An equivalent-circuit model, possibly consisting of various RLC elements, could be built to model the mechanical impedance. A foreseeable challenge would be to relate these various electrical components to mechanical properties of the cell. According to Maxwell analogy [173], inertia of a mechanical system impedes motion in the same way as an inductor impedes current; compressibility stores energy in a similar way as a capacitor; and viscosity causes dissipation. An experi-

ment where the cell is mechanically vibrated to obtain a voltage response, without the flow of current, could be conducted to exclude or downplay some of the effects related to Warburg impedance. If designed to recover measurable voltage drops across the cells, results from such an experiment could validate the present model.

To conclude this chapter, we want to utilise the insights gained in the parameter study section to propose a material whose properties would make the mechanical effects an intrinsically important part of its impedance spectra. To achieve this goal it is desirable to: increase the diffusion Mach number $\mathrm{Ma}_{\mathrm{D}}^{\infty}$, the volume fraction of solvent B_0, and the solvent the mole fraction y_0^{∞}; to decrease the Maxwell Mach number $\mathrm{Ma}_{\mathrm{M}}^{\infty}$, the transference number $t_+^{0,\infty}$, and the activity coefficient χ^{∞} leading to non-ideality; and to keep the Schmidt number $\mathrm{Sc}_{\mathrm{shear}}^{\infty}$ (or viscosity) and the mass fraction of solvent m_0 constant.

The choice of parameters to achieve the above modifications is a trade-off between different properties: let us lead with increasing the bulk modulus to make the material more rigid, a relatively easy goal to achieve, which would decrease $\mathrm{Ma}_{\mathrm{M}}^{\infty}$. This route also decreases $\mathrm{Ma}_{\mathrm{D}}^{\infty}$, however, which is undesirable. In addition, it further increases the acoustic frequency, making experimental observation more challenging. These issues can be countered effectively by increasing the thickness of the membrane, to maintain the acoustic frequency constant ~ 0.5MHz, but then the diffusion coefficient D^{∞} should also be increased to prevent $\mathrm{Ma}_{\mathrm{D}}^{\infty}$ from becoming too small. Along with this, the membrane partial molar volume should be changed so that it occupies a volume fraction comparable to water, which changes B_0; χ and $t_+^{0,\infty}$ should be reduced as well. Changing the water content will probably not accomplish much, and hence could be kept constant at $\lambda = 10$. Table 4.9 summarises the desirable values of the model parameters, and Figure 4.23 shows the resulting impedance spectra. The

mechanical peaks are broader, which would be easier to observe on the impedance plots, while the fundamental acoustic frequencies remain in the MHz range.

property	value	property	value	dimensionless no	value
K^∞	$\mathcal{O}(10^{10}$ Pa)	B_0	1	$\mathrm{Ma}_\mathrm{D}^\infty$	$\mathcal{O}(10^{-9})$
D^∞	$\mathcal{O}(10^{-7}$ m^2/s)	$t_+^{0,\infty}$	0.4	$\mathrm{Ma}_\mathrm{M}^\infty$	$\mathcal{O}(10^{-2})$
L^∞	$\mathcal{O}(10^{-2}$ m)	χ^∞	0.1		

Table 4.9: Values of membrane properties and resulting dimensionless parameters chosen to play up the electrochemical/mechanical coupling.

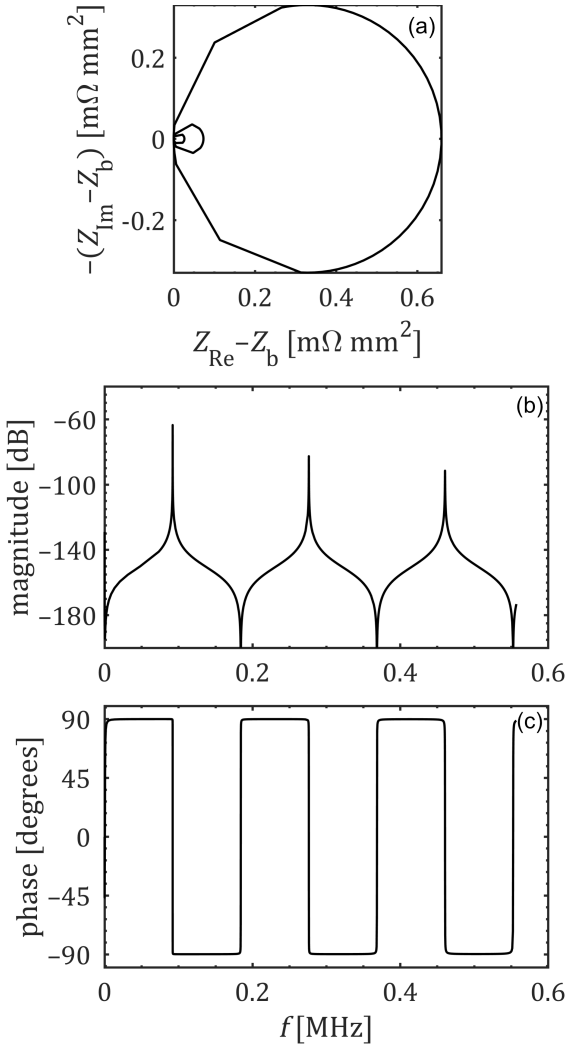

Figure 4.23: Impedance plots with parameters selected to play up the electrochemical/mechanical coupling (a) Nyquist plot with loops (b) Bode gain plot and (c) Bode phase plot, show peaks with large bandwidths.

Chapter 5

Alternate Applications: Steady-State Case

Electrochemical impedance spectroscopy was chosen as the first application for the transport model developed in this thesis because it looked at first-order perturbation of the model, making it easier to identify mechanical effects and their time scales, as well as illustrating coupling between mechanics and diffusion. It is also interesting to study this system at steady state, to inform a better understanding of long-term behaviour. Investigation of steady states is similar to low-frequency impedance, except nonlinearities due to higher-order effects such as inertia are also included.

As a start, consider a standalone Nafion membrane in VE mode exposed to gases of differing relative humidities on either side, resembling the anode and cathode gas channels in a PEM fuel cell. It is assumed that water molecules in the VE membrane are strongly bound to the ionic sites on the backbone and form a part of the membrane phase itself. The principal mode of transport in VE mode is diffusion, driven by concentration and pressure gradients, as well as electroosmosis in the presence of charge flow.

At this stage, the model is focused on the isothermal description of steady-state distributions in the thickness direction of the membrane; it can be extended to obtain transient behaviour, however. The system of equations is based in a coordinate that moves with the deformed membrane, instead of being fixed in space. This allows us to solve the problem with static boundaries ($X\,[=x/L]=0$ to $X=1$) for any level of hydration). For this preliminary discussion, an assumption of uniform pressure is applied,

$$\vec{\nabla}p=0, \tag{5.1}$$

as has often been done in the literature [3, 95]. An assumption of constant pressure requires us assume that inertia is negligible and there are no deviatoric stresses at play. Despite this reductive assumption, the formulation is still novel in the way that pressure can affect local volume through the equation of state, and allows for the relationship between water transport, swelling behaviour, and the associated integral pressure to be studied.

Although still coupled, this reduced uniform pressure model (in $1d$) can be tracked analytically. The mole-fraction sum (equation 3.15),

$$y_0+\nu y_\mathrm{e}=1, \tag{5.2}$$

and the volumetric equation of state (equation 3.30), with explicit consideration of the pressure dependence of partial molar volumes,

$$c_\mathrm{T}\left(\overline{V}_0^{\mathrm{ref}}y_0+\overline{V}_\mathrm{e}^{\mathrm{ref}}y_\mathrm{e}\right)\pi=1, \tag{5.3}$$

hold locally, where $\pi=\exp\left(-\frac{p-p^{\mathrm{ref}}}{K}\right)$. The material balance turns into a condition of constant flux

$$\vec{\nabla}\cdot\vec{N}_0=0, \tag{5.4}$$

similar to current density $\vec{\nabla} \cdot \vec{i} = 0$. The volume balance for the steady state case, under uniform pressure conditions, becomes

$$\vec{\nabla} \cdot \vec{v}^{\square} = 0, \tag{5.5}$$

simplifying the conservation equations to a great extent. Finally, to close the system of equations, there is a solvent flux law, which simplifies in the absence of stress gradients to,

$$\vec{N}_0 = -c_{\mathrm{T}}^2 \overline{V}_{\mathrm{e}} \frac{D}{\nu} \vec{\nabla} y_0 + c_{\mathrm{T}} y_0 \vec{v}^{\square}. \tag{5.6}$$

This system of equations (differential equations 4.4, 5.1, 5.4, 5.5, 5.6 with algebraic equations 5.2, 5.3) is simple enough to be solved analytically with the following boundary conditions: prescribe solvent mole fraction at both ends $y_0|_0 = y_0^0$, $y_0|_L = y_0^L$, prescribe reference pressure at one end $p|_L = p^{\infty}$, and apply the constraint that membrane cannot cross the boundary $\vec{N}_-\big|_0 = 0$. When no current is being passed through the system, one can just solve for water transport. The solvent composition distribution along the thickness of the membrane is then

$$y_0 = \frac{1 - \left(\frac{1-y_0^L}{1-a y_0^L}\right)^{x/L} \left(\frac{1-y_0^0}{1-a y_0^0}\right)^{(1-x/L)}}{1 - a\left[\left(\frac{1-y_0^L}{1-a y_0^L}\right)^{x/L} \left(\frac{1-y_0^0}{1-a y_0^0}\right)^{(1-x/L)}\right]}, \tag{5.7}$$

where $a = 1 - \nu B_0$. As expected, the mole-fraction distribution is independent of pressure and temperature, and is only governed by relative humidity specifications at the boundaries. Figure 5.1 presents solvent mole fraction profiles in situations where the left boundary is kept dry while the humidity at the right boundary is increased.

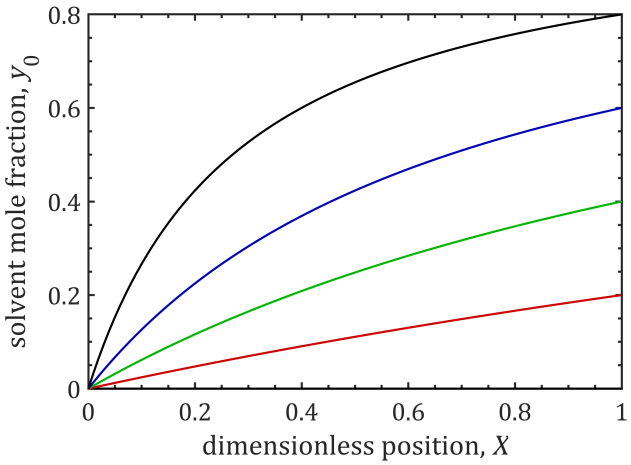

Figure 5.1: Solvent mass fraction profile across the thickness of the membrane. The left boundary is kept completely dry while the right boundary is progressively humidified: red ($y_0^L = 0.2$) ; green ($y_0^L = 0.4$); blue ($y_0^L = 0.6$); black ($y_0^L = 0.8$), resulting in increasingly non-linear profiles.

Dimensionless solvent flux $\eta_0^0 = N_0^0 L\overline{V}_e^0/D$, a constant with respect to position, can be computed through

$$\eta_0^0 = \frac{1}{\nu B_0 \pi} \ln\left[\frac{(1-y_0^L)(1-ay_0^0)}{(1-y_0^0)(1-ay_0^L)}\right]. \tag{5.8}$$

The dependence of η_0^0 on both the boundary compositions is presented as a contour plot in Figure 5.2. Note that the axes are restricted to the range of boundary conditions that is accessible in VE mode $[\lambda = 0, y_0 = 0\,(\text{dry})$ to $\lambda = 14, y_0 = 0.875\,(\text{saturated})]$. When $y_0^0 = y_0^L$, there is no solvent flux across the membrane at steady state. However, as the difference in y_0^0 and y_0^L rises, so does the flux, whose direction of flux depends on the polarity of the composition gradient. The logarithmic function of composition makes the flux contour lines non-linear and leads to the symmetric clustering of contour lines for the higher mole-fraction values, implying that flux changes faster at higher compositions. Also, equation 5.8 shows that flux increases with increasing ambient pressure (as p increases, π decreases). Typically, one electrode in a PEM fuel cell is saturated, and the other runs the risk of drying up due to electroosmosis; a higher pressure may enhance back diffusion by a small amount, given $y_0^L > y_0^0$.

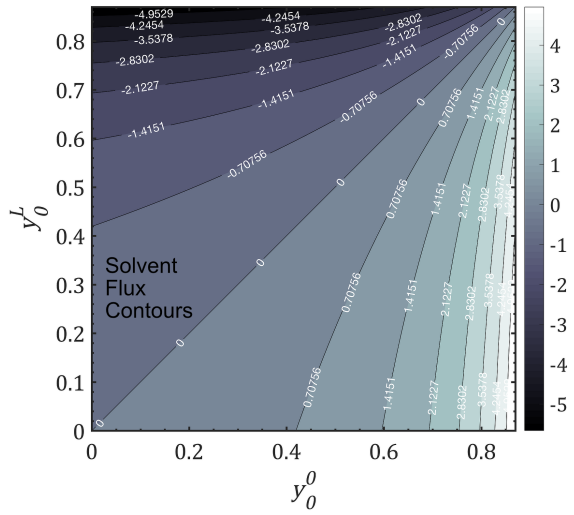

Figure 5.2: Contour plot of solvent flux as a function of solvent mole fraction at the left (x-axis) and at the right (y-axis) boundaries.

We implement global volumetric strain computations based on the local equation of state, making them thermodynamically sound. Similar to Meyers and Newman [81], conservation of membrane mass is enforced through tracking the following auxiliary variable,

$$n_{\mathrm{e}} = A \int_0^x c_{\mathrm{T}} y_{\mathrm{e}} dx. \tag{5.9}$$

Here n_{e} gives the number of moles of electrolyte membrane moles contained within volume Ax. Assuming that the cross-section remains uniform through hydration; the membrane thickness goes from a dry value of L^{ref} to a hydrated value L. Since the total number of membrane moles remains constant at different levels of membrane hydration or under different physical constraints, this new variable should remain constant at its dry value after the membrane is hydrated or deformed:

$$n_{\mathrm{e}}(L) = A \int_0^L c_{\mathrm{T}} y_{\mathrm{e}} dx = A c_{\mathrm{T}}^{\mathrm{ref}} y_{\mathrm{e}}^{\mathrm{ref}} L^{\mathrm{ref}} \Rightarrow A L^{\mathrm{ref}} = n_{\mathrm{e}}(L) \overline{V}_{\mathrm{e}}^{\mathrm{ref}} \tag{5.10}$$

We should emphasise that a dry membrane acts as a reference state, for which $c_{\mathrm{T}}^{\mathrm{ref}} y_{\mathrm{e}}^{\mathrm{ref}} \overline{V}_{\mathrm{e}}^{\mathrm{ref}} = 1$. With this constraint in mind, it is relatively simple to define the

global volumetric strain ϵ_g,

$$\epsilon_g = \frac{V}{V^{ref}} - 1 = \frac{L}{n_e(L)\,\overline{V}_e^{ref}} - 1. \tag{5.11}$$

For a given set of boundary humidity and pressure conditions this strain is,

$$\epsilon_g = \frac{L - L^{ref}}{L^{ref}} = \frac{\pi\,(1 - a y_0^0)\,(1 - a y_0^L)}{\nu B_0\,(y_0^L - y_0^0)} \ln\left[\frac{(1 - y_0^0)\,(1 - a y_0^L)}{(1 - y_0^L)\,(1 - a y_0^0)}\right] - 1. \tag{5.12}$$

Given certain water-content/flux boundary conditions, one can either fix strain to calculate the compressive force or pressure developed in the membrane, or change the pressure acting on the membrane to calculate the corresponding strain. Figure 5.3(a) presents a contour plot of global strain in a freely swelling membrane. Dry, freely swelling conditions yield no strain in the membrane, whereas having saturated vapour on both sides yields the maximum strain of 35%. Figure 5.3(b) shows the membrane under exaggerated compression (corresponding to $\pi = 0.9$); at lower compositions the swelling from hydration is not enough to compensate for the compression from pressure. Even under saturated conditions, the strain is lower than the freely-swelling membrane by ~10–15%.

The complexity of this model can be increased gradually by passing current through the system to understand the electroosmotic effect, allowing pressure to vary, accounting for deviatoric stress and strain, and even by relaxing the condition of constant temperature and electroneutrality. As in the impedance case, elastic, viscous, viscoelastic models of stress can be explored and compared. However, as seen from the impedance case, pressure changes resulting from low-frequency or steady-state current are very small for Nafion systems. This model can nevertheless simulate conditions where external pressure or stress gradients are imposed on the system. Such external forces would affect the solvent and cation flux through the membrane, essential for water management, as well as impacting the effective strain on the membrane, which is important from a durability viewpoint.

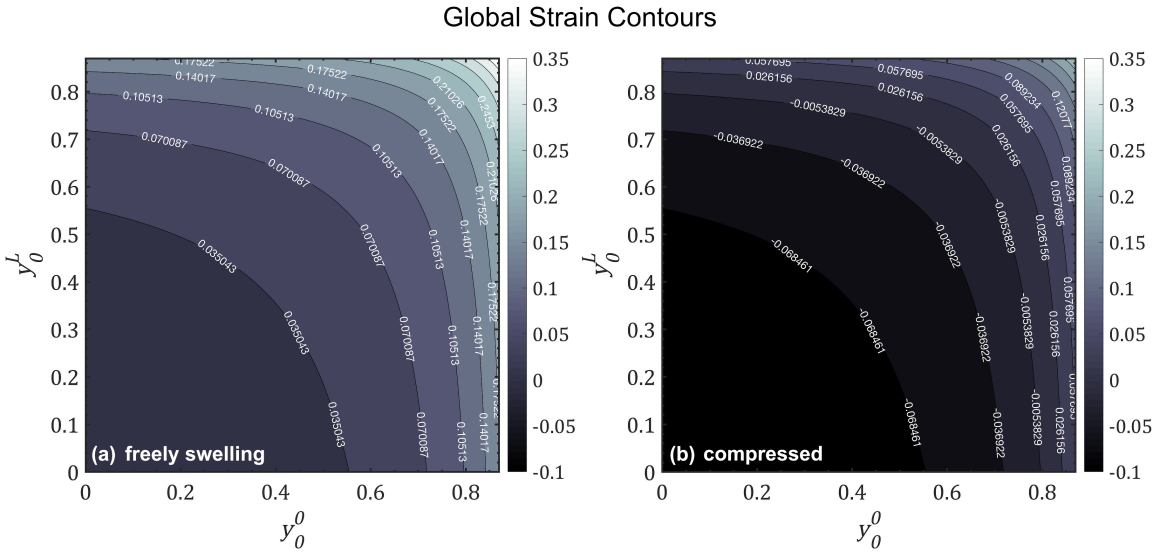

Figure 5.3: Contour plot of global strain ϵ_g as a function of solvent mole fraction at the left (x-axis) and at the right (y-axis) boundaries for (a) freely-swelling membrane (b) uniformly compressed membrane.

Chapter 6

Status and Outlook

The primary aim of the thesis was to develop a macroscopic continuum-level transport model incorporating electrochemical/mechanical coupling, specifically for viscoelastic electrolytes that can sustain deformation. A case was presented for investigating the particular case of Nafion membranes, which are commonly used in polymer-electrolyte membrane fuel cells; solutions to the issues of water management and durability for Nafion are closely dependent on understanding the two-way interaction between the mechanical-stress distribution and ionic and water transport. The focus was to root the multiphysics transport model of this viscoelastic electrolyte in thermodynamics, to ensure consistency across the various physical phenomena that manifest in a given application.

Classical thermodynamics was revisited to account for the strain energy, which adds to the compressive energy to make up the total mechanical energy of a solid material. This theoretical analysis led to rigorous conditions for microscopic equilibrium valid locally within the material, as well as producing irreversible transport laws consistent with solid mechanics/elasticity. A local momentum balance, compressive effects on local volume, along with the modified mass-flux laws including pressure and deformation-stress gradients, and momentum-flux constitutive laws for viscoelas-

tic materials constituted the additions needed to extend Newman's concentrated-electrolyte transport model [23, 27]. The closed system of transport equations based on concentrated-solution theory is already considered complex; our modification introduced additional nuance making the coupling of physical phenomena even more intricate. Before solving the whole model as it stood, we sought to understand the time- and length-scales at which different physical effects might dominate, especially focusing on conditions that would make mechanical effects important.

Electrochemical impedance spectroscopy was identified as a tool that could be used to interpret the novel features of the transport model without obfuscation by the model's higher-order complexity. Assuming the membrane was subjected to a small-amplitude sinusoidal current, the transport equations were linearised. Impedance signatures in this linear-response regime showed resonance events when the frequency of the input signal matched the fundamental acoustic frequency of the membrane, which was typically in the MHz range. By contrast, diffusion effects become visible around 0.1 Hz. The peaks on the Bode gain and phase plots that signified resonance were very narrow, and thus deemed difficult to observe experimentally.

A parameter study focused on the diffusion Mach number, Maxwell Mach number, and Schmidt number, as well as some thermodynamic and material properties, provided insights into how the shape of impedance signatures could be controlled, while mitigating the need to perform computationally expensive simulations. Towards the end of this study, a hypothetical material was designed with a high bulk modulus [$\sim \mathcal{O}\,(10\mathrm{GPa})$], diffusion coefficient [$\sim \mathcal{O}\,(10^{-7}\mathrm{m^2s^{-1}})$], and thickness [$\sim \mathcal{O}\,(10^{-2}\mathrm{m})$] along with lower transference number and activity coefficient, and a solvent-membrane combination with very similar partial molar volumes, to achieve experimentally observable impedance features which could be technologically exploited.

6.1 What Questions does our Model Answer?

The literature review in Chapter 2 helped to identify some gaps in existing models, raised some questions about thermodynamic consistency of multiphysical models, and laid out suggestions for development of an improved transport model. In this section, we take stock of the progress made, by means of tackling those requirements one at a time:

- ***A thermodynamic basis should be preferred over a phenomenological one, to ensure first, that no physical constraints are violated, and second, that all model variables and properties have physical definitions that clearly explicate how they can be measured***

  The transport model developed to address electrochemical/mechanical coupling in viscoelastic electrolytes established a foundation in classical as well as irreversible thermodynamics. All the flux laws, for both material and momentum, as well as local equilibrium state equations, were derived from the same thermodynamic basis instead of bringing together elements from distinct phenomenological or empirical theories. This rigour also ensured that every property in the model had an explicit thermodynamic definition, giving clear physical meanings and suggesting routes for experimental measurement.

- ***A macroscopic model will not account for structural features explicitly, but material- and transport-property variations within the membrane could ideally embody relevant nano/micro/mesoscale dependencies, if any***

  The model was constructed at a continuum level, where each volume element is assumed to contain enough particles to make its properties representative of

statistical averages, thereby allowing the use of classical thermodynamic laws. Further, the assumption of local equilibrium permits the use of classical thermodynamic relations in dynamical laws describing irreversible processes. The incorporation of thermodynamic state equations still permits system properties to reflect behaviour that originates in microstructure. One example is the activity coefficient derived from solvent uptake isotherms, which is extensively measured in experiments [174, 175] and modelled through equilibrium models [60],

$$\chi = 1 + \frac{d\ln\lambda_{y_0}}{d\ln y_0}.$$

- ***Given the uncertainty about morphology, an effort should be made to make as few assumptions about the structure of Nafion as possible; the only such differentiation in our model is based on the VE vs. LE classification***

  All the model properties assumed effective values for hydrated Nafion, assuming that the material comprises a single thermodynamic phase. Any variation in these properties was a function only of macroscopic state variables such as composition, pressure, deviatoric stress, and temperature instead of any structural parameters.

- ***The model should have consistency checks in place so that it converges to correct physical limits; for example, it should include parameters that match known values when the membrane is dry***

  Since conservation laws for mass, momentum, and energy, as well as the flux laws are ensured to be thermodynamically rigorous and the model is closed, it can be extended easily to account for any number of species with varying properties.

- ***The scope of our model will be limited to vapour-equilibrated modes, a restriction that allows Nafion to be treated as a single phase, with possibly non-uniform internal distributions of mass, momentum, and energy***

  It was fair to treat hydrated Nafion like a concentrated liquid binary electrolytic solution because in the vapour-equilibrated mode, it is all one phase. Mole fraction, volume fraction, or some other composition basis can provide the information about what fractions different components occupy in a unit element of the electrolyte. While transitioning to the liquid-equilibrated case, the material should be treated as porous, with two distinct phases described by *e.g.* Eikerling's poroelectroelastic approach [73] or Coussy's model of soil mechanics approach [128]. Newman and Weber discussed the conundrum of applying a force across a single-phase material without moving the entire system [75]. Distributing the pressure driving force among all species in proportion to their mass fractions may resolve that problem.

- ***The model should be based in concentrated solution theory, incorporating a generalised diffusion driving force similar to the one developed by Hirschfelder, Curtis, and Bird [93], but revisited for the case of a viscoelastic polymer capable of storing strain energy at equilibrium***

  The modification of the first law of thermodynamics by including strain energy term led to a mass-diffusion driving force with contributions from stress gradients as shown in equation 3.58,

$$\vec{d}_i = -c_{\mathrm{T}} y_i \left[\vec{\nabla}\mu_i + \overline{S}_i \vec{\nabla} T \; - \frac{\overline{m}_i}{\rho} \left(\vec{\nabla} p + \vec{\bar{\epsilon}}' : \vec{\nabla} \vec{\bar{\tau}} \right) \right].$$

This expression can be simplified for a liquid electrolyte under non-isobaric conditions, in which case $\vec{\vec{\epsilon}}' \to 0$ and the stress term reduces to the pressure gradient. It is worthwhile to recall that $\vec{\nabla}\mu_i$ also has a pressure dependence, $\overline{V}_i \vec{\nabla} p$.

- ***The model should be macroscopic in its outlook, but swelling and stresses should be recognised as locally variable quantities; it is critical to include local relationships that establish how water content and stresses define swelling and deformation***

  Volumetric equation of state 3.30 prescribes local swelling as a function of local composition and pressure,

$$\frac{1}{c_{\mathrm{T}}} = \sum_i \overline{V}_i (p)\, y_i,$$

  and deformational equation of state 3.45 which takes the form of localised Hooke's law,

$$\vec{\vec{\tau}} = -2G_{\mathrm{shear}} \vec{\vec{\epsilon}}',$$

  with $G_{\mathrm{shear}} = G_{\mathrm{shear}} (c_{\mathrm{T}}, y_i)$, was developed to denote conditions of local mechanical equilibrium for compressive and deformation effects, respectively.

- ***A local momentum balance with carefully considered boundary conditions should be included***

  Species momentum balances are added up to form the overall momentum balance 3.114:

$$\rho \frac{D\vec{v}}{Dt} = -\vec{\nabla} \cdot \left(\vec{\vec{\sigma}}_{\mathrm{t}} + \vec{\vec{\Xi}} \right) + \sum_i \vec{b}_i.$$

  The internal forces $\vec{f}_i$ sum to zero for all species, therefore playing no role in this momentum balance. The surprising modification to the standard Cauchy

momentum balance is the diffusion stress,

$$\vec{\vec{\Xi}} = \sum_i \frac{\overline{m}_i}{c_{\mathrm{T}} y_i} \vec{J}_i \otimes \vec{J}_i,$$

which is usually clubbed with deviatoric stress in the literature. Tensor $\vec{\vec{\Xi}}$ recognizes that there is momentum in excess of $\rho\vec{v} \otimes \vec{v}$, which only accounts for momentum convected at the mass-average velocity. Diffusion stress is, however, a second-order effect, and therefore plays no part in the impedance model. Further, note that the total stress $\vec{\vec{\sigma}}_{\mathrm{t}}$ contains both thermodynamic as well as purely dynamic stresses. Including this excess dynamic stress enables us to build in bulk viscosity, plasticity *etc.* to the model.

- ***A distinction should be made between spherical stress or pressure (which causes volume change, preserving shape) and deviatoric stress, such as a viscous or elastic stress (which causes shape change, preserving volume). Would deformation stress, identified as separate from pressure, affect local volume/density?***

  At the classical thermodynamics level, while defining the mechanical energy of a system at equilibrium, the total stress was broken down into a spherical and a deviatoric part, as required. This distinction helped arrive at the conclusion that local swelling does not depend on deviatoric stresses, so shearing the material or deforming it at constant pressure should not cause the local composition or swelling to change. Maxwell relation 3.29,

  $$\left(\frac{\partial V}{\partial \tau_i}\right)_{T,p,\tau_{j\neq i},n_k} = \left(\frac{\partial D_i}{\partial p}\right)_{T,\tau_1,\tau_2,n_j} = 0,$$

  impresses this point succinctly. It also implies that deformation or shape change in the material cannot be brought about by just changing pressure, if the deviatoric stresses are held constant.

- ***A rigorous description of deformation stress is needed, along with a stress constitutive law that describe the viscoelastic phenomena of creep and stress relaxation***

- ***One must ensure that stress is rooted in classical thermodynamics, rather than being obtained from an ad hoc phenomenological description; this requires revisiting the entropy generation law that governs all dissipative processes, and examining how it depends on deformation stress***

  The entropy-generation expression, from the second law of thermodynamics (in transient form), equation 3.132,

$$Tg_S = \sum_{i \neq n} \left(\frac{\vec{J}_i}{c_{\mathrm{T}} y_i} - \frac{\vec{J}_n}{c_{\mathrm{T}} y_n} \right) \cdot \left(\vec{d}_i + \vec{\vec{\epsilon}} \cdot \overline{m}_i \vec{J}_i \right) + \vec{q}' \cdot \left(-\vec{\nabla} \ln T \right) + \vec{\vec{\tau}} : \left(\vec{\vec{\epsilon}} + \vec{\vec{\epsilon}}' \vec{\nabla} \cdot \vec{v} + \frac{D\vec{\vec{\epsilon}}'}{Dt} \right) + \vec{\vec{\sigma}}_{\mathrm{dy}} : \vec{\vec{\epsilon}}$$

  identifies that the driving force $\left(\vec{\vec{\epsilon}} + \vec{\vec{\epsilon}}' \vec{\nabla} \cdot \vec{v} + \frac{D\vec{\vec{\epsilon}}'}{Dt} \right)$ is conjugate to the deviatoric momentum flux. The driving force expression implies that momentum flux may result from a velocity gradient $\vec{\vec{\epsilon}}$ (~ viscous fluids), from the deformation of materials which are transiently compressed or dilated $\vec{\vec{\epsilon}}' \vec{\nabla} \cdot \vec{v}$, and from transient changes in deformation strain, $\frac{D\vec{\vec{\epsilon}}'}{Dt}$. This is one of the first times that a general stress-constitutive law has been derived solely from thermodynamic principles, yielding equation 3.143,

$$\vec{\vec{\tau}} = \frac{2\mu_{\mathrm{shear}} \left(\vec{\vec{\epsilon}} + \frac{1}{3} \vec{\vec{I}} \vec{\nabla} \cdot \vec{v} \right) - t_{\mathrm{shear}} \dfrac{D\vec{\vec{\tau}}}{Dt}}{1 - t_{\mathrm{shear}} \frac{D \ln \rho G_{\mathrm{shear}}}{Dt}}.$$

  This law has elements of the Maxwell model, which typically describes stress relaxation well through the transient deformation stress term. There is a possibility that this model may explain creep better than the standard Maxwell model owing to the $1 - t_{\mathrm{shear}} \frac{D \ln \rho G_{\mathrm{shear}}}{Dt}$ term.

- ***Would gradients in deformation stress be linked to transport in the material, and would such transport be diffusive or convective?***

  As discussed earlier, stress gradients form a part of the mass-diffusion driving force, and hence drive diffusive flux. This can be seen explicitly in the flux-explicit laws for water, equation 4.19, and for hydrogen ions, equation 4.21 used in Chapter 4,

$$\vec{N}_0 = -c_T^2 \overline{V}_e y_0 \frac{D}{\nu} \left\{ \vec{\nabla} \ln y_0 + \frac{1}{RT\chi} \left[\left(\overline{V}_0 - \frac{\overline{m}_0}{\rho} \right) \left(\vec{\nabla} p + \vec{\vec{\epsilon}}' : \vec{\nabla} \vec{\vec{\tau}} \right) \right] \right\} + c_T y_0 \vec{v}^{\square},$$

$$\vec{\nabla}\Phi = -\frac{\vec{i}}{\kappa} - \frac{\nu RT\left(1-t_+^0\right)\chi}{Fz_+\nu_+\left(1-y_0\right)} \vec{\nabla} y_0 + \frac{1}{Fz_+} \left[\frac{\overline{m}_+}{\rho} - \frac{\nu\left(1-t_+^0\right) y_0}{\nu_+\left(1-y_0\right)} \left(\overline{V}_0 - \frac{\overline{m}_0}{\rho} \right) \right] \left(\vec{\nabla} p + \vec{\vec{\epsilon}}' : \vec{\nabla} \vec{\vec{\tau}} \right),$$

  Here we can clearly see that it's the product of deformation strain $\vec{\vec{\epsilon}}'$ and $\vec{\nabla}\vec{\vec{\tau}}$ that affects mass flux, suggesting that this effect will ne negligibly small for liquids or for materials with exceptionally high elastic moduli.

- ***A consistency check is required to ensure that any stress/strain relationship proposed properly describes the extremes of a Newtonian liquid and a Hookean solid***

  Hooke's law 3.45 can be used to simplify the viscoelastic flux law 3.140 to eliminate deformation strain as in equation 3.143,

$$\vec{\vec{\tau}} = \frac{2\mu_{\text{shear}} \left(\vec{\vec{\epsilon}} + \frac{1}{3} \vec{\vec{I}} \vec{\nabla} \cdot \vec{v} \right) - t_{\text{shear}} \frac{D\vec{\vec{\tau}}}{Dt}}{1 - t_{\text{shear}} \frac{D \ln \rho G_{\text{shear}}}{Dt}}.$$

  When the relaxation time $t_{\text{shear}} = \mu_{\text{shear}}/G_{\text{shear}}$ is small, this reduces to Newton's law of viscosity, and the material tends to behave like a liquid. Alternatively, in the limit where t_{shear} is very large, this reduces to an expression like Hooke's law, in which the material behaves like a linear elastic solid. In the case of Nafion, it appears that there exists a wide range of stress relaxation times [32, 116] depending on hydration, temperature, strain, and other factors.

6.2 What Questions Remain Open?

- ***Analytical Solution for VE models***

  The theoretical formulation of the VE model is complete at this stage, and is intended to be thermodynamically consistent. The nonlinear coupling in the model does not permit an analytical solution. Validation of the numerical implementations in the previous section with the help of the analytical solution, even though at a simpler stage, provides the confidence to proceed with the numerical approaches in the future.

- ***Robust Implementation of Diverse Boundary Conditions***

  This system should be numerically investigated over the whole range of physically possible boundary conditions—be it fixing the thickness of the membrane or the external pressure acting on it, in addition to the water content/flux and other electrochemical conditions at each of the boundaries. The results thus obtained should be validated against appropriate experimental data from the literature. The stress profile obtained from such a model could be used to analyse membrane fatigue and durability, as measured by experiments.

- ***Modelling LE Mode***

  The Nafion model was specifically developed solely for VE mode, containing only collapsed channels. A step-change introducing porosity would incorporate the structural reorganization that accompanies the switch from ambient water vapour to ambient liquid water. Coussy's model [128] for porous solids could act as the starting point for a consistent LE model. The first step can assume uniform water concentration in the membrane, which could further be associated with a fixed value of porosity throughout the thickness, instead of using a local porosity value corresponding to the water concentration at that location.

This case would require an additional momentum balance which incorporates Darcy flow in the water-filled pores, in addition to pressure and deformation stress in the membrane solution phase. It would make sense not to differentiate between bound and free water at the outset of such a study. Even with that simplification, partitioning of the total stress at any point between the polymer (deformation), and water (permeation) in a thermodynamically consistent manner is a foreseeable challenge. Borrowing certain assumptions from Coussy's model [128] for the sake of simplicity, however, might be helpful in determining how porosity changes with the forces arising from swelling of the pores *vs* external forces. Once a reliable stress appropriation scheme has been decided on, water concentration can be allowed to vary, which in turn would cause the porosity to vary locally.

One of the end goals of the project would be to arrive at a comprehensive model, which could switch between VE and LE modes, and should also be able to handle mixed VE/LE conditions. The mixed mode would need a parameter, to decide the fraction of collapsed channels expanded into water-filled pores. Weber and Newman [55] proposed a similar parameter, fraction of expanded channels, in their model. It could be useful to start with this approach to judge how it can be integrated into our models.

- ***Full Transient Model (without Linearisation)***

  Once a steady state model with all the desired features is functional, it can be extended to a transient model similar to the extended Nernst–Planck model of Doi *et al.* [41, 97]. This would involve careful treatment of the moving membrane boundary because of dynamic swelling. A dimensional analysis of the transient model, similar to the one performed here for the impedance model, might be a better investment from a cost/benefit perspective, because the mov-

ing boundary condition can make solving the transient comprehensive model immensely complex.

- ***Incorporating Electrode Kinetics***

  The case for liquid electrolytes with asymmetric reactions at the two electrodes is interesting because it would lead to a first-order change in electrolyte volume. In our current analysis it was also assumed that reactions at the electrodes are infinitely fast. If Butler–Volmer kinetics is used to model the reaction overpotential, one might expect to see an additional parallel RC impedance, which should lie between the characteristic Warburg and acoustic frequencies. Adding this functionality would make experimental validation more straightforward.

- ***Forced Convection Impedance Signatures***

  The MacInnes equation (modified Ohm's law) establishes a relationship between stress gradients and potential drop across the electrolyte. The stress gradients studied in Chapter 4 originated as a result of a sinusoidal applied current: an electrical stimulus led to a mechanical force, and the impact of that force on impedance was studied. This is similar to the composition polarisation that results from passing current through an electrolyte. One might also observe a voltage difference, and hence an impedance signature, if stress gradients are induced mechanically without passing any current. Exploring this case further could confirm the reverse piezoelectric nature of the membrane, opening a whole new avenue for sensor and actuator applications.

- ***Relaxing Electroneutrality***

  For some solid electrolytes, such as ceramic LLZO, space-charge layers near the electrodes dominate both the electrochemical and mechanical physics in the cell. The Lorentz forces developed in these non-electroneutral layers can help explain the origin of critical currents which lead to the mechanical failure of these electrolytes. The present model structure provides the basis for a non-electroneutral model as studied by Li and Monroe [176].

- ***Describing Anisotropic Elastic & Non-Newtonian Materials***

  The thermodynamic model was developed specifically for elastic isotropic materials, but it can be made more general to include anisotropic and various kinds of non-Newtonian materials. This would entail reformulating the deformation equation of state and the stress constitutive law. Since Onsager's basic formulation of constitutive laws assumes the irreversible flux and driving force to be linearly related, some fundamental extensions of the theory would be needed to handle power-law fluids.

- ***Accounting for Thermo-Electrochemical-Mechanical Coupling***

  There is possibility for an immense gain in knowledge from a thermal analysis, which would require us to relax the assumed constraint of constant temperature. Treating thermal energy in the OSM formalism would introduce the familiar Dufour and Soret fluxes, but due to the strain energy modification in our model, there would also be heat production from transient changes in elastic strain and stress in the solid. Thermodynamic, material, and mechanical properties of the system tend to be strong functions of temperature, leading to multiphysical coupling. Further, solid-state batteries and solid-oxide fuel cells

are generally manufactured at very high temperatures to ensure good bonding between solid layers. Upon cooling, large thermo-mechanical stresses can thus develop, if the thermal expansion coefficients of these layers are very different. It could be interesting to account for such behaviour in the future.

- ***Describing Viscoplastic Behaviour***

  Certain materials, which can be linear or non-linear elastic or viscoelastic below a certain yield stress, are capable of withstanding purely dynamic irrecoverable deformation upon yielding. This deformation, usually termed plastic, does not contribute to the thermodynamic strain energy by virtue of its irreversibility but can be a source of energy dissipation or entropy generation [177, 178]. Many practical materials such as Nafion ionomer membranes exhibit a special kind of plastic behavior—viscoplasticity—where the rate of plastic deformation depends on the magnitude of the applied stress [123]. Dissipation from the deviatoric dynamic part of total Cauchy stress can be used to write the appropriate stress laws in the viscoplastic regime when the stress exceeds the yield limit.

Appendix A

Mathematical Properties of Tensors

The 3-tuple $\{\vec{e}_i\}_3$ represents a right-handed, orthornormal set of basis vectors. Between a vector $\vec{v}$ and a tensor $\vec{\vec{\sigma}}$ there are two ways of forming a new vector with a scalar product,

$$\vec{\vec{\sigma}} \cdot \vec{v} = \sum_{i,j} \sigma_{ij} v_j \vec{e}_i \quad \text{and} \quad \vec{v} \cdot \vec{\vec{\sigma}} = \sum_{i,j} v_j \sigma_{ji} \vec{e}_i. \tag{A.1}$$

The *transpose* of $\vec{\vec{\sigma}}$ is the unique tensor $\vec{\vec{\sigma}}^{\,\mathrm{T}}$ that satisfies

$$\vec{\vec{\sigma}} \cdot \vec{v} = \vec{v} \cdot \vec{\vec{\sigma}}^{\,\mathrm{T}} \tag{A.2}$$

for every $\vec{v}$. Between tensors $\vec{\vec{\sigma}}$ and $\vec{\vec{\tau}}$,

$$\vec{\vec{\sigma}} \cdot \vec{\vec{\tau}} = \sum_{i,j,k} \sigma_{ik} \tau_{kj} \vec{e}_i \otimes \vec{e}_j \tag{A.3}$$

forms a tensor; this product does not generally commute.

The *trace* of tensor $\vec{\vec{\sigma}}$ is defined as

$$\mathrm{tr}(\vec{\vec{\sigma}}) = \sum_k \sigma_{kk}. \tag{A.4}$$

Generally $\mathrm{tr}(\vec{\vec{\sigma}}) = \mathrm{tr}(\vec{\vec{\sigma}}^{\,\mathrm{T}})$ and $\mathrm{tr}(\vec{\vec{\sigma}} \cdot \vec{\vec{\tau}}) = \mathrm{tr}(\vec{\vec{\tau}} \cdot \vec{\vec{\sigma}})$. The *adjugate trace* of $\vec{\vec{\sigma}}$ is defined in terms of the trace and scalar product as

$$\mathrm{tr}\big[\mathrm{adj}(\vec{\vec{\sigma}})\big] = \tfrac{1}{2}\left[\mathrm{tr}^2(\vec{\vec{\sigma}}) - \mathrm{tr}(\vec{\vec{\sigma}} \cdot \vec{\vec{\sigma}})\right], \tag{A.5}$$

and the *determinant* of $\vec{\vec{\sigma}}$ is

$$\det(\vec{\vec{\sigma}}) = \tfrac{1}{6}\left[\mathrm{tr}^3(\vec{\vec{\sigma}}) - 3\mathrm{tr}(\vec{\vec{\sigma}})\mathrm{tr}(\vec{\vec{\sigma}}\cdot\vec{\vec{\sigma}}) + 2\mathrm{tr}(\vec{\vec{\sigma}}\cdot\vec{\vec{\sigma}}\cdot\vec{\vec{\sigma}})\right]. \tag{A.6}$$

The determinant distributes over the scalar product of tensors as $\det(\vec{\vec{\sigma}}\cdot\vec{\vec{\tau}}) = \det(\vec{\vec{\sigma}})\det(\vec{\vec{\tau}})$.

The *identity tensor* $\vec{\vec{I}}$ satisfies $\vec{v}\cdot\vec{\vec{I}} = \vec{\vec{I}}\cdot\vec{v} = \vec{v}$ for all $\vec{v}$ and $\vec{\vec{\sigma}}\cdot\vec{\vec{I}} = \vec{\vec{I}}\cdot\vec{\vec{\sigma}} = \vec{\vec{\sigma}}$ for all $\vec{\vec{\sigma}}$. In component form,

$$\vec{\vec{I}} = \sum_{i,j}\delta_{ij}\vec{e}_i\otimes\vec{e}_j, \tag{A.7}$$

where δ_{ij} is the Kronecker delta, equal to 1 if $i = j$ and 0 otherwise. The *inverse* of $\vec{\vec{\sigma}}$ is the unique tensor $\vec{\vec{\sigma}}^{-1}$ for which

$$\vec{\vec{\sigma}}\cdot\vec{\vec{\sigma}}^{-1} = \vec{\vec{\sigma}}^{-1}\cdot\vec{\vec{\sigma}} = \vec{\vec{I}}. \tag{A.8}$$

Note that $\mathrm{tr}[\mathrm{adj}(\vec{\vec{I}})] = 3$ and $\det(\vec{\vec{I}}) = 1$. Since $\det(\vec{\vec{\sigma}}\cdot\vec{\vec{\sigma}}^{-1}) = \det(\vec{\vec{\sigma}})\det(\vec{\vec{\sigma}}^{-1}) = 1$, the determinant of a tensor must be nonzero for its inverse to exist.

The *vertical scalar product* between tensors $\vec{\vec{\sigma}}$ and $\vec{\vec{\tau}}$ is given by

$$\vec{\vec{\sigma}} : \vec{\vec{\tau}} = \sum_{i,j}\sigma_{ij}\tau_{ij} = \mathrm{tr}(\vec{\vec{\sigma}}\cdot\vec{\vec{\tau}}^{\mathrm{T}}). \tag{A.9}$$

With this definition one can also write the trace of $\vec{\vec{\sigma}}$ as a vertical scalar product with the identity, $\mathrm{tr}(\vec{\vec{\sigma}}) = \vec{\vec{\sigma}} : \vec{\vec{I}}$, whence $\mathrm{tr}(\vec{\vec{I}}) = \vec{\vec{I}} : \vec{\vec{I}} = 3$. Properties of the trace imply that the vertical scalar product commutes, $\vec{\vec{\sigma}} : \vec{\vec{\tau}} = \vec{\vec{\tau}} : \vec{\vec{\sigma}}$.

One can understand how the components of a tensor transform under a rigid rotation of coordinate axes by observing that the act of rotating a vector $\vec{v}$ without changing its magnitude can be expressed by projecting a *rotation tensor* $\vec{\vec{Q}}$ onto $\vec{v}$, where $\vec{\vec{Q}}^{\mathrm{T}} = \vec{\vec{Q}}^{-1}$ and $\det(\vec{\vec{Q}}) = 1$. The most primitive rotation is expressed by the identity tensor $\vec{\vec{I}}$, which merely maps a vector or tensor into itself.

If $\vec{\vec{T}}$ is any tensor, then rotation of the basis vectors under $\vec{\vec{T}}$ by $\vec{\vec{Q}}$ sends $\vec{\vec{T}}$ into a new tensor $\vec{\vec{T}}'$ according to

$$\vec{\vec{T}}' = \vec{\vec{Q}}\cdot\vec{\vec{T}}\cdot\vec{\vec{Q}}^{\mathrm{T}}, \tag{A.10}$$

whose components stand in the rotated coordinate frame. The trace, adjugate trace, and determinant defined by equations A.4 through A.6 remain unchanged under transformations like the one in equation A.10, and are therefore known as a tensor's *three principal invariants*, which express its essential physical content.

The *spectral theorem* from linear algebra codifies a few general consequences of tensor symmetry: given any tensor $\vec{\vec{T}} = \vec{\vec{T}}^{\mathrm{T}}$, with components over a right-handed, ordered orthonormal basis $\{\vec{e}_1, \vec{e}_2, \vec{e}_3\}$, there is some rotation tensor $\vec{\vec{Q}}_T$ with $\det(\vec{\vec{Q}}_T) = 1$ such that

$$\vec{\vec{T}} = \vec{\vec{Q}}_T^{\mathrm{T}} \cdot \vec{\vec{d}}_T \cdot \vec{\vec{Q}}_T, \quad \text{where} \quad \vec{\vec{d}}_T = \sum_k T_k \vec{e}_k^T \otimes \vec{e}_k^T. \tag{A.11}$$

The ordered list $\{\vec{e}_1^T, \vec{e}_2^T, \vec{e}_3^T\}$, where $\vec{e}_i^T = \vec{\vec{Q}}_T \cdot \vec{e}_i$, represents a rigidly rotated, right-handed, ordered orthonormal set of principal axes for tensor $\vec{\vec{T}}$, the nontrivial entries $\{T_1, T_2, T_3\}$ of the diagonal tensor $\vec{\vec{d}}_T$ are the associated principal values. The similarity transformation stated in equation A.11, along with the corresponding pair of tensors $\vec{\vec{Q}}_T$ and $\vec{\vec{d}}_T$, is called the *principal representation* of $\vec{\vec{T}}$.

The principal stresses of a tensor $\vec{\vec{T}}$ generally relate to its three principal invariants through

$$\begin{aligned} \mathrm{tr}(\vec{\vec{T}}) &= T_1 + T_2 + T_3, \\ \mathrm{tr}[\mathrm{adj}(\vec{\vec{T}})] &= T_1T_2 + T_1T_3 + T_2T_3, \\ \det(\vec{\vec{T}}) &= T_1T_2T_3. \end{aligned} \tag{A.12}$$

Appendix B

Inversion of Flux Laws

Onsager–Stefan–Maxwell formalism casts mass transport laws in a force-explicit form involving microscopic binary interaction parameters. These are then converted to the more useful flux-explicit form characterised by macroscopic transport properties. For the hydrated Nafion system, we chose to write two force-explicit flux laws for solvent and cations, understanding that the third flux law of anions would be linearly dependent on the first two according to the Gibbs–Duhem equation (equation 3.57).

B.1 Solvent Flux Law to Extended Nernst–Planck Law

Starting with the force-explicit form of the equation (equation 4.19)

$$- c_{\mathrm{T}} y_0 \left[RT\chi \vec{\nabla} \ln y_0 + \left(\overline{V}_0 - \frac{\overline{m}_0}{\rho} \right) \left(\vec{\nabla} p + \vec{\vec{\epsilon}}' : \vec{\nabla} \vec{\vec{\tau}} \right) \right] = \frac{RT}{\mathscr{D}_{0+}} \left(y_+ \vec{N}_0 - y_0 \vec{N}_+ \right) + \frac{RT}{\mathscr{D}_{0-}} \left(y_- \vec{N}_0 - y_0 \vec{N}_- \right), \quad \text{(B.1)}$$

we divide throughout by RT, combine solvent flux terms, and substitute for anion flux using Faraday's law (eq 3.91) to get $\left(\overline{V}_0 - \dfrac{\overline{m}_0}{\rho}\right)\left(\vec{\nabla}p + \vec{\bar{\epsilon}}' : \vec{\nabla}\vec{\bar{\tau}}\right)$

$$- c_{\mathrm{T}} y_0 \left[\chi \vec{\nabla} \ln y_0 + \frac{1}{RT}\left(\overline{V}_0 - \frac{\overline{m}_0}{\rho}\right)\left(\vec{\nabla}p + \vec{\bar{\epsilon}}' : \vec{\nabla}\vec{\bar{\tau}}\right)\right] = \left(\frac{y_+}{\mathscr{D}_{0+}} + \frac{y_-}{\mathscr{D}_{0-}}\right)\vec{N}_0 - \left(\frac{1}{\mathscr{D}_{0+}} - \frac{z_+}{z_-}\frac{1}{\mathscr{D}_{0-}}\right) y_0 \vec{N}_+ - \frac{y_0}{\mathscr{D}_{0-}}\frac{\vec{i}}{F z_-}. \quad \text{(B.2)}$$

Before proceeding further, apply the principle of electroneutrality to replace the anion mole fraction from the equation:

$$- c_{\mathrm{T}} y_0 \left[\chi \vec{\nabla} \ln y_0 + \frac{1}{RT}\left(\overline{V}_0 - \frac{\overline{m}_0}{\rho}\right)\left(\vec{\nabla}p + \vec{\bar{\epsilon}}' : \vec{\nabla}\vec{\bar{\tau}}\right)\right] = \left(\frac{1}{\mathscr{D}_{0+}} - \frac{z_+}{z_-}\frac{1}{\mathscr{D}_{0-}}\right) y_+ \vec{N}_0 - \left(\frac{1}{\mathscr{D}_{0+}} - \frac{z_+}{z_-}\frac{1}{\mathscr{D}_{0-}}\right) y_0 \vec{N}_+ - \frac{y_0}{\mathscr{D}_{0-}}\frac{\vec{i}}{F z_-}. \quad \text{(B.3)}$$

Identify the thermodynamic diffusion coefficient as $\frac{1}{\mathscr{D}} = \frac{z_-}{z_+ - z_-}\left(\frac{z_+}{z_-}\frac{1}{\mathscr{D}_{0-}} - \frac{1}{\mathscr{D}_{0+}}\right)$ to make the expression more compact:

$$- c_{\mathrm{T}} y_0 \left[\chi \vec{\nabla} \ln y_0 + \frac{1}{RT}\left(\overline{V}_0 - \frac{\overline{m}_0}{\rho}\right)\left(\vec{\nabla}p + \vec{\bar{\epsilon}}' : \vec{\nabla}\vec{\bar{\tau}}\right)\right] = -\frac{z_+ - z_-}{z_- \mathscr{D}} y_+ \vec{N}_0 + \frac{z_+ - z_-}{z_- \mathscr{D}} y_0 \vec{N}_+ - \frac{y_0}{\mathscr{D}_{0-}}\frac{\vec{i}}{F z_-}. \quad \text{(B.4)}$$

In the next step, apply Guggenheim principle to switch from charges z_k to stoichiometric coefficients ν_k and more significantly, replace the cation flux by using the definition of volume-average velocity $\left(\vec{N}_+ = \frac{\nu_+}{\overline{V}_{\mathrm{e}}}\vec{v}^{\square} - \frac{\nu_+ \overline{V}_0}{\overline{V}_{\mathrm{e}}}\vec{N}_0 - \frac{\nu_+ \overline{V}_-}{\overline{V}_{\mathrm{e}}}\frac{\vec{i}}{F z_-}\right)$, defining the electrolyte partial molar volume as $\overline{V}_e = \nu_+ \overline{V}_+ + \nu_- \overline{V}_-$, and multiplying throughout by $\frac{\mathscr{D}}{\nu}$

$$- \frac{\mathscr{D}}{\nu} c_{\mathrm{T}} y_0 \left[\chi \vec{\nabla} \ln y_0 + \frac{1}{RT}\left(\overline{V}_0 - \frac{\overline{m}_0}{\rho}\right)\left(\vec{\nabla}p + \vec{\bar{\epsilon}}' : \vec{\nabla}\vec{\bar{\tau}}\right)\right] = \left(\frac{y_+}{\nu_+} + y_0 \frac{\overline{V}_0}{\overline{V}_{\mathrm{e}}}\right)\vec{N}_0 + \left(\frac{\overline{V}_-}{\overline{V}_{\mathrm{e}}} - \frac{\mathscr{D}}{\nu \mathscr{D}_{0-}}\right) y_0 \frac{\vec{i}}{F z_-} - \frac{y_0}{\overline{V}_{\mathrm{e}}}\vec{v}^{\square}. \quad \text{(B.5)}$$

Equation of state for this system [recast as $c_{\mathrm{T}} \overline{V}_{\mathrm{e}}\left(\frac{y_+}{\nu_+} + y_0 \frac{\overline{V}_0}{\overline{V}_{\mathrm{e}}}\right) = 1$] can help simplify the cofactor of solvent flux, and the equation can then be rearranged to a flux-explicit

form:

$$\vec{N}_0 = -\frac{\mathscr{D}\chi}{\nu} c_{\mathrm{T}}^2 \overline{V}_{\mathrm{e}} y_0 \left[\vec{\nabla} \ln y_0 + \frac{1}{RT\chi} \left(\overline{V}_0 - \frac{\overline{m}_0}{\rho} \right) \left(\vec{\nabla} p + \vec{\vec{\epsilon}}' : \vec{\nabla} \vec{\vec{\tau}} \right) \right] + c_{\mathrm{T}} y_0 \left[\vec{v}^{\square} - \left(\overline{V}_- - \frac{\mathscr{D} \overline{V}_{\mathrm{e}}}{\nu \mathscr{D}_{0-}} \right) \frac{\vec{i}}{F z_-} \right] \quad \text{(B.6)}$$

From the definition of transference number and thermodynamic coefficient, $\frac{\mathscr{D}}{\nu \mathscr{D}_{0-}} = \frac{t_+^0}{\nu_-}$, the last term can thus be processed further and Fickian diffusion coefficient $D = \mathscr{D}\chi$ should be introduced,

$$\vec{N}_0 = -\frac{D}{\nu} c_{\mathrm{T}}^2 \overline{V}_{\mathrm{e}} y_0 \left[\vec{\nabla} \ln y_0 + \frac{1}{RT\chi} \left(\overline{V}_0 - \frac{\overline{m}_0}{\rho} \right) \left(\vec{\nabla} p + \vec{\vec{\epsilon}}' : \vec{\nabla} \vec{\vec{\tau}} \right) \right] + c_{\mathrm{T}} y_0 \left(\vec{v}^{\square} - \frac{\vec{i} Q}{F} \right) \quad \text{(B.7)}$$

where the quantity $Q = \left(\frac{t_+^0}{z_+} \overline{V}_+ + \frac{t_-^0}{z_-} \overline{V}_- \right)$ is the same as that appeared in Newman and Chapman's derivation in the restricted diffusion paper [133] where they arbitrarily set it to 0, since it can't be measured independently. Also note that $t_-^0 = 1 - t_+^0$. The assumption of $Q = 0$ when combined with the definition of the electrolyte partial molar volume yields useful relationships for the ionic partial molar volumes as follows:

$$\overline{V}_+ = \frac{1 - t_+^0}{\nu_+} \overline{V}_{\mathrm{e}} \qquad \text{and} \qquad \overline{V}_- = \frac{t_+^0}{\nu_-} \overline{V}_{\mathrm{e}}. \quad \text{(B.8)}$$

Thus, the final inverted form of the solvent balance can be written in terms of explicit driving forces for diffusion,

$$\boxed{\vec{N}_0 = -\frac{D}{\nu} c_{\mathrm{T}}^2 \overline{V}_{\mathrm{e}} y_0 \left[\vec{\nabla} \ln y_0 + \frac{1}{RT\chi} \left(\overline{V}_0 - \frac{\overline{m}_0}{\rho} \right) \left(\vec{\nabla} p + \vec{\vec{\epsilon}}' : \vec{\nabla} \vec{\vec{\tau}} \right) \right] + c_{\mathrm{T}} y_0 \vec{v}^{\square}}. \quad \text{(B.9)}$$

B.2 Cation Flux Law to Modified Ohm's Law

In a similar way as the solvent flux law, the force-explicit cation flux law can also be inverted to obtain the MacInnes equation,

$$-c_{\mathrm{T}} y_+ \left[\vec{\nabla}\mu_+ - \frac{\overline{m}_+}{\rho}\left(\vec{\nabla}p + \vec{\vec{\epsilon}}' : \vec{\nabla}\vec{\vec{\tau}}\right)\right] = \frac{RT}{\mathscr{D}_{+0}}\left(y_0\vec{N}_+ - y_+\vec{N}_0\right) + \frac{RT}{\mathscr{D}_{+-}}\left(y_-\vec{N}_+ - y_+\vec{N}_-\right). \quad \text{(B.10)}$$

Dividing throughout by RT, collecting the flux terms together, and substituting for the anion flux from Faraday's law:

$$\begin{aligned} -c_{\mathrm{T}} y_+ &\left[\frac{1}{RT}\vec{\nabla}\mu_+ - \frac{\overline{m}_+}{\rho RT}\left(\vec{\nabla}p + \vec{\vec{\epsilon}}' : \vec{\nabla}\vec{\vec{\tau}}\right)\right] \\ &= \left[\frac{y_0}{\mathscr{D}_{+0}} + \frac{1}{z_-\mathscr{D}_{+-}}\left(\underbrace{z_-y_- + z_+y_+}_{=0}\right)\right]\vec{N}_+ - \frac{y_+}{\mathscr{D}_{+0}}\vec{N}_0 - \frac{y_+}{\mathscr{D}_{+-}}\frac{\vec{i}}{Fz_-} \end{aligned} \quad \text{(B.11)}$$

Using electroneutrality,

$$-c_{\mathrm{T}} y_+ \left[\frac{1}{RT}\vec{\nabla}\mu_+ - \frac{\overline{m}_+}{\rho RT}\left(\vec{\nabla}p + \vec{\vec{\epsilon}}' : \vec{\nabla}\vec{\vec{\tau}}\right)\right] = \frac{y_0}{\mathscr{D}_{+0}}\vec{N}_+ - \frac{y_+}{\mathscr{D}_{+0}}\vec{N}_0 - \frac{y_+}{\mathscr{D}_{+-}}\frac{\vec{i}}{Fz_-}. \quad \text{(B.12)}$$

Now replacing the cation flux using the volume-average velocity

$$\begin{aligned} -c_{\mathrm{T}} y_+ &\left[\frac{1}{RT}\vec{\nabla}\mu_+ - \frac{\overline{m}_+}{\rho RT}\left(\vec{\nabla}p + \vec{\vec{\epsilon}}' : \vec{\nabla}\vec{\vec{\tau}}\right)\right] = \frac{\nu_+ y_0}{\mathscr{D}_{+0}\overline{V}_{\mathrm{e}}}\vec{v}^{\square} - \frac{\nu_+}{\mathscr{D}_{+0}}\left(y_0\frac{\overline{V}_0}{\overline{V}_{\mathrm{e}}} + \frac{y_+}{\nu_+}\right)\vec{N}_0 \\ &- \left(\frac{y_0}{\mathscr{D}_{+0}}\frac{\nu_+\overline{V}_-}{\overline{V}_{\mathrm{e}}} + \frac{y_+}{\mathscr{D}_{+-}}\right)\frac{\vec{i}}{Fz_-}. \end{aligned} \quad \text{(B.13)}$$

Plugging in the equation of state,

$$\begin{aligned} -c_{\mathrm{T}} y_+ &\left[\frac{1}{RT}\vec{\nabla}\mu_+ - \frac{\overline{m}_+}{\rho RT}\left(\vec{\nabla}p + \vec{\vec{\epsilon}}' : \vec{\nabla}\vec{\vec{\tau}}\right)\right] \\ &= \frac{\nu_+ y_0}{\mathscr{D}_{+0}\overline{V}_{\mathrm{e}}}\vec{v}^{\square} - \frac{1}{c_{\mathrm{T}}\overline{V}_{\mathrm{e}}}\frac{\nu_+}{\mathscr{D}_{+0}}\vec{N}_0 - \left(\frac{y_0}{\mathscr{D}_{+0}}\frac{\nu_+\overline{V}_-}{\overline{V}_{\mathrm{e}}} + \frac{y_+}{\mathscr{D}_{+-}}\right)\frac{\vec{i}}{Fz_-}. \end{aligned} \quad \text{(B.14)}$$

Finally, use the inverted form of the solvent flux law obtained in eq B.9 and $1 - t_+^0 = \frac{\nu_+\mathscr{D}}{\nu\mathscr{D}_{0+}}$,

$$\begin{aligned} \vec{\nabla}\mu_+ = \frac{RT}{c_{\mathrm{T}} y_+}&\left(\frac{y_0}{\mathscr{D}_{+0}}\frac{\nu_+\overline{V}_-}{\overline{V}_{\mathrm{e}}} + \frac{y_+}{\mathscr{D}_{+-}}\right)\frac{\vec{i}}{Fz_-} - \frac{RT\left(1-t_+^0\right)\chi}{y_+}\vec{\nabla}y_0 \\ &- \left[\frac{\left(1-t_+^0\right)y_0}{y_+}\left(\overline{V}_0 - \frac{\overline{m}_0}{\rho}\right) - \frac{\overline{m}_+}{\rho}\right]\left(\vec{\nabla}p + \vec{\vec{\epsilon}}' : \vec{\nabla}\vec{\vec{\tau}}\right) \end{aligned} \quad \text{(B.15)}$$

Next, writing the cation mole fraction as a function of the solvent mole fraction, identifying conductivity as

$$\frac{1}{\kappa} = -\frac{RT}{F^2 z_+ z_- c_{\mathrm{T}}}\left(\frac{1}{\mathscr{D}_{+-}} + \frac{\nu_+ y_0 \overline{V}_-}{y_+ \mathscr{D}_{+0} \overline{V}_{\mathrm{e}}}\right),$$

and

$$\vec{\nabla}\Phi = \frac{\vec{\nabla}\mu_+}{F z_+}$$

to get a modified Ohm's law,

$$\vec{\nabla}\Phi = -\frac{\vec{i}}{\kappa} - \frac{\nu RT\left(1-t_+^0\right)\chi}{F z_+ \nu_+ \left(1-y_0\right)}\vec{\nabla} y_0 + \frac{1}{F z_+}\left[\frac{\overline{m}_+}{\rho} - \frac{\nu\left(1-t_+^0\right) y_0}{\nu_+\left(1-y_0\right)}\left(\overline{V}_0 - \frac{\overline{m}_0}{\rho}\right)\right]\left(\vec{\nabla} p + \vec{\vec{\epsilon}}' : \vec{\nabla}\vec{\vec{\tau}}\right). \tag{B.16}$$

B.3 Derivation of Transport Coefficient and Electroosmotic Coefficient Expressions

The expression for the transport coefficient in terms of the thermodynamic diffusion coefficient can be obtained by comparing the solvent flux law obtained in terms of the two properties. The transport coefficient, α is defined through the following equation, based on Fuller's thesis [79]

$$\vec{N}_0 = -\alpha\vec{\nabla}\mu_0, \tag{B.17}$$

which represents the flux of solvent in the absence of current through an isothermal, isobaric system. Applying the same constraints (isobaric conditions: $\vec{\nabla} p = 0, \vec{\vec{\tau}} = 0$, no current flow: $\vec{i} = \vec{N}_+ = \vec{N}_- = 0, \vec{v}^{\square} = \overline{V}_0 \vec{N}_0$) to the solvent flux law, equation 4.19, and using equation of state 3.30, we get,

$$\vec{N}_0 = -\frac{c_{\mathrm{T}}}{RT}\frac{y_0}{1-y_0}\mathscr{D}\underbrace{RT\chi\vec{\nabla}\ln y_0}_{\vec{\nabla}\mu_0}. \tag{B.18}$$

Comparing the two equivalent forms of the solvent flux law, equation B.17 and equation B.18, we get the following expression relating the transport coefficient with the

thermodynamic diffusion coefficient,

$$\alpha = \frac{c_{\mathrm{T}}}{RT}\frac{y_0}{1-y_0}\mathscr{D}. \tag{B.19}$$

Going down a similar path, the expression for the electroosmotic coefficient in terms of the cation transference number can be obtained by comparing the cation flux law, alternatively called the MacInnes equation, obtained in terms of the two properties. The electroosmotic coefficient, ξ can be assumed to be defined through the following equation, also based on Fuller's thesis [79]

$$\vec{i} = -\frac{\kappa}{F}\vec{\nabla}\mu_+ - \frac{\kappa}{F}\xi\vec{\nabla}\mu_0. \tag{B.20}$$

The isobaric form of the MacInnes equation (equation 4.21) obtained in Chapter 4 can be cast in a similar form for more convenient comparison (plug $z_+ = 1, \nu_+ = 1, \nu = 2$),

$$\vec{i} = -\frac{\kappa}{Fz_+}\vec{\nabla}\mu_+ - 2\frac{\kappa}{Fz_+}\frac{y_0}{1-y_0}\left(1-t_+^0\right)\underbrace{RT\chi\vec{\nabla}\ln y_0}_{\vec{\nabla}\mu_0}. \tag{B.21}$$

A straightforward comparison between equations B.20 and B.21 gives us the expression we are seeking,

$$\xi = 2\frac{y_0}{1-y_0}\left(1-t_+^0\right). \tag{B.22}$$

Appendix C

Mathematical Behaviour of Composition and Pressure

C.1 Derivation of Diffusion Equation

The scaled linear solvent balance (equation 4.48) is combined with the following space-differentiated scaled linear solvent flux law (equation 4.61),

$$\frac{d\eta_0^{(1)}}{dX} = -\frac{\theta_T^{\infty^2}}{\nu}\left[\frac{d^2y_0^{(1)}}{dX^2} + \beta^\infty \frac{\mathrm{Ma}_D^\infty}{\mathrm{Ma}_M^{\infty^2}} y_0^\infty \left(1 - y_0^\infty\right) \frac{d^2P^{(1)}}{dX^2}\right] + \theta_T^\infty y_0^\infty \frac{d\mathrm{Pe}^{\square,(1)}}{dX} \quad \text{(C.1)}$$

to give

$$j\Omega\frac{\nu}{\theta_T^\infty}y_0^{(1)} = \frac{d^2y_0^{(1)}}{dX^2} + \beta^\infty \frac{\mathrm{Ma}_D^\infty}{\mathrm{Ma}_M^{\infty^2}} y_0^\infty \left(1 - y_0^\infty\right) \frac{d^2P^{(1)}}{dX^2} - \frac{\nu y_0^\infty}{\theta_T^\infty}\frac{d\mathrm{Pe}^{\square,(1)}}{dX} - j\Omega\frac{\nu y_0^\infty}{\theta_T^{\infty^2}}\theta_T^{(1)}. \quad \text{(C.2)}$$

This form of the equation can be simplified significantly by using the scaled linear volume balance (equation 4.50) to replace the gradient of volume-average velocity (Peclet-box number), $d\mathrm{Pe}^{\square,(1)}/dX$,

$$j\Omega\frac{\nu}{\theta_T^\infty}y_0^{(1)} = \frac{d^2y_0^{(1)}}{dX^2} + \beta^\infty \frac{\mathrm{Ma}_D^\infty}{\mathrm{Ma}_M^{\infty^2}} y_0^\infty \left(1 - y_0^\infty\right) \frac{d^2P^{(1)}}{dX^2} + j\Omega\mathrm{Ma}_D^\infty\frac{\nu y_0^\infty}{\theta_T^\infty}P^{(1)} - j\Omega\frac{\nu y_0^\infty}{\theta_T^{\infty^2}}\theta_T^{(1)}. \quad \text{(C.3)}$$

followed by the scaled linear equation of state (equation 4.52) and the zero-order total concentration $\theta_T^\infty = \frac{\nu}{1+(\nu B_0 - 1)y_0^\infty}$ to replace the temporal derivative of scaled concen-

tration, $j\Omega\theta_{\mathrm{T}}^{(1)}$,

$$\underbrace{\boxed{j\Omega y_0^{(1)} = \frac{d^2 y_0^{(1)}}{dX^2}}}_{\text{Fick's law}} + \underbrace{\beta^{\infty} \frac{\mathrm{Ma}_{\mathrm{D}}^{\infty}}{\mathrm{Ma}_{\mathrm{M}}^{\infty^2}} y_0^{\infty} \left(1 - y_0^{\infty}\right) \frac{d^2 P^{(1)}}{dX^2}}_{\text{pressure diffusion correction}}. \tag{C.4}$$

C.2 Derivation of Wave Equation

Three different wave equations can be derived for the three respective cases of elastic, viscous, and viscoelastic materials. In general, we start with time-differentiating the volume balance

$$j\Omega \frac{d\mathrm{Pe}^{\square,(1)}}{dX} = -j^2 \Omega^2 \mathrm{Ma}_{\mathrm{D}}^{\infty} P^{(1)}, \tag{C.5}$$

and space-differentiating the momentum balance;

for the elastic case

$$3\frac{d^2 P^{(1)}}{dX^2} = -j\Omega \mathrm{Ma}_{\mathrm{D}}^{\infty} \frac{d\mathrm{Pe}^{(1)}}{dX}; \tag{C.6}$$

for the viscous case,

$$j\Omega \mathrm{Ma}_{\mathrm{D}}^{\infty} \frac{d\mathrm{Pe}^{(1)}}{dX} = -\frac{d^2 P^{(1)}}{dX^2} + \tfrac{4}{3}\mathrm{Sc}^{\infty} \mathrm{Ma}_{\mathrm{D}}^{\infty} \frac{d^3 \mathrm{Pe}^{(1)}}{dX^3}; \tag{C.7}$$

for the viscoelastic case,

$$j\Omega \mathrm{Ma}_{\mathrm{D}}^{\infty} \frac{d\mathrm{Pe}^{(1)}}{dX} = -\frac{d^2 P^{(1)}}{dX^2} + \frac{\frac{4}{3}\mathrm{Sc}^{\infty} \mathrm{Ma}_{\mathrm{D}}^{\infty}}{1 + j\Omega \frac{2(1+\nu_{\mathrm{PR}})}{3(1-2\nu_{\mathrm{PR}})} \mathrm{Sc}^{\infty} \mathrm{Ma}_{\mathrm{D}}^{\infty}} \frac{d^3 \mathrm{Pe}^{(1)}}{dX^3}. \tag{C.8}$$

The next step, which requires us to relate the gradients of mass-based and volume-based Peclet numbers (dimensionless velocities) is general again. Start with differentiating the kinematic relationship between these reference velocities with respect to time and space as well as identifying that current density is solenoidal (equation 4.49),

$$j\Omega \frac{d\mathrm{Pe}^{(1)}}{dX} = -\frac{j\Omega}{\varphi^{\infty}} \left(B_0 - m_0\right) \frac{d\eta_0^{(1)}}{dX} + \frac{j\Omega}{\varphi^{\infty}} \frac{d\mathrm{Pe}^{\square,(1)}}{dX}. \tag{C.9}$$

Use the time-differentiated scaled volume balance, the scaled solvent balance, and the scaled equation of state to simplify this derivative,

$$j\Omega\frac{d\mathrm{Pe}^{(1)}}{dX} = j^2\Omega^2\frac{\theta_{\mathrm{T}}^{\infty}}{\varphi^{\infty}}\left(B_0 - m_0\right)\left[1 - y_0^{\infty}\theta_{\mathrm{T}}^{\infty}\left(B_0 - \frac{1}{\nu}\right)\right]y_0^{(1)} - j^2\Omega^2\frac{1}{\varphi^{\infty}}\mathrm{Ma}_{\mathrm{D}}^{\infty}\left(1 - \theta_{\mathrm{T}}^{\infty}y_0^{\infty}B_0 + \theta_{\mathrm{T}}^{\infty}y_0^{\infty}m_0\right)P^{(1)}. \quad \text{(C.10)}$$

The definitions of zero-order total concentration $\theta_{\mathrm{T}}^{\infty} = \nu/1 + \left(\nu B_0 - 1\right)y_0^{\infty}$ and density $\varphi^{\infty} = \theta_{\mathrm{T}}^{\infty}\left[1 + \left(\nu m_0 - 1\right)y_0^{\infty}\right]/\nu$ help further,

$$j\Omega\frac{d\mathrm{Pe}^{(1)}}{dX} = j^2\Omega^2\beta^{\infty}y_0^{(1)} - j^2\Omega^2\mathrm{Ma}_{\mathrm{D}}^{\infty}P^{(1)}. \quad \text{(C.11)}$$

The viscous and viscoelastic momentum balances need a third-order derivative of the mass-based Peclet number. The second derivative can be written by differentiating C.11,

$$\frac{d^2\mathrm{Pe}^{(1)}}{dX^2} = j\Omega\beta^{\infty}\frac{dy_0^{(1)}}{dX} - j\Omega\mathrm{Ma}_{\mathrm{D}}^{\infty}\frac{dP^{(1)}}{dX}. \quad \text{(C.12)}$$

The composition gradient in C.12 can be replaced using the scaled solvent flux law 4.61

$$\frac{d^2\mathrm{Pe}^{(1)}}{dX^2} = -j\Omega\beta^{\infty}\frac{\nu}{\theta_{\mathrm{T}}^{\infty^2}}\eta_0^{(1)} + j\Omega\beta^{\infty}\frac{\nu}{\theta_{\mathrm{T}}^{\infty}}y_0^{\infty}\mathrm{Pe}^{\square,(1)} - j\Omega\mathrm{Ma}_{\mathrm{D}}^{\infty}\left[1 + \frac{\beta^{\infty^2}}{\mathrm{Ma}_{\mathrm{M}}^{\infty^2}}y_0^{\infty}\left(1 - y_0^{\infty}\right)\right]\frac{dP^{(1)}}{dX}. \quad \text{(C.13)}$$

By employing the equation of state, volume balance, and solvent balance, the third-order derivative can be obtained as

$$\frac{d^3\mathrm{Pe}^{(1)}}{dX^3} = j^2\Omega^2\beta^{\infty}y_0^{(1)} - j\Omega\mathrm{Ma}_{\mathrm{D}}^{\infty}\left[1 + \frac{\beta^{\infty^2}}{\mathrm{Ma}_{\mathrm{M}}^{\infty^2}}y_0^{\infty}\left(1 - y_0^{\infty}\right)\right]\frac{d^2P^{(1)}}{dX^2}. \quad \text{(C.14)}$$

Substituting these derivatives of Pe into the space-differentiated momentum balances

yield the three different wave equations:

elastic

$$\underbrace{\boxed{j^2\Omega^2\frac{\mathrm{Ma}_\mathrm{D}^{\infty^2}}{3}P^{(1)} = \frac{d^2P^{(1)}}{dX^2}}}_{\text{pressure wave equation}} + \underbrace{j^2\Omega^2\frac{\mathrm{Ma}_\mathrm{D}^{\infty}}{3}\beta^{\infty}y_0^{(1)}}_{\text{composition correction}}, \tag{C.15}$$

viscous

$$\begin{aligned} &j^2\frac{\Omega^2\mathrm{Ma}_\mathrm{D}^{\infty^2}}{1+j\Omega\frac{4}{3}\mathrm{Sc}^{\infty}\mathrm{Ma}_\mathrm{D}^{\infty^2}\left[1+\frac{\beta^{\infty^2}}{\mathrm{Ma}_\mathrm{M}^{\infty^2}}y_0^{\infty}\left(1-y_0^{\infty}\right)\right]}P^{(1)} \\ &\qquad = \frac{d^2P^{(1)}}{dX^2} + j^2\frac{\Omega^2\mathrm{Ma}_\mathrm{D}^{\infty}\beta^{\infty}\left(1-\frac{4}{3}\mathrm{Sc}^{\infty}\right)}{1+j\Omega\frac{4}{3}\mathrm{Sc}^{\infty}\mathrm{Ma}_\mathrm{D}^{\infty^2}\left[1+\frac{\beta^{\infty^2}}{\mathrm{Ma}_\mathrm{M}^{\infty^2}}y_0^{\infty}\left(1-y_0^{\infty}\right)\right]}y_0^{(1)}, \end{aligned} \tag{C.16}$$

viscoelastic

$$\begin{aligned} &j^2\frac{\Omega^2\mathrm{Ma}_\mathrm{D}^{\infty^2}}{1+\frac{j\Omega\frac{4}{3}\mathrm{Sc}^{\infty}\mathrm{Ma}_\mathrm{D}^{\infty^2}}{1+j\Omega\frac{2(1+\nu)}{3(1-2\nu)}\mathrm{Sc}^{\infty}\mathrm{Ma}_\mathrm{D}^{\infty}}\left[1+\frac{\beta^{\infty^2}}{\mathrm{Ma}_\mathrm{M}^{\infty^2}}y_0^{\infty}\left(1-y_0^{\infty}\right)\right]}P^{(1)} \\ &\qquad = \frac{d^2P^{(1)}}{dX^2} + j^2\frac{\Omega^2\mathrm{Ma}_\mathrm{D}^{\infty}\beta^{\infty}\left[1-\frac{\frac{4}{3}\mathrm{Sc}^{\infty}}{1+j\Omega\frac{2(1+\nu)}{3(1-2\nu)}\mathrm{Sc}^{\infty}\mathrm{Ma}_\mathrm{D}^{\infty}}\right]}{1+\frac{j\Omega\frac{4}{3}\mathrm{Sc}^{\infty}\mathrm{Ma}_\mathrm{D}^{\infty^2}}{1+j\Omega\frac{2(1+\nu)}{3(1-2\nu)}\mathrm{Sc}^{\infty}\mathrm{Ma}_\mathrm{D}^{\infty}}\left[1+\frac{\beta^{\infty^2}}{\mathrm{Ma}_\mathrm{M}^{\infty^2}}y_0^{\infty}\left(1-y_0^{\infty}\right)\right]}y_0^{(1)}. \end{aligned} \tag{C.17}$$

C.3 Eigenvalues of the System

C.3.1 Elastic Case

The elastic wave equation, equation C.15, can be substituted in the diffusion equation, equation C.4, to give,

$$\frac{d^2 y_0^{(1)}}{dX^2} = jWC_{\text{elas}}^{\infty}\left(1 + jW\xi_{\text{coup}}^{\infty}\right) y_0^{(1)} - j^2W^2\frac{\sqrt{3}}{\beta^{\infty}}\xi_{\text{coup}}^{\infty}P^{(1)}, \tag{C.18}$$

where parameters have been grouped for compactness to give dimensionless speed of sound in an elastic medium, $C_{\text{elas}}^{\infty} = \sqrt{3}/\text{Ma}_{\text{D}}^{\infty}$, scaled frequency, $W = \Omega/C_{\text{elas}}^{\infty}$, and $\xi_{\text{coup}}^{\infty} = \frac{{\beta^{\infty}}^2}{\text{Ma}_{\text{M}}^{\infty 2}} y_0^{\infty}\left(1 - y_0^{\infty}\right)/C_{\text{elas}}^{\infty}$, which quantifies the coupling between composition and pressure. The elastic wave equation can also be moulded in a similar form to give,

$$\frac{d^2 P^{(1)}}{dX^2} = -j^2W^2C_{\text{elas}}^{\infty}\frac{\beta^{\infty}}{\sqrt{3}}y_0^{(1)} + j^2W^2P^{(1)}. \tag{C.19}$$

Together, the system of equations C.18 and C.19 can be written in a matrix form as follows,

$$\frac{d^2}{dX^2}\begin{bmatrix} y_0^{(1)} \\ P^{(1)} \end{bmatrix} = jW\begin{bmatrix} C_{\text{elas}}^{\infty}\left(1 + jW\xi_{\text{coup}}^{\infty}\right) & -jW\frac{\sqrt{3}}{\beta^{\infty}}\xi_{\text{coup}}^{\infty} \\ -jWC_{\text{elas}}^{\infty}\frac{\beta^{\infty}}{\sqrt{3}} & jW \end{bmatrix}\begin{bmatrix} y_0^{(1)} \\ P^{(1)} \end{bmatrix}. \tag{C.20}$$

The eigenvalues of the coefficient matrix can be computed as follows,

$$\begin{vmatrix} C_{\text{elas}}^{\infty}\left(1 + jW\xi_{\text{coup}}^{\infty}\right) - \text{K}^2 & -jW\frac{\sqrt{3}}{\beta^{\infty}}\xi_{\text{coup}}^{\infty} \\ -jWC_{\text{elas}}^{\infty}\frac{\beta^{\infty}}{\sqrt{3}} & jW - \text{K}^2 \end{vmatrix} = 0. \tag{C.21}$$

The characteristic equation then provides the dispersion relations between wavenumber, K and frequency W:

$$\text{K}^4 - \left[jW + C_{\text{elas}}^{\infty}\left(1 + jW\xi_{\text{coup}}^{\infty}\right)\right]\text{K}^2 + jWC_{\text{elas}}^{\infty} = 0. \tag{C.22}$$

The solution of this quadratic (in K^2) equation gives us the dispersion relation we seek,

$$\text{K}^2 = \frac{\left[jW + C_{\text{elas}}^{\infty}\left(1 + jW\xi_{\text{coup}}^{\infty}\right)\right] \pm \sqrt{\left[jW + C_{\text{elas}}^{\infty}\left(1 + jW\xi_{\text{coup}}^{\infty}\right)\right]^2 - 4jWC_{\text{elas}}^{\infty}}}{2}. \tag{C.23}$$

When the coupling between composition and pressure ($\xi^{\infty}_{\text{coupl}} \sim 0$) is insignificant, the wavenumber solution points to two clear eigenmodes:

- Diffusion mode, $\mathrm{K} = \pm\sqrt{jW}$,
- Wave mode, $\mathrm{K} = \pm\sqrt{C^{\infty}_{\text{elas}}}$.

However, when coupling does play a role, it damps the wave mode, approximately according to $C^{\infty}_{\text{elas}}\sqrt{1 + jW\xi^{\infty}_{\text{coup}}}$. The coupling or damping factor for the elastic case is revisited to clarify its dependence on dimensionless parameters,

$$\xi^{\infty}_{\text{coup}} = \frac{\mathrm{Ma}^{\infty}_{\mathrm{D}}}{\sqrt{3}} \frac{1}{\mathrm{Ma}^{\infty^2}_{\mathrm{M}}} \left[\frac{\theta^{\infty^2}_{\mathrm{T}} \left(B_0 - m_0\right)}{\nu\varphi^{\infty}} \right]^2 y^{\infty}_0 \left(1 - y^{\infty}_0\right). \tag{C.24}$$

This expression corroborates the major numerical results obtained during parameter study: increasing diffusion Mach number by $\mathcal{O}(1)$ increases damping proportionally, decreasing Maxwell Mach number by $\mathcal{O}(1)$ increases damping by $\mathcal{O}(2)$. A more damped system directly implies a broader resonance peak.

C.3.2 Viscous Case

The viscous wave equation, equation C.16, can be substituted in the diffusion equation, equation C.4, to give,

$$\frac{d^2 y^{(1)}_0}{dX^2} = jWC^{\infty}_{\text{visc}} \frac{1 + jW\left(\xi^{\infty}_{\text{visc}} + \xi^{\infty}_{\text{coup}}\right)}{1 + jW\xi^{\infty}_{\text{visc}}\left(1 + C^{\infty}_{\text{visc}}\xi^{\infty}_{\text{coup}}\right)} y^{(1)}_0 - \frac{j^2W^2/\beta^{\infty}\xi^{\infty}_{\text{coup}}}{1 + jW\xi^{\infty}_{\text{visc}}\left(1 + C^{\infty}_{\text{visc}}\xi^{\infty}_{\text{coup}}\right)} P^{(1)}, \tag{C.25}$$

where the speed of sound in the viscous medium is defined as $C^{\infty}_{\text{visc}} = 1/\mathrm{Ma}^{\infty}_{\mathrm{D}}$, the scaled frequency and coupling coefficient are defined with respect to C^{∞}_{visc}, and a new viscous coefficient is given by $\xi^{\infty}_{\text{visc}} = \frac{4}{3}\mathrm{Sc}^{\infty}/\mathrm{C}^{\infty}_{\text{visc}}$. Combining this with the viscous wave equation, also simplified using the new variable definitions,

$$\frac{d^2 P^{(1)}}{dX^2} = \frac{j^2W^2}{1 + jW\xi^{\infty}_{\text{visc}}\left(1 + C^{\infty}_{\text{visc}}\xi^{\infty}_{\text{coup}}\right)} P^{(1)} - \frac{j^2W^2 C^{\infty}_{\text{visc}}\beta^{\infty}\left(1 - C^{\infty}_{\text{visc}}\xi^{\infty}_{\text{visc}}\right)}{1 + jW\xi^{\infty}_{\text{visc}}\left(1 + C^{\infty}_{\text{visc}}\xi^{\infty}_{\text{coup}}\right)} y^{(1)}_0. \tag{C.26}$$

Together, the system of equations C.25 and C.26 can be written in a matrix form as follows,

$$\frac{d^2}{dX^2}\begin{bmatrix} y_0^{(1)} \\ P^{(1)} \end{bmatrix} = \frac{jW}{1+jW\xi_{\text{visc}}^{\infty}\left(1+C_{\text{visc}}^{\infty}\xi_{\text{coup}}^{\infty}\right)} \cdot \begin{bmatrix} C_{\text{visc}}^{\infty}\left[1+jW\left(\xi_{\text{visc}}^{\infty}+\xi_{\text{coup}}^{\infty}\right)\right] & -jW\frac{1}{\beta^{\infty}}\xi_{\text{coup}}^{\infty} \\ -jWC_{\text{visc}}^{\infty}\beta^{\infty}\left(1-C_{\text{visc}}^{\infty}\xi_{\text{visc}}^{\infty}\right) & jW \end{bmatrix}\begin{bmatrix} y_0^{(1)} \\ P^{(1)} \end{bmatrix} \tag{C.27}$$

The eigenvalues/wavenumber of the coefficient matrix are then given by solving the following characteristic equation,

$$\mathrm{K}^4 - \left\{jW + C_{\text{visc}}^{\infty}\left[1+jW\left(\xi_{\text{visc}}^{\infty}+\xi_{\text{coup}}^{\infty}\right)\right]\right\}\mathrm{K}^2 \tag{C.28}$$

$$+jWC_{\text{visc}}^{\infty}\left[1+jW\xi_{\text{visc}}^{\infty}\left(1+\xi_{\text{coup}}^{\infty}C_{\text{visc}}^{\infty}\right)\right] = 0. \tag{C.29}$$

The wavenumber forms are understandably more complex than the elastic case,

$$\mathrm{K}^2 = \tfrac{1}{2}\left\{jW + C_{\text{visc}}^{\infty}\left[1+jW\left(\xi_{\text{visc}}^{\infty}+\xi_{\text{coup}}^{\infty}\right)\right]\right\} \pm \tfrac{1}{2}\sqrt{\left\{jW - C_{\text{visc}}^{\infty}\left[1+jW\left(\xi_{\text{visc}}^{\infty}+\xi_{\text{coup}}^{\infty}\right)\right]\right\}^2 - 4W^2C_{\text{visc}}^{\infty}\xi_{\text{coup}}^{\infty}\left(1-C_{\text{visc}}^{\infty}\xi_{\text{visc}}^{\infty}\right)}. \tag{C.30}$$

When the viscous coefficient is insignificant ($\xi_{\text{visc}}^{\infty} \sim 0$), the system reduces to the elastic system. However, when the viscous coefficient is significant but the coupling coefficient is not, we again get 2 clear eigenmodes

- Diffusion mode, $\mathrm{K} = \pm\sqrt{j\Omega}$,
- Wave mode (with viscous damping), $\mathrm{K} = \pm\sqrt{C_{\text{visc}}^{\infty}\left(1+jW\xi_{\text{visc}}^{\infty}\right)}$.

The viscous coefficient is therefore, unsurprisingly, acting like a damper. Taking a closer look at it,

$$\xi_{\text{visc}} = \frac{4}{3}\mathrm{Sc}^{\infty}\mathrm{Ma}_{\mathrm{D}}^{\infty} \tag{C.31}$$

we see that is directly proportional to the Schmidt number and the diffusion Mach number. The coupling coefficient adds further to this damping; its dependences on the dimensionless parameters were discussed in the previous section.

C.3.3 Viscoelastic Case

It was observed that the viscoelastic equations can be obtained by simply replacing the viscous damping factor, with a complex viscoelastic damping factor,

$$\xi^{*,\infty}_{\text{visc,elas}} = \frac{\xi^{\infty}_{\text{visc}}}{1 + jW\frac{1+\nu_{\text{PR}}}{2(1-2\nu_{\text{PR}})}C^{\infty}_{\text{visc}}\xi^{\infty}_{\text{visc}}}. \tag{C.32}$$

The solution to the characteristic equation can, therefore, be obtained by directly replacing $\xi^{\infty}_{\text{visc}}$ with $\xi^{*,\infty}_{\text{visc,elas}}$,

$$\begin{aligned}\text{K}^2 = {} & \tfrac{1}{2}\left\{jW + C^{\infty}_{\text{visc}}\left[1 + jW\left(\xi^{*,\infty}_{\text{visc, elas}} + \xi^{\infty}_{\text{coup}}\right)\right]\right\} \pm \\ & \tfrac{1}{2}\sqrt{\left\{jW - C^{\infty}_{\text{visc}}\left[1 + jW\left(\xi^{*,\infty}_{\text{visc, elas}} + \xi^{\infty}_{\text{coup}}\right)\right]\right\}^2 - 4W^2C^{\infty}_{\text{visc}}\xi^{\infty}_{\text{coup}}\left(1 - C^{\infty}_{\text{visc}}\xi^{*,\infty}_{\text{visc, elas}}\right)}\end{aligned} \tag{C.33}$$

Further, whereas the viscous coefficient is a real number, the viscoelastic coefficient is a complex number, with a real and imaginary part, shown as follows,

$$\xi^{*,\infty}_{\text{visc,elas}} = \underbrace{\frac{\xi^{\infty}_{\text{visc}}}{1 + W^2\left[\frac{1+\nu}{2(1-2\nu)}\right]^2 C^{\infty^2}_{\text{visc}}\xi^{\infty^2}_{\text{visc}}}}_{\text{REAL}} + j\underbrace{\frac{-W\frac{1+\nu}{2(1-2\nu)}C^{\infty}_{\text{visc}}\xi^{\infty^2}_{\text{visc}}}{1 + W^2\left[\frac{1+\nu}{2(1-2\nu)}\right]^2 C^{\infty^2}_{\text{visc}}\xi^{\infty^2}_{\text{visc}}}}_{\text{IMAGINARY}} \tag{C.34}$$

Finally, the magnitude and phase of the viscoelastic damping coefficient vary with the impedance frequency.

Appendix D

Warburg Impedance for Symmetric Cells

At low frequencies, the diffusion equation, equation C.4, is reduced to

$$j\Omega y_0^{(1)} = \frac{d^2 y_0^{(1)}}{dX^2}, \tag{D.1}$$

with the general solution:

$$y_0^{(1)} = A\exp\left(\sqrt{j\Omega}X\right) + B\exp\left(-\sqrt{j\Omega}X\right). \tag{D.2}$$

The constants A and B depend on the boundary conditions. Section 4.2.1 discusses the boundary conditions for a symmetric hydrogen cell used for an impedance experiment. For use in this analytical solution, the following boundary conditions

1. Apply the condition that solvent doesn't cross either boundary to the solvent flux balance, equation 4.19

$$\eta_0^{(1)}\Big|_{0,1} = -\frac{{\theta_{\mathrm{T}}^{\infty}}^2}{\nu}\left.\frac{dy_0^{(1)}}{dX}\right|_{0,1} + \theta_{\mathrm{T}}^{\infty} y_0^{\infty}\,\mathrm{Pe}^{\square,(1)}\Big|_{0,1} = 0, \tag{D.3}$$

2. Volume-average velocity introduced due to both electrode reactions is proportional to the current

$$\mathrm{Pe}^{\square,(1)}\Big|_{0,1} = \left.\frac{s_+ z_+}{n_{\mathrm{e}^-} z_{\mathrm{e}^-}} B_+ \mathrm{I}^{(1)}\right|_{0,1}, \tag{D.4}$$

3. Since current density is solenoidal ($\vec{\nabla}\cdot\vec{i}=0$) in this electroneutral system,

$$\mathrm{I}^{(1)}\big|_1 = \mathrm{I}^{(1)}\big|_0 = \mathrm{I}_0, \tag{D.5}$$

should be combined to give the composition gradient at the boundaries,

$$\left.\frac{dy_0^{(1)}}{dX}\right|_{0,1} = \left.\left(\frac{s_+ z_+}{n_{e^-} z_{e^-}}\frac{\nu y_0^\infty}{\theta_T^\infty} B_+\right)\right|_{0,1} \mathrm{I}_0. \tag{D.6}$$

Note that pressure gradients are seen to be negligible at the frequencies relevant for this analysis. To apply the composition gradient boundary conditions, differentiate the general solution,

$$\frac{dy_0^{(1)}}{dX} = A\sqrt{j\Omega}\exp\left(\sqrt{j\Omega}X\right) - B\sqrt{j\Omega}\exp\left(-\sqrt{j\Omega}X\right) \tag{D.7}$$

and set it equal to the values prescribed at the left boundary:

$$A - B = \frac{1}{\sqrt{j\Omega}}\frac{s_+ z_+}{n_{e^-} z_{e^-}}\frac{\nu y_0^\infty}{\theta_T^\infty} B_+ \mathrm{I}_0 \tag{D.8}$$

and at the right boundary

$$A\exp\left(\sqrt{j\Omega}\right) - B\exp\left(-\sqrt{j\Omega}\right) = \frac{1}{\sqrt{j\Omega}}\frac{s_+ z_+}{n_{e^-} z_{e^-}}\frac{\nu y_0^\infty}{\theta_T^\infty} B_+ \mathrm{I}_0. \tag{D.9}$$

Solving these two equations for the 2 unknowns—A and B, we have

$$A = \frac{s_+ z_+}{n_{e^-} z_{e^-}}\frac{\nu y_0^\infty}{\theta_T^\infty} B_+ \mathrm{I}_0 \frac{1}{\sqrt{j\Omega}} \frac{1-\exp\left(-\sqrt{j\Omega}\right)}{\exp\left(\sqrt{j\Omega}\right)-\exp\left(-\sqrt{j\Omega}\right)} \quad \text{and} \tag{D.10}$$

$$B = \frac{s_+ z_+}{n_{e^-} z_{e^-}}\frac{\nu y_0^\infty}{\theta_T^\infty} B_+ \mathrm{I}_0 \frac{1}{\sqrt{j\Omega}} \frac{1-\exp\left(\sqrt{j\Omega}\right)}{\exp\left(\sqrt{j\Omega}\right)-\exp\left(-\sqrt{j\Omega}\right)}. \tag{D.11}$$

Use hyperbolic trigonometric identities

$$\sinh\theta = \frac{\exp(\theta)-\exp(-\theta)}{2} \quad \text{and} \quad \cosh\theta = \frac{\exp(\theta)+\exp(-\theta)}{2} \tag{D.12}$$

to write solvent composition distribution in the electrolyte, at low frequencies when pressure change is negligible, as a function of the dimensionless frequency Ω:

$$y_0^{(1)} = \frac{s_+ z_+}{n_{e^-} z_{e^-}}\frac{\nu y_0^\infty}{\theta_T^\infty} B_+ \mathrm{I}_0 \frac{1}{\sqrt{j\Omega}} \frac{\cosh\left(\sqrt{j\Omega}X\right) - \cosh\left[\sqrt{j\Omega}(1-X)\right]}{\sinh\left(\sqrt{j\Omega}\right)}. \tag{D.13}$$

This can be simplified even further through some more identities

$$\cosh(\theta_1) - \cosh(\theta_2) = 2\sinh\left(\tfrac{\theta_1+\theta_2}{2}\right)\sinh\left(\tfrac{\theta_1-\theta_2}{2}\right) \tag{D.14}$$

$$\text{and} \quad \sinh(2\theta) = 2\sinh\theta\cosh\theta \tag{D.15}$$

to give the final form of the solvent composition distribution,

$$y_0^{(1)} = \frac{1}{2}\frac{s_+ z_+}{n_{e^-} z_{e^-}}\frac{\nu y_0^\infty}{\theta_T^\infty} B_+ I_0 \frac{1}{\sqrt{\frac{j\Omega}{4}}}\frac{\sinh\left[\sqrt{\frac{j\Omega}{4}}(2X-1)\right]}{\cosh\left(\sqrt{\frac{j\Omega}{4}}\right)}. \tag{D.16}$$

The composition overpotential can be derived as follows:

$$Z_y = \frac{s_+ z_+}{n_{e^-} z_{e^-}}\frac{\nu^2\left(1-t_+^{0,\infty}\right)^2\chi^\infty}{z_+\nu_+\left(1-y_0^\infty\right)}\frac{y_0^\infty}{\theta_T^\infty}\frac{\overline{V}_e^\infty L^\infty}{F z_+ D^\infty}\frac{RT}{F}\frac{1}{\sqrt{\frac{j\Omega}{4}}}\tanh\left(\sqrt{\frac{j\Omega}{4}}\right). \tag{D.17}$$

The complex number component $\dfrac{1}{\sqrt{\frac{j\Omega}{4}}}\tanh\left(\sqrt{\frac{j\Omega}{4}}\right)$ can be resolved further to separate the real and imaginary parts of impedance. According to Euler's identity,

$$\exp(j\theta) = \cos\theta + j\sin\theta, \tag{D.18}$$

implying that $j = \exp\left(\frac{j\pi}{2}\right)$. Taking the square root of j,

$$j^{1/2} = \exp\left(\tfrac{j\pi}{4}\right) = \cos\left(\tfrac{\pi}{4}\right) + j\sin\left(\tfrac{\pi}{4}\right) = \frac{1+j}{\sqrt{2}}, \tag{D.19}$$

we have

$$\frac{1}{\sqrt{\frac{j\Omega}{4}}}\tanh\left(\sqrt{\frac{j\Omega}{4}}\right) = \frac{(1-j)}{\sqrt{\frac{\Omega}{2}}}\tanh\left[2\sqrt{\frac{\Omega}{2}}(1+j)\right]. \tag{D.20}$$

Using more trigonometric and hyperbolic identities, we identify

$$\frac{1-j}{\sqrt{\frac{\Omega}{2}}}\tanh\left[\frac{(1+j)\sqrt{\Omega}}{2\sqrt{2}}\right] = \underbrace{\frac{1}{\sqrt{\frac{\Omega}{2}}}\frac{\sin\left(\sqrt{\frac{\Omega}{2}}\right)+\sinh\left(\sqrt{\frac{\Omega}{2}}\right)}{\cos\left(\sqrt{\frac{\Omega}{2}}\right)+\cosh\left(\sqrt{\frac{\Omega}{2}}\right)}}_{\textbf{REAL}}$$

$$+ j\underbrace{\frac{1}{\sqrt{\frac{\Omega}{2}}}\frac{\sin\left(\sqrt{\frac{\Omega}{2}}\right)-\sinh\left(\sqrt{\frac{\Omega}{2}}\right)}{\cos\left(\sqrt{\frac{\Omega}{2}}\right)+\cosh\left(\sqrt{\frac{\Omega}{2}}\right)}}_{\textbf{IMAGINARY}}. \tag{D.21}$$

Bibliography

[1] J. Newman, D. Bennion, and C. W. Tobias. "Mass Transfer in Concentrated Binary Electrolytes". In: *Berichte der Bunsengesellschaft für physikalische Chemie* 69.7 (1965), pp. 608–612.

[2] A. Kusoglu and A. Z. Weber. "Electrochemical/Mechanical Coupling in Ion-Conducting Soft Matter". In: *Journal of Physical Chemistry Letters* 6.22 (2015), pp. 4547–4552.

[3] A. Z. Weber and J. Newman. "A Theoretical Study of Membrane Constraint in Polymer-Electrolyte Fuel Cells". In: *AIChE Journal* 50.12 (2004), pp. 3215–3226.

[4] P. Goyal and C. W. Monroe. "New Foundations of Newman's Theory for Solid Electrolytes: Thermodynamics and Transient Balances". In: *Journal of the Electrochemical Society* 164.11 (2017), E3647–E3660.

[5] B. P. Setzler and T. F. Fuller. "A Physics-Based Impedance Model of Proton Exchange Membrane Fuel Cells Exhibiting Low-Frequency Inductive Loops". In: *Journal of the Electrochemical Society* 162.6 (2015), F519–F530.

[6] L. Onsager. "Reciprocal Relations in Irreversible Processes. II". In: *Physical Review* 38.12 (1931), pp. 2265–2279.

[7] C. W. Monroe and J. Newman. "Onsager's Shortcut to Proper Forces and Fluxes". In: *Chemical Engineering Science* 64.22 (2009), pp. 4804–4809.

[8] H. B. G. Casimir. "On Onsager's Principle of Microscopic Reversibility". In: *Reviews of Modern Physics* 17.2-3 (1945), pp. 343–350.

[9] C. W. Monroe, D. R. Wheeler, and J. Newman. "Nonequilibrium Linear Response Theory: Application to Onsager–Stefan–Maxwell Diffusion". In: *Industrial & Engineering Chemistry Research* 54.16 (2015), pp. 4460–4467.

[10] D. R. Wheeler and J. Newman. "Molecular Dynamics Simulations of Multicomponent Diffusion. 1. Equilibrium Method". In: *Journal of Physical Chemistry B* 108.47 (2004), pp. 18353–18361.

[11] D. R. Wheeler and J. Newman. "Molecular Dynamics Simulations of Multicomponent Diffusion. 2. Nonequilibrium Method". In: *Journal of Physical Chemistry B* 108.47 (2004), pp. 18362–18367.

[12] R. Darling and J. Newman. "Modeling a Porous Intercalation Electrode with Two Characteristic Particle Sizes". In: *Journal of the Electrochemical Society* 144.12 (1997), pp. 4201–4208.

[13] P. Arora, R. E. White, and M. Doyle. "Capacity Fade Mechanisms and Side Reactions in Lithium-Ion Batteries". In: *Journal of the Electrochemical Society* 145.10 (1998), pp. 3647–3667.

[14] P. M. Gomadam et al. "Mathematical Modeling of Lithium-Ion and Nickel Battery Systems". In: *Journal of Power Sources* 110.2 (2002), pp. 267–284.

[15] C. Monroe and J. Newman. "Dendrite Growth in Lithium/Polymer Systems - A Propagation Model for Liquid Electrolytes Under Galvanostatic Conditions". In: *Journal of the Electrochemical Society* 150.10 (2003), A1377–A1384.

[16] A. Z. Weber, R. M. Darling, and J. Newman. "Modeling Two-Phase Behavior in PEFCs". In: *Journal of the Electrochemical Society* 151.10 (2004), A1715–A1727.

[17] L. Cai and R. E. White. "An Efficient Electrochemical-Thermal Model for a Lithium-Ion Cell by Using the Proper Orthogonal Decomposition Method". In: *Journal of the Electrochemical Society* 157.11 (2010), A1188–A1195.

[18] S. K. Rahimian, S. Rayman, and R. E. White. "Extension of Physics-Based Single Particle Model for Higher Charge-Discharge Rates". In: *Journal of Power Sources* 224 (2013), pp. 180–194.

[19] A. M. Bizeray, D. A. Howey, and C. W. Monroe. "Resolving a Discrepancy in Diffusion Potentials, with a Case Study for Li-Ion Batteries". In: *Journal of the Electrochemical Society* 163.8 (2016), E223–E229.

[20] R. B. Smith and M. Z. Bazant. "Multiphase Porous Electrode Theory". In: *Journal of the Electrochemical Society* 164.11 (2017), E3291–E3310.

[21] A. M. Bizeray et al. "Identifiability and Parameter Estimation of the Single Particle Lithium-Ion Battery Model". In: *IEEE Transactions on Control Systems Technology* (2018), pp. 1–16.

[22] J. Newman. "Thermoelectric Effects in Electrochemical Systems". In: *Industrial & Engineering Chemistry Research* 34.10 (1995), pp. 3208–3216.

[23] C. W. Monroe and C. Delacourt. "Continuum Transport Laws for Locally Non-Neutral Concentrated Electrolytes". In: *Electrochimica Acta* 114 (2013), pp. 649–657.

[24] J. Newman and K. E. Thomas-Alyea. *Electrochemical Systems*. 3rd. Hoboken, New Jersey: John Wiley & Sons, Inc., 2004.

[25] M. Doyle, T. F. Fuller, and J. Newman. "Modeling of Galvanostatic Charge and Discharge of the Lithium Polymer Insertion Cell". In: *Journal of the Electrochemical Society* 140.6 (1993), pp. 1526–1533.

[26] T. F. Fuller, M. Doyle, and J. Newman. "Simulation and Optimization of the Dual Lithium Ion Insertion Cell". In: *Journal of the Electrochemical Society* 141.1 (1994), pp. 1–10.

[27] J. Liu and C. W. Monroe. “Solute-Volume Effects in Electrolyte Transport”. In: *Electrochimica Acta* 135 (2014), pp. 447–460.

[28] J. Liu and C. W. Monroe. “On the Characterization of Battery Electrolytes with Polarization Cells”. In: *Electrochimica Acta* 167 (2015), pp. 357–363.

[29] T. H. Etsell and S. N. Flengas. “Electrical Properties of Lanthanum Oxide-Calcium Oxide Solid Electrolytes”. In: *Journal of the Electrochemical Society* 116.6 (1969), pp. 771–778.

[30] T. H. Etsell and S. N. Flengas. “Electrical Properties of Solid Oxide Electrolytes”. In: *Chemical Reviews* 70.3 (1970), pp. 339–376.

[31] W. Grot. “Perfluorinated Ion Exchange Membranes of High Chemical and Thermal Stability”. In: *Chemie Ingenieur Technik* 44.4 (1972), pp. 167–169.

[32] S. C. Yeo and A. Eisenberg. “Physical-Properties and Supermolecular Structure of Perfluorinated Ion-Containing (Nafion) Polymers”. In: *Journal of Applied Polymer Science* 21.4 (1977), pp. 875–898.

[33] R. S. Yeo and J. Mcbreen. “Transport Properties of Nafion Membranes in Electrochemically Regenerative Hydrogen-Halogen Cells”. In: *Journal of the Electrochemical Society* 126.10 (1979), pp. 1682–1687.

[34] D. R. MacFarlane, J. H. Huang, and M. Forsyth. “Lithium-Doped Plastic Crystal Electrolytes Exhibiting Fast Ion Conduction for Secondary Batteries”. In: *Nature* 402.6763 (1999), pp. 792–794.

[35] J. W. Fergus. “Ceramic and Polymeric Solid Electrolytes for Lithium-Ion Batteries”. In: *Journal of Power Sources* 195.15 (2010), pp. 4554–4569.

[36] F. M. Du et al. “All Solid State Lithium Batteries Based on Lamellar Garnet-Type Ceramic Electrolytes”. In: *Journal of Power Sources* 300 (2015), pp. 24–28.

[37] J. C. Li et al. “Solid Electrolyte: the Key for High-Voltage Lithium Batteries”. In: *Advanced Energy Materials* 5.4 (2015).

[38] J. Wolfenstine et al. “High Conductivity of Dense Tetragonal $Li_7La_3Zr_2O_{12}$”. In: *Journal of Power Sources* 208 (2012), pp. 193–196.

[39] Y. Wang et al. “A Review of Polymer Electrolyte Membrane Fuel Cells: Technology, Applications, and Needs on Fundamental Research”. In: *Applied Energy* 88.4 (2011), pp. 981–1007.

[40] K. Asaka et al. “Bending of Polyelectrolyte Membrane-Platinum Composites by Electric Stimuli I. Response Characteristics to Various Waveforms”. In: *Polymer Journal* 27.4 (1995), pp. 436–440.

[41] T. Yamaue et al. “Electrostress Diffusion Coupling Model for Polyelectrolyte Gels”. In: *Macromolecules* 38.4 (2005), pp. 1349–1356.

[42] A. Kusoglu and A. Z. Weber. “New Insights into Perfluorinated Sulfonic-Acid Ionomers”. In: *Chemical Reviews* 117.3 (2017), pp. 987–1104.

[43] D. T. Hallinan and N. P. Balsara. “Polymer Electrolytes”. In: *Annual Review of Materials Research* 43 (2013), pp. 503–525.

[44] H. L. Yeager and A. Steck. “Cation and Water Diffusion in Nafion Ion Exchange Membranes - Influence of Polymer Structure”. In: *Journal of the Electrochemical Society* 128.9 (1981), pp. 1880–1884.

[45] H. L. Yeager and A. Eisenberg. “Perfluorinated Ionomer Membranes - Introduction”. In: *ACS Symposium Series* 180 (1982), pp. 1–6.

[46] K. A. Mauritz and R. B. Moore. “State of Understanding of Nafion”. In: *Chemical Reviews* 104.10 (2004), pp. 4535–4585.

[47] W. Y. Hsu and T. D. Gierke. “Elastic Theory for Ionic Clustering in Perfluorinated Ionomers”. In: *Macromolecules* 15.1 (1982), pp. 101–105.

[48] T. D. Gierke and W. Y. Hsu. “The Cluster-Network Model of Ion Clustering in Perfluorosulfonated Membranes”. In: *ACS Symposium Series* 180 (1982), pp. 283–307.

[49] M. Fujimura, T. Hashimoto, and H. Kawai. “Small-Angle X-Ray-Scattering Study of Perfluorinated Ionomer Membranes .1. Origin of 2 Scattering Maxima”. In: *Macromolecules* 14.5 (1981), pp. 1309–1315.

[50] M. Fujimura, T. Hashimoto, and H. Kawai. “Small-Angle X-Ray-Scattering Study of Perfluorinated Ionomer Membranes .2. Models for Ionic Scattering Maximum”. In: *Macromolecules* 15.1 (1982), pp. 136–144.

[51] S. Kumar and M. Pineri. “Interpretation of Small-Angle X-Ray and Neutron-Scattering Data for Perfluorosulfonated Ionomer Membranes”. In: *Journal of Polymer Science Part B-Polymer Physics* 24.8 (1986), pp. 1767–1782.

[52] M. Eikerling, A. A. Kornyshev, and E. Spohr. “Proton-Conducting Polymer Electrolyte Membranes: Water and Structure in Charge”. In: *Fuel Cells I* 215 (2008), pp. 15–54.

[53] K. D. Kreuer. *Hydrocarbon Membranes*. Handbook of Fuel Cells-Fundamentals, Technology, and Applications. Chichester, West Sussex: John Wiley & Sons, Inc., 2003.

[54] A. Z. Weber and J. Newman. “Transport in Polymer-Electrolyte Membranes - I. Physical Model”. In: *Journal of the Electrochemical Society* 150.7 (2003), A1008–A1015.

[55] A. Z. Weber and J. Newman. “Transport in Polymer-Electrolyte Membranes - II. Mathematical Model”. In: *Journal of the Electrochemical Society* 151.2 (2004), A311–A325.

[56] M. Eikerling et al. “Phenomenological Theory of Electro-Osmotic Effect and Water Management in Polymer Electrolyte Proton-Conducting Membranes”. In: *Journal of the Electrochemical Society* 145.8 (1998), pp. 2684–2699.

[57] E.C. Kumbur and M.M. Mench. “Fuel Cells - Proton-Exchange Membrane Fuel Cells - Water Management”. In: (2009).

[58] A. Kusoglu, B. L. Kienitz, and A. Z. Weber. “Understanding the Effects of Compression and Constraints on Water Uptake of Fuel-Cell Membranes”. In: *Journal of the Electrochemical Society* 158.12 (2011), B1504–B1514.

[59] M. K. Budinski and A. Cook. “Osmotic Pressure of Water in Nafion”. In: *Tsinghua Science and Technology* 15.4 (2010), pp. 385–390.

[60] P. Choi, N. H. Jalani, and R. Datta. “Thermodynamics and Proton Transport in Nafion - I. Membrane Swelling, Sorption, and Ion-Exchange Equilibrium”. In: *Journal of the Electrochemical Society* 152.3 (2005), E84–E89.

[61] P. Choi, N. H. Jalani, and R. Datta. “Thermodynamics and Proton Transport in Nafion - II. Proton Diffusion Mechanisms and Conductivity”. In: *Journal of the Electrochemical Society* 152.3 (2005), E123–E130.

[62] P. Choi, N. H. Jalani, and R. Datta. “Thermodynamics and Proton Transport in Nafion - III. Proton Transport in Nafion/Sulfated ZrO_2 Nanocomposite Membranes”. In: *Journal of the Electrochemical Society* 152.8 (2005), A1548–A1554.

[63] N. H. Jalani, P. Choi, and R. Datta. “TEOM: A Novel Technique for Investigating Sorption in Proton-Exchange Membranes”. In: *Journal of Membrane Science* 254.1-2 (2005), pp. 31–38.

[64] P. Choi et al. “Consideration of Thermodynamic, Transport, and Mechanical Properties in the Design of Polymer Electrolyte Membranes for Higher Temperature Fuel Cell Operation”. In: *Journal of Polymer Science Part B-Polymer Physics* 44.16 (2006), pp. 2183–2200.

[65] P. J. Flory. “Thermodynamics of Dilute Solutions of High Polymers”. In: *The Journal of Chemical Physics* 13.11 (1945), pp. 453–465.

[66] P. J. Flory and W. R. Krigbaum. “Thermodynamics of High Polymer Solutions”. In: *Annual Review of Physical Chemistry* 2 (1951), pp. 383–402.

[67] M. L. Huggins. “Solutions of Long Chain Compounds”. In: *The Journal of Chemical Physics* 9.5 (1941), pp. 440–440.

[68] P. J. Flory and J. Rehner. “Statistical Mechanics of Cross-Linked Polymer Networks I. Rubber-like Elasticity”. In: *The Journal of Chemical Physics* 11.11 (1943), pp. 512–520.

[69] P. J. Flory and J. Rehner. “Statistical Mechanics of Cross-Linked Polymer Networks II. Swelling”. In: *The Journal of Chemical Physics* 11.11 (1943), pp. 521–526.

[70] V. Freger. “Elastic Energy in Microscopically Phase-Separated Swollen Polymer Networks”. In: *Polymer* 43.1 (2002), pp. 71–76.

[71] A. Kusoglu et al. “Micromechanics Model Based on the Nanostructure of PFSA Membranes”. In: *Journal of Polymer Science Part B-Polymer Physics* 46.22 (2008), pp. 2404–2417.

[72] A. Kusoglu, M. H. Santare, and A. M. Karlsson. “Mechanics-Based Model for Non-Affine Swelling in Perfluorosulfonic Acid (PFSA) Membranes”. In: *Polymer* 50.11 (2009), pp. 2481–2491.

[73] M. H. Eikerling and P. Berg. “Poroelectroelastic Theory of Water Sorption and Swelling in Polymer Electrolyte Membranes”. In: *Soft Matter* 7.13 (2011), pp. 5976–5990.

[74] M. Eikerling and A. A. Kornyshev. “Proton Transfer in a Single Pore of a Polymer Electrolyte Membrane”. In: *Journal of Electroanalytical Chemistry* 502.1-2 (2001), pp. 1–14.

[75] A. Z. Weber and J. Newman. “Modeling Transport in Polymer-Electrolyte Fuel Cells”. In: *Chemical Reviews* 104.10 (2004), pp. 4679–4726.

[76] T. E. Springer, T. A. Zawodzinski, and S. Gottesfeld. “Polymer Electrolyte Fuel-Cell Model”. In: *Journal of the Electrochemical Society* 138.8 (1991), pp. 2334–2342.

[77] T. A. Zawodzinski et al. “Characterization of Polymer Electrolytes for Fuel-Cell Applications”. In: *Solid State Ionics* 60.1-3 (1993), pp. 199–211.

[78] T. V. Nguyen and R. E. White. “A Water and Heat Management Model for Proton-Exchange-Membrane Fuel-Cells”. In: *Journal of the Electrochemical Society* 140.8 (1993), pp. 2178–2186.

[79] T. F. Fuller. “Solid Polymer Electrolyte Fuel Cells”. Thesis. University of California, Berkeley, 1992.

[80] J. P. Meyers and J. Newman. “Simulation of the Direct Methanol Fuel Cell - I. Thermodynamic Framework for a Multicomponent Membrane”. In: *Journal of the Electrochemical Society* 149.6 (2002), A710–A717.

[81] J. P. Meyers and J. Newman. “Simulation of the Direct Methanol Fuel Cell - II. Modeling and Data Analysis of Transport and Kinetic Phenomena”. In: *Journal of the Electrochemical Society* 149.6 (2002), A718–A728.

[82] J. P. Meyers and J. Newman. “Simulation of the Direct Methanol Fuel Cell - III. Design and Optimization”. In: *Journal of the Electrochemical Society* 149.6 (2002), A729–A735.

[83] D. M. Bernardi and M. W. Verbrugge. “Mathematical-Model of a Gas-Diffusion Electrode Bonded to a Polymer Electrolyte”. In: *AIChE Journal* 37.8 (1991), pp. 1151–1163.

[84] D. M. Bernardi and M. W. Verbrugge. “A Mathematical-Model of the Solid-Polymer-Electrolyte Fuel-Cell”. In: *Journal of the Electrochemical Society* 139.9 (1992), pp. 2477–2491.

[85] R. Schlögl. “Membrane Permeation in Systems Far from Equilibrium”. In: *Berichte der Bunsengesellschaft für physikalische Chemie* 70.4 (1966), p. 400.

[86] S. Whitaker. “Flow in Porous-Media .1. A Theoretical Derivation of Darcy’s Law”. In: *Transport in Porous Media* 1.1 (1986), pp. 3–25.

[87] C. W. Monroe et al. “A Vaporization-Exchange Model for Water Sorption and Flux in Nafion”. In: *Journal of Membrane Science* 324.1-2 (2008), pp. 1–6.

[88] P. W. Majsztrik et al. “Water Sorption, Desorption and Transport in Nafion Membranes”. In: *Journal of Membrane Science* 301.1-2 (2007), pp. 93–106.

[89] J. Fuhrmann. “Comparison and Numerical Treatment of Generalised Nernst–Planck Models”. In: *Computer Physics Communications* 196 (2015), pp. 166–178.

[90] F. Helfferich. *Ion Exchange*. New York: Dover Publications, Inc., 1962.

[91] P. N. Pintauro and D. N. Bennion. “Mathematical-Model for the Determination of Ion and Solvent Transport in Membranes”. In: *Journal of the Electrochemical Society* 127.3 (1980), pp. C121–C121.

[92] P. N. Pintauro and D. N. Bennion. “Mass-Transport of Electrolytes in Membranes .1. Development of Mathematical Transport Model”. In: *Industrial & Engineering Chemistry Fundamentals* 23.2 (1984), pp. 230–234.

[93] J. O. Hirschfelder, R. B. Bird, and C. F. Curtiss. *Molecular Theory of Gases and Liquids*. New York: John Wiley & Sons, Inc., 1954.

[94] R. B. Bird, W. E. Stewart, and E. N. Lightfoot. *Transport Phenomena*. New York: John Wiley & Sons, Inc., 1960, p. 780.

[95] J. P. Meyers. “Simulation and Analysis of the Direct Methanol Fuel Cell”. Thesis. University of California, Berkeley, 2000.

[96] I. Nazarov and K. Promislow. “The Impact of Membrane Constraint on PEM Fuel Cell Water Management”. In: *Journal of the Electrochemical Society* 154.7 (2007), B623–B630.

[97] T. Yamaue and M. Doi. “The Stress Diffusion Coupling in the Swelling Dynamics of Cylindrical Gels”. In: *The Journal of Chemical Physics* 122.8 (2005).

[98] T. Yamaue and M. Doi. “Swelling Dynamics of Constrained Thin-Plate Gels under an External Force”. In: *Physical Review E* 70.1 (2004), pp. 011401–1.

[99] T. Yamaue and M. Doi. “Theory of One-Dimensional Swelling Dynamics of Polymer Gels under Mechanical Constraint”. In: *Physical Review E* 69.4 (2004).

[100] M. Doi et al. “Electro-Mechanical Coupling in Ionic Gels”. In: *Reactive & Functional Polymers* 73.7 (2013), pp. 891–893.

[101] O. Coussy and J. M. Pereira. “Modelling Plasticity of Unsaturated Soils in a Thermodynamically Consistent Framework”. In: *Poromechanics IV - Proceedings of the 4th Biot Conference on Poromechanics* (2009), pp. 252–257.

[102] O. Coussy, J. M. Pereira, and J. Vaunat. “Revisiting the Thermodynamics of Hardening Plasticity for Unsaturated Soils”. In: *Computers and Geotechnics* 37.1-2 (2010), pp. 207–215.

[103] O. Coussy. *Mechanics and Physics of Porous Solids*. Chichester, West Sussex: John Wiley & Sons, Inc., 2011.

[104] C. W. MacMinn, E. R Dufresne, and J. S Wettlaufer. "Large Deformations of a Soft Porous Material". In: *Physical Review Applied* 5.4 (2016), p. 044020.

[105] K. A. Page et al. "In Situ Method for Measuring the Mechanical Properties of Nafion Thin Films during Hydration Cycles". In: *ACS Applied Materials & Interfaces* 7.32 (2015), pp. 17874–17883.

[106] R. Borup et al. "Scientific Aspects of Polymer Electrolyte Fuel Cell Durability and Degradation". In: *Chemical Reviews* 107.10 (2007), pp. 3904–3951.

[107] J. P. Melchior et al. "About the Interactions Controlling Nafion's Viscoelastic Properties and Morphology". In: *Macromolecules* 48.23 (2015), pp. 8534–8545.

[108] Y. Lai et al. "Viscoelastic Stress Analysis of Constrained Proton Exchange Membranes under Humidity Cycling". In: *Journal of Fuel Cell Science and Technology* 6.2 (2009), pp. 021002–1.

[109] R. Mukundan et al. "Membrane Accelerated Stress Test Development for Polymer Electrolyte Fuel Cell Durability Validated Using Field and Drive Cycle Testing". In: *Journal of the Electrochemical Society* 165.6 (2018), F3085–F3093.

[110] K. A. Patankar et al. "Linear Hygrothermal Viscoelastic Characterization of Nafion NRE 211 Proton Exchange Membrane". In: *Fuel Cells* 12.5 (2012), pp. 787–799.

[111] Y. L. Tang et al. "An Experimental Investigation of Humidity and Temperature Effects on the Mechanical Properties of Perfluorosulfonic Acid Membrane". In: *Materials Science and Engineering: A* 425.1-2 (2006), pp. 297–304.

[112] Y. L. Tang et al. "Mechanical Properties of a Reinforced Composite Polymer Electrolyte Membrane and its Simulated Performance in PEM Fuel Cells". In: *Journal of Power Sources* 175.2 (2008), pp. 817–825.

[113] P. Majsztrik, A. Bocarsly, and J. Benziger. "Water Permeation through Nafion Membranes: The Role of Water Activity". In: *Journal of Physical Chemistry B* 112.51 (2008), pp. 16280–16289.

[114] P. W. Majsztrik, A. B. Bocarsly, and J. B. Benziger. "Viscoelastic Response of Nafion. Effects of Temperature and Hydration on Tensile Creep". In: *Macromolecules* 41.24 (2008), pp. 9849–9862.

[115] M. B. Satterfield et al. "Mechanical Properties of Nafion and Titania/Nafion Composite Membranes for Polymer Electrolyte Membrane Fuel Cells". In: *Journal of Polymer Science Part B-Polymer Physics* 44.16 (2006), pp. 2327–2345.

[116] M. B. Satterfield. "Mechanical and Water Sorption Properties of Nafion and Composite Nafion/Titanium Dioxide Membranes for Polymer Electrolyte Membrane Fuel Cells". Thesis. Princeton University, 2007.

[117] P. W. Majsztrik. "Mechanical and Transport Properties of Nafion for PEM Fuel Cells: Temperature and Hydration Effects". Thesis. Princeton University, 2008.

[118] L. E. Malvern. *Introduction to the Mechanics of a Continuous Medium*. Engelwood Cliffs, New Jersey: Prentice-Hall, Inc., 1969.

[119] A. Y. Malkin and A. I. Isayev. *Rheology: Concepts, Methods, and Applications*. Toronto: ChemTec Publishing, 2017.

[120] D. Jou, J. Casas-Vázquez, and G. Lebon. *Extended Irreversible Thermodynamics*. Berlin, Heidelberg: Springer, 1996.

[121] M. N. Silberstein and M. C. Boyce. "Constitutive Modeling of the Rate, Temperature, and Hydration Dependent Deformation Response of Nafion to Monotonic and Cyclic Loading". In: *Journal of Power Sources* 195.17 (2010), pp. 5692–5706.

[122] R. Solasi et al. "A Time and Hydration Dependent Viscoplastic Model for Polyelectrolyte Membranes in Fuel Cells". In: *Mechanics of Time-Dependent Materials* 12.1 (2008), pp. 15–30.

[123] W. Yoon and X. Y. Huang. "A Nonlinear Viscoelastic-Viscoplastic Constitutive Model for Ionomer Membranes in Polymer Electrolyte Membrane Fuel Cells". In: *Journal of Power Sources* 196.8 (2011), pp. 3933–3941.

[124] A. Latz and J. Zausch. "Thermodynamic Consistent Transport Theory of Li-ion Batteries". In: *Journal of Power Sources* 196.6 (2011), pp. 3296–3302.

[125] M. Z. Bazant. "Theory of Chemical Kinetics and Charge Transfer Based on Nonequilibrium Thermodynamics". In: *Accounts of Chemical Research* 46.5 (2013), pp. 1144–1160.

[126] M. Pavelka. "Thermodynamic Analysis of Processes in Hydrogen Fuel Cells". Thesis. Charles University in Prague, 2015.

[127] A. E. Green and P. M. Naghdi. "A Re-Examination of the Basic Postulates of Thermomechanics". In: *Proceedings of the Royal Society of London Series A - Mathematical Physical and Engineering Sciences* 432.1885 (1991), pp. 171–194.

[128] O. Coussy. *Poromechanics*. Chichester, West Sussex: John Wiley & Sons, Inc., 2004.

[129] R. S. Rivlin. "Large Elastic Deformations of Isotropic Materials IV. Further Developments of the General Theory". In: *Philosophical Transactions of the Royal Society. A. Mathematical and Physical Sciences* 241.835 (1948), pp. 379–397.

[130] R. W. Ogden and R. Hill. "Large Deformation Isotropic Elasticity—On the Correlation of Theory and Experiment for Incompressible Rubberlike Solids". In: *Proceedings of the Royal Society of London. A. Mathematical and Physical Sciences* 326.1567 (1972), pp. 565–584.

[131] G. T Houlsby and A. M. Puzrin. *Principles of hyperplasticity: an approach to plasticity theory based on thermodynamic principles*. Springer Science & Business Media, 2007.

[132] C. Truesdell. “Mechanical Basis of Diffusion”. In: *The Journal of Chemical Physics* 37.10 (1962), pp. 2336–2344.

[133] J. Newman and T. W. Chapman. “Restricted Diffusion in Binary Solutions”. In: *AIChE Journal* 19.2 (1973), pp. 343–348.

[134] H. Brenner. “Fluid Mechanics Revisited”. In: *Physica A: Statistical Mechanics and its Applications* 370.2 (2006), pp. 190–224.

[135] H. Brenner. “Kinematics of Volume Transport”. In: *Physica A* 349 (2005), pp. 11–59.

[136] H. Brenner. “Bivelocity Hydrodynamics. Diffuse Mass Flux vs. Diffusive Volume Flux”. In: *Physica A* 392 (2013), pp. 558–566.

[137] I. Gyarmati. *Nonequilibrium Thermodynamics: Field Theory and Variational Principles*. 1st. New York: Springer-Verlag, 1970.

[138] S. Whitaker. “Role of the Species Momentum Equation in the Analysis of the Stefan Diffusion Tube”. In: *Industrial & Engineering Chemistry Research* 30.5 (1991), pp. 978–983.

[139] R. J. Bearman and J. G. Kirkwood. “Statistical Mechanics of Transport Processes. XI. Equations of Transport in Multicomponent Systems”. In: *The Journal of Chemical Physics* 28.1 (1958), pp. 136–145.

[140] F. M. Snell and R. A. Spangler. “A Phenomenological Theory of Transport in Multicomponent Systems”. In: *The Journal of Physical Chemistry* 71.8 (1967), pp. 2503–2510.

[141] R. Datta and S. A. Vilekar. “The Continuum Mechanical Theory of Multicomponent Diffusion in Fluid Mixtures”. In: *Chemical Engineering Science* 65 (2010), pp. 5976–5989.

[142] L. Onsager. “Theories and Problems of Liquid Diffusion”. In: *Annals of the New York Academy of Sciences* 46.5 (1945), pp. 241–265.

[143] S. R. de Groot. *Thermodynamics of Irreversible Processes*. New York: Interscience Publishers, 1951.

[144] C. W. Monroe and J. Newman. “An Introduction to the Onsager Reciprocal Relations”. In: *Chemical Engineering Education* 41 (2007), p. 223.

[145] T. F. Fuller and J. Newman. “Experimental-Determination of the Transport Number of Water in Nafion-117 Membrane”. In: *Journal of the Electrochemical Society* 139.5 (1992), pp. 1332–1337.

[146] C. W. Monroe and J. Newman. “Onsager Reciprocal Relations for Stefan–Maxwell Diffusion”. In: *Industrial & Engineering Chemistry Research* 45.15 (2006), pp. 5361–5367.

[147] J. N. Agar. *Thermogalvanic Cells*. P. Delahay, Ed. Vol. 3. Advances in Electrochemistry and Electrochemical Engineering. New York: Interscience Publishers, 1963.

[148] D. Bernardi, E. Pawlikowski, and J. Newman. “A General Energy-Balance for Battery Systems”. In: *Journal of the Electrochemical Society* 132.1 (1985), pp. 5–12.

[149] T. W. Chapman and J. Newman. *A Compilation of Selected Thermodynamic and Transport Properties of Binary Electrolytes in Aqueous Solution*. Report. University of California, Lawrence Radiation Laboratory, 1968.

[150] J. C. Maxwell. “On the Dynamical Theory of Gases”. In: *Philosophical Transactions of the Royal Society of London* 157 (1867), pp. 49–88.

[151] J. Stefan. “Über das Gleichgewicht und Bewegung, insbesondere die Diffusion von Gemischen”. In: *Sitzungsberichte der Kaiserlichen Akademie der Wissenschaften Wien* 63 (1871), pp. 63–124.

[152] M. E. Orazem and B. Tribollet. *Electrochemical Impedance Spectroscopy*. Hoboken, New Jersey: John Wiley & Sons, Inc., 2008.

[153] J. E. B. Randles. “Kinetics of Rapid Electrode Reactions”. In: *Discussions of the Faraday Society* 1 (1947), pp. 11–19.

[154] E. Warburg. “Über das Verhalten sogenannter unpolarisirbarer Elektroden gegen Wechselstrom”. In: *Annalen der Physik* 303.3 (1899), pp. 493–499.

[155] K. S. Cole and R. H. Cole. “Dispersion and Absorption in Dielectrics I. Alternating Current Characteristics”. In: *The Journal of Chemical Physics* 9.4 (1941), pp. 341–351.

[156] P. M. Gomadam and J. W. Weidner. “Analysis of Electrochemical Impedance Spectroscopy in Proton Exchange Membrane Fuel Cells”. In: *International Journal of Energy Research* 29.12 (2005), pp. 1133–1151.

[157] M. Eikerling and A. A. Kornyshev. “Electrochemical Impedance of the Cathode Catalyst Layer in Polymer Electrolyte Fuel Cells”. In: *Journal of Electroanalytical Chemistry* 475.2 (1999), pp. 107–123.

[158] G. A. Futter et al. “Physical Modeling of Polymer-Electrolyte Membrane Fuel Cells: Understanding Water Management and Impedance Spectra”. In: *Journal of Power Sources* 391 (2018), pp. 148–161.

[159] T. E. Springer et al. “Characterization of Polymer Electrolyte Fuel Cells using AC Impedance Spectroscopy”. In: *Journal of the Electrochemical Society* 143.2 (1996), pp. 587–599.

[160] Z. Xie and S. Holdcroft. “Polarisation-dependent Mass Transport Parameters for ORR in Perflourosulfonic Acid Ionomer Membranes: an EIS Study using Microelectrodes”. In: *Journal of the Electroanalytical Chemistry* 568 (2004), pp. 247–260.

[161] D. J. L. Brett et al. “Localized Impedance Measurements along a Single Channel of a Solid Polymer Fuel Cell”. In: *Electrochemical and Solid-State Letters* 6.4 (2003), A63–A66.

[162] I. A. Schneider et al. “Fast Locally Resolved Electrochemical Impedance Spectroscopy in Polymer Electrolyte Fuel Cells”. In: *Journal of the Electrochemical Society* 152.10 (2005), A2092–A2103.

[163] R. Pollard and T. Comte. “Determination of Transport Properties for Solid Electrolytes from the Impedance of Thin Layer Cells”. In: *Journal of the Electrochemical Society* 136.12 (1989), pp. 3734–3748.

[164] J. Evans, C. A. Vincent, and P. G. Bruce. “Electrochemical Measurement of Transference Numbers in Polymer Electrolytes”. In: *Polymer* 28.13 (1987), pp. 2324–2328.

[165] N. Wagner. “Characterization of Membrane Electrode Assemblies in Polymer Electrolyte Fuel Cells using AC Impedance Spectroscopy”. In: *Journal of Applied Electrochemistry* 32.8 (2002), pp. 859–863.

[166] M. N. Silberstein and M. C. Boyce. “Hygro-Thermal Mechanical Behavior of Nafion during Constrained Swelling”. In: *Journal of Power Sources* 196.7 (2011), pp. 3452–3460.

[167] K. B. Daly et al. “Viscosity of Nafion Oligomers as a Function of Hydration and Counterion Type: A Molecular Dynamics Study”. In: *The Journal of Physical Chemistry B* 118.48 (2014), pp. 13981–13991.

[168] C. Delacourt and J. Newman. “Mathematical Modeling of a Cation-Exchange Membrane Containing Two Cations”. In: *Journal of the Electrochemical Society* 155.11 (2008), B1210–B1217.

[169] R. E. Graves and B. M. Argrow. “Bulk Viscosity: Past to Present”. In: *Journal of Thermophysics and Heat Transfer* 13 (1999), pp. 337–342.

[170] A. S. Dukhin and P. J. Goetz. “Bulk Viscosity and Compressibility Measurement using Acoustic Spectroscopy”. In: *The Journal of Chemical Physics* 130 (2009), p. 124519.

[171] M. S. Cramer. “Numerical Estimates for the Bulk Viscosity of Ideal Gases”. In: *Physics of Fluids* 24 (2012), p. 066102.

[172] H. Metiu and K. F. Freed. “Bulk Viscosity of Polymer-Solutions”. In: *The Journal of Chemical Physics* 67 (1977), pp. 3303–3315.

[173] R. P. Paganelli et al. “Modeling and Characterization of Piezoelectric Transducers by Means of Scattering Parameters. Part I: Theory”. In: *Sensors and Actuators A: Physical* 160.1-2 (2010), pp. 9–18.

[174] T. A. Zawodzinski et al. “Water-Uptake by and Transport through Nafion 117 Membranes”. In: *Journal of the Electrochemical Society* 140.4 (1993), pp. 1041–1047.

[175] A. C. Olesen, T. Berning, and S. K. Kaer. “On the Diffusion Coefficient of Water in Polymer Electrolyte Membranes”. In: *ECS Transactions* 50.2 (2013), pp. 979–991.

[176] G. Li and C. W. Monroe. “Electrochemomechanics in Doped Garnet Lithium-Ion Conductors”. In: *Meeting Abstracts, 233rd ECS Meeting* (2018).

[177] P. W. Bridgman. “The Thermodynamics of Plastic Deformation and Generalized Entropy”. In: *Review of Modern Physics* 22 (1950), pp. 56–63.

[178] I. F. Collins and G. T. Houlsby. “Application of Thermomechanical Principles to the Modelling of Geotechnical Materials”. In: *Proceedings of the Royal Society of London. Series A, Mathematical, Physical and Engineering Sciences* 453 (1997), pp. 1975–2001.